

JSCSEN 74(8–9)847–1019(2009)

Journal of the Serbian Chemical Society

Electronic
version

VOLUME 74

No 8–9

BELGRADE 2009

Available on line at



www.shd.org.rs/JSCS

The full search of JSCS
is available through

DOAJ DIRECTORY OF
OPEN ACCESS
JOURNALS
www.doaj.org

J. Serb. Chem. Soc. Vol. 74, No. 8–9 (2009)

CONTENTS

Organic Chemistry and Biochemistry

- I. M. C. Ienaşcu, A. X. Lupea, I. M. Popescu, M. A. Pădure and A. D. Zamfir: The synthesis and characterization of some novel 5-chloro-2-(substituted alkoxy)-*N*-phenylbenzamide derivatives..... 847
- S. E. Kevrešan, Đ. R. Malenčić, M. T. Popović, K. N. Kuhajda and J. E. Kandrač: The effect of cholic acid treatment on the oxidative status of soybean plants..... 857
- J. M. Aćimović, B. D. Stanimirović and Lj. M. Mandić: The role of the thiol group in protein modification with methylglyoxal 867
- J. P. Marković, J. B. Radović, R. T. Štrbanović, D. S. Bajić and M. M. Vrvic: Changes in the infrared attenuated total reflectance (ATR) spectra of lignins from alfalfa stem with growth and development..... 885
- V. Doubnerová, L. Potůčková, K. Müller and H. Ryšlavá: The regulation and catalytic mechanism of the NADP-malic enzyme from tobacco leaves 893

Inorganic Chemistry

- S. Chandra, M. Tyagi and M. S. Refat: Spectroscopic, thermal and antibacterial studies on Mn(II) and Co(II) complexes derived from thiosemicarbazone 907
- N. Kurtoglu: Synthesis, characterization, chelation with transition metal ions, and antibacterial and antifungal studies of the 4-[(*E*)-phenyldiazenyl]-2-[(*E*)-(phenylimino)methyl]phenol dye..... 917
- P. Tharmaraj, D. Kodimunthiri, C. D. Sheela and C. S. S. Priya: Synthesis, spectral studies and antibacterial activity of Cu(II), Co(II) and Ni(II) complexes of 1-(2-hydroxyphenyl)-3-phenyl-2-propen-1-one, *N*²-[(3,5-dimethyl-1*H*-pyrazol-1-yl)methyl]hydrazone..... 927
- F. Firdaus, K. Fatma, A. U. Khan and M. Shakir: Metal ion controlled synthesis of 16- and 18-membered binuclear octaazamacrocyclic complexes with Co(II), Ni(II), Cu(II) and Zn(II): a comparative spectroscopic approach to DNA binding to Cu(II) complexes..... 939

Physical Chemistry

- C. Balan, D. Bilba and M. Macoveanu: Studies on chromium(III) removal from aqueous solutions by sorption on *Sphagnum* moss peat..... 953

Electrochemistry

- K. Dj. Popović, J. D. Lović, A. V. Tripković and P. K. Olszewski: Activity of carbon supported Pt₃Ru₂ nanocatalyst in CO oxidation 965

Analytical Chemistry

- S. M. Rančić and S. D. Nikolić-Mandić: Kinetic spectrophotometric determination of Bi(III) based on its catalytic effect on the oxidation of phenylfluorone by hydrogen peroxide (Short communication) 977
- H. Z. Mousavi and H. Shir Khanloo: Spectrophotometric determination of nitrite based on its catalytic effect on the reaction of nuclear fast red and potassium bromated (Short communication) 985

Chemical Engineering

- Z. J. Predojević and B. D. Škrbić: Alkali-catalyzed production of biodiesel from waste frying oils 993

Environmental Chemistry

- B. M. Žarković and S. D. Blagojević: The effects of some agrotechnical measures on the uptake of nickel by maize plants 1009

- Errata (printed version)..... 1019

Published by the Serbian Chemical Society
Karnegijeva 4/III, 11000 Belgrade, Serbia
Printed by the Faculty of Technology and Metallurgy
Karnegijeva 4, P.O. Box 35-03, 11120 Belgrade, Serbia



J. Serb. Chem. Soc. 74 (8–9) 847–855 (2009)
JSCS–3881

Journal of
the Serbian
Chemical Society

JSCS@tmf.bg.ac.rs • www.shd.org.rs/JSCS

UDC 547.272'11+547.564.7:542.913:
547–304.6

Original scientific paper

The synthesis and characterization of some novel 5-chloro-2-(substituted alkoxy)-*N*-phenylbenzamide derivatives

IOANA M. C. IENAȘCU^{1,3}, ALFA X. LUPEA^{1*}, IULIANA M. POPESCU²,
MIRABELA A. PĂDURE¹ and ALINA D. ZAMFIR^{3,4}

¹"Politehnica" University, Faculty of Industrial Chemistry and Environment Engineering, Department of Organic Chemistry, 2 P-ța Victoriei, 300006 Timisoara, ²Banat's Agricultural Science University, Faculty of Agriculture, Department of Chemistry and Biochemistry, 119 Calea Aradului, 300645 Timisoara, ³Mass Spectrometry Laboratory, National Institute for Research and Development in Electrochemistry and Condensed Matter, 1 Plautius Andronescu, 300224 Timisoara and ⁴"Aurel Vlaicu" University of Arad, 77 Revoluției Blvd., 310130 Arad, Romania

(Received 26 November 2007, revised 27 April 2009)

Abstract: To obtain biologically active compounds, the synthesis of some new derivatives with an *o*-hydroxybenzamide structure was performed. The ethyl esters **4–6** were obtained by the reaction of 5-chloro-2-hydroxy-*N*-phenylbenzamide and chloro-substituted acid ethyl esters **1–3** in ethyl methyl ketone. The obtained ethyl esters were condensed with hydrazine yielding the hydrazides **7–8**. The hydrazones **11–14** were obtained by the reaction of the hydrazides and the chloro-substituted benzaldehydes **9–10**. All the newly synthesized compounds were characterized by FTIR, ¹H-NMR, ¹³C-NMR, MS and elemental analyses.

Keywords: 5-chloro-2-(substituted alkoxy)-*N*-phenylbenzamide derivatives; ethyl esters; hydrazides; hydrazones; *O*-substituted salicylanilides.

INTRODUCTION

Searching for novel biologically active compounds with improved and highly selective effects and lower toxicity remains a challenge for pharmaceutical chemistry, while the incidence of the systemic diseases as well as the spectrum of pathogens have been steadily increasing over the past few years.

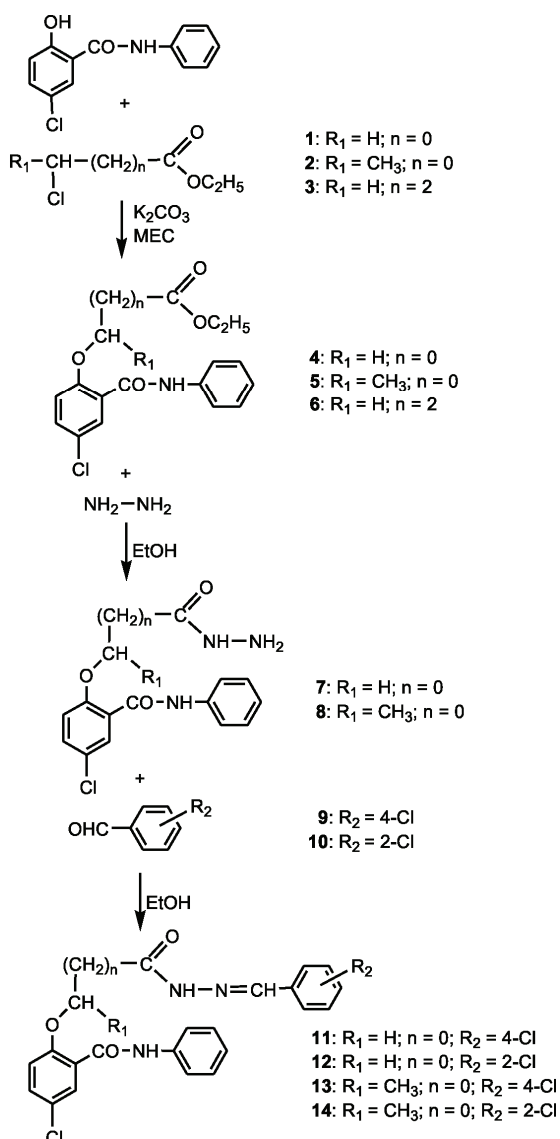
Salicylanilides, as well as *O*-substituted salicylanilides, represent a class of compounds with a broad spectrum of biological activity,^{1,2} including antimicrobial effects against a number of yeast and filamentous fungi. Substitution of phenoxyacetic acid with an electrophilic group in the *ortho* or *para* position increases their activity against human pathogenic fungi.^{3–9}

* Corresponding author. E-mail: alfaxenialupea@yahoo.com
doi: 10.2298/JSC0909847I

2-(Hydrazinocarbonylmethoxy)benzamide and its hydrazones obtained with substituted benzaldehydes show anti-inflammatory and analgesic activity superior to salicylamide itself and lower ulcerogenic activity.^{10,11}

In order to obtain such active compounds, some *ortho*-substituted phenoxyalkanoic acids and their derivatives were synthesized and characterized.^{12,13}

The aim of this research was to synthesize new 5-chloro-2-(substituted alkoxy)-*N*-phenylbenzamide derivatives (Scheme 1) with potential antibacterial and antifungal activity and to characterize them.



Scheme 1. Synthesis of 5-chloro-2-(substituted alkoxy)-*N*-phenylbenzamide derivatives.

RESULTS AND DISCUSSION

The synthesized compounds are crystalline substances (needles or prisms) and were obtained with reaction yields ranging from 66 to 92 %. Their physical, chemical and spectral properties are given below.

2-[4-Chloro-(2-phenylamino)carbonyl]phenoxy}acetic acid, ethyl ester (4). Yield: 78 %; m.p. 150 °C; Anal. Calcd. for $C_{17}H_{16}ClNO_4$ (333.08 g/mol): C, 61.18, H, 4.83, N, 4.20 %. Found: C, 61.20, H, 4.80, N, 4.24 %; IR (KBr, cm^{-1}): 3328 *m*, 1751 *i*, 1652 *i*, 1596 *m*, 1541 *i*, 1502 *m*, 1483 *m*, 1442 *m*, 1388 *s*, 1321 *m*, 1282 *s*, 1222 *i*, 1112 *m*, 1074 *m*, 1062 *m*, 1024 *s*, 906 *s*, 823 *m*, 758 *m*, 706 *s*, 690 *s*, 547 *s*, 511 *s*; 1H -NMR (400 MHz, DMSO- d_6 , δ / ppm): 1.21 (3H, *t*, $COOCH_2CH_3$, $J = 7.2$ Hz), 4.22 (2H, *q*, $COOCH_2CH_3$, $J = 7.2$ Hz), 4.99 (2H, *s*, $-O-CH_2-CO-$), 7.13 (1H, *t*, H_{10} , $J = 7.6$ Hz), 7.22 (1H, *d*, H_3 , $J = 8.8$ Hz), 7.37 (2H, *t*, H_9, H_{11} , $J = 8.0$ Hz), 7.57 (1H, *d*, H_4 , $J = 8.8$ Hz), 7.78 (2H, *d*, H_8, H_{12} , $J = 8.0$ Hz), 7.83 (1H, *s*, H_6), 10.39 (1H, *s*, $-CO-NH-$); ^{13}C -NMR (400 MHz, $CDCl_3$, δ / ppm): 14.14 ($COOCH_2CH_3$), 61.48 ($COOCH_2CH_3$), 66.25 ($-O-CH_2-CO-$), 115.91 (C_3), 120.16 (C_8, C_{12}), 124.28 (C_1), 125.12 (C_{10}), 125.81 (C_5), 129.03 (C_9, C_{11}), 130.13 (C_6), 132.43 (C_4), 138.58 (C_7), 154.05 (C_2), 162.07 ($-CO-NH-$), 168.80 ($COOC_2H_5$); (+)MS¹ (m/z): 356.1 ($[M+Na]^+$), 334.0 ($[M+H]^+$); (+)MSⁿ (m/z): 334.0, 258.9, 240.8, 212.8, 184.8, 154.9.

2-[4-Chloro-(2-phenylamino)carbonyl]phenoxy}propionic acid, ethyl ester (5). Yield: 72 %; m.p. 69–73 °C; Anal. Calcd. for $C_{18}H_{18}ClNO_4$ (347.09 g/mol): C, 62.16, H, 5.22, N, 4.03 %. Found C, 62.11, H, 5.25, N, 4.05 %; IR (KBr, cm^{-1}): 3338 *m*, 2989 *s*, 1745 *i*, 1660 *i*, 1596 *m*, 1541 *i*, 1494 *m*, 1479 *m*, 1440 *m*, 1379 *s*, 1367 *m*, 1303 *s*, 1271 *m*, 1232 *i*, 1149 *m*, 1118 *m*, 1053 *s*, 1020 *s*, 910 *s*, 866 *s*, 802 *s*, 758 *m*, 719 *s*, 702 *s*, 677 *s*, 648 *s*, 515 *s*, 418 *s*; 1H -NMR (400 MHz, DMSO- d_6 , δ / ppm): 1.18 (3H, *t*, $COOCH_2CH_3$, $J = 6.8$ Hz), 1.58 (3H, *d*, $-O-CH(CH_3)CO-$, $J = 6.8$ Hz), 4.17 (2H, *q*, $COOCH_2CH_3$, $J = 6.8$ Hz), 5.23 (1H, *q*, $-O-CH(CH_3)CO-$, $J = 6.8$ Hz), 7.12 (1H, *t*, H_{10} , $J = 7.6$ Hz), 7.18 (1H, *d*, H_3 , $J = 8.8$ Hz), 7.37 (2H, *t*, H_9, H_{11} , $J = 8.0$ Hz), 7.54 (1H, *d*, H_4 , $J = 8.8$ Hz), 7.72 (2H, *d*, H_8, H_{12} , $J = 8.0$ Hz), 7.75 (1H, *s*, H_6), 10.29 (1H, *s*, $-CO-NH-$); ^{13}C -NMR (400 MHz, $CDCl_3$, δ / ppm): 14.05 ($COOCH_2CH_3$), 18.11 ($-O-CH(CH_3)CO-$), 61.70 ($COOCH_2CH_3$), 73.60 ($-O-CH(CH_3)CO-$), 116.42 (C_3), 119.80 (C_8, C_{12}), 124.19 (C_1), 125.85 (C_{10}), 126.39 (C_5), 129.10 (C_9, C_{11}), 130.04 (C_6), 132.15 (C_4), 138.60 (C_7), 153.49 (C_2), 162.39 ($-CO-NH-$), 171.65 ($COOC_2H_5$); (+)MS¹ (m/z): 386.0 ($[M+K]^+$), 370.1 ($[M+Na]^+$), 348.1 ($[M+H]^+$); (+)MSⁿ (m/z): 370.0, 342.0, 276.9, 268.9, 250.9.

4-[4-Chloro-(2-phenylamino)carbonyl]phenoxy}butyric acid, ethyl ester (6). Yield: 66%; m.p. 168–172 °C; Anal. Calcd. for $C_{19}H_{20}ClNO_4$ (361.11 g/mol): C, 62.16, H, 5.22, N, 4.03 %. Found: C, 62.15, H, 5.20, N, 4.04 %; IR (KBr, cm^{-1}): 3323 *s*, 3020 *m*, *l*, 1720 *m*, 1630 *i*, 1596 *m*, 1558 *i*, 1498 *m*, 1488 *m*, 1417 *m*, 1365 *m*, 1278 *m*, 1224 *m*, 1190 *s*, 1074 *s*, 894 *s*, 821 *m*, 773 *s*, 754 *s*, 698 *m*, 686

m, 651 *m*, 543 *s*, 509 *s*, 418 *s*; $^1\text{H-NMR}$ (400 MHz, $\text{DMSO-}d_6$, δ / ppm): 1.06 (3H, *t*, $\text{COOCH}_2\text{CH}_3$, $J = 7.2$ Hz), 1.13 (2H, *t*, $-\text{CH}_2-\text{CH}_2-\text{COO}-\text{CH}_2-$, $J = 7.2$ Hz), 2.00 (2H, *cv*, $-\text{CH}_2-\text{CH}_2-\text{CH}_2-\text{COO}-\text{CH}_2-$), 4.01 (2H, *q*, $\text{COOCH}_2\text{CH}_3$, $J = 7.2$ Hz), 4.12 (2H, *t*, $-\text{O}-\text{CH}_2-\text{CH}_2-\text{CH}_2-$, $J = 6.4$ Hz), 6.95 (1H, *d*, H_3 , $J = 8.8$ Hz), 7.11 (1H, *t*, H_{10} , $J = 7.2$ Hz), 7.34–7.38 (3H, *m*, H_4 , H_9 , H_{11}), 7.70 (2H, *d*, H_8 , H_{12} , $J = 8.4$ Hz), 7.92 (1H, *s*, H_6), 10.16 (1H, *s*, $-\text{CO}-\text{NH}-$); $^{13}\text{C-NMR}$ (400 MHz, CDCl_3 , δ / ppm): 13.98 ($\text{COOCH}_2\text{CH}_3$), 23.95 ($-\text{O}-\text{CH}_2-\text{CH}_2-\text{CH}_2-\text{CO}-$), 29.83 ($-\text{O}-\text{CH}_2-\text{CH}_2-\text{CH}_2-\text{CO}-$), 59.78 ($\text{COOCH}_2\text{CH}_3$), 67.76 ($-\text{O}-\text{CH}_2-\text{CH}_2-\text{CH}_2-\text{CO}-$), 119.68 (C_3), 119.83 (C_1), 120.31 (C_8 , C_{12}), 120.65 (C_{10}), 123.74 (C_5), 128.54 (C_6), 128.77 (C_9 , C_{11}), 132.67 (C_4), 138.50 (C_7), 159.45 (C_2), 164.65 ($-\text{CO}-\text{NH}-$), 172.40 (COOC_2H_5); (+)MS¹ (*m/z*): 400.1 ($[\text{M}+\text{K}]^+$), 384.1 ($[\text{M}+\text{Na}]^+$), 362.1 ($[\text{M} + \text{H}]^+$); (+)MS^{*n*} (*m/z*): 400.0, 362.1, 316.0, 286.9, 115.1.

5-Chloro-2-(hydrazinocarbonylmethoxy)-N-phenylbenzamide (7). Yield: 92 %; m.p. 194–196 °C; Anal. Calcd. for $\text{C}_{15}\text{H}_{14}\text{ClN}_3\text{O}_3$ (319.07 g/mol): C, 56.35, H, 4.41, N, 13.14 %. Found: C, 56.33, H, 4.38, N, 13.16 %; IR (KBr, cm^{-1}): 3303 *m*, *l*, 3051 *s*, *l*, 1705 *m*, 1654 *i*, 1639 *i*, 1595 *i*, 1541 *i*, 1488 *m*, 1444 *m*, 1272 *m*, 1234 *m*, 1076 *s*, 985 *m*, 914 *s*, 815 *s*, 752 *m*, 717 *m*, 688 *m*, 542 *m*; $^1\text{H-NMR}$ (400 MHz, $\text{DMSO-}d_6$, δ / ppm): 4.79 (2H, *s*, $-\text{O}-\text{CH}_2-\text{CO}$), 5.20 (2H, *s*, $-\text{NH}-\text{NH}_2$), 7.11 (1H, *t*, H_{10} , $J = 6.8$ Hz), 7.18 (1H, *d*, H_3 , $J = 8.8$ Hz), 7.37 (2H, *t*, H_9 , H_{11} , $J = 6.8$ Hz), 7.57 (1H, *d*, H_4 , $J = 8.8$ Hz), 7.75 (1H, *d*, H_8 , $J = 6.8$ Hz), 7.80 (1H, *d*, H_{12} , $J = 6.8$ Hz), 7.86 (1H, *s*, H_6), 8.96, 9.49 (2 conformers: *Z*, *E*) (1H, *s*, $-\text{CO}-\text{NH}-\text{NH}_2$), 10.72, 11.20 (2 conformers: *Z*, *E*) (1H, *s*, $-\text{CO}-\text{NH}-\text{Ar}$); $^{13}\text{C-NMR}$ (400 MHz, CDCl_3 , δ / ppm): 67.23 ($-\text{O}-\text{CH}_2-\text{CO}$), 116.14 (C_3), 120.06 (C_8 , C_{12}), 124.20 (C_1), 125.89 (C_{10}), 126.31 (C_5), 129.03 (C_9 , C_{11}), 130.01 (C_6), 132.29 (C_4), 138.75 (C_7), 154.23 (C_2), 162.66 ($-\text{CO}-\text{NH}-\text{Ar}$), 167.21 ($-\text{CO}-\text{NH}-\text{NH}_2$); (+)MS¹ (*m/z*): 358.0 ($[\text{M}+\text{K}]^+$), 342.1 ($[\text{M}+\text{Na}]^+$), 320.0 ($[\text{M}+\text{H}]^+$); (+)MS^{*n*} (*m/z*): 320.0, 247.9, 226.8, 198.8, 154.8.

5-Chloro-2-[1-(hydrazinocarbonyl)ethoxy]-N-phenylbenzamide (8). Yield: 90 %; m.p. 208–210 °C; Anal. Calcd. for $\text{C}_{16}\text{H}_{16}\text{ClN}_3\text{O}_3$ (333.09 g/mol) C, 57.58, H, 4.83, N, 12.59 %. Found: C, 57.60, H, 4.81, N, 12.54 %; IR (KBr, cm^{-1}): 3355 *m*, 3300 *m*, 1660 *i*, 1598 *m*, 1548 *m*, 1494 *m*, 1473 *m*, 1446 *m*, 1398 *s*, 1323 *m*, 1267 *m*, 1228 *i*, 1110 *s*, 1076 *s*, 1041 *s*, 970 *s*, 893 *s*, 808 *s*, 750 *s*, 677 *s*, 650 *s*; $^1\text{H-NMR}$ (400 MHz, $\text{DMSO-}d_6$, δ / ppm): 1.50 (3H, *d*, $-\text{O}-\text{CH}(\text{CH}_3)\text{CO}-$, $J = 6.8$ Hz), 4.43 (2H, *s*, $-\text{NH}-\text{NH}_2$), 5.10 (1H, *q*, $-\text{O}-\text{CH}(\text{CH}_3)\text{CO}-$, $J = 6.8$ Hz), 7.12 (1H, *t*, H_{10} , $J = 7.2$ Hz), 7.18 (1H, *d*, H_3 , $J = 8.8$ Hz), 7.37 (2H, *t*, H_9 , H_{11} , $J = 8.4$ Hz), 7.57 (1H, *d*, H_4 , $J = 8.8$ Hz), 7.68 (1H, *s*, H_6), 7.78 (2H, *d*, H_8 , H_{12} , $J = 8.4$ Hz), 9.67 (1H, *s*, $-\text{CO}-\text{NH}-\text{NH}_2$), 10.84 (1H, *s*, $-\text{CONH}-\text{Ar}$); $^{13}\text{C-NMR}$ (400 MHz, CDCl_3 , δ / ppm): 19.01 ($-\text{O}-\text{CH}(\text{CH}_3)\text{CO}-$), 73.88 ($-\text{O}-\text{CH}(\text{CH}_3)\text{CO}-$), 116.88 (C_3), 119.33 (C_8 , C_{12}), 123.72 (C_1), 125.85 (C_{10}), 127.35 (C_5), 128.86 (C_9 , C_{11}), 129.81 (C_6), 131.80 (C_4), 138.85 (C_7), 153.15

(C₂), 162.57 (–CO–NH–Ar), 170.29 (–CO–NH–NH₂); (+)MS¹ (*m/z*): 356.1 ([M+Na]⁺), 334.1 ([M+H]⁺); (+)MS^{*n*} (*m/z*): 334.0, 247.9.

5-Chloro-2-[(4-chlorobenzylidene)hydrazinocarbonylmethoxy]-N-phenylbenzamide (11). Yield: 83 %; m.p. 205–208 °C; Anal. Calcd. for C₂₂H₁₇Cl₂N₃O₃ (441.06 g/mol): C, 59.74, H, 3.87, N, 9.50 %. Found: C, 59.80, H, 3.85, N, 9.46 %; IR (KBr, cm⁻¹): 3303 *m*, 3240 *m*, *l*, 1701 *i*, 1651 *i*, 1596 *i*, 1541 *i*, 1481 *i*, 1444 *i*, 1263 *m*, 1230 *m*, 1087 *m*, 806 *s*, 758 *m*, 731 *s*, 692 *s*, 542 *m*, 511 *s*, 459 *s*; ¹H-NMR (400 MHz, DMSO-*d*₆, δ / ppm): 4.97 (2H, *s*, –O–CH₂–CO–), 7.12 (1H, *t*, H₁₀, *J* = 7.6 Hz), 7.24 (1H, *d*, H₃, *J* = 8.0 Hz), 7.38 (2H, *t*, H₉, H₁₁, *J* = 8.4 Hz), 7.52 (1H, *d*, H₄, *J* = 8.0 Hz), 7.62 (2H, *d*, H₁₅, H₁₇, *J* = 8.8 Hz), 7.81 (2H, *d*, H₈, H₁₂, *J* = 8.4 Hz), 7.93 (2H, *d*, H₁₄, H₁₈, *J* = 8.8 Hz), 8.04 (1H, *s*, H₆), 8.19 (1H, *s*, –N=CH–), 10.64 (1H, *s*, –CO–NH–Ar), 10.96, 11.96 (2 conformers: *Z*, *E*) (1H, *s*, –CO–NH–N=CH–); ¹³C-NMR (400 MHz, CDCl₃, δ / ppm): 66.86 (–O–CH₂–CO–), 116.28 (C₃), 120.06 (C₈, C₁₂), 123.82 (C₁), 124.33 (C₁₀), 125.54 (C₅), 128.68 (C₉, C₁₁), 128.79 (C₁₅, C₁₇), 128.83 (C₁₄, C₁₈), 130.34 (C₆), 132.50 (C₁₃), 132.75 (C₄), 134.64 (C₁₆), 138.82 (C₇), 143.66 (–N=CH–), 154.52 (C₂), 161.62 (–CO–NH–Ar), 169.45 (–CO–NH–N=CH–); (+)MS¹ (*m/z*): 464.1 ([M+Na]⁺), 442.1 ([M+H]⁺); (+)MS^{*n*} (*m/z*): 442.0, 348.9, 320.9, 287.9, 259.9, 211.8, 166.9, 137.95.

5-Chloro-2-[(2-chlorobenzylidene)hydrazinocarbonylmethoxy]-N-phenylbenzamide (12). Yield: 90 %; m.p. 222–223 °C; Anal. Calcd. for C₂₂H₁₇Cl₂N₃O₃ (441.06 g/mol): C, 59.74, H, 3.87, N, 9.50 %. Found: C, 59.76, H, 3.85, N, 9.47 %; IR (KBr, cm⁻¹): 3336 *m*, 3224 *m*, *l*, 1720 *i*, 1703 *m*, 1645 *i*, 1593 *m*, 1552 *i*, 1473 *m*, 1446 *m*, 1257 *i*, 1238 *i*, 1062 *m*, 800 *m*, 752 *i*, 727 *m*, 715 *m*, 688 *s*, 542 *m*, 507 *s*, 418 *s*; ¹H-NMR (400 MHz, DMSO-*d*₆, δ / ppm): 4.97 (2H, *s*, –O–CH₂–CO–), 7.12 (1H, *t*, H₁₀, *J* = 7.2 Hz), 7.35–7.48 (4H, *m*, H₃, H₉, H₁₁, H₁₇), 7.54 (1H, *d*, H₄, *J* = 8.8 Hz), 7.62 (1H, *d*, H₁₅, *J* = 8.6 Hz), 7.81–7.93 (3H, *m*, H₁₆, H₈, H₁₂), 8.13 (1H, *d*, H₁₈, *J* = 8.8 Hz), 8.43 (1H, *s*, H₆), 8.67 (1H, *s*, –N=CH–), 10.34, 10.64 (2 conformers: *Z*, *E*) (1H, *s*, –CO–NH–Ar), 10.92, 12.08 (2 conformers: *Z*, *E*) (1H, *s*, –CO–NH–N=CH–); ¹³C-NMR (400 MHz, CDCl₃, δ / ppm): 66.87 (–O–CH₂–CO–), 116.30 (C₃), 120.01 (C₈, C₁₂), 123.81 (C₁), 124.40 (C₁₀), 125.49 (C₅), 127.22 (C₁₇), 127.52 (C₆), 128.68 (C₉, C₁₁), 129.84 (C₁₅), 130.26 (C₁₈), 130.96 (C₁₃), 131.58 (C₁₆), 132.45 (C₄), 134.05 (C₁₄), 138.77 (C₇), 140.83 (–N=CH–), 154.48 (C₂), 161.62 (–CO–NH–Ar), 169.56 (–CO–NH–N=CH–); (+)MS¹ (*m/z*): 464.1 ([M+Na]⁺), 442.1 ([M+H]⁺); (+)MS^{*n*} (*m/z*): 442.0, 348.9, 321.0, 287.9, 259.9, 211.8, 166.9, 154.9, 137.9.

5-Chloro-2-[1-[(4-chlorobenzylidene)hydrazinocarbonyl]ethoxy]-N-phenylbenzamide (13). Yield: 81 %; m.p. 197–198 °C; Anal. Calcd. for C₂₃H₁₉Cl₂N₃O₃ (455.08 g/mol): C, 60.54, H, 4.20, N, 9.21 %. Found: C, 60.54, H, 4.26, N, 9.18 %; IR (KBr, cm⁻¹): 3178 *m*, *l*, 1652 *i*, 1622 *i*, 1595 *i*, 1560 *i*, 1498 *m*, 1456 *i*, 1315 *i*, 1269 *m*, 1238 *i*, 1103 *i*, 1062 *s*, 1035 *m*, 950 *s*, 898 *s*, 765 *m*, 756 *m*, 677

m, 648 *s*, 524 *s*; $^1\text{H-NMR}$ (400 MHz, $\text{DMSO-}d_6$, δ / ppm): 1.65 (3H, *d*, $-\text{O}-\text{CH}(\text{CH}_3)\text{CO}-$, $J = 6.8$ Hz), 6.09 (1H, *q*, $-\text{O}-\text{CH}(\text{CH}_3)\text{CO}-$, $J = 6.8$ Hz), 7.12 (1H, *t*, H_{10} , $J = 7.2$ Hz), 7.25 (1H, *d*, H_3 , $J = 8.8$ Hz), 7.33–7.40 (2H, *m*, H_9 , H_{11}), 7.57 (1H, *d*, H_4 , $J = 8.8$ Hz), 7.60 (2H, *d*, H_{15} , H_{17} , $J = 8.8$ Hz), 7.73 (2H, *d*, H_8 , H_{12} , $J = 8.4$ Hz), 7.78–7.81 (2H, *m*, H_{14} , H_{18}), 8.08 (1H, *s*, H_6), 8.28 (1H, *s*, $-\text{N}=\text{CH}-$), 10.65, 10.89 (2 conformers: *Z*, *E*) (1H, *s*, $-\text{CO}-\text{NH}-\text{Ar}$), 11.97 (1H, *s*, $-\text{CO}-\text{NH}-\text{N}=\text{CH}-$); $^{13}\text{C-NMR}$ (400 MHz, CDCl_3 , δ / ppm): 19.01 ($-\text{O}-\text{CH}(\text{CH}_3)\text{CO}-$), 73.51 ($-\text{O}-\text{CH}(\text{CH}_3)\text{CO}-$), 117.02 (C_3), 119.32 (C_8 , C_{12}), 123.34 (C_1), 124.29 (C_{10}), 126.57 (C_5), 128.51 (C_9 , C_{11}), 128.62 (C_{15} , C_{17}), 128.66 (C_{14} , C_{18}), 130.14 (C_6), 132.30 (C_{13}), 132.56 (C_4), 134.25 (C_{16}), 138.92 (C_7), 142.58 ($-\text{N}=\text{CH}-$), 153.45 (C_2), 161.33 ($-\text{CO}-\text{NH}-\text{Ar}$), 169.46 ($-\text{CO}-\text{NH}-\text{N}=\text{CH}-$); (+)MS¹ (*m/z*): 478.1 ([M+Na]⁺), 456.1 ([M+H]⁺); (+)MS^{*n*} (*m/z*): 456.1, 363.0, 335.0, 274.0, 247.9, 225.9, 180.9, 154.8.

5-Chloro-2-[1-[(2-chlorobenzylidene)hydrazinocarbonyl]ethoxy]-N-phenylbenzamide (14). Yield: 82 %; m.p. 187–189 °C; Anal. Calcd. for $\text{C}_{23}\text{H}_{19}\text{Cl}_2\text{N}_3\text{O}_3$ (455.08 g/mol) C, 60.54, H, 4.20, N, 9.21 %. Found: C, 60.55, H, 4.24, N, 9.20 %; IR (KBr, cm^{-1}): 3394 *m*, 3178 *m*, *l*, 3099 *s*, 2979 *s*, 1681 *i*, 1598 *m*, 1548 *m*, 1483 *s*, 1446 *i*, 1398 *m*, 1269 *m*, 1226 *m*, 1093 *s*, 819 *s*, 750 *s*, 686 *s*, 542 *s*, 505 *s*, 462 *s*. $^1\text{H-NMR}$ (400 MHz, $\text{DMSO-}d_6$, δ / ppm): 1.65 (3H, *d*, $-\text{O}-\text{CH}(\text{CH}_3)\text{CO}-$, $J = 6.8$ Hz), 6.09 (1H, *q*, $-\text{O}-\text{CH}(\text{CH}_3)\text{CO}-$, $J = 6.8$ Hz), 7.13 (1H, *t*, H_{10} , $J = 7.2$ Hz), 7.27–7.61 (5H, *m*, H_3 , H_9 , H_{11} , H_{16} , H_{17}), 7.75 (1H, *d*, H_4 , $J = 8.8$ Hz), 7.79 (2H, *d*, H_8 , H_{15} , $J = 8.6$ Hz), 7.97 (1H, *d*, H_{12} , $J = 8.4$ Hz), 8.12 (1H, *d*, H_{18} , $J = 8.8$ Hz), 8.48 (1H, *s*, H_6), 8.74 (1H, *s*, $-\text{N}=\text{CH}-$), 10.65, 10.83 (2 conformers: *Z*, *E*) (1H, *s*, $-\text{CO}-\text{NH}-\text{Ar}$), 12.05, 12.17 (2 conformers: *Z*, *E*) (1H, *s*, $-\text{CO}-\text{NH}-\text{N}=\text{CH}-$); $^{13}\text{C-NMR}$ (400 MHz, CDCl_3 , δ / ppm): 19.00 ($-\text{O}-\text{CH}(\text{CH}_3)\text{CO}-$), 73.53 ($-\text{O}-\text{CH}(\text{CH}_3)\text{CO}-$), 117.04 (C_3), 119.28 (C_8 , C_{12}), 123.32 (C_1), 124.35 (C_{10}), 126.52 (C_5), 127.25 (C_{17}), 127.32 (C_6), 128.50 (C_9 , C_{11}), 129.68 (C_{15}), 130.09 (C_{18}), 130.76 (C_{13}), 131.75 (C_{16}), 132.25 (C_4), 133.88 (C_{14}), 138.87 (C_7), 140.11 ($-\text{N}=\text{CH}-$), 153.40 (C_2), 161.34 ($-\text{CO}-\text{NH}-\text{Ar}$), 169.58 ($-\text{CO}-\text{NH}-\text{N}=\text{CH}-$); (+)MS¹ (*m/z*): 478.2 ([M+Na]⁺), 456.1 ([M+H]⁺); (+)MS^{*n*} (*m/z*): 456.1, 381.0, 363.0, 335.0, 274.0, 247.9, 180.9.

The experimental results suggested that the 5-chloro-2-(substituted alkoxy)-*N*-phenylbenzamide derivatives were readily purified.

The IR spectral data of the ethyl esters **4–6** indicate the presence of an ether bond between the phenolic hydroxyl group and the alkyl α - or γ -C atom of the ester by signals in the range 1222–1232 and 1053–1074 cm^{-1} . The carbonyl groups from the esters appear in the range 1720–1751 cm^{-1} ; however, in the IR spectra of the hydrazides, this band is missing, which indicates the conversion of the esters into hydrazides. The signals corresponding to the vibrations of the amide and hydrazide group appear between 3178–3394 and 1630–1720 cm^{-1} , respectively.

The synthesized compounds were also analysed by $^1\text{H-NMR}$ spectroscopy in $\text{DMSO-}d_6$ and $^{13}\text{C-NMR}$ spectroscopy in CDCl_3 . In order to facilitate the NMR data interpretation, the numbering of the aromatic rings is presented in Fig. 1. The $^1\text{H-NMR}$ shifts of the ethyl group from the esters appear between 1.0 and 4.3 ppm, that of the amide group between 10.2 and 11.2 ppm, that of the hydrazide group, from both hydrazides and hydrazones, between 8.9 and 12.1 ppm and that of the imine group between 8.1 and 8.8 ppm. The $^{13}\text{C-NMR}$ signals corresponding to the carbons from the hydrazide and amide groups appear in the range 162–171 ppm and those of the aromatic carbons between 115 and 160 ppm.

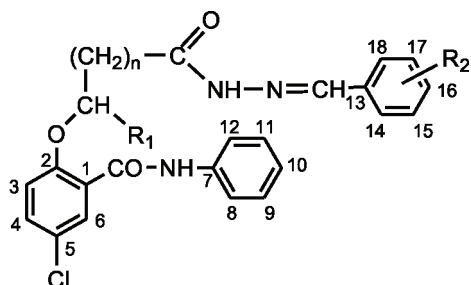


Fig. 1. Numbering of the aromatic rings used for the identification of the NMR signals.

Compound characterization was further realised by high performance mass spectrometry using an advanced methodology based on positive electrospray ionization ((+)ESI) high capacity ion trap multistage collision-induced dissociations (CID) at low energies. For the MS investigation, the samples were dissolved in pure methanol and both (+) ESI MS^1 and tandem mass spectra (+) ESI MS^n ($n = 2-6$) were acquired. MS^1 and mass calculation revealed only the presence of the molecular ions corresponding to monoprotonated molecules, $[\text{M}+\text{H}]^+$, and/or species exhibiting sodiated and potassiated adducts $[\text{M}+\text{Na}]^+$ and $[\text{M}+\text{K}]^+$. Fine and detailed structural analyses were performed by multistage mass spectrometry from MS^2 to MS^6 , which was for the first time employed here for accurate determination of compounds belonging to this particular class. Multistage MS was performed by application of an ion isolation width of 1 Da followed by He-assisted CID at low and variable energies. Unlike classical tandem MS in a single dissociation phase, the consecutive fragmentation episodes of up to MS^6 applied to the precursor ion and its derived fragments, provided not only a strict control of the dissociation process but also the unique possibility to re-sequence small fragment ions of the same precursor until unequivocal structure elucidation. Interpretation of the MS^2 – MS^6 spectra showed that the obtained multistage sequencing data unambiguously corroborated the structure of the synthesized compounds.

EXPERIMENTAL

Materials

Reagents: ethyl chloroacetate, ethyl 2-chloropropionate, ethyl 4-chlorobutyrate, 5-chloro-2-hydroxy-*N*-phenylbenzamide (Aldrich, for synthesis); hydrazine monohydrate (N₂H₄·H₂O) (Merck, for synthesis); 4-chlorobenzaldehyde, 2-chlorobenzaldehyde (Merck, for synthesis); solvents: absolute ethanol, ethyl methyl ketone, dimethylformamide (Merck, analytical purity).

*Synthesis of the ethyl esters 4–6*¹⁴

Ethyl esters were obtained by the reaction of 5-chloro-2-hydroxy-*N*-phenylbenzamide with chloro-substituted acid ethyl esters **1–3** in ethyl methyl ketone. A mixture of 5-chloro-2-hydroxy-*N*-phenylbenzamide (0.010 mol) and anhydrous K₂CO₃ (0.010 mol) was refluxed in 50 mL ethyl methylketone. The halogenated acid ethyl ester (0.010 mol) was added dropwise. The optimum molar ratio was amide:ester:K₂CO₃ = 1:1:1. The mixture was stirred and heated on a steam bath for 5 h. After cooling to room temperature, the mixture was poured onto water and shaken intensively. The organic phase was separated and dried over MgSO₄. After filtration and evaporation of the solvent under vacuum, the esters crystallized. The solid esters were re-crystallized from ethanol.

*Synthesis of the hydrazides 7 and 8*¹⁰

A mixture of ethyl ester **4** or **5** (0.010 mol) and hydrazine hydrate (2.2 mL, 0.010 mol) was refluxed in 25 mL ethanol for 3 h. The reaction mixture was cooled, the separated solid filtered off and then re-crystallized from ethanol.

*Synthesis of the hydrazones 11–14*¹⁰

To a solution of hydrazide **7** or **8** (0.0030 mol) in 25 mL ethanol, the appropriate benzaldehyde **9** or **10** (0.0030 mol) was added. The reaction mixture was refluxed for 5 h. The solid obtained after cooling was filtered off, washed with water and re-crystallized from dimethylformamide.

Melting points were determined with a Böetius Carl-Zeiss Jena apparatus. The IR spectra, as KBr pellet, were recorded on a Jaskow FT/IR-430 instrument and the NMR spectra were recorded in DMSO-*d*₆ and CDCl₃ on a Bruker Avance DRX 400 instrument. Mass spectra were recorded in methanol on a high capacity ion trap, HCT Ultra PTM instrument (Bruker, Daltonics, Bremen), interfaced to a PC running the CompassTM integrated software package, version 1.2, which includes the HystarTM module, version 3.2.37, for instrument controlling and spectrum acquisition, and Esquire ControlTM, version 6.1.512, and Data AnalysisTM, version 3.4.179, modules for storing the ion chromatograms and processing the MS data. Elemental analysis was performed on a Vario EL analyzer.

CONCLUSIONS

Nine novel compounds with the *ortho*-hydroxybenzamide structure were synthesized and characterized.

The 1:1 molar ratio of reagents gave good yields (>66 %) after the final purification. The purity of the synthesized compounds was higher than 95 %.

The employed analytical methods confirmed the identity and provided the elemental composition of all the investigated compounds.

Some of these compounds were found to be active against a series of bacterial and fungal strains.^{15,16} Therefore they can be considered as a group of potentially antimicrobial compounds.

ИЗВОД

СИНТЕЗА И КАРАКТЕРИЗАЦИЈА НЕКИХ НОВИХ 5-ХЛОРО-2-(СУПСТИТУИСАНИ АЛКОКСИ)-N-ФЕНИЛБЕНЗАМИДНИХ ДЕРИВАТА

IOANA M.C. IENAȘCU¹, ALFA X. LUPEA¹, IULIANA M. POPESCU²,
MIRABELA A. PĂDURE¹ и ALINA D. ZAMFIR^{3,4}

¹"Politehnica" University, Faculty of Industrial Chemistry and Environment Engineering, Department of Organic Chemistry, 2 P-ța Victoriei, 300006 Timicoara, ²Banat's Agricultural Science University, Faculty of Agriculture, Department of Chemistry and Biochemistry, 119 Calea Aradului, 300645 Timicoara, ³Mass Spectrometry Laboratory, National Institute for Research and Development in Electrochemistry and Condensed Matter, 1 Plautius Andronescu, 300224 Timișoara и ⁴"Aurel Vlaicu" University of Arad, 77 Revoluției Blvd., 310130 Arad, Romania

У циљу добијања биолошки активних једињења извршена је синтеза неких нових деривата *o*-хидроксибензамида. Етил-естри су добијени реакцијом *N*-фенил-2-хидрокси-5-хлоро-бензамида и хлоро-супституисаних етил-естара **1–3** у етил-метил-кетону. Добијени етил-естри кондензовани су са хидразином градећи хидразиде **7** и **8**. Хидразони **11–14** су затим добијени реакцијом хидразида са хлоро-супституисаним бензалдехидима **9** и **10**. Нова једињења су окарактерисана помоћу FTIR, ¹H-NMR, ¹³C-NMR, MS и елементалном анализом.

(Примљено 26. новембра 2007, ревидирано 27. априла 2009)

REFERENCES

1. J. Matyk, K. Waisser, K. Drazkova, J. Kunes, V. Klimensova, K. Palat Jr., J. Kaustova, *Farmaco* **60** (2005) 399
2. K. Waisser, J. Matyk, H. Divisova, P. Husakova, J. Kunes, V. Klimensova, J. Kaustova, U. Mollmann, H. M. Dahse, M. Miko, *Arch Pharm.* **339** (2006) 616
3. I. Zawadowska, *Acta Polon. Pharmacol.* **20** (1963) 25
4. A. X. Lupea, RO 98000 (C14: E04, B1/72), 1989
5. K. Waisser, O. Bures, P. Holy, J. Kunes, R. Oswald, L. Jiraskova, M. Pour, V. Klimesova, L. Kubicova, J. Kaustova, *Arch. Pharm. Pharm. Med. Chem.* **336** (2003) 53
6. K. Waisser, M. Pesina, O. Bures, P. Holy, M. Pour, J. Kunes, V. Klimesova, V. Buchta, P. Kubanova, J. Kaustova, *Arch. Pharm. Pharm. Med. Chem.* **336** (2003) 322
7. P. Kubanova, V. Buchta, M. Perina, K. Waisser, M. Pour, *Folia Microbiol.* **48** (2003) 346
8. K. Waisser, M. Pesina, V. Klimesova, J. Kaustova, *Collect. Czech. Chem. Commun.* **68** (2003) 1275
9. A. X. Lupea, C. Tărăbășanu, M. Pădure, *Rev. Chim.* **54** (2003) 752
10. H. H. Fahmy, W. El-Eraky, *Arch. Pharm. Res.* **24** (2001) 171
11. H. H. Fahmy, G. A. Soliman, *Arch. Pharm. Res.* **24** (2001) 180
12. A. X. Lupea, I. Popescu, C. Tărăbășanu, I. Ienașcu, V. Badea, *J. Serb. Chem. Soc.* **71** (2006) 1247
13. A. X. Lupea, I. Popescu, C. Tărăbășanu, I. Ienașcu, M. Pădure, *Rev. Roum. Chem.* **51** (2006) 517
14. H. Kwiecien, *Pol. J. Chem.* **70** (1996) 733
15. I. Ienașcu, I. Popescu, A. Borozan, A. X. Lupea, *Ann. West Univer. Timisoara* **16** (2007) 49 (in Romanian)
16. I. Ienașcu, A. X. Lupea, D. Hădărugă, N. Hădărugă, I. Popescu, *Rev. Chim.* **59** (2008) 247.



J. Serb. Chem. Soc. 74 (8–9) 857–865 (2009)
JSCS–3882

The effect of cholic acid treatment on the oxidative status of soybean plants

SLAVKO E. KEVREŠAN^{1*#}, ĐORĐE R. MALEŃČIĆ^{1#}, MILAN T. POPOVIĆ^{1#},
KSENIJA N. KUHAJDA^{2#} and JULIJAN E. KANDRAČ^{1#}

¹Faculty of Agriculture, University of Novi Sad, Trg Dositeja Obradovića 8, 21000 Novi Sad
and ²Faculty of Science, Department of Chemistry, University of Novi Sad,
Trg Dositeja Obradovića 3, 21000 Novi Sad, Serbia

(Received 18 February, revised 29 March 2009)

Abstract: The objective of this work was to study the effect of treatment of young soybean plants with cholic acid of different concentrations on their oxidative status. Young soybean plants, grown hydroponically for two weeks, were treated by adding cholic acid to the nutrient solution at the concentrations 20, 40, 60 and 80 mg/L, the control being without cholic acid. After one week, several parameters of the oxidative status were determined in the leaves and roots of the plants: contents of superoxide ($O_2^{\bullet-}$), hydroxyl radicals ($\bullet OH$) and glutathione (GSH), lipid peroxidation (LP), the superoxide dismutase (SOD) activity and the soluble protein accumulation, as well as the contents of chlorophylls and carotenoids. Treatments with cholic acid increased $O_2^{\bullet-}$, LP, $\bullet OH$ and GSH in the leaves of the treated plants, while only the OH content increased in the roots at higher cholic acid concentrations. The obtained results support the idea that cholic acid, as an elicitor of defence responses in plants, might act through the generation of an oxidative burst.

Keywords: cholic acid; soybean; oxidative status.

INTRODUCTION

Plants have evolved efficient mechanisms to combat pathogen attacks. One of the earliest responses to an attempted pathogen attack is the generation of an oxidative burst, which can trigger hypersensitive cell death. This is called a hypersensitive response (HR) and is considered a major element of plant disease resistance. The HR is thought to deprive the pathogens of their food supply and confine them to the initial infection site.¹ It occurs when a plant can specifically recognize the pathogen during an “incompatible” interaction.² The cell death is manifested as a rapid collapse of tissue and shows some typical morphological

* Corresponding author. E-mail: kevresan@polj.ns.ac.rs

Serbian Chemical Society member.

doi: 10.2298/JSC0909857K

features: membrane blebbing, nucleus condensation, fragmentation of DNA, shrinkage of the cell, *etc.* Cell death is also a feature of disease symptoms but it occurs very late in the infection process during a 'compatible' interaction. The HR is not due to the action of pathogen virulence factors that kill the plant cells, but rather appears to be a form of programmed cell death (PCD) in plants.³

Recently, it was established that cholic acid is an elicitor of hypersensitive cell death, pathogenesis-related protein synthesis and phytoalexin accumulation and could induce defence responses in rice plants.⁴ Elicitor molecules, beside inducing accumulation of phytoalexins, trigger a plant defence response called an oxidative burst, which involves the production of reactive oxygen species.^{5,6} Bile acids can also promote the generation of reactive oxygen species and the increase in reactive oxygen species caused by bile acids is well documented only in mammalian tissues.^{7,8} The effect of bile acids on plants, especially on the antioxidative status, has hitherto not been studied. Antioxidant systems are produced during interactions between pathogens and plant hosts.^{9,10} The susceptibility of a plant to oxidative stress may depend on the overall balance between factors that increase oxidant generation and those cellular components that exhibit an antioxidant capability.¹¹

The aim of this work was to study the effect on their oxidative status of the treatment of young soybean plants with cholic acid of different concentrations.

EXPERIMENTAL

All employed chemicals were of reagent grade, purchased from Merck (Darmstadt, Germany) or Sigma Aldrich.

Plant material and treatment

Soybean seeds, genotype Bečejka, were obtained from the Institute of Field and Vegetable Crops, Novi Sad, Serbia. Prior to germination, the seeds were surface sterilized by soaking in a 5 % solution of commercial bleach for 20 min and washed with distilled water. The seeds were sterilized again by dipping in 70 % ethanol for one minute, followed by soaking in commercial bleach for ten minutes and then rinsed three times with sterile distilled water. The seeds were germinated on wet paper towels in a thermostat for 3 days at 25 °C. Subsequently, the seedlings were transferred to pots with full nutrient solution (1 mmol/L MgSO₄, 3 mmol/L Ca(NO₃)₂, 0.19 mmol/L KH₂PO₄, 0.31 mmol/L NH₄H₂PO₄, 46 µmol/L B, 9 µmol/L Mn, 0.8 µmol/L Zn, 0.3 µmol/L Cu, 0.8 µmol/L Mo and 75 µmol/L Fe as Fe-EDTA) and grown in a controlled environment (temperature 25 °C, relative humidity 60 % and light intensity 16000 lux) for two weeks. The treatments with cholic acid were realised by adding cholic acid (as sodium cholate) to the nutrient solution at concentrations of 20, 40, 60 and 80 mg/L, the control plants being grown in nutrient solution without the addition of cholic acid. Samples of roots and leaves were taken for biochemical analyses 7 days after treatment.

Biochemical assays

For the determination of the oxidative status parameters, 1 g of fresh plant material was homogenized with 10 cm³ 0.10 M K₂HPO₄ at pH 7.0. After centrifugation at 15000 g for 10 min at 4 °C, aliquots of the supernatant were used for the biochemical assays.

A UV/visible spectrophotometer model 6105, Jenway, Dunmon, UK was used for the spectroscopic measurements.

The superoxide radical was measured by the inhibition of adrenalin auto-oxidation.¹² The hydroxyl radical was assayed by the inhibition of deoxyribose degradation.¹³ The superoxide-dismutase (SOD; EC 1.15.1.1) activity was measured by monitoring the inhibition of nitroblue tetrazolium (NBT) reduction at 560 nm.¹⁴ Lipid peroxidation (LP) was measured spectrophotometrically as malonyldialdehyde (MDA) production at 532 nm with thiobarbituric acid (TBA), as described by Placer *et al.*¹⁵ and Gidrol *et al.*¹⁶. The chlorophyll and carotenoid contents were estimated according to Sairam *et al.*⁸ and soluble protein content was determined according to Bradford.¹⁷ The results of the oxidative status parameters were normalized per milligram of homogenate soluble protein; the chlorophyll and carotenoid contents are expressed per gram of fresh leaf matter (f.m.).

Statistical analyses

All determinations were made in triplicate and the values are expressed as the mean \pm standard deviation. The statistical significance was tested by one-way Anova, followed by comparisons of the means by the Duncan multiple range test ($p < 0.05$).

RESULTS AND DISCUSSION

One of the earliest biochemical changes observed after pathogen recognition is an increased production of reactive oxygen species (ROS), *i.e.*, the so-called "oxidative burst". Numerous reports showed a rapid production of ROS in response to various infections or elicitor treatments.^{18–20} The superoxide radical and H₂O₂ play various roles in the signal transduction pathway leading to HR cell death. They can act directly as antimicrobial compounds or induce a rapid cross-linking of proteins in the cell wall. They can also act as messengers, triggering, for example, modification of ion fluxes or the production of secondary messengers such as salicylic acid.¹⁰ In this work, a similar response was observed in the leaves of soybean after treatments with cholic acid (Figs. 1 and 2). This is in agreement with the findings of Delledonne *et al.*²⁰ that inoculation of soybean cell suspensions with *Pseudomonas syringae* stimulated a strong oxidative burst.

ROS are known to be produced very locally and at high levels during the HR. Hence, in addition to their predicted signalling role, they can also act in a direct way. Cytochemical studies showed that the accumulation of ROS is related to rapid death of infected cells and is correlated with a rapid loss of membrane integrity.¹⁰ The superoxide content in the leaves of the investigated plants increased significantly compared to the control with increasing cholic acid concentration. At the same time, this effect was not observed in the root tissue (Fig. 1). This is probably because the photosynthetic apparatus is absent from this plant organ. Photosynthesis is one of the most important metabolic pathways in which the generation of ROS occurs.²¹ In addition, the activity of the antioxidant enzyme SOD was increased in the roots and the increase was higher compared to that observed in the leaves (Fig. 3). SOD is of utmost importance since it catalyzes the dismutation of the superoxide radical to molecular oxygen and hydro-

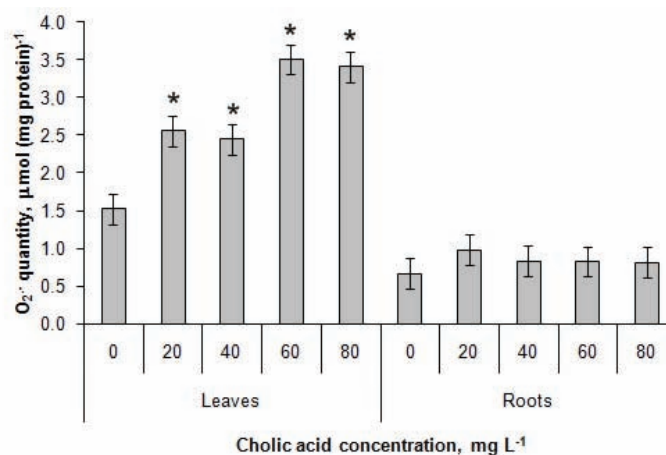


Fig 1. Superoxide content in leaves and roots of young soybean plants treated with cholic acid of different concentrations. Bars represent the standard deviation. Columns labelled with an asterisk are significantly different (Duncan test, $p < 0.05$) from the corresponding control.

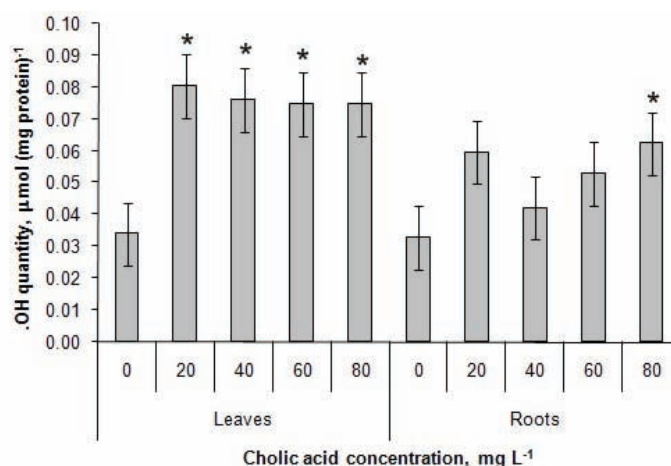


Fig. 2. ·OH content in the leaves and roots of young soybean plants treated with cholic acid of different concentrations. Bars represent the standard deviation. Columns labelled with an asterisk are significantly different (Duncan test, $p < 0.05$) from the corresponding control.

gen peroxide,¹⁴ thus preventing the formation of other, more toxic oxygen species, such as the ·OH radical. Some other authors also reported an increase in the SOD activity in plants under oxidative stress.^{22,23} Aggressive oxygen radicals are thought to cause lipid peroxidation (LP) and membrane damage that might be directly responsible for the collapse of the cells. This is in agreement with the present findings for the quantities of ·OH and MDA, the main end product of LP (Figs. 2 and 4). The quantity of ·OH increased significantly for most of the treatments with cholic acid, which was particularly pronounced in the

soybean leaves and to a smaller extent in the roots (only treatment with highest cholic acid concentration, 80 mg L⁻¹, had an effect). These results suggest that the most intensive process of destruction of cell membranes occurred in the leaves, due to higher quantity of the most reactive oxygen species – OH, thus confirming the hypothesis that the accumulation of ROS is in positive correlation with the peroxidation of membrane lipids.

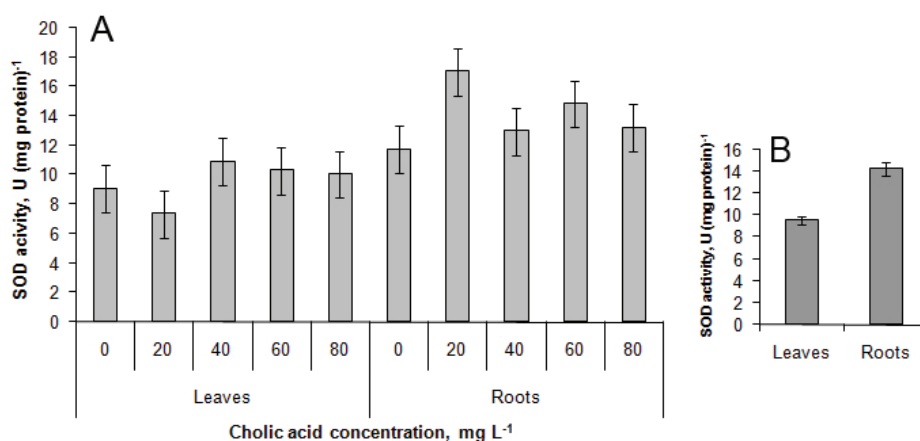


Fig. 3. A) SOD activity in leaves and roots of young soybean plants treated with cholic acid of different concentrations. Bars represent the standard deviation. B) Averages of SOD activity for all treatments in the leaves and roots of young soybean plants. Bars represent standard deviation. Values are significantly different (Duncan test, $p < 0.05$).

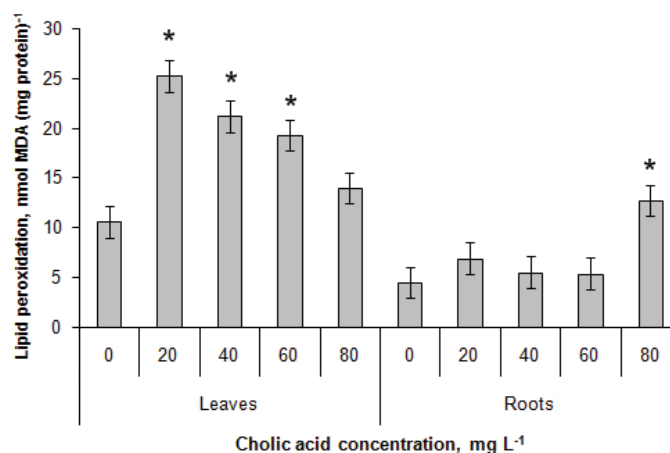


Fig. 4. Lipid peroxidation in the leaves and roots of young soybean plants treated with cholic acid of different concentrations. Bars represent the standard deviation. Columns labelled with an asterisk are significantly different (Duncan test, $p < 0.05$) from the corresponding control.

The tripeptide glutathione (γ -Glu-Cys-Gly) is involved in many aspects of metabolism: removal of hydroperoxides, protection from ionizing radiation, maintenance of the sulphhydryl status of proteins, complexation of xenobiotic or endogenous reactive compounds, aiding in their detoxification and excretion, *etc.*²⁴ Many of these functions are accomplished by reactions at the cysteinyl sulphhydryl group, catalyzed by glutathione-requiring enzymes. The obtained results showed that the glutathione (GSH) content increased significantly in soybean leaves on cholic acid treatment (Fig. 5). Even the lowest applied concentration of cholic acid (20 mg L⁻¹) caused a significant increase in the GSH content in soybean roots compared to the control. It seems that GSH plays an active role in the leaves in the detoxification and removal of ROS produced by cholic acid treatment.

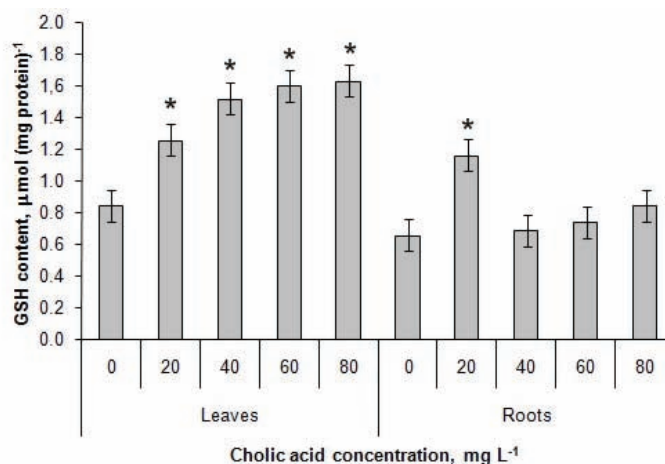


Fig. 5. GSH content in the leaves and roots of young soybean plants treated with cholic acid of different concentrations. Bars represent the standard deviation. Columns labelled with an asterisk are significantly different (Duncan test, $p < 0.05$) from the corresponding control.

The chlorophyll and carotenoid contents in soybean leaves increased due to cholic acid treatment, being highest with the treatment of 80 mg L⁻¹ (Fig. 6). Some other authors^{8,25} reported a decrease in the content of plant pigments under oxidative stress conditions. It seems that under the present experimental conditions, a *de novo* biosynthesis of chlorophylls and carotenoids occurred in the leaves of soybean as a response to cholic acid treatment. These mechanisms should be further investigated since there are no previous studies in this area.

CONCLUSIONS

Increased quantities of O₂^{•-}, LP and [•]OH in leaves of treated plants support the idea that cholic acid, as an elicitor of defence responses, could act through the generation of an oxidative burst. The GSH content increased significantly in soy-

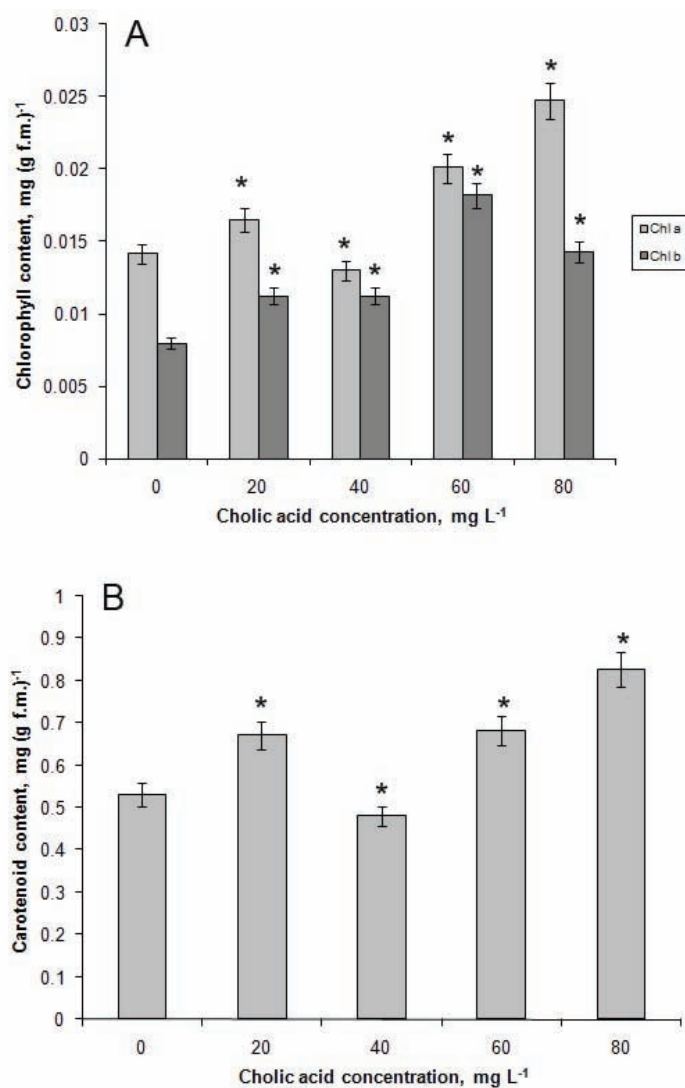


Fig. 6. Chlorophyll *a* and *b* (A) and carotenoid (B) content in the leaves of young soybean plants treated with cholic acid of different concentrations. Bars represent the standard deviation. Columns labelled with an asterisk are significantly different (Duncan test, $p < 0.05$) from the control.

bean leaves as affected by cholic acid treatments, which could mean that GSH plays an active role in leaves in the detoxification and removal of ROS produced because of the treatments.

Acknowledgement. This study was supported by the Ministry of Science and Technological Development of the Republic of Serbia, project No. 142005B.

ИЗВОД

ЕФЕКАТ ТРЕТМАНА ХОЛНОМ КИСЕЛИНОМ НА ОКСИДАТИВНИ
СТАТУС БИЉАКА СОЈЕСЛАВКО Е. КЕВРЕШАН¹, ЂОРЂЕ Р. МАЛЕНЧИЋ¹, МИЛАН Т. ПОПОВИЋ¹,
КСЕНИЈА Н. КУХАЈДА² и ЈУЛИЈАН Е. КАНДРАЧ¹¹Пољопривредни факултет, Универзитет у Новом Саду, Трз Досијеја Обрадовића 8, 21000 Нови Сад и²Природно-математички факултет, Департаман за хемију, Универзитет у Новом Саду,
Трз Досијеја Обрадовића 3, 21000 Нови Сад

Циљ овог рада је био да се испита ефекат третмана различитим концентрацијама холне киселине на оксидативни статус младих биљака соје. Младе биљке соје, узгајане хидропонски две недеље, третиране су додавањем холне киселине у хранљиви раствор у концентрацијама од 20, 40, 60 и 80 mg/L, док код контролних биљака није додавана холна киселина. Недељу дана након почетка третмана одређено је неколико показатеља оксидативног статуса у листовима и корену биљака: количина супероксида ($O_2^{\bullet-}$) и хидроксил радикала ($\bullet OH$), као и глутатиона (GSH), липидна пероксидација (LP), активност супероксид-дисмутазе (SOD), садржај растворљивих протеина, хлорофила и каротеноида. Третмани холном киселином довели су до повећања $O_2^{\bullet-}$, LP, $\bullet OH$ и GSH у листовима биљака, док је у корену утврђен повећани садржај $\bullet OH$ у третманима са већим концентрацијама холне киселине. Добијени резултати говоре у прилог претпоставци да холна киселина као молекул покретач може деловати путем стварања реактивних кисеоничних врста код биљака.

(Примљено 18. фебруара, ревидирано 29. марта 2009)

REFERENCES

1. E. M. Govrin, A. Levine, *Curr. Biol.* **10** (2000) 751
2. D. Pontier, C. Balague, D. Roby, *C. R. Acad. Sci Paris* **321** (1998) 721
3. J. T. Greenberg, *Annu. Rev. Plant Physiol. Plant Mol. Biol.* **48** (1997) 525
4. J. Koga, H. Kubota, S. Gomi, K. Umemura, M. Ohnishi, T. Kono, *Plant Physiol.* **140** (2006) 1475
5. K. A. Blee, S. C. Jupe, G. Richard, A. Zimmerlin, D. R. Davies, G. P. Bolwell. *Plant Mol. Biol.* **47** (2001) 607
6. T. Kawano, R. Pinontoan, N. Uozumi, Y. Morimitsu, C. Miyake, K. Asada, S. Muto, *Plant Cell Physiol.* **41** (2000) 1259
7. R. J. Sokol, B. M. Winkhofer-Roob, M. W. Devereaux, J. M. McKim Jr., *Gastroenterology* **109** (1995) 1249
8. C. M. Palmeira, A. P. Rolo, *Toxicology* **203** (2004) 1
9. S. I. Kwon, A. J. Anderson, *Physiol. Mol. Plant Pathol.* **58** (2001) 73
10. Dj. Malenčić, J. Miladinović, M. Popović, *Cent. Eur. J. Biol.* **3** (2008) 155
11. R. K. Sairam, D. V. Singh, G. C. Srivastava, *Biol. Plant.* **47** (2003/4) 61
12. H. P. Misra, I. Fridovich, *J. Biol. Chem.* **247** (1972) 3170
13. K. H. Cheesman, A. Beavis, H. Esterbauer, *Biochem. J.* **252** (1988) 649
14. C. N. Giannopolitis, S. K. Ries, *Plant Physiol.* **59** (1977) 309
15. Z. A. Placer, L. L. Cushman, B. C. Johnson, *Anal. Biochem.* **16** (1966) 359
16. H. Gidrol, H. Sergihini, B. Nobhani, B. Mocquot, P. Mazilak, *Physiol. Plant.* **76** (1987) 591
17. M. M. Bradford, *Anal. Biochem.* **72** (1976) 248
18. N. Doke, *Physiol. Plant Pathol.* **23** (1983) 359

19. C. Lamb, R. A. Dixon, *Annu. Rev. Plant Physiol. Plant Mol. Biol.* **48** (1997) 251
20. M. Delledonne, J. Zeier, A. Marocco, C. Lamb, *Proc. Natl. Acad. Sci. USA* **98** (2001) 13454
21. B. Halliwell, *Chloroplast Metabolism*, Oxford University Press, New York, 1984, p. 160
22. S. Gupta, R. P. Webb, A. S. Holaday, R. D. Allen, *Plant Physiol.* **103** (1993)1067
23. H. M. Kang, E. Saltveit, *Plant Cell Environ.* **25** (2002) 1233
24. M. Arias, W. B. Jakoby, *Glutathione: Metabolism and Function*, Raven Press, New York, 1976, p. 103
25. D. Štajner, M. Popović, M. Štajner, *Biol. Plant.* **47** (2003/4) 575.



J. Serb. Chem. Soc. 74 (8–9) 867–883 (2009)
JSCS–3883

The role of the thiol group in protein modification with methylglyoxal

JELENA M. AĆIMOVIĆ[#], BOJANA D. STANIMIROVIĆ and LJUBA M. MANDIĆ^{*#}

*Faculty of Chemistry, Department of Biochemistry, University of Belgrade,
P.O. Box 51, 11158 Belgrade, Serbia*

(Received 26 November 2008, revised 9 February 2009)

Abstract: Methylglyoxal is a highly reactive α -oxoaldehyde with elevated production in hyperglycemia. It reacts with nucleophilic Lys and Arg side-chains and N-terminal amino groups causing protein modification. In the present study, the importance of the reaction of the Cys thiol group with methylglyoxal in protein modification, the competitiveness of this reaction with those of amino and guanidine groups, the time course of these reactions and their role and contribution to protein cross-linking were investigated. Human and bovine serum albumins were used as model systems. It was found that despite the very low levels of thiol groups on the surface of the examined protein molecules (approx. 80 times lower than those of amino and guanidino groups), a very high percentage of it reacts (25–85 %). The amount of reacted thiol groups and the rate of the reaction, the time for the reaction to reach equilibrium, the formation of a stable product and the contribution of thiol groups to protein cross-linking depend on the methylglyoxal concentration. The product formed in the reaction of thiol and an insufficient quantity of methylglyoxal (compared to the concentrations of the groups accessible for modification) participates to a significant extent (4 %) to protein cross-linking. Metformin applied in equimolar concentration with methylglyoxal prevents its reaction with amino and guanidino groups but, however, not with thiol groups.

Keywords: methylglyoxal; protein thiol group reaction; protein modification and cross-linking; AGEs.

INTRODUCTION

Advanced glycation end products (AGEs) are elevated in diabetes and are involved in the pathogenesis of its vascular complications,^{1–6} as well as in other pathological states. They are formed in the reaction of carbonyl-containing materials with N-terminal and Lys side-chain amino groups, the guanidino group of

* Corresponding author. E-mail: ljmandic@helix.chem.bg.ac.rs

[#] Serbian Chemical Society member.

doi: 10.2298/JSC0909867A

Arg, the sulfhydryl group of Cys in proteins, and through a series of reactions and rearrangement.⁷ Some of the final products of these reactions are the well-characterized conjugates (*N*-(carboxymethyl)lysine, *N*-(carboxyethyl)lysine, *N*-(carboxymethyl)arginine, *S*-(carboxymethyl)cysteine, *S*-(carboxyethyl)cysteine and pentosidine), which are used as markers in clinical practice.

Methylglyoxal (MG) is an α -oxoaldehyde which is formed in cells primarily from triose phosphate intermediates of glycolysis, dihydroxyacetone phosphate and glyceraldehydes-3-phosphate.⁸ It is accumulated in hyperglycemia,^{9,10} oxidative stress, uremia,¹¹ in the aging process and inflammation. As a highly reactive compound (α -dicarbonyl compounds are 20,000-fold more reactive than glucose in glycation reactions¹²), it participates in the modification of proteins¹³ and DNA¹⁴ and leads to the formation of AGEs. Molecules modified with methylglyoxal and their derivatives can affect cellular functionality *via* gene expression,¹⁵ lead to micro- and macro-vascular complications in diabetes,¹⁶ contribute to upregulation of inflammatory and tissue-injury-provoking molecules (interaction of AGEs and receptor RAGE), protein cross-linking and apoptosis.¹⁷

Amino, guanidine¹⁶ and thiol groups¹³ present on protein surfaces participate in protein modification with methylglyoxal. The products formed in the first phase of the reaction change in a series of subsequent reactions.¹⁸ The thiol group is a strong nucleophile, at physiological pH values stronger than the amino and guanidine groups of Lys and Arg side chains. Yet, the role of thiol group in protein modification with MG has not been sufficiently investigated. The proposed mechanism of reaction of thiol with glyoxal¹⁹ or MG¹³ proved the formation of carboxymethylcysteine^{19–21} and carboxyethylcysteine. These products were proposed for use as markers in pathological states¹⁹ and attempts were made for their quantification.²² The research on Cys side-chain modifications of thiol-dependent enzymes glyceraldehyde-3-phosphate dehydrogenase²³ and creatine kinase¹⁹ with MG showed their inactivation during incubation. The formation of protein aggregates was observed in the treatment of albumin with MG.¹⁸ The role of amino and thiol groups in cross-linking *via* reactive compounds, such as glutaraldehyde,²⁴ 4-hydroxynonenal²⁵ and acrolein²⁶ was stressed. The potential importance of SH and MG reaction in protein cross-linking has only been reported by Zeng and Davies.²⁷ They proposed that the product of the initial reaction between a thiol group and MG can be a target for the next reaction with an amino group or, *vice versa*, the initial product of a reaction between an amino group and MG can be a target for an SH group. Since the presence and availability of thiol groups on the protein surface is marginal compared to amino groups, the question is: what is the importance and contribution of the initial reaction between SH and MG to cross-linking? What are the target proteins for this reaction and what is the physiological role of the formed adducts?

Therefore, in this study, the time progression of the reaction of protein thiol groups (as well as of amino and guanidino groups) with methylglyoxal, detection of protein modifications, the role and contribution of the initial reaction between thiol and MG, *i.e.*, the product of that reaction, as a target for protein cross-linking were examined. Also, the effects of inhibitors on the above-mentioned reactions, especially during low-dose long-term exposition of albumin to MG, were analyzed. Human (HSA) and bovine serum (BSA) albumins were chosen as model-systems by virtue of the considerably lower thiol group content on the molecule surface compared to amino (and guanidino) group and because of their abundance and reported antioxidant properties.

EXPERIMENTAL

Materials

All chemicals were purchased from Sigma, Steinheim, Germany, unless otherwise stated. The 20 % solution of HSA was purchased from Octapharma AB, Stockholm, Sweden; thymol, 3',3'',5',5''-tetrabromo-*m*-cresolsulphonophthalein (BCG), hydroquinone and bromine were from Merck, Darmstadt, Germany.

Preparation of glycated samples

HSA or BSA solutions (33 mg/mL, *i.e.*, 0.50 mM) were prepared in 0.10 M phosphate buffer (pH 7.2) under sterile conditions (sterile zone) and incubated in capped vials at 37 °C with different concentrations of MG as follows: BSA with 50 mM MG for 168 h; HSA with 100 mM MG for 24 h; HSA with 10 mM MG for 24 days. All solutions were sterile-filtered prior to incubation. For the investigations of the inhibition of the reactions, glutathione (GSH) and metformin (10 and 20 mM) were used.

Monitoring of changes of HSA and BSA molecules during incubation with MG

Aliquots of the reaction mixtures were taken at predetermined intervals during incubation and subsequently extensively dialyzed against deionized water (3 times within an hour). The albumin concentrations after dialysis were assayed by the BCG method.²⁸ Protein changes during incubation with different methylglyoxal concentrations were monitored using native and SDS PAGE. In brief, to 5.0 mL of 0.04 mM BCG in 0.10 M Gly buffer (pH 3.8), 0.02 mL of sample was added. The absorbance at 628 nm was measured against the reagent after 30 s.

Protein changes during the incubation with different MG concentrations were monitored using native and SDS PAG (10 % of acrylamide) electrophoresis according to protocol of Hofer scientific instruments.²⁹ 7 µL of protein samples (0.05–0.15 mg/mL) were applied. Gels were stained by Coomassie Brilliant Blue G-250 (CBB).

In each aliquot, the contents of the reactive groups were determined in triplicate.

Thiol assays

Free thiol groups were assayed spectrophotometrically according to a modified Ellman method.³⁰ 5,5'-Dithiobis(2-nitrobenzoic acid) reagent (100 µL of 2.0 mM solution) was mixed with 10 µL–100 µL of the sample, 100 µL of 1.0 M Tris buffer (pH 8.0) and filled up with water to 1300 µL. To avoid interferences of the browning state of modified albumin, the absorbance was measured at 412 nm against a sample blank, using a Beckman DU 50 spectrophotometer. In addition, dilution of samples (13–130 times) contributed to the minimization of the influences. Standard solutions of 2-mercaptoethanol (0.143–1.43 mM) were used for the

construction of a standard curve ($y = 0.01013 + 0.7225x$; $r = 0.9999$, $p < 0.0001$). The SH group concentration was also calculated using the extinction coefficient $13600 \text{ mol}^{-1} \text{ dm}^3 \text{ cm}^{-1}$.

As commercially available albumin preparations already contain oxidized Cys34,³¹ the content of free thiol group was determined in untreated BSA/HSA (0.73/0.76 mole per mole of protein, respectively). The amounts of reacted thiol groups were expressed as percentages of these contents.

Guanidine assay

A spectrophotometric method³² was used for the determination of guanidino groups. To 1.0 mL 0.020 % thymol in 1.0 M NaOH, 10 μL –100 μL sample and 100 μL 2.0 % Br_2 in 5.0 % NaOH were added and the mixture was filled up with water to 2.1 mL. The absorbance at 470 nm was measured against a reagent blank. A standard curve was prepared with standard arginine solutions in the concentration range 0.125–1.25 mM (standard curve: $y = -0.01407 + 0.30933x$, $r = 0.9992$, $p < 0.0001$).

Determination of amino groups

The spectrophotometric determination of amino groups was performed as follows:³³ 100 μL sample, 100 μL 1.0 M phosphate buffer (pH 7.2), and 40 μL 0.10 M *p*-benzoquinone in dimethyl sulfoxide were mixed and water was added to a volume of 1500 μL . The absorbance at 480 nm was measured against reagent blank. A standard curve was constructed with alanine in the concentration range from 10–90 mM ($y = 0.03225 + 0.00695x$, $r = 0.9966$, $p < 0.0001$).

Statistical analysis

Data are expressed as the mean \pm standard deviation (*SD*) from a minimum of three experiments. Statistical analysis was performed by the Student's *t*-test.

RESULTS AND DISCUSSION

BSA and HSA were used as model systems to investigate the role of thiol groups in the modification and cross-linking of protein molecules *via* methylglyoxal. These proteins were chosen due to the fact that the number of amino acid side-chains is known, *i.e.*, the number of reactive groups on the protein surface that MG can react with,^{18,34} and the number of thiol groups (only one) is considerably lower compared to the number of Lys (59) and Arg (24) side-chains. Considering the higher reactivity of the SH-group compared to the amino and guanidine groups at physiological pH values and the substantially lower availability for reaction, it was of interest to investigate the importance of this reaction for protein modification at different MG concentrations. On the other hand, the abundance of HSA in the serum may point to its additional role in carbonyl stress.

Modification of BSA in reaction with methylglyoxal

A reaction mixture of BSA (0.50 mM) and methylglyoxal (50 mM) in 0.10 M phosphate buffer (pH 7.2) was incubated for 7 days at 37 °C. A considerably higher concentration of MG than the physiological one (free MG in plasma is $< 5 \mu\text{M}$ ³⁵ with > 90 % MG bound to proteins¹³) was used in order to monitor and compare the reaction rates of each group (thiol, amino and guanidino) accessible

for modification. In addition, the employed MG concentration was higher (by 19 %) than the sum of reactive groups per mole of BSA surface of the protein molecule. BSA modification was monitored over time by native and SDS PAGE (Figs. 1A and 1B, respectively).

A considerable change in the mobility of BSA during native electrophoresis, *i.e.*, a decrease in the positive charge of the protein, was observed after 2 and 4 h of incubation (Fig. 1A, lanes 2 and 4, respectively). The mobility of the protein band increased with incubation time. A broadening and higher diffuseness of the protein bands during native and SDS PAGE was detected as early as after 4–6 h of incubation, which continued as the incubation proceeded further. These bands tailed to higher molecular mass values in the period from 1 to 7 days of incubation.

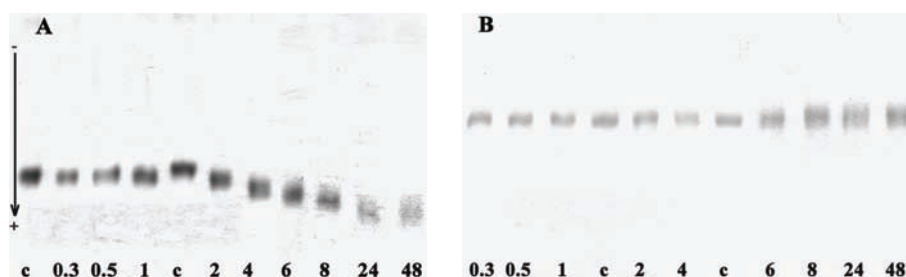


Fig. 1. Native (A) and SDS-PAGE (B) showing the changes of BSA electrophoretic mobility resulting from reaction with methylglyoxal. BSA (0.50 mM) was treated with 50 mM MG in 0.10 M phosphate buffer (pH 7.2) at 37 °C for 7 days. Lane c shows nontreated BSA. The marks of other lines correspond to time of incubation (h) of BSA with MG. The electrophoresis was performed on 10 % polyacrylamide gels and the bands were visualized by CBB, as detailed in the Experimental.

Comparison of the reactivity of the thiol, amino and guanidine groups of the BSA amino acid side chains with methylglyoxal

In order to determine the role and contribution of the thiol groups and to compare them with the contributions of the amino and guanidino groups to the changes in BSA as observed in the electrophoregrams, the progress of reactions of these groups with MG was monitored by their quantification in aliquots of the reaction mixture during incubation (Fig. 2).

The changes in the amounts, *i.e.*, the percentages, of reacted guanidino and thiol groups in the reaction mixture after 7 days were very similar. After 24-hour incubation, 66 % of the arginine side chains, 53 % of the thiol groups and only 21 % of the amino groups had reacted. In the following two days of incubation, the percentage of the reacted guanidino groups rose to 81 % and of thiol to 77 %, at which levels they remained until the end of incubation (7 days). The content of amino groups changed moderately from the first to the seventh day of incubation (24.8 ± 2.4 %).

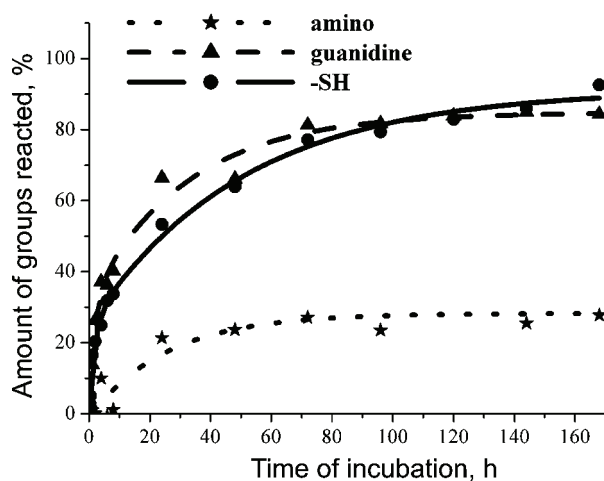


Fig. 2. Quantification of thiol, amino and guanidino groups (% of the ones reacted) during the incubation of 0.50 mM BSA with 50 mM MG in 0.10 M phosphate buffer (pH 7.2) at 37 °C for 7 days. Data are the means from three determinations. *SD* data for particular reactive group and specific time points are presented in Table I.

It is of interest to compare the changes in the contents of the reactive groups during the first 8 h of reaction, the period when modification of the protein molecules was detected by electrophoresis. The amount of guanidino groups decreased by 26 % in the first 2 h of incubation and had decreased by 37 % after 4 h. In the same time period, the amount of thiol groups decreased by 20 and 30 %, respectively. After 8 h, under the employed incubation conditions, only about 8 % of amino groups had reacted.

The contribution of the reaction of individual reactive groups to the changes of the BSA molecules observed by electrophoresis can be better realized if the percentages of the reactive groups are converted to the corresponding number of amino acid side-chains (mole) reacted per molecule (mole) of BSA (Table I). After a three-day incubation (the equilibrium state), the total content of amino acid side-chains reacted per BSA molecule was 36 (43.1 %). The contribution of MG reaction with guanidino groups to the decrease of the positive charge of BSA was higher compared to the contribution of the amino groups. The percentage of modified thiol groups to the total content of modified amino acid residues (1.55 %) was almost two times higher than that in untreated BSA (0.87 %). Modification of the SH groups can contribute to a broadening of protein bands in electrophoresis. The increased broadening of the protein bands with time reflects the production of multiple modified forms of the protein (modification with different numbers of MG molecules and different sites).

Some previous studies³⁶ showed that a decrease in the free thiol content in BSA could be the result of an oxidation process rather than of the glycation process with MG. For this reason, the potential oxidation of thiol group in BSA due to influence of temperature (37 °C) and the presence of oxygen in the solutions was followed by determining of the -SH content in untreated albumin (control). During the incubation, the content of -SH groups changed insignificantly. After

168 h, it had decreased by only 8 %. Since in the first hours of BSA incubation with MG, the registered decrease of free SH groups was by 20–30 % (Table I), this is mainly the result of the glycation reaction. According to the proposed mechanism,^{7,13} thiohemiacetal is formed in the reaction of SH group and MG, which is converted by a Cannizzaro-type rearrangement into (1-carboxyethyl)cysteine or participates in the cross-linking of protein molecules.²⁷

TABLE I. Content of reacted amino acid side-chains. BSA (0.50 mM) was treated with 50 mM MG in 0.10 M phosphate buffer (pH 7.2) at 37 °C for various time periods

Incubation time, h	Reacted groups (mol/mol of BSA)				% ^a
	Thiol	Amino	Guanidino	Total	
2	0.149±0.010	0.66±0.12	6.29±0.15	7.10	8.50
4	0.220±0.012	3.25±0.15	8.91±0.39	12.36	14.8
8	0.247±0.001	4.72±0.32	9.64±0.15	15.77	18.9
24	0.390±0.007	12.59±1.15	15.93±0.15	28.91	34.5
48	0.468±0.011	13.96±0.92	15.86±1.08	30.29	36.2
72	0.564±0.014	15.98±1.15	19.51±0.77	36.05	43.1
168	0.677±0.009	16.36±1.01	20.25±0.77	37.28	44.5

^aTotal reacted groups as the percent of the total number of available groups

Inhibition of methylglyoxal-induced modifications of BSA by GSH and metformin

The experiment of BSA (0.50 mM) incubation with MG (50 mM) was also performed in the presence of glutathione (GSH) and metformin as inhibitors of MG reaction with amino acid side chains. The experiments were performed separately; the concentration of the inhibitors was 20 mM (2.5 times lower compared to the MG concentration). The results of monitoring BSA modification by native and SDS electrophoresis in the presence of GSH and metformin are shown in Fig. 3.

Changes in BSA mobility in native electrophoresis were observed in the presence of both inhibitors (Fig. 3A) but to a smaller extent in the presence of metformin (lanes 3, 6, and 9). Relative electrophoretic migration (REM) was determined by calculating the ratio of migration of modified BSA with nontreated albumin (Table II). Significant decreases in REM were found for BSA modified in presence of metformin compared to BSA-MG and BSA-MG + GSH after four ($p < 0.01$ for both) and eight ($p < 0.001$; $p < 0.05$, resp.) hours of incubation. These results are consistent with the findings which underlined metformin as potent glycation inhibitor.^{37,38} On the other hand, in the presence of GSH, significant decrease of REM ($p < 0.001$ vs. BSA-MG) was found only after eight hours of incubation. Thus, positive charge of BSA molecules in presence of metformin is higher than in presence of GSH. A broadening of MG modified BSA (BSA-MG) bands in SDS PAGE was also found in the presence of both inhibitors after only 4 hours of incubation (Fig. 3B), but to a smaller extent in the presence of GSH (lanes 2, 5, 8) compared to the system with metformin (lanes 3, 6, 9) and without

inhibitor (lanes 1, 4, 7) for the same period of time. These findings confirm the importance of $-SH$ reaction with MG in protein modification as well as the role of compounds that contain reactive thiol group as competitive inhibitor of glycation. The obtained results are in agreement with the established depletion of serum thiol levels and erythrocytic GSH in diabetics compared to healthy individuals.^{39,40}

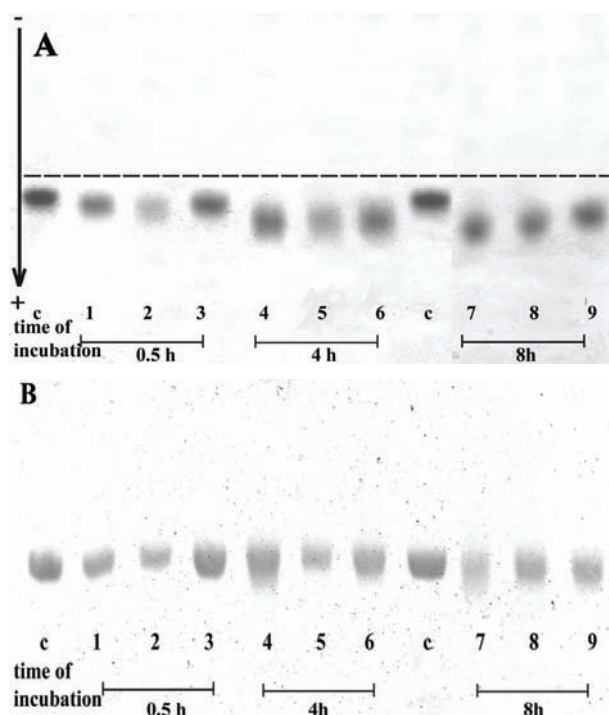


Fig. 3. Native (A) and SDS-PAGE (B) showing the changes of BSA (0.50 mM) resulting from the reaction with MG (50 mM) in the presence (20 mM) and absence of GSH and metformin. The incubation was performed in 0.10 M phosphate buffer (pH 7.2) at 37 °C for 7 days. The marks of the lanes: lane c – untreated BSA; lanes 1, 4 and 7 – BSA+MG; lanes 2, 5 and 8 – BSA+MG+GSH; lanes 3, 6 and 9 – BSA+MG+metformin. The electrophoresis was performed on 10 % polyacrylamide gels and the bands were visualized with CBB, as detailed in the Experimental.

TABLE II. Relative electrophoretic migrations (REM) of BSA modified with MG (BSA-MG) and in the presence of inhibitors (BSA-MG + GSH; BSA-MG + metformin). Data of REM are presented as mean \pm SD ($n = 3$) and statistical analyses were performed using the t -test

Time, h	REM		
	BSA-MG	BSA-MG + GSH	BSA-MG + metformin
0.5	1.044 \pm 0.007	1.055 \pm 0.027	1.043 \pm 0.008
4	1.222 \pm 0.007	1.220 \pm 0.008	1.186 \pm 0.009 ^a
8	1.347 \pm 0.011	1.259 \pm 0.013 ^b	1.222 \pm 0.012 ^{c,d}

^a $p < 0.01$ compared with BSA-MG and BSA-MG + GSH; ^{b,c} $p < 0.001$, compared with BSA-MG; ^d $p < 0.05$, compared with BSA-MG + GSH

HSA modification in the reaction with methylglyoxal

The investigation of BSA modification with a small excess (19 %) of MG compared to the total amount of reactive groups (84¹⁸) showed a significant re-

duction in the content of thiol groups and did not give cross-linking of the protein molecules. The obtained results were the basis for design of the experiments (regarding the MG concentration and duration of incubation) for the examination of HSA changes with MG. In order to determine the dependence of modification of the amino acids of the protein side chains on the MG concentration, HSA was incubated in the presence of an excess or shortage of MG compared to the total amount of reactive groups on the protein surface.

First, HSA (0.50 mM) was incubated with MG at a concentration (100 mM), considerably higher than the physiological concentration³⁵ and higher than the total amount of reactive groups on the protein surface¹⁸. The reaction mixture in 0.10 M phosphate buffer pH 7.2 was incubated at 37 °C for 24 h because after this time, intensive modification of protein molecules was detected in the experiment with BSA. The progress of MG reaction with thiol, amino and guanidino group of HSA was monitored by measuring levels of these groups in aliquots of the reaction mixture with time.

The reaction rate of the guanidine group was the highest: 48 % of available groups reacted during the first 30 min of the reaction, after which it remained unchanged (48.6 ± 3.9 %) during the next 10 h of reaction. In the first 30 min, only 20 % of the available amino groups had reacted and after 4 h the percentage had doubled, after which time there was a gradual increase (to 49 %) after up to 10 h of incubation. The data for the progress of SH-group reaction indicates that 30 % of the groups had reacted after 30 min, 55 % after 2 h and 65 % after 10 h. At the end of the incubation period (24 h), approx. 70 % of the amino and guanidine groups and 85 % of the SH-groups had reacted.

HSA modification under these conditions was also monitored by native and SDS PAGE (Fig. 4). Changes in the charge of HSA were detected by native electrophoresis after 15 min of incubation (Fig. 4A). During 24 h of incubation, the positive charge of HSA continually declined. The changes in the charge of the HSA molecules are consistent with the change in the amounts of reacted guanidino and amino groups per HSA molecule (Table III). They were the most pronounced during the first two hours of incubation (maximum percentage of guanidino and a significant percentage of amino groups had reacted). The contribution of MG reaction with the amino groups to the change of the HSA charge increased with time.

SDS PAGE analysis (Fig. 4B) of MG modified HSA (MG-HSA) showed marked changes from unmodified HSA: there was a broadening of the peak of molecular mass 66 kDa corresponding to MG-HSA monomers. This band tailed to higher molecular mass values (extending to 90 kDa) after a very short time of incubation (about 30 min) and became more intensive with time. Also, the presence of dimers (of molecular mass *ca.* 130 kDa) and oligomers was found. These findings indicate intensive fragmentation and cross-linking of fragments (a broad band ranging between molecular masses 48–90 kDa), as well as HSA cross-

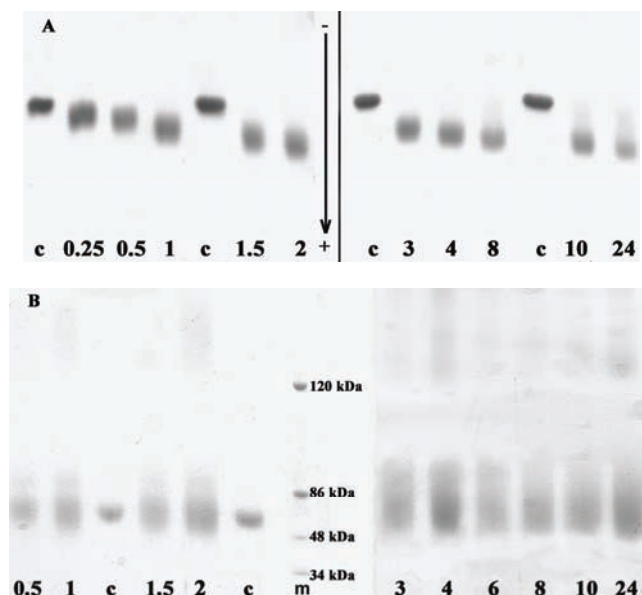


Fig. 4. Native (A) and SDS-PAGE (B) showing the changes in the mobility of HSA resulting from the reaction with MG. HSA (0.50 mM) was treated with 100 mM MG in 0.10 M phosphate buffer (pH 7.2) at 37 °C for 24 h. Lane c shows untreated HSA. The marks of other lanes correspond to the time incubation (h) of BSA with MG. Lane m – high-molecular mass standards (34, 48, 86 and 120 kDa). The electrophoresis was performed on 10 % polyacrylamide gels and the bands were visualized with CBB, as detailed in the Experimental.

-linking under the employed incubation conditions during this period of time. Taking into account that:

- the percentage of reacted guanidino groups was the highest during the first 30 min and did not change during further incubation,
- oligomers were easily detected during SDS-PAGE after two hours of incubation, during which time the amount of reacted amino and SH-groups increased (Table III) and

– the cross-linking of proteins increased with time (and the amounts of free amino and SH-groups decreased),

it can be concluded that lysine and cysteine residues play a more important role in the cross-linking of protein molecules than those of arginine.

Lysine side chains participate in HSA cross-linking *via* MG-SH (hemithioacetal) or MG-NH₂ products formed during the first step, which is consistent with an earlier proposal.²⁷ The obtained results are also in agreement with the proposed mechanism of MG reaction with the guanidino group,¹³ in which the product of the first step participates in an intramolecular reaction with the guanidino residues of arginine, forming an imidazolone derivative, thus preventing any further linking.

TABLE III. Content of reacted amino acid side-chains. HSA (0.50 mM) was treated with 100 mM MG in 0.10 M phosphate buffer (pH 7.2) at 37 °C for various time periods

Incubation time, h	Reacted group (mol/mol of HSA)				% ^a
	Thiol	Amino	Guanidino	Total	
0.5	0.222±0.009	11.80±0.52	11.52±0.35	23.54	28.10
2	0.413±0.009	18.90±0.38	10.15±0.17	29.46	35.17
4	0.417±0.004	24.06±0.61	11.80±0.52	36.27	43.31
8	0.459±0.013	25.28±0.52	10.96±0.43	36.70	43.81
10	0.495±0.006	28.91±0.46	11.93±0.40	41.34	49.35
24	0.647±0.004	40.71±0.48	16.8±0.33	58.16	69.43

^atotal reacted groups as the percent of the total number of available groups

Comparison of results obtained for modified BSA and HSA (Tables I and III) indicate that the total amount of reacted amino acid side-chains per mole of HSA, after 24 h of incubation, was two times higher than per mole of BSA (58.16 vs. 28.91). It could be said that this result conforms to the fact that the concentration of MGO in reaction mixtures with HSA was two times higher. During the entire incubation period, the amounts of reacted –SH groups were also approximately two times higher in HSA compared to BSA. The amounts of reacted Arg residues in HSA and BSA were similar after 8 and 24 h of incubation. However, it is noticeable that during the entire incubation period, the contribution of the reaction of MG with amino groups to the modification of HSA was several times higher compared to BSA. Changes in the content of amino groups brought about differences in electrophorograms of the modified HSA compared to those obtained for BSA.

The HSA modifications and the contributions of the amino acid side chains to the changes described above result from HSA incubation with an amount of MG (200 mmol/mol HSA) that was considerably higher than the sum of the available groups (84¹⁸). However, it was important not only to determine the role, contributions and reactivity of each type of group (–SH, amino and guanidino) in protein modification when the amount of MG was lower than the sum of the available groups, but also to monitor changes over a longer period of time. Therefore, HSA (0.50 mM) was incubated with 10 mM MG in 0.10 mM phosphate buffer (pH 7.2) at 37 °C for 24 days. The chosen MG concentration was 10 times lower than the concentration used in the previous HSA incubation experiment and approx. 4 times lower than the sum of amino, guanidino and SH-groups on the surface of the protein molecule.

The changes in the amount (mol) of the thiol, amino and guanidino groups per mole of HSA during 24 days are shown in Table IV. In the case of MG reaction with guanidino and amino group, equilibrium was achieved after one day of incubation, with approx. 50 % (47.2±3.8 %) of the guanidino and 35 % of the amino groups reacted. Also, HSA mobility during native electrophoresis changed

considerably after the first day of incubation (Fig. 5A, lane 1), and changed slightly in the following days (lanes 2–8); differences between REM values obtained for those bands are not significant). Due to the high reaction rate of MG with the guanidino group, the percentages of Arg residues reacted during 24 h both in the case of insufficient and excess amount of MG were very high (50 and 70 %, respectively, Table V). This indicates a similar contribution of this reaction to the change in the HSA charge at different MG concentrations. The difference in the percentage of reacted amino groups at both shortage and excess of MG was more significant (35 and 69 %, respectively). Yet, the contribution of the reaction of the amino groups to the change of the HSA charge even at insufficient amount of MG was very high. After 24 h of incubation, 20.7 mol of Lys residues per mole of HSA had reacted (Table IV), which makes approx. 63 % of the total number of modified amino acid residues.

TABLE IV. Content of reacted amino acid side-chains. HSA (0.50 mM) was treated with 10 mM MG in 0.10 M phosphate buffer (pH 7.2) at 37 °C for 24 days

Incubation time, days	Reacted group (mol/mol of HSA)				% ^a
	Thiol	Amino	Guanidino	Total	
1	0.198±0.009	20.75±0.70	11.97±0.08	32.92	39.3
3	0.430±0.006	20.39±0.83	10.40±0.23	31.22	37.3
5	0.494±0.003	23.69±0.96	11.51±0.39	35.69	42.6
7	0.528±0.012	24.08±1.11	12.22±0.23	36.83	44.0
9	0.509±0.015	28.70±0.42	13.20±0.08	42.40	50.6
15	0.514±0.010	27.45±0.14	10.85±0.23	38.81	46.3
24	0.550±0.008	29.13±0.36	10.51±0.20	40.19	48.0

^atotal reacted groups as the percent of the total number of available groups

The broadening of the HSA bands in SDS PAGE with tails to higher molecular mass values (Fig. 5B, lanes 3 and 5, obtained after 3 and 5 days of incubation) points to cross-linking of the protein molecules even with an insufficient amount of MG. The high content of reacted amino groups (compared to the MG concentration, 20 mM) as early as after 24 h of incubation points to their role in the cross-linking. Over a longer incubation period (from 9–24 days), fragmentation also emerges (the occurrence of bands with lower molecular mass values, lanes 9 and 24, Fig. 5B). Zeng and Davies²⁷ suggested that the initial addition of the thiol to the dicarbonyl compound and subsequent reaction with an amine can lead to cross-link formation. It could be asked what is the contribution of the SH-groups in the formation of aggregates under conditions of an insufficient amount of MG, since the number of SH-groups on the surface of the HSA molecule is negligible compared to the number of amino and guanidino groups (1:59:24).¹⁸ After the first day of HSA incubation with 10 mM MG, 26 % of the SH-groups had reacted (0.198 mol/mol HSA), 51 % after the second day (0.388 mol/mol HSA) and equilibrium was achieved after 5 days when 65 % of the groups had

reacted (0.494 mol per mole HSA) (Table III). During this period, bands with expressed tailing to higher molecular mass values were obtained during SDS PAGE. In addition, a slight increase of reacted amino groups was found (from 35 to 40 %), which indicates the possibility of reaction with the hemithioacetal and the role of SH-group in protein modification and cross-linking. Taking into account the MG concentration (10 mM) in reaction mixture, the HSA concentration (0.50 mM), the number of reactive groups on the protein surface, the amount of reacted amino (40 %) and guanidino (50 %) groups, it can be concluded that 8.0 mM amino groups participated in cross-linking after 5 days of incubation under these conditions. Based on the amount of reacted SH-groups (65 %), *i.e.*, hemithioacetals formed during 5 days of incubation, it could be concluded that approx. 4 % of the cross-linking of the protein molecules was a consequence of hemithioacetal reaction with an amino group. This percentage is not negligible taking into account the extremely low distribution of SH-groups on the protein surface compared to amino and guanidino groups.

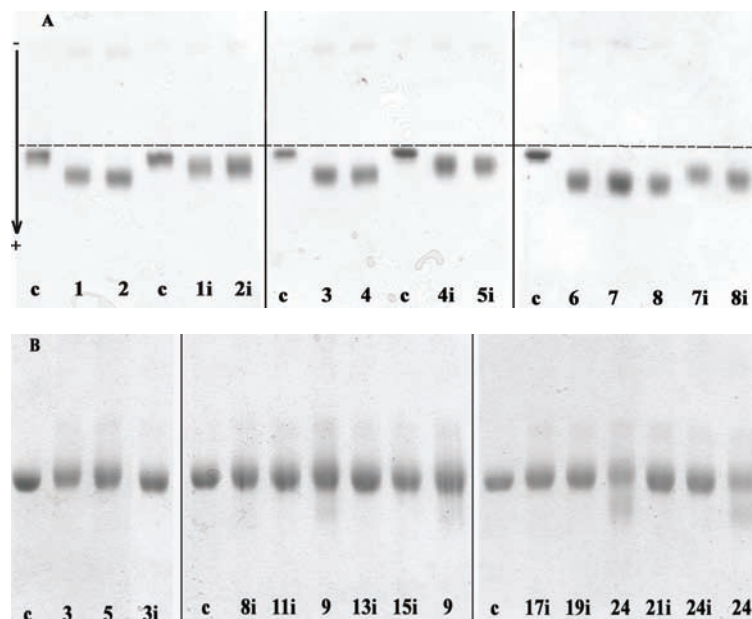


Fig. 5. Native (A) and SDS-PAGE (B) showing the changes of the mobility of HSA (0.50 mM) resulting from the reaction with methylglyoxal (10 mM). The incubation was performed in 0.10 M phosphate buffer (pH 7.2) at 37 °C for 24 days, with (10 mM) and without metformin. Lane c shows HSA without metformin and lanes 2–24 with MG. The number of the lane corresponds to the number of incubation days. The label i beside the lane number shows that the incubation was performed in the presence of metformin. The electrophoresis was performed on 10 % polyacrylamide gels and the bands were visualized with CBB, as detailed in the Experimental.

TABLE V. Dependence of the levels of reacted thiol, amino and guanidino groups of HSA (%) on the MG concentration and incubation time. The concentration of HSA was 0.50 mM

Group	MG concentration, mM						
	100				10		
	Incubation time						
	30 min	2 h	10 h	1 day	1 day	2 days	5 days
Thiol	30	55	65	85	26	51	65
Amino	20	34	49	69	35	35	40
Guanidino	48	No change		70	50	No change	

The modification of albumin through glycation and the subsequent formation of AGEs have been shown to contribute to vascular complications in patients with diabetes. Some studies have focused on the changes of its antioxidant properties^{36,41–43} and role of the thiol group (Cys 34) in these changes. Faure⁴³ suggested that MG can strongly impair the structure and antioxidant properties of albumin *in vitro*, leading to a modified protein similar to that isolated from diabetic patients. The results of the quantification of the reactive groups and parallel electrophoretic monitoring of HSA changes, especially at low-dose long-term exposition of albumin to MG (obtained in this paper) showed that the –SH group, in addition to the amino group, plays a role in the modification of proteins with MG and cross-linking. The significant decrease of the content of –SH groups by 26 % after 1 h incubation, *i.e.*, 72 % after 24 h of incubation, in the presence of MG may have as a consequence a decrease of the anti-oxidative capacity of albumin, which is consistent with the results of Faure *et al.*⁴³

To investigate the influence of inhibitor on low-dose long-term exposition of HSA to MG, metformin was chosen. It was found that oxidative stress and glycation were significantly lower in metformin-treated patients with Type 2 diabetes mellitus.³⁸ In addition, experiments with BSA showed that the change of the positive charge of the BSA molecule was lower in the presence of metformin than in the presence of GSH.

The inhibitor metformin in an equimolar concentration with MG (during low-dose long-term exposition of albumin to MG), under conditions of an insufficient amount of MG, decreased the amounts of amino and guanidino groups that reacted in the first day by two to three times compared to the system without inhibitor. After a 24-h incubation, 15 % of the guanidino groups, (3.6 mol Arg residues per mole of HSA), approx. 8 % of the amino (4.7 moles of Lys side-chain per mole of HSA) and 86 % of the –SH groups (0.653 mol Cys thiol per mole of HSA) had reacted (Fig. 6). The obtained results are in agreement with the smaller changes in HSA mobility (protein charge) during native electrophoresis in the presence of metformin (Fig. 5A, lanes 1i, 2i, 4i, 5i, 7i and 8i) compared to the bands obtained without this inhibitor. Relative electrophoretic mobilities obtained for HSA bands in the presence of metformin were significantly lower

($p < 0.001$ for 1i to 7i and $p < 0.01$ for 8i) compared to the same ones without inhibitors. However, in the presence of this inhibitor, a broadening of the bands with tails to higher molecular mass values was recorded in SDS PAGE (Fig. 5B). Since all thiol groups reacted under these conditions, the product of reaction between SH-group and MG is the target for the Lys side-chain amino groups in protein cross-linking.

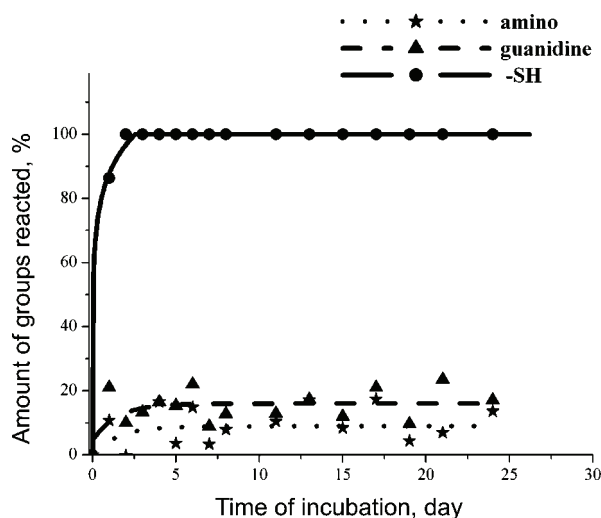


Fig. 6. Quantification of thiol, amino and guanidino groups (% of the ones reacted) during the incubation of 0.50 mM HSA with 10 mM methylglyoxal in the presence of metformin (10 mM), in 0.10 M phosphate buffer (pH 7.2) at 37 °C for 24 days. The data are the means from three determinations.

In hyperglycemia, the glycation process is accompanied by an oxidation process. By applying metformin as an antihyperglycemic agent in patients with Type 2 diabetes mellitus, the oxidation of the albumin thiol group was decreased.³⁸ Metformin decreases the content of toxic dicarbonyl and thereby inhibits the development of AGEs. In the present study, at the equimolar concentration of MG and metformin almost all the -SH groups reacted. This indicates that in the mixture where MG is the only reactive species, the glycation reaction of the albumin thiol group is proceeding.

An absence of fragments of lower molecular mass value (formed during 9–24 days of incubation, lanes 9 and 24, Fig. 5B) in the presence of metformin (Fig. 5B, lanes 13i, 15i, 17i, 19i, 21i, 24i), indicates the role of the reaction of guanidino with MG in the unfolding and fragmentation of the protein.

CONCLUSIONS

The results obtained indicate that thiol group reaction, despite the very small presence of thiol groups on the surface of the protein molecule, (80 times less available compared to amino and guanidino groups in HSA¹⁸) plays an important role in protein modification with MG and in cross-linking. Since these changes in proteins can be a cause of the development of secondary complications in dia-

betes,¹⁶ modification of signal transduction^{15,44} and the cause of various pathological states,¹⁷ the application of MG scavenger substances is of importance in clinical practice. To date, various inhibitors of MG reactions with thiol, amino and guanidino groups have been tested, providing differences in their inhibition potency. The results presented in this paper show that metformin at equimolar concentration with MG inhibits its reaction with guanidino group but not, however, with the thiol group.

Acknowledgements. This paper was supported by the Ministry of Science and Technological Development of the Republic of Serbia (Project No. 142020). Our special thanks go to Dr. Dragan Marinkovic from Del Mar, CA, for help in editing.

ИЗВОД

УЛОГА ТИОЛНЕ ГРУПЕ У МОДИФИКАЦИЈИ ПРОТЕИНА СА МЕТИЛГЛИОКСАЛОМ

ЈЕЛЕНА М. АЋИМОВИЋ, БОЈАНА Д. СТАНИМИРОВИЋ и ЉУБА М. МАНДИЋ

Хемијски факултет, Универзитет у Београду, б.бр. 51, 11158 Београд

Метилглиоксал је веома реактивни α -оксоалдехид који се повећано ствара у хипергликемији. Реагује са нуклеофилним групама бочних остатака Lys, Arg и N-терминалном аминок-групом, што доводи до модификације протеина. У овом раду испитивани су значај реакције SH групе са метилглиоксалом у модификацији протеина, конкурентност ове реакције у односу на реакције са аминок- и гванидино-групом, ток ових реакција и њихова улога и допринос у умрежавању протеина. Као модел-системи употребљени су хумани и говеђи серум-албумин. Утврђено је да и поред веома мале заступљености SH групе на површини испитиваних молекула протеина (око 80 пута мања у односу на укупан број аминок- и гванидино-група), она реагује у великом проценту (од 25–85 %). Количина изреагованих SH група и брзина реакције, време успостављања равнотеже реакције, стварања стабилног производа и допринос SH група умрежавању протеина зависе од концентрације метилглиоксала. Производ створен у реакцији SH група и недовољне количине метилглиоксала (у односу на концентрацију група доступних за модификацију) учествује у умрежавању протеина са значајним уделом (4 %). У еквимоларној концентрацији са метилглиоксалом метформин спречава његову реакцију са аминок- и гванидино групама албумина, али не и са тиол групом.

(Примљено 26. новембра 2008, ревидирано 9. фебруара 2009)

REFERENCES

1. P. J. Beisswenger, L. L. Moore, T. Brinck-Johnsen, T. J. Curphey, *J. Clin. Invest.* **92** (1993) 212
2. T. J. Berg, H. J. Bangstad, P. A. Torjesen, R. Osterby, R. Bucala, K. F. Hanssen, *Metab. Clin. Exp.* **46** (1997) 661
3. Y. Aso, T. Inukai, K. Tayama, Y. Takemura, *Acta Diabetol.* **37** (2000) 87
4. M. Kalousova, J. Skrha, T. Zima, *Physiol. Res.* **51** (2002) 597
5. J. Misselwitz, S. Franke, E. Kauf, U. John, G. Stein, *Pediatr. Nephrol.* **17** (2002) 316
6. K. Hirata, K. Kubo, *Endocr. J.* **51** (2004) 537
7. M. Brownlee, A. Cerami, H. Vlassara, *N. Eng. J. Med.* **318** (1988) 1315
8. S. A. Phillips, P. J. Thornalley, *Eur. J. Biochem.* **212** (1993) 101
9. A. C. McLellan, P. J. Thornalley, J. Benn, P. H. Sonksen, *Clin. Sci.* **87** (1994) 21

10. A. Lapolla, R. Flamini, A. Dalla Vedova, A. Senesi, R. Reitano, D. Fedele, E. Basso, R. Seraglia, P. Traldi, *Clin. Chem. Lab. Med.* **41** (2003) 1166
11. H. Odani, T. Shinzato, Y. Matsumoto, J. Usami, K. Maeda, *Biochem. Biophys. Res. Commun.* **256** (1999) 89
12. P. J. Thornalley, *Ann. NY Acad. Sci.* **1043** (2005) 111
13. T. W. Lo, M. E. Westwood, A. C. McLellan, T. Selwood, P. J. Thornalley, *J. Biol. Chem.* **269** (1994) 32299
14. P. J. Thornalley, *Biochem. Soc. Trans.* **31** (2003) 1372
15. D. Yao, T. Taguchi, T. Matsumura, R. Pestell, D. Edelstein, I. Giardino, G. Suske, N. Ahmed, P. J. Thornalley, V. P. Sarthy, H. P. Hammes, M. Brownlee, *Cell* **24** (2006) 275
16. J. W. Baynes, S. R. Thorpe, *Free Radical Biol. Med.* **28** (2000) 1708
17. R. Ramasamy, S. F. Yan, A. M. Schmidt, *Cell* **124** (2006) 258
18. M. E. Westwood, P. J. Thornalley, *J. Protein Chem.* **14** (1995) 359
19. J. Zeng, M. J. Davies, *Chem. Res. Toxicol.* **18** (2005) 1232
20. S. R. Thorpe, J. W. Baynes, *Amino Acids* **25** (2003) 275
21. N. Alt, J. A. Carson, N. L. Alderson, Y. Wang, R. Nagai., T. Henle, S. R. Thorpe, J. W. Baynes, *Arch. Biochem. Biophys.* **425** (2004) 200
22. A. A. Mostafa, E. W. Randell, S. C. Vasdev, V. D. Gill, Y. Han, V. Gadag, A. A. Raouf, H. El Said, *Mol. Cell Biochem.* **302** (2007) 35
23. P. E. Morgan, R. T. Dean, M. J. Davies, *Arch. Biochem. Biophys.* **403** (2002) 259
24. K. Okuda, I. Urabe, Y. Yamada, H. Okada, *J. Ferment. Bioeng.* **71** (1991) 100
25. T. Ishii, E. Tatsuda, S. Kumazawa, T. Nakayama, K. Uchida, *Biochemistry* **42** (2003) 3474
26. A. Furuhashi, M. Nakamura, T. Osawa, K. Uchida, *J. Biol. Chem.* **277** (2002) 27919
27. J. Zeng, M. J. Davies, *Chem. Res. Toxicol.* **19** (2006) 1668
28. B. T. Dumas, W. A. Watson, H. G. Biggs, *Clin. Chim. Acta* **31** (1971) 87
29. Hoeffer Scientific Instruments. *Electrophoresis Instruments and Accessories. Techniques and Exercises*, Hoeffer scientific instruments. San Francisco. USA, 1991
30. G. Bulaj, T. Kortemme, D. P. Goldenberg, *Biochemistry* **37** (1998) 8965
31. D. Bar-Or, R. Bar-Or, L. T. Rael, D. K. Gardner, D. S. Slone, M. L. Craun, *Crit. Care Med.* **33** (2005) 1638
32. C. S. P. Sastry, M. K. Tummuru, *Food. Chem.* **15** (1984) 257
33. D. A. M. Zaia, W. J. Barreto, *Anal. Chim. Acta* **277** (1993) 89
34. S. Sridharan, A. Nicholls, B. Honig, *Biophys. J.* **61** (1992) A174.
35. P. J. Thornalley, *Gen. Pharmacol.* **27** (1996) 565
36. P. Rondeau, N. R. Singh, H. Caillens, F. Tallet, E. Bourdon, *Rad. Biol. Med.* **45** (2008) 799
37. S. Rahbar, J. L. Figarola, *Arch. Biochem. Biophys.* **419** (2003) 63
38. P. Faure, C. Polge, A. Faviere, S. Halimi, *Clin. Sci.* **114** (2008) 251
39. H. Pasaoglu, B. Sancak, N. Bukan, *Tohoku J. Exp. Med.* **203** (2004) 211
40. P. J. Thornalley, A. C. McLellan, T. W. Lo, J. Benn, P. H. Sonksen, *Clin. Sci (London)* **91** (1996) 575
41. M. Soriani, D. Pietraforte, M. Minetti, *Arch. Biochem. Biophys.* **312** (1994) 180
42. M. Roche, P. Rondeau, N. R. Singh, E. Tarnus, E. Bourdon, *FEBS Lett.* **582** (2008) 1783
43. P. Faure, L. Troncy, M. Lecomte, N. Wiernsperger, M. Lagarde, D. Ruggiero, S. Halimi, *Diabetes Metab.* **31** (2005) 169
44. A. A. Akhand, K. Hossain, H. Mitsui, M. Kato, T. Miyata, R. Inagi, J. Du, K. Takeda, Y. Kawamoto, H. Suzuki, K. Kurokawa, I. Nakashima, *Free Radical Biol. Med.* **31** (2001) 20.



J. Serb. Chem. Soc. 74 (8–9) 885–892 (2009)
JSCS–3884

Changes in the infrared attenuated total reflectance (ATR) spectra of lignins from alfalfa stem with growth and development

JORDAN P. MARKOVIĆ^{1*}, JASMINA B. RADOVIĆ¹, RATIBOR T. ŠTRBANOVIĆ¹,
DANICA S. BAJIĆ^{2#} and MIROSLAV M. VRVIĆ^{2,3#}

¹Institute for Forage Crops, 37000 Kruševac, Trg Kosturnica 50, 37000, ²Department of Chemistry, Institute of Chemistry, Technology and Metallurgy, 11001 Belgrade, Njegoševa 12, P.O. Box 473, Belgrade and ³Faculty of Chemistry, University of Belgrade, 11158 Belgrade, Studentski trg 16, P.O. Box 51, Belgrade, Serbia

(Received 24 February, revised 30 March 2009)

Abstract: Lignin is a poorly characterized polymer and its exact properties vary depending on both the species of the plant and its location within the plant. Three classes of lignins taken from alfalfa stem were examined. The investigation was concentrated on the determination of chemical changes in the lignins during growth and development by the attenuated total reflectance (ATR) infrared (IR) spectrometric technique. The spectrum of permanganate lignin was comparable to that of acid detergent lignin. The main differences were in the different relative absorbance of the peaks. The predominant component of acid detergent lignin and permanganate lignin was guaiacyl-type lignin. The predominant component of Klason lignin was syringyl-type lignin. A comparison between the signals from lignin in different development stages revealed the appearance of new peaks, which are indications of new bonds and changes in the structure of the lignins.

Keywords: alfalfa; acid detergent; permanganate and Klason lignin; ATR infrared spectra.

INTRODUCTION

Lignin is a complex polymer of high carbon content, which is distinct from carbohydrates, that impregnates the plant cell wall. Thus, lignin confers compressive strength and bending stiffness necessary for mechanical support; it also provides a hydrophobic surface, essential for longitudinal water transport, and provides a barrier against pathogens. Lignins are composed of three main units, named *p*-hydroxyphenyl, guaiacyl and syringyl units. These components originate from

* Corresponding author. E-mail: jordan.markovic@ikbks.com

Serbian Chemical Society member.

doi: 10.2298/JSC0909885M

the polymerization of the three monolignols, *p*-coumaryl, coniferyl and sinapyl alcohols (Fig. 1).¹ The proportions of these three units in the cell wall vary according to plant species and tissue type.² During the early stages, coniferyl alcohol with small amounts of *p*-coumaryl alcohol is copolymerized into the primary wall to form mixed guaiacyl and *p*-hydroxyphenyl lignins (Fig. 2).^{1,2} Later, during secondary wall development, coniferyl alcohol and increasing amounts of sinapyl alcohol are copolymerized to form mixed guaiacyl and syringyl lignins.³

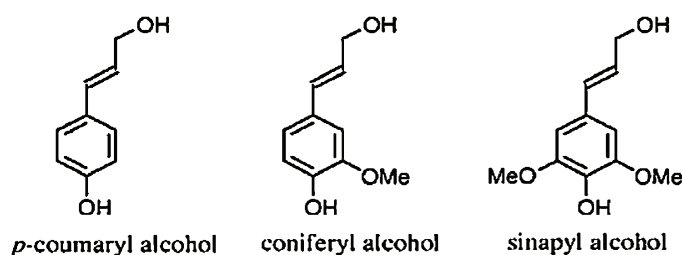


Fig. 1. The monolignols.

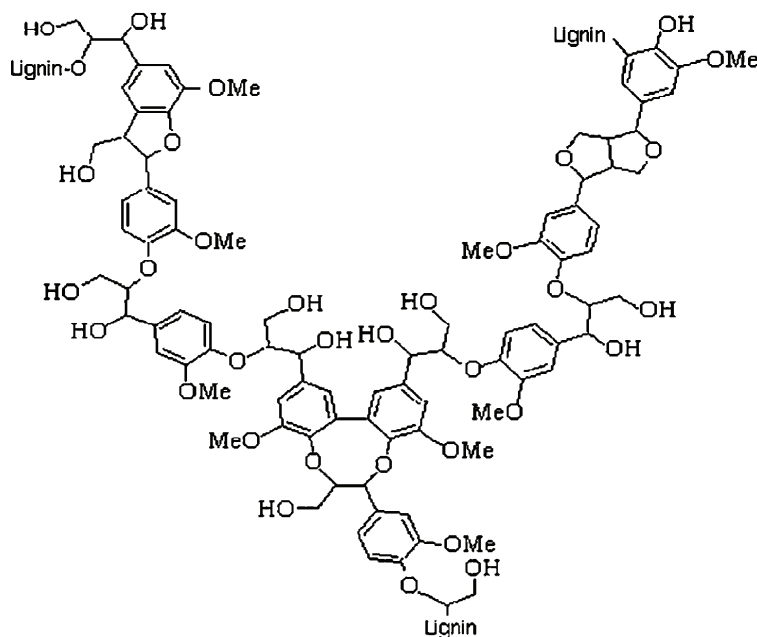


Fig. 2. Fragment of the hypothetical structural formula of lignin.

Many methods of lignin analysis have been developed because of the negative association of lignin with digestibility. In this study, the composition and structure of the lignin isolated by different methods from alfalfa stem at different stage of growth and development were investigated by the ATR-IR spectroscopic method.

EXPERIMENTAL

Material

A new cultivar K-22 of alfalfa (*Medicago sativa* L.) was created in the Institute for Forage Crops, Kruševac, Serbia. Three maturities of alfalfa after the first cut were chosen for this study. The first sample of forage crop was harvested on June 17th, 2008. The alfalfa was 0.38 m tall and at the mid-bud stage. The second was harvested on June 24th, 2008, when the plants were 0.68 m tall and at about 55 % bloom. The third harvest was harvested on July 1st, 2008, when the alfalfa was 0.91 m tall and in full bloom. All values are averages.

Methods

The acid detergent lignin (ADL) was determined as the lignin insoluble in 72 % (w/w) sulfuric acid, applying the method of Van Soest and Robertson.⁴ The permanganate lignin (PerL) was determined as the residue remaining after oxidation with potassium permanganate by the method of Van Soest and Wine.⁵ The Klason lignin (KL) was determined as the residue remaining after total hydrolysis of the cell wall polysaccharides by the method of Theander and Westerlund.⁶

The ATR spectra (1700–500 cm⁻¹) were obtained using a Nicolet Model 6700 FT-IR spectrometer. The crystal-diamond spectra were obtained with 4 cm⁻¹ resolution and 32 scans for each sample spectrum were performed. The spectral values are in cm⁻¹.

RESULTS AND DISCUSSION

ATR-IR spectrometry was used as a structural, non-destructive and simple tool for the qualitative analysis of the chemical composition of lignins isolated by different methods and in different stages of herbal development.

The spectrum of ADL (the first stage of development) is presented in Fig. 3a. Peaks were observed at (cm⁻¹): 1727.7 (C=O unconjugated groups in lignin and carboxylic acid ester⁷); 1602.8 and 1490.7 (aromatic skeletal vibrations^{8,9}); 1455.4 (benzene ring vibration in lignin, CH₃ and CH₂ substituted⁸); 1166.7 (C–O–C bonds of allyl ether¹⁰); 1031.3 (primary alcoholic and aliphatic ether groups⁹) and 960.0 (aromatic C–H out-of-plane deformations¹¹). At the second stage of development (Fig. 3b), the signal at 1031.5 arises from the C–O bond of primary alcohols⁹. At the third stage of alfalfa development (Fig. 3c), the assigned peaks are: 1568.0 (vibrations of the aromatic rings present in lignin⁸); 1506.6 (C=C in plane aromatic vibrations from lignin¹⁰); 1420.5 (C–H deformation in lignin and carbohydrates¹¹); 1316.9 (C–H vibrations in cellulose and the C₁–O vibration in syringyl derivatives¹²); 1244.4 (syringyl ring and C–O stretching in lignin and xylan¹³); 1027.3 (C–O–C vibration in cellulose and hemicelluloses¹⁰) and 896.4 (C–H deformation).

The spectrum of PerL (Fig. 4) is comparable to that of ADL. Peaks were observed at (cm⁻¹): 1731.7 (carbonyl stretching – unconjugated ketones and carboxyl groups¹⁴); 1316.3 (syringyl ring breathing with C–O stretching⁸); 1244.8 (guaiacyl ring breathing with C–O stretching⁸); an intensive signal at: 1159.1 (may represent aromatic C–H in plane deformation of the guaiacyl-type) and 897.3 (aromatic C–H out of plane deformation⁸). This spectrum of PerL could be

explained by alkylation, which protects the phenolic aromatic rings from degradation, while all the other aromatic rings are degraded in the permanganate oxidation. Some biphenyls and biphenyl ethers also survived the oxidative degradation.¹⁰ On the other hand, the signals at (cm^{-1}): 1427.5 at the second stage of development and 1592.8 and at 1417.0 at the third stage of development (aromatic skeletal vibrations combined with C–H in plane deformation¹¹) and 1245.7 (syringyl ring and C–O stretching in lignin and xylan¹²) disappeared.

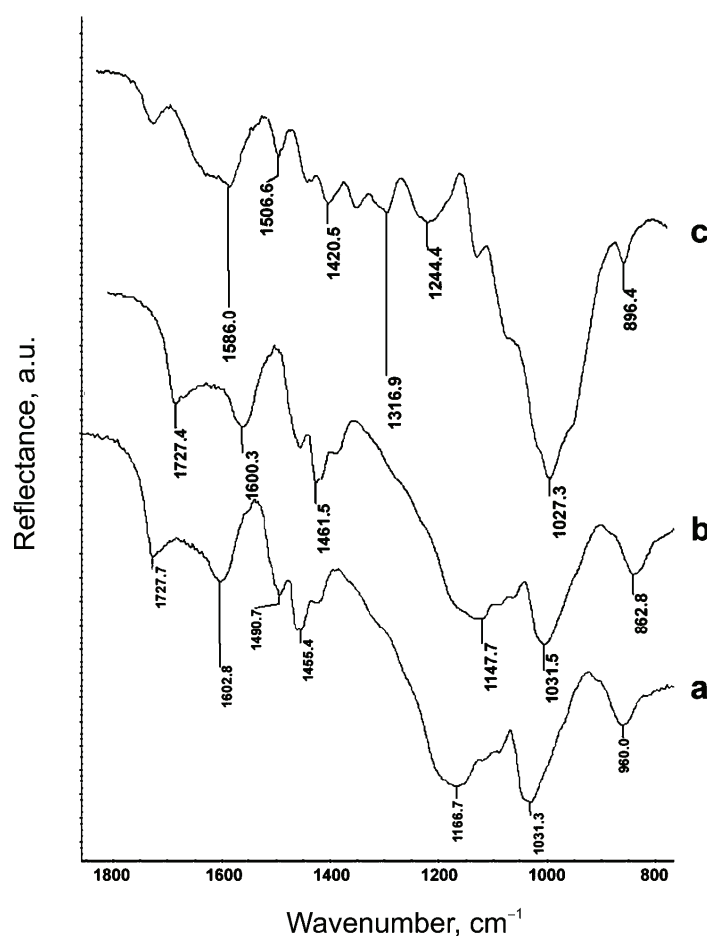


Fig. 3. IR spectrum of ADL from alfalfa stem by ATR spectrometry, a) the first stage, b) the second stage and c) the third stage of development.

At the first development stage, in the spectrum of KL (Fig. 5a), intensive signals at (cm^{-1}): 1090.1 and 1028.6 (syringyl units or condensed guaiacyl units⁹) and signals 1455.2, 1495.9 and 1613.5 (aromatic skeletal vibration as well as CH deformations, guaiacyl–syringyl-type¹⁰) were observed. At the second

development stage (Fig. 5b), signal at (cm^{-1}): 1651.0 (carbonyl groups of oxycelluloses, found in degraded materials¹¹); 1423.2 (C–H vibrations and aromatic ring vibrations^{7,15}) and 1210.1 (vibrations of guaiacyl rings and stretching vibrations of C–O bonds⁹) were registered. The spectrum of KL in the third development stage of alfalfa (Fig. 5c) showed syringyl ring and C–O stretching at 1232.8 in lignin and xylan.^{10,15}

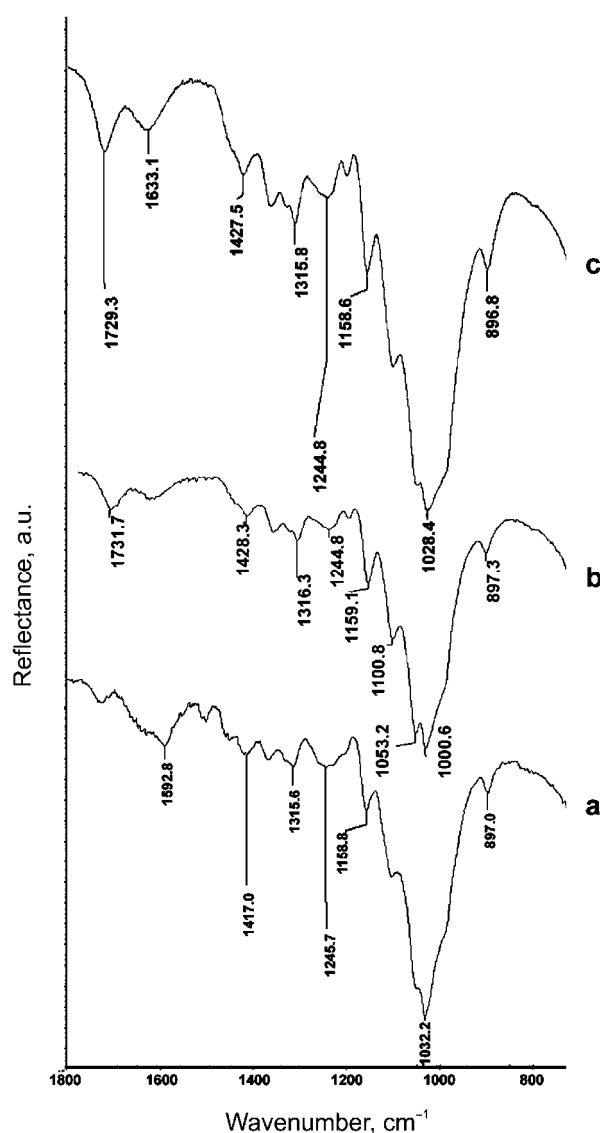


Fig. 4. IR spectrum of PerL from alfalfa stem by ATR spectrometry, a) the first stage, b) the second stage and c) the third stage of development.

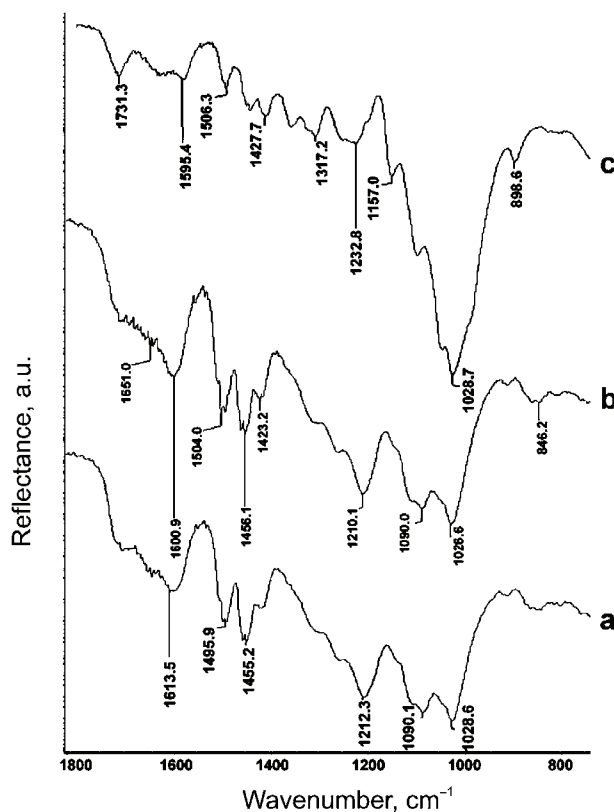


Fig. 5. IR spectrum of KL from alfalfa stem by ATR spectrometry, a) the first stage, b) the second stage and c) the third stage of development.

In other detailed structural study,^{16–18} contemporary comparison of the composition of lignin from alfalfa stem with growth and development were made. The spectra of ADL and PerL were similar. The main difference was that in the PerL spectrum, guaiacyl and syringyl ring breathing signals were registered, whereas in the ADL spectrum, only a guaiacyl ring breathing signal was observed. The spectra of KL showed syringyl and condensed guaiacyl units from the first to the third stage of alfalfa stem development. The spectral data of lignins from alfalfa stem indicate changes of peaks in fingerprint region at different stages of growth. Comparison between the peaks from different development stages revealed the appearance of new signals after 7-day intervals, which are indications of new bonds. The increases of the new bands indicate that new bonds were formed owing to the breakdown of lignin and hemicellulose polymers. During this period, many chemical changes occurred in these constituents, primarily in the structure and amount of lignins.

Acknowledgments. This work was supported in part by the Ministry of Science and Technological Development of the Republic of Serbia (Grants: 142018B and 20131B).

ИЗВОД

ПРОМЕНЕ У ИНФРАЦРВЕНИМ АТР СПЕКТРИМА ЛИГНИНА ИЗ СТАБЛА ЛУЦЕРКЕ
У ЗАВИСНОСТИ ОД ФАЗЕ РАЗВИЋА

ЈОРДАН П. МАРКОВИЋ¹, ЈАСМИНА Б. РАДОВИЋ¹, РАТИБОР Т. ШТРБАНОВИЋ¹,
ДАНИЦА С. БАЈИЋ² и МИРОСЛАВ М. ВРВИЋ^{2,3}

¹Институт за крмно биље, Трз Коштурница 50, 37000 Крушевац, ²Институт за хемију, технологију и
механику, Центар за хемију, Њежицева 12, б. бр. 473, 11001 Београд и ³Хемијски факултет,
Универзитет у Београду, Студентски брз 16, б. бр. 51, 11158 Београд

Лигнини су врло мало проучавани, и њихова структура се разликује у зависности од врсте биљака и његове заступљености у биљци. Испитивања су обављена на три типа лигнина изолованих из стабла нове крушевачке сорте луцерке, К-22. Ово истраживање је обављено да би се боље упознале хемијске промене различитих типова лигнина, са напредовањем фазе развића, применом АТР спектрометрије. Спектар перманганатног лигнина је сличан спектру киселог детерцентног лигнина. Основна разлика је у интензитету сигнала. Главне компоненте киселог детерцентног лигнина и перманганатног лигнина јесу јединице „гвајацил“ типа, док су код Класон лигнина основне структурне јединице „сирингил“ типа. Поређењем спектра у различитим фазама развића бележи се појава нових сигнала, што указује на нове хемијске везе – промене у структури лигнина.

(Примљено 24. фебруара, ревидирано 30. марта 2009)

REFERENCES

1. O. Derkacheva, D. Sukhov, *Macromol. Symp.* **265** (2008) 61
2. W. Boerjan, J. Ralph, M. Boucher, *Annu. Rev. Plant Biol.* **54** (2003) 519R
3. R. Sibout, A. Eudes, G. Mouille, B. Pollet, C. Lapiere, L. Jounanin, A. Seguin, *Plant Cell* **17** (2005) 2059
4. P. J. Van Soest, J. B. Robertson, in *Standardization of analytical methodology in feeds*, W. J. Pigden, C. C. Balch, M. Graham, Eds., International Research Development Center, Ottawa, 1980, p. 49
5. P. J. Van Soest, R. H. Wine, *J. AOAC* **50** (1967) 50
6. O. Theander, E. A. Westerlund, *J. Agric. Food Chem.* **34** (1986) 330
7. H. L. Hergert, in *Lignins, occurrence, formation, structure and reaction*, K. V. Sarkanen, C. H. Ludwig, Eds., Wiley-Interscience, New York, 1971, p. 267
8. G. Brunow, in *Lignin, humic substances and coal*, M. Hofrichter, A. Steinbüchel, Eds., Wiley-VCH, Weinheim, 2001, p. 89
9. I. Bykov, *M.Sc. Thesis*, University of Technology, Luleå, 2008, p. 9
10. K. K. Pandey, *J. Appl. Polym. Sci.* **71** (1999) 1969
11. M. Behbood, *Int. Biodeterior Biodegrad.* **55** (2005) 247
12. J. Rodrigues, O. Faix, H. Pereira, *Holzforchung* **52** (1998) 46
13. P. D. Evans, A. J. Micchell, K. J. Schmalzl, *Wood Sci. Technol.* **26** (1992) 151
14. P. Garside, P. Wyeth, *Polym. Prepr.* **41** (2000) 1792
15. S. Raikola, M. Pulkkinen, T. Laakso, K. Fagerstedt, M. Löjja, R. Mahlberg, L. Paajanen, A. C. Ritschkoff, P. Saranpää, *Silva Fennica* **41** (2007) 351

16. V. Nikolić, Lj. Nikolić, M. Stanković, A. Kapor, M. Popsavin, D. Cvetković, *J. Serb. Chem. Soc.* **72** (2007) 737
17. D. Godjevac, B. Pejin, G. Zdunić, K. Šavikin, D. Stešević, V. Vajs, S. Milosavljević, *J. Serb. Chem. Soc.* **73** (2008) 525
18. B. M. Mandić, D. N. Godjevac, V. P. Beškoski, M. R. Simić, S. S. Trifunović, V. V. Tešević, V. V. Vajs, S. M. Milosavljević, *J. Serb. Chem. Soc.* **74** (2009) 27.



J. Serb. Chem. Soc. 74 (8–9) 893–906 (2009)
JSCS–3885

The regulation and catalytic mechanism of the NADP-malic enzyme from tobacco leaves

VERONIKA DOUBNEROVÁ*, LUCIE POTŮČKOVÁ,
KAREL MÜLLER and HELENA RYŠLAVÁ

*Department of Biochemistry, Faculty of Science, Charles University, Hlavova 2030,
CZ-128 40 Prague 2, Czech Republic*

(Received 5 February, revised 7 May 2009)

Abstract: The non-photosynthetic NADP-malic enzyme EC 1.1.1.40 (NADP-ME), which catalyzes the oxidative decarboxylation of L-malate and NADP⁺ to produce pyruvate and NADPH, respectively, and which could be involved in plant defense responses, was isolated from *Nicotiana tabacum* L. leaves. The mechanism of the enzyme reaction was studied by the initial rate method and was found to be an ordered sequential one. Regulation possibilities of purified cytosolic NADP-ME by cell metabolites were tested. Intermediates of the citric acid cycle (α -ketoglutarate, succinate, fumarate), metabolites of glycolysis (pyruvate, phosphoenolpyruvate, glucose-6-phosphate), compounds connected with lipogenesis (coenzyme A, acetyl-CoA, palmitoyl-CoA) and some amino acids (glutamate, glutamine, aspartate) did not significantly affect the NADP-ME activity from tobacco leaves. In contrast, macroergic compounds (GTP, ATP and ADP) were strong inhibitors of NADP-ME; the type of inhibition and the inhibition constants were determined in the presence of the most effective cofactors (Mn²⁺ or Mg²⁺), required by NADP-ME. Predominantly non-competitive type of inhibitions of NADP-ME with respect to NADP⁺ and mixed type to L-malate were found.

Keywords: NADP-malic enzyme; macroergic compounds; *Nicotiana tabacum* L.; kinetic mechanism; inhibition.

INTRODUCTION

The NADP-malic enzyme (L-malate: NADP⁺ oxidoreductase (decarboxylating)), EC 1.1.1.40, NADP-ME) catalyzes the oxidative decarboxylation of L-malate using NADP⁺ as a coenzyme in the presence of divalent metal ions to produce pyruvate, NADPH and CO₂.^{1,2} The presence of a cofactor and the coenzyme is required for the reaction. The most effective cations are Mg²⁺ and Mn²⁺.³ NADP-MEs have been found in prokaryotic and eukaryotic micro-organisms,

* Corresponding author. E-mail: doubnerova@volny.cz
doi: 10.2298/JSC0909893D

plants (C₃, C₄ and CAM), animals and humans. Their amino acid sequences are highly conserved among various living organisms, suggesting that NADP-MEs may have an important biological function.⁴

The best-known role of plant NADP-ME is the photosynthetic one; L-malate is decarboxylated and the released CO₂ is fixed into the Calvin Cycle *via* ribulose-1,5-bisphosphate carboxylase/oxygenase. This process occurs in the chloroplasts of bundle sheath cells of some C₄ plants or during the day in the cytosol of CAM plants.¹ The function of the non-photosynthetic NADP-ME isoform, present in C₃ plants and in non-photosynthetic tissues of C₄ plants, is not fully explained. It is assumed that its main role is to supply reduced equivalents (NADPH) for synthetic metabolic pathways, such as the synthesis of fatty acids. NADP-ME together with phosphoenolpyruvate carboxylase serves to maintain the intracellular pH.¹ NADP-ME also participates in the mechanism of stomatal closure and can affect the water economy of a plant.⁵ Moreover, NADP-ME function seems to be associated with the metabolic response of plants to stress.^{6–17} In animals, the cytosolic isoform (c-NADP-ME) is involved in the generation of NADPH for the biosynthesis of fatty acids and steroids in the liver and adipose tissues. Cytosolic NADP-ME may also have a role in microsomal drug detoxification.¹⁸

The structure and reaction mechanism of animal malic enzyme has been best studied because the crystal structures of pigeon and rat cytosolic NADP-ME are known.^{4,18} The structure of plant and animal NADP-MEs is predominantly tetrameric, with a relative molecular mass of one subunit ranging from 62000 to 67000 Da.^{2,4,17,19}

In plants, NADP-MEs are encoded by a small gene family, the expression of which is tissue and ontogenetic stage specific. The best-studied family of malic enzymes is from *Arabidopsis thaliana* (C₃ dicot plant) and rice (C₃ monocot plant), for which the complete genome sequence is known.^{12,20} Two recombinant isoforms of *Nicotiana tabacum* L. were characterized (chloroplastic Nt-NADP-ME1 and cytosolic Nt-NADP-ME2) and the transcript of a third putative NADP-ME has also been identified.¹⁷

The photosynthetic isoform (NADP-ME from maize leaves) is up-regulated by light,²¹ or by pH (NADP-ME from sugar cane leaves), which affects the oligomerization state of the enzyme.¹ The enzyme can readily undergo changes between monomer, dimer and tetramer. All three forms of the enzyme possess enzyme activity but the highest specific activity occurs at pH 8 for the tetramer form.¹ Finally, regulation of maize NADP-ME occurs by various compounds: either *via* inhibition by an excess of the substrate (L-malate), or by other effectors. Several organic acids have been found to inhibit the C₄ NADP-ME; the strongest inhibition was observed in the presence of oxaloacetate and α -ketoglutarate.¹ Recombinant non-photosynthetic isoforms of NADP-ME from *Arabidopsis thaliana*

and *Nicotiana tabacum* L. were found to be differently regulated by various intermediates of the citric acid cycle (oxaloacetate, fumarate, and succinate) and ATP.^{17,22}

Previously, NADP-ME from tobacco leaves was characterized by kinetic constants and the effect of divalent metal ions on the enzyme activity.²³

The objective of the present communication was the study of the kinetic mechanism of NADP-ME reaction, which has not been described for C₃ plant enzyme and detailed inhibition studies including the determination of inhibition constants and type of inhibition for important regulators.

EXPERIMENTAL

Plant material

Tobacco plants (*Nicotiana tabacum* L. cv. Petit Havana SR1) were grown in a greenhouse under 22/18 °C day/night temperatures. The seeds were sown in pots with sand and the plantlets were transferred to soil after 3 weeks. The leaves of seven-week old plants were collected, frozen immediately in liquid N₂ and stored at –80 °C.

Enzyme purification

A modified procedure described by Ryšlavá *et al.*²³ was used for the purification of NADP-ME enzyme from tobacco leaves. In contrast to the previously used method, the homogenization buffer contained in addition 330 mM sorbitol, which ensures that the chloroplasts remained intact and were removed by centrifugation. Chromatography on DEAE-cellulose, sephacryl S-300 and finally on a 2',5'-ADP-sepharose 4B column yielded a purified enzyme preparation with specific activity 0.95 μmol min⁻¹ mg⁻¹. The purified NADP-ME was stored at 4 °C for further studies.

Enzyme activity assays

The NADP-ME activity was determined spectrophotometrically (Hellios α, Thermo Spectronic) at 21 °C by monitoring the NADPH production at 340 nm, as previously described by Ryšlavá *et al.*⁹

Kinetic studies

The initial-rate study of the kinetic mechanism of NADP-ME was performed by varying the concentrations of free NADP⁺ (0.025–0.166 mmol/l) and varying the concentration of free L-malate (0.879–14.633 mmol/l). The association constants for Me²⁺-NADP⁺ and Me²⁺-L-malate complexes described by Grover *et al.* were used.²⁴ The concentrations of the other compounds were constant (4 mmol/l MgCl₂, 80 mmol/l MOPS–20 mmol/l sodium acetate–NaOH buffer (pH 7.4)). The experimental data were fitted using the equations characterizing a two-substrate mechanism. The sequential initial-rate pattern (Eq. (1)) was found to be the most suitable. Differentiation between ordered sequential and random sequential mechanisms was achieved by scrutinizing the constants K' and constants V'_{lim} (calculated from Eqs. (2)–(4)) vs. the NADP⁺ concentration and vs. the L-malate concentration, respectively.

$$v = \frac{V_{lim} [A][B]}{[B]K_{MA} + [A]K_{MB} + [A][B] + K_A K_{MB}} \quad (1)$$

$$K' = \frac{K_A K_{MB}}{[A]} + K_{MB} \quad (2)$$

$$K' = \frac{K_A K_{MB}}{K_{MB} + [B]} \quad (3)$$

$$V'_{lim} = \frac{V_{lim}[B]}{K_{MB} + [B]} \quad (4)$$

where v is the initial reaction rate, V_{lim} is the apparent maximal reaction rate, $[A]$ and $[B]$ are the substrate concentrations; $K_{MA(B)}$ is the Michaelis constant for the particular substrate, K_A the dissociation constant for the complex enzyme–substrate A, B, K' the apparent Michaelis constant.²⁵

Effect of various compounds on the NADP-ME reaction rate

The NADP-ME assay mixture contained 80 mmol/l MOPS–20 mmol/l sodium acetate–NaOH buffer (pH 7.4), 16 mmol/l L-malate, 4 mmol/l $MgCl_2$ and 0.2 mmol/l $NADP^+$ in a total volume of 1 cm³. Alternatively, the reaction mixture contained a subsaturation concentration of some substrate: 2 mmol/l L-malate and 0.05 mmol/l $NADP^+$, respectively. The reaction was started by addition of the enzyme. The tested concentration of the potential modulators (GTP, ATP, ADP, puruvate, α -ketoglutarate, succinate, fumarate, glutamate, glutamine, aspartate, phosphoenolpyruvate, 3-phosphoglycerate and glucose-6-phosphate) in the reaction mixture was 2 or 5 mmol/l. In the case of coenzyme A, acetyl-coenzyme A and palmitoyl-coenzyme A, their concentration in the reaction mixture was 0.01 or 0.1 mmol/l. The reaction rate of NADP-ME without additions of potential regulators was taken as 100 %.

Inhibition studies

The inhibition constants and type of inhibition for GTP, ATP and ADP were established with 3 concentrations of inhibitor towards 5 various concentrations of L-malate (free concentrations result from particular graphs in Figs. 2–4A and 4B) or 5 various concentrations of $NADP^+$ (free concentrations result from particular graphs in Figs. 2–4C and 4D) and in the presence of Mg^{2+} (Figs. 2–4A and 4C) or Mn^{2+} (Figs. 2–4B and 4D). The NADP-ME assay mixture for the inhibition studies together with varying substrates and inhibitors contained 80 mmol/l MOPS, 20 mmol/l sodium acetate–NaOH buffer (pH 7.4), 2.0 mmol/l $MgCl_2$ or 0.10 mmol/l $MnCl_2$ in a total volume of 1 cm³. The reaction was started by addition of the enzyme (50 μ l). The concentrations of the free inhibitors ATP, ADP and GTP are listed in the Figure legends (Figs. 2, 3 and 4, respectively). The free ATP (GTP, ADP) was calculated using the association constants of the complexes ATP– Mg^{2+} ($\log \beta = 4.29$), ATP– Mn^{2+} ($\log \beta = 5.01$), GTP– Mg^{2+} ($\log \beta = 4.31$), GTP– Mn^{2+} ($\log \beta = 5.36$), ADP– Mg^{2+} ($\log \beta = 3.36$) and ADP– Mn^{2+} ($\log \beta = 4.22$).^{26–28} In the presence of ATP (GTP and ADP), the chelations by the substrate or cofactors are negligible.²⁹ The inhibition constants were obtained by fitting the experimental data to Eq. (5) (equation characterizing non-competitive inhibition), Eq. (6) (equation characterizing competitive inhibition) and Eq. (7) (equation characterizing mixed inhibition):³⁰

$$v = \frac{V_{lim}[A]}{(K_M + [A]) \left(1 + \frac{[I]}{K_i} \right)} \quad (5)$$

$$v = \frac{V_{lim}[A]}{K_M \left(1 + \frac{[I]}{K_{ic}} \right) + [A]} \quad (6)$$

$$v = \frac{V_{\text{lim}}[A]}{K_M \left(1 + \frac{[I]}{K_{\text{ic}}}\right) + \left(1 + \frac{[I]}{K_{\text{iu}}}\right)[A]} \quad (7)$$

where V_{lim} is the apparent maximal reaction rate, $[A]$ the substrate concentration; $[I]$ the inhibitor concentration; K_M the Michaelis constant for the substrate, K_{ic} and K_{iu} the inhibition constants for the inhibitor (free ATP, ADP or free GTP) derived from the slope and intercept, respectively in a Lineweaver-Burk plot. The data were processed by non-linear regression with the MS Excel program.

RESULTS

Mechanism of reaction catalyzed by NADP-ME

The kinetic mechanism of the reaction catalyzed by the isoform of NADP-ME present in the cytosol of the leaves of *Nicotiana tabacum* L., cv. Petit Havana, SR1 was analyzed by initial rate studies with five various concentrations of NADP^+ at five fixed concentrations of L-malate as sequential (Figs. 1A and 1B). This type

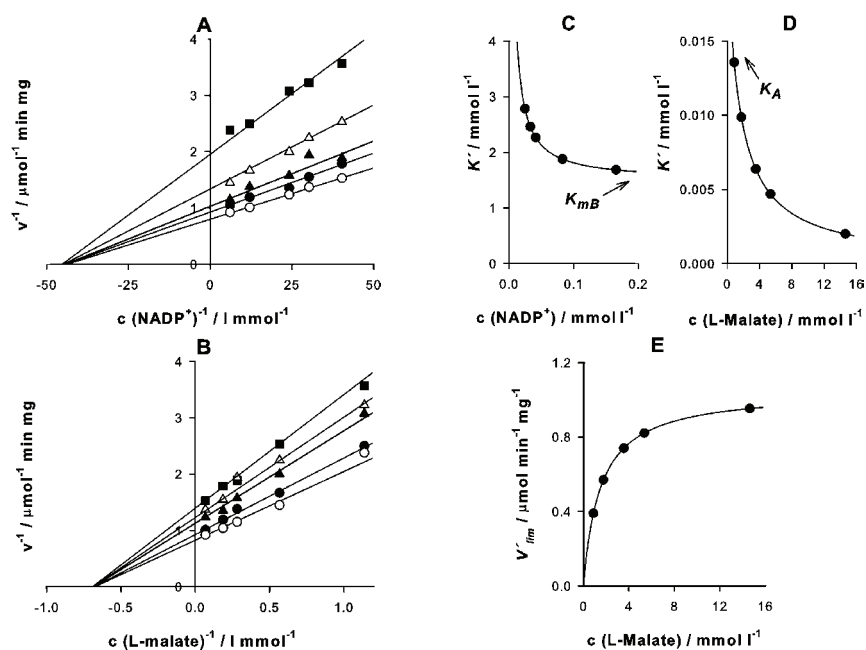


Fig. 1. Double reciprocal plots of the dependence of the reaction rate on the concentration of NADP^+ (A) and L-malate (B) fitted to Eq. (1) and the dependences of the apparent Michaelis constants (K') and constants V_{lim} calculated from Eqs. (2), (3) and (4), respectively, on the concentration of NADP^+ (C) and L-malate (D and E) specified sequential mechanism as ordered. Plot C also indicated the Michaelis constant for substrate B (K_{mB}) and plot D dissociation constant for complex enzyme–substrate A, B (K_A) (both labeled with arrows).

Concentrations of the free (chelation-corrected) NADP^+ : 0.025–0.166 mmol/l;
concentration of free L-malate: 0.879–14.633 mmol/l.

of two-substrate reaction is characterized by all lines intercepting in one point at (or above) the x -axis in a double reciprocal plot (Figs. 1A and 1B). The ping-pong mechanism, characterized by a set of parallel lines in a double reciprocal plot, was excluded. The dependence of the apparent Michaelis constants (K') and V'_{lim} , calculated from Eqs. (2), (3) and (4), respectively, on the concentration of the fixed substrate, was used for an additional specification of the sequential mechanism, which was determined as ordered (Figs. 1C–1E). Fig. 1E (the dependence of the concentration of the on V'_{lim}) indicates that the second substrate binding to the enzyme is L-malate. From determinations of K' at different concentrations of substrate, it is possible to obtain estimations of K_{MB} and K_A (Figs. 1C and 1D).

Inhibition of NADP-ME by macroergic compounds

NADP-ME from tobacco leaves was inhibited by ATP, ADP and GTP. ATP and GTP were stronger inhibitors than ADP (Table I). Detailed inhibition studies were performed with ATP, ADP and GTP as inhibitors with respect to L-malate and $NADP^+$ in the presence of Mg^{2+} or Mn^{2+} as NADP-ME cofactors (Figs. 2–4). The obtained results based on various diagnostic plots of experimental sets of data (double reciprocal plot (Figs. 2–4), the Dixon plot, the Hanes-Woolf plot and the Woolf-Augustinsson-Hoffstee plot (data not shown)) showed that the ATP (GTP, ADP) concentration had to be corrected for Me^{2+} -ATP (Me^{2+} -GTP,

TABLE I. Inhibition constants ($mmol\ l^{-1}$) and types of inhibition of NADP-ME from tobacco leaves by ATP, ADP or GTP with respect to $NADP^+$ or L-malate in the presence of Mg^{2+} or Mn^{2+} as cofactors. Standard deviations from 3 independent measurements are shown. K_{ic} and K_{iu} inhibition constants for the inhibitor: free ATP, ADP or free GTP, derived from slope and intercept, respectively, of Lineweaver-Burk plots, calculated from Eqs. (5)–(7)

Inhibitor with respect to	Constant	Mg^{2+}	Mn^{2+}
		Mixed	
ATP/L-malate	K_{ic}	0.19±0.06	0.053±0.013
	K_{iu}	0.94±0.13	0.39±0.06
ATP/ $NADP^+$	K_i	Non-competitive	
		0.54±0.20	0.40±0.13
ADP/L-malate	K_{ic}	Competitive	
		Mixed	
		0.68±0.15	0.45±0.02
ADP/ $NADP^+$	K_{iu}	Mixed	
		Non-competitive	
		–	2.76±0.64
GTP/L-malate	K_i	Competitive	
		Mixed	
		5.08±0.43	3.58±0.39
GTP/L-malate	K_{ic}	0.23±0.08	0.047±0.025
	K_{iu}	1.65±0.32	0.35±0.10
GTP/ $NADP^+$	K_i	Non-competitive	
		0.70±0.20	0.23±0.03

Mg^{2+} -ADP) complex, because only free ATP (GTP, ADP) was assumed to be the inhibitory species. These results are also in agreement with those of Hsu *et al.*²⁹

ATP, ADP and GTP are non-competitive inhibitors with respect to NADP⁺

The dependences of the enzyme reaction rate on the NADP⁺ concentration were measured in the presence of Mg^{2+} or Mn^{2+} and three concentrations of inhibitors (ATP, GTP or ADP). The lines in the double reciprocal plots of these dependences in all cases intercepted the *x*-axis (Figs. 2C and 2D, 3C and 3D and 4C and 4D), indicating a non-competitive type of inhibition.

This means that macroergic inhibitors (ATP, GTP or ADP) are bound to another site than the binding site for the coenzyme NADP⁺. The relevant inhibi-

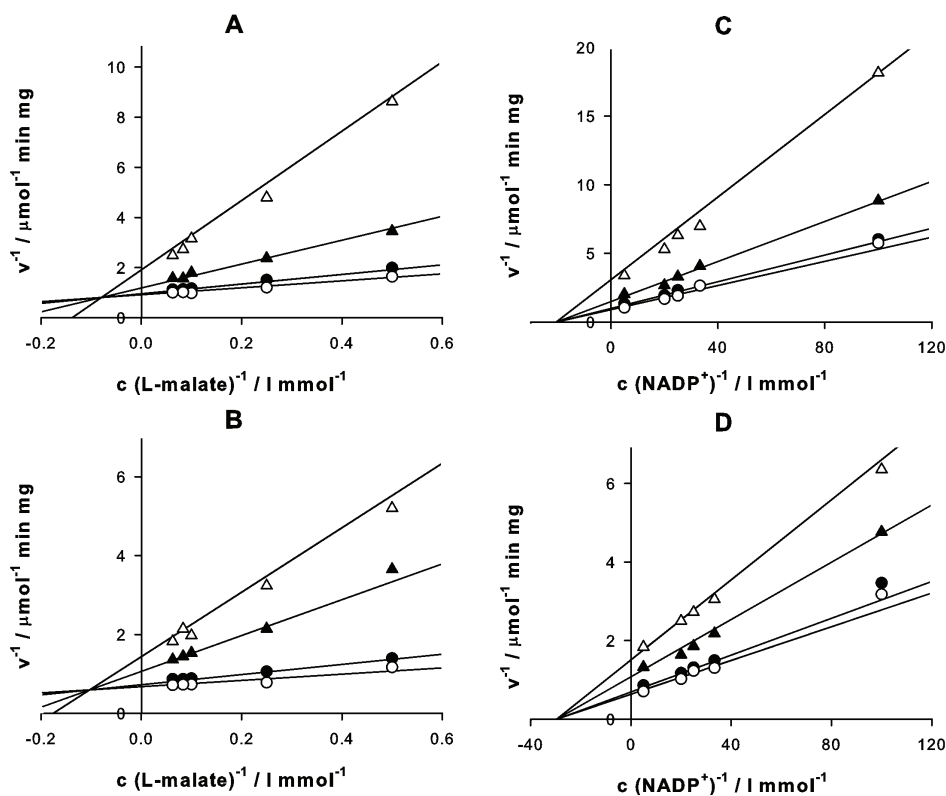


Fig. 2. Mixed and non-competitive type of inhibition of NADP-ME from tobacco leaves by ATP with respect to L-malate and NADP⁺ in the presence of Mg^{2+} (A and C) or Mn^{2+} (B and D). The NADP-ME activity was measured at different concentrations of L-malate (A and B) or NADP⁺ (C and D) at various concentrations of free ATP (from top to bottom, the chelation-corrected free ATP concentrations were 1.090, 0.296, 0.047 and 0 mmol/l in A and C, and 0.402, 0.200, 0.027 and 0 mmol/l in B and D).

The experimental data were fitted to Eqs. (5) and (7).

tion constants are summarized in Table I. $K_{i,ADP(\text{free})}$ in the presence of Mg^{2+} is approximately 10-times higher than $K_{i,ATP(\text{free})}$ and $K_{i,GTP(\text{free})}$, and in the presence of Mn^{2+} , the value of $K_{i,ADP(\text{free})}$ was the highest (7-times higher than $K_{i,ATP(\text{free})}$ and 12-times higher than $K_{i,GTP(\text{free})}$).

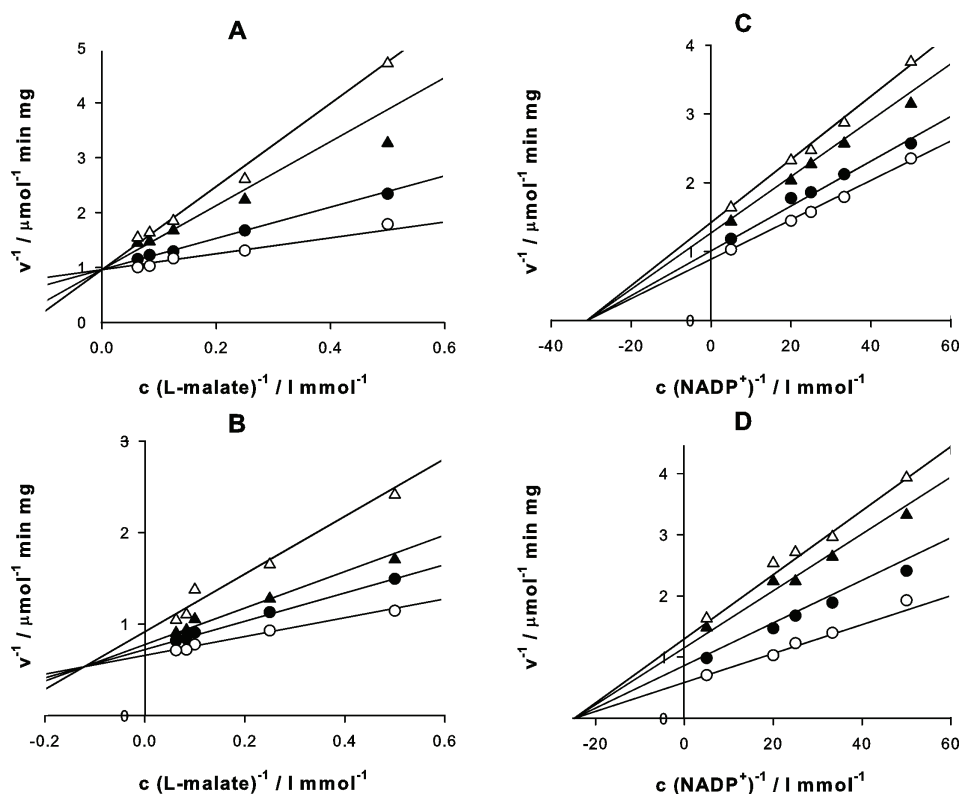


Fig. 3. Competitive, mixed and non-competitive type of inhibition of NADP-ME from tobacco leaves by ADP with respect to L-malate and $NADP^+$ in the presence of Mg^{2+} (A and C) or Mn^{2+} (B and D). The NADP-ME activity was measured at different concentrations of L-malate (A and B) or $NADP^+$ (C and D) at various concentrations of free ADP (from top to bottom, the chelation-corrected free ADP concentrations were 3.238, 2.317, 0.741 and 0 mmol/l in A and C, 1.903, 0.906, 0.510 and 0 in B and 4.901, 3.902, 1.903 and 0 mmol/l in D). The experimental data were fitted to Eqs. (5)–(7).

ATP, ADP and GTP are predominantly mixed inhibitors with respect to L-malate

Detailed kinetic studies of NADP-ME inhibition by ATP (GTP) with respect to L-malate in the presence of Mg^{2+} or Mn^{2+} showed a mixed type of inhibition. In double reciprocal plot, all lines met at a joint intercept left of the ordinate, *i.e.*, they differed in slope and ordinate intercept, because this type of inhibition influences both the apparent Michaelis constant and the maximum rate, Figs. 2A

and 2B; 3A and 3B; 4A and 4B. The two constants, K_{ic} and K_{iu} , characterizing this type of inhibition are summarized in Table I for both inhibitors (ATP and GTP) and cofactors (Mg^{2+} and Mn^{2+}). ADP with respect to L-malate was a milder inhibitor than ATP. Inhibition of NADP-ME by ADP toward L-malate was evaluated as competitive in the presence of Mg^{2+} and mixed in the presence of Mn^{2+} , analogous to the inhibitors ATP and GTP.

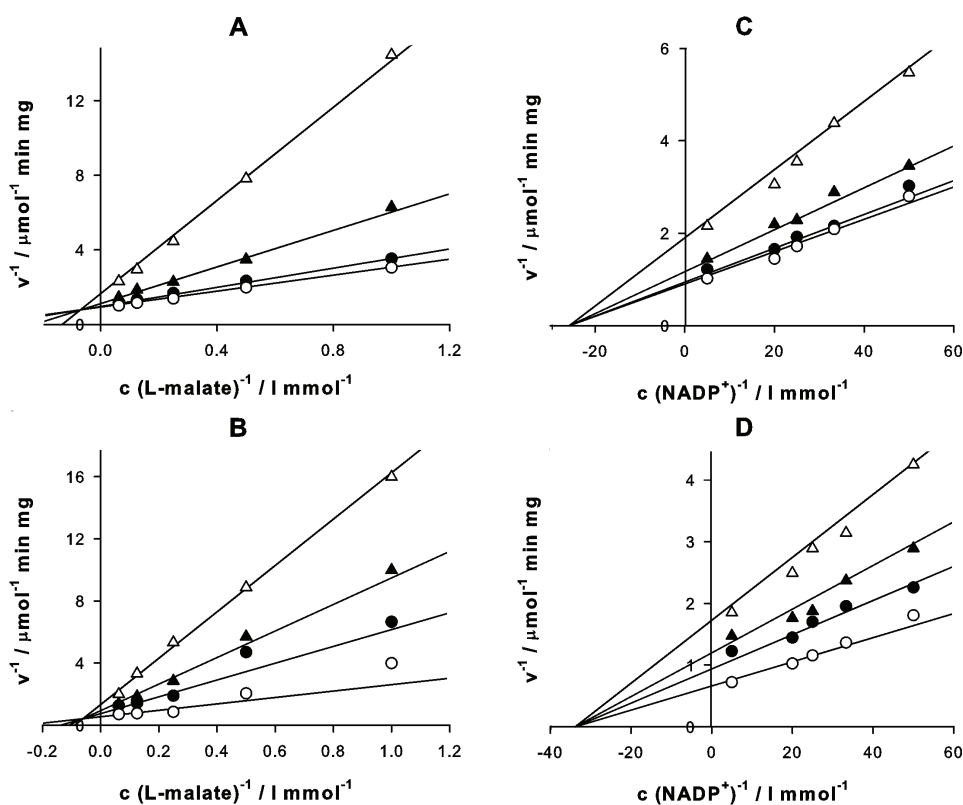


Fig. 4. Mixed and non-competitive type of inhibition of NADP-ME from tobacco leaves by GTP with respect to L-malate and $NADP^+$ in the presence of Mg^{2+} (A and C) or Mn^{2+} (B and D). The NADP-ME activity was measured at different concentrations of L-malate (A and B) or $NADP^+$ (from top to bottom, the chelation-corrected free GTP concentrations were 1.086, 0.289, 0.049 and 0 mmol/l in A and C, and 0.401, 0.202, 0.104 and 0 mmol/l in B and D.

The experimental data were fitted to Eqs. (5) and (7).

Effect of other compounds on the NADP-ME reaction rate

Five groups of compounds important in metabolism were tested as inhibitors or modulators of NADP-ME activity: macroergic compounds (ATP, ADP, and GTP), intermediates of the citric acid cycle (α -ketoglutarate, succinate and fumarate), metabolites of glycolysis (glucose-6-phosphate, 3-phosphoglycerate, phos-

phoenolpyruvate and pyruvate), compounds related to lipogenesis (coenzyme A, acetyl-CoA, palmitoyl-CoA) and some amino acids (glutamate, glutamine, aspartate). The influences of these compounds were tested as possible modulators with respect to L-malate and to NADP⁺ not only at saturation concentrations, but also at subsaturation concentrations to indicate *e.g.* competition between the inhibitor and the NADP-ME substrate. Only the macroergic compounds (ATP, ADP and GTP) significantly affected (inhibited) the reaction rate of NADP-ME. The other compounds, with exception of a slight inhibition effect of intermediates of glycolysis, did not influence the reaction rate of NADP-ME within the frame of standard deviations (Table II).

TABLE II. Effect of different compounds on the reaction rate of NADP-ME from tobacco leaves. The activity of the enzyme is expressed in percentage, control experiment without inhibitors or modulators were taken as 100 %. Standard deviations from 3 independent measurements are shown

Compounds	Composition of the reaction mixture			
	16 mmol/l L-malate 0.2 mmol/l NADP ⁺ 4 mmol/l MgCl ₂	2 mmol/l L-malate 0.2 mmol/l NADP ⁺ 4 mmol/l MgCl ₂	16 mmol/l L-malate 0.05 mmol/l NADP ⁺ 4 mmol/l MgCl ₂	
Macroergic compounds ^a	GTP	59±2	50±2	62±2
	ATP	54±4	46±8	51±2
	ADP	71±8	70±5	78±4
Intermediates of glycolysis ^a	Glucose-6-phosphate	98±4	97±6	100±3
	3-Phosphoglycerate	92±5	84±9	90±5
	Phosphoenolpyruvate	94±6	100±17	85±5
	Pyruvate	97±4	91±2	98±3
Metabolites of citric acid cycle ^a	α-Ketoglutarate	97±2	91±6	101±1
	Succinate	100±4	109±14	104±6
	Fumarate	102±4	103±9	100±4
Compounds related to lipogenesis ^b	Coenzyme A	103±10	103±4	96±5
	Acetyl-CoA	106±4	99±6	97±3
Amino acids ^a	Palmitoyl-CoA	101±2	97±18	95±5
	Glutamate	105±10	104±4	107±17
	Glutamine	102±3	102±6	99±4
	Aspartate	100±2	102±5	101±4

Concentration of tested compounds: ^a5.0 mmol/l; ^b0.10 mmol/l

DISCUSSION

In this study, the mechanism of the reaction catalyzed by the non-photosynthetic NADP-ME from tobacco leaves and its regulation possibilities were investigated.

Although the enzyme is present in tobacco both in the chloroplasts and the cytosol, the enzyme used in this study was most probably the cytosolic isoform, because the chloroplasts were removed during the enzyme isolation (see Experimental, *Enzyme purification*).

It was previously found that the reaction mechanism of cytosolic NADP-MEs is ordered sequential for NADP-ME from pigeon liver and from human breast cancer cell lines^{31,32} but random sequential for mitochondrial (NAD(P)-ME from *Ascaris suum* and from hepatoma tumor cells).^{33,34} The reaction mechanism catalyzed by NADP-ME from tobacco leaves was found to be ordered sequential (Fig. 1). This means that the enzyme binds only one substrate first (substrate A), followed by the binding of substrate B, to form a ternary enzyme–substrate A–substrate B complex.²⁵ With respect to Fig. 1E, which can be used as an indicator of substrate-binding order (a fixed dependence of V_{lim} on a substrate concentration is associated with the second substrate to bind the enzyme)²⁵ and from results shown in Figs. 1C and 1D, it is supposed that NADP⁺ is the leading substrate, followed by L-malate. This mechanism is in agreement with the results published for animal cytosolic NADP-ME.^{31,32} The kinetic mechanism for plant NADP-ME was studied only for photosynthetic chloroplastic NADP-ME from maize leaves and an ordered sequential mechanism was also determined.³⁵

In the present study, the regulation of cytosolic NADP-ME from tobacco leaves by cell metabolites, the most important of which were ATP, GTP and ADP (Table II), was also investigated. ATP was previously found to be an inhibitor for all NADP-ME isoenzymes of *Arabidopsis thaliana* and both chloroplastic and cytosolic ones of *Nicotiana tabacum* L. plants.^{17,22} The inhibition was characterized in detail by the type of inhibition and the inhibition constants (Figs. 2–4, Table I). A non-competitive inhibition of NADP-ME by ATP, GTP and the ADP with respect to NADP⁺ and a predominantly mixed inhibition by ATP, GTP and ADP with respect to L-malate in the presence of Mg²⁺ or Mn²⁺ were established. The type of inhibition of human m-NAD-ME by ATP toward NAD⁺ and L-malate was reported to be competitive in both cases.²⁹ Free ATP (GTP, ADP, respectively) was assumed to be the inhibiting species of both tobacco NADP-ME (by evaluating the various diagnostic plots) and of human m-NAD-ME (from structural studies).²⁹ Divalent metal ions (cofactors) significantly influenced the inhibition constants. The values of $K_{i,ATP(free)}$, $K_{i,GTP(free)}$ and $K_{i,ADP(free)}$ for non-competitive inhibition by ATP (GTP, ADP) toward NADP⁺ were lower in the presence of Mn²⁺ than in the presence of Mg²⁺; this means that ATP (GTP, ADP) is a stronger inhibitor in the presence of Mn²⁺ as the cofactor. Also, the $K_{ic,ATP(GTP)free}$ and $K_{iu,ATP(GTP)free}$ constants of the mixed type of inhibition by ATP (GTP) to L-malate were lower in the presence of Mn²⁺ than in the presence of Mg²⁺. The only exception was the inhibition by ADP with respect to L-malate,

which is, however, competitive in the presence of Mg^{2+} and mixed in the presence of Mn^{2+} .

The structural derivate of $NADP^+$, β -nicotinamide mononucleotide had no effect on the activity of tobacco NADP-ME (data not shown), suggesting that the adenosine diphosphate part of the molecule is important for $NADP^+$ binding.

Regulation of NADP-ME from tobacco leaves by its cofactors was studied previously.²³ Not only Mg^{2+} and Mn^{2+} , but also Co^{2+} and Ni^{2+} were found to be cofactors of NADP-ME. The dependence of the reaction rates on the Mg^{2+} , Mn^{2+} , Co^{2+} and Ni^{2+} concentrations does not correspond to Michaelis-Menten kinetics. Two binding sites were determined for Mg^{2+} and binding of Mn^{2+} caused a strong positive cooperation.²³ NADP-ME from tobacco leaves was not regulated *via* inhibition by L-malate, which is a characteristic trait for C_3 plants.²

Other metabolites, such as intermediates of glycolysis, intermediates of the citric acid cycle, compounds related to lipogenesis and amino acids, did not affect significantly the activity of cytosolic NADP-ME from tobacco leaves, neither at saturation nor subsaturation concentrations of the substrate or coenzyme (Table II). Mild inhibition was observed with 3-phosphoglycerate (Table II). Müller *et al.*¹⁷ obtained slightly different results, *i.e.*, pyruvate, glucose-6-phosphate, fumarate, succinate and oxaloacetate inhibited recombinant cytosolic tobacco NADP-ME. The reason lies in the different experimental conditions (especially the substrate and coenzyme concentrations, the employed buffer and its concentration, pH). Furthermore, the recombinant protein could be differently folded compared with protein isolated from plant material. Oxaloacetate was not tested in this study because this compound could also be a substrate and could be decarboxylated in a reaction catalyzed by NADP-ME. The regulation of NADP-ME by cell metabolites depended on the particular isoform; chloroplastic NADP-ME was activated by aspartate, while the cytosolic one was not.¹⁷ The regulation of NADP-ME isoenzymes in *Arabidopsis thaliana* was different but all isoenzymes were inhibited by ATP.²²

NADP-ME from germinating *Ricinus communis* cotyledons was activated by coenzyme A, acetyl-CoA, palmitoyl-CoA and succinate. Therefore, cotyledon NADP-ME was suggested to play a role in the metabolism of fatty acids.³⁶

The regulation of NADP-ME by macroergic compounds (ATP, ADP and GTP) (Figs. 2–4) and the slight inhibition by intermediates of glycolysis (Table II) indicate that the enzyme could participate in maintaining the energy balance in the plant. It could be more important under stress than under physiological conditions. Higher activity of NADP-ME caused by viral infection⁹ and by abiotic stress factors in plants were found.^{6–8,10–17}

In regard to the significance of NADP-ME in plant defense response, and the quite different regulation of NADP-ME in respective organism, cells and cell compartments, it is important to bring new information into this field.

CONCLUSIONS

The kinetic mechanism of reactions catalyzed by cytosolic NADP-ME from tobacco leaves was determined as ordered sequential. This enzyme was inhibited by ATP, GTP and ADP; the type of inhibition was non-competitive toward NADP⁺ and predominantly mixed toward L-malate.

Other cell metabolites, such as intermediates of the citric acid cycle, amino acids and compounds related to fatty acids metabolism did not significantly affect the activity of cytosolic NADP-ME from tobacco leaves, neither in saturation nor in subsaturation concentrations of L-malate and NADP⁺.

ABBREVIATIONS

CAM	– Crassulacean acids metabolism
C ₃ plant	– A plant that produces the 3-carbon compound 3-phosphoglyceric acid as the first photosynthetic product
C ₄ plant	– A plant that produces the 4-carbon compound oxaloacetic acid as the first photosynthetic product
MOPS	– 3-Morpholinopropanesulfonic acid
NADP-ME	– NADP-dependent malic enzyme EC 1.1.1.40

ИЗВОД

РЕГУЛАЦИЈА И МЕХАНИЗАМ КАТАЛИЗЕ NADP-МАЛАТНОГ ЕНЗИМА ИЗ ЛИСТА ДУВАНА

VERONIKA DOUBNEROVÁ, LUCIE POTŮČKOVÁ, KAREL MÜLLER и HELENA RYŠLAVÁ

Department of Biochemistry, Faculty of Science, Charles University, Hlavova 2030, CZ-128 40 Prague 2, Czech Republic

Из листа *Nicotiana tabacum* L. је изолован нефотосинтетишући NADP-малатни ензим EC 1.1.1.40 (NADP-ME), који катализује оксидативну декарбоксилацију L-малата и стварање пирувата и NADPH, укључених у одбрамбени одговор биљке. Механизам ензимске реакције је проучаван методом почетне брзине, за коју је нађено да је првог реда. Испитане су могућности регулације пречишћеног цитосолног NADP-ME ћелијским метаболитима. На активност NADP-ME из листа дувана нису значајно утицали интермедијери циклуса лимунске киселине (α -кетоглутарат, сукцинат, фумарат), метаболити гликолизе (пируват, фосфоенол-пируват, глукоза-6-фосфат), једињења која учествују у липогенези (коензим А, ацетил-СоА, палмитоил-СоА), и неке аминокиселине (глутамат, глутамин, аспартат). Супротно томе, једињења GTP, ATP и ADP су јаки инхибитори NADP-ME; тип и константа инхибиције су одређени у присуству најефикаснијих кофактора NADP-ME (Mn²⁺ и Mg²⁺). Констатован је претежно некомпетитивни тип инхибиције NADP-ME у односу на NADP⁺ и мешовити тип у односу на L-малат.

(Примљено 5. фебруара, ревидирано 7. маја 2009)

REFERENCES

1. G. E. Edwards, C. S. Andreo, *Phytochemistry* **31** (1992) 1845
2. M. F. Drincovich, P. Casati, C. S. Andreo, *FEBS Lett.* **490** (2001) 1
3. R. T. Wedding, *Plant Physiol.* **90** (1989) 367

4. Z. Yang, H. Zhang, H.-C. Hung, C.-C. Kuo, L.-C. Tsai, H. S. Yuan, W.-Y. Chou, G. G. Chang, L. Tong, *Protein Sci.* **11** (2002) 332
5. M. M. Laporte, B. Shen, M. C. Tarczynski, *J. Exp. Bot.* **53** (2002) 699
6. V. G. Maurino, M. Saigo, C. S. Andreo, M. F. Drincovich, *Plant Mol. Biol.* **45** (2001) 409
7. H. Synková, R. Valcke, *Physiol. Plant.* **112** (2001) 513
8. F. Crecelius, P. Streb, J. Feierabend, *J. Exp. Bot.* **54** (2003) 1075
9. H. Ryšlavá, K. Muller, Š. Semorádová, H. Synková, N. Čeřovská, *Photosynthetica* **41** (2003) 357
10. S.-B. Sun, Q.-R. Shen, J.-M. Wan, Z.-P. Liu, *Acta Biochim. Biophys. Sinica* **35** (2003) 423
11. H. Synková, Š. Semorádová, L. Burketová, *Plant Cell Tissue Organ. Cult.* **79** (2004) 169
12. W. Chi, J. Yang, N. Wu, F. Zhang, *Biosci. Biotechnol. Biochem.* **68** (2004) 1865
13. K. Smeets, A. Cuypers, A. Lambrechts, B. Semane, P. Hoet, A. Van Laere, J. Vangronsveld, *Plant Physiol. Biochem.* **43** (2005) 437
14. S. Saher, N. Fernández-García, A. Piqueras, E. Hellín, E. Olmos, *Plant Physiol. Biochem.* **43** (2005) 573
15. R. Valderrama, F. J. Corpas, A. Carreras, M. V. Gómez-Rodríguez, M. Chaki, J. R. Pedrajas, A. Fernández-Ocana, L. A. Del Río, J. B. Barroso, *Plant Cell Environ.* **29** (2006) 1449
16. S. Liu, Y. Cheng, X. Zhang, Q. Guang, S. Nishiuchi, K. Hase, T. Takano, *Plant Mol. Biol.* **64** (2007) 49
17. G. L. Müller, M. F. Drincovich, C. S. Andreo, M. V. Lara, *Plant Cell Physiol.* **49** (2008) 469
18. Y. Xu, G. Bhargava, H. Wu, G. Loeber, L. Tong, *Structure* **7** (1999) 877
19. G. Bukato, Z. Kochan, J. Swierczyński, *Int. J. Biochem. Cell Biol.* **27** (1995) 47
20. M. C. Gerrard Wheeler, M. A. Tronconi, M. F. Drincovich, C. S. Andreo, U. I. Flüge, V. G. Maurino, *Plant Physiol.* **139** (2005) 39
21. S.-L. Tausta, H. M. Coyle, B. Rothermael, V. Stiefel, T. Nelson, *Plant Mol. Biol.* **50** (2002) 635
22. M. C. Gerrard Wheeler, C. L. Arias, M. A. Tronconi, V. G. Maurino, C. S. Andreo, M. F. Drincovich, *Plant Mol. Biol.* **67** (2008) 231
23. H. Ryšlavá, V. Doubnerová, K. Muller, P. Bařková, R. Schnablová, J. Liberda, H. Synková, N. Čeřovská, *Collect. Czech. Chem. Commun.* **72** (2007) 1420
24. S. D. Grover, P. F. Canellas, R. T. Wedding, *Arch. Biochem. Biophys.* **209** (1981) 396
25. A. G. Marangoni, *Enzyme kinetics. A modern approach*, Wiley, Hoboken, NJ, 2003, p. 90
26. H. Sigel, E. M. Bianchi, N. A. Corfu, Y. Kinjo, R. Tribolet, R. B. Martin, *Chem. Eur. J.* **7** (2001) 3729
27. H. Sigel, *Pure Appl. Chem.* **76** (2004) 375
28. E. M. Bianchi, S. A. S. Sajadi, B. Song, H. Sigel, *Chem. Eur. J.* **9** (2003) 881
29. W.-C. Hsu, H.-C. Hung, L. Tong, G.-G. Chang, *Biochemistry* **43** (2004) 7382
30. H. Bisswanger, *Enzyme kinetics. Principles and methods*, Wiley-VCH Verlag GmbH, Weinheim, 2002, p. 80
31. R. Y. Hsu, H. A. Lardy, W. W. Cleland, *J. Biol. Chem.* **242** (1967) 5315
32. G.-G. Gang, T.-M. Huang, J.-K. Wang, H.-J. Lee, W.-Y. Chou, C.-L. Meng, *Arch. Biochem. Biophys.* **296** (1992) 468
33. J. K. Teller, L. A. Fahien, J. W. Davis, *J. Biol. Chem.* **267** (1992) 10423
34. D. F. Aktas, P. F. Cook, *Biochemistry* **47** (2008) 2539
35. C. P. Spampinato, C. S. Andreo, *Photosynth. Res.* **43** (1995) 1
36. S. L. Colombo, C. S. Andreo, F. E. Podestá, *Physiol. Plant.* **101** (1997) 821.



J. Serb. Chem. Soc. 74 (8–9) 907–915 (2009)
JSCS–3886

Journal of
the Serbian
Chemical Society

JSCS@tmf.bg.ac.rs • www.shd.org.rs/JSCS

UDC 546.712'732:547.495.1/2:615.281

Original scientific paper

Spectroscopic, thermal and antibacterial studies on Mn(II) and Co(II) complexes derived from thiosemicarbazone

SULEKH CHANDRA^{1*}, MONIKA TYAGI¹ and MOAMEN S. REFAT²

¹Department of Chemistry, Zakir Husain College, University of Delhi, JLN-Marg, New Delhi - 110002, India and ²Department of Chemistry, Faculty of Science, Port-Said, Suez Canal University, Port-Said, Egypt

(Received 1 December 2008, revised 15 April 2009)

Abstract: Mn(II) and Co(II) complexes having the general composition $[M(L)_2X_2]$ (where L = 2-pyridinecarboxaldehyde thiosemicarbazone, M = Mn(II) and Co(II), X = Cl⁻ and NO₃⁻) were synthesized. All the metal complexes were characterized by elemental analysis, molar conductance, magnetic susceptibility measurements, mass, IR, EPR, electronic spectral studies and thermogravimetric analysis (TG). Based on the spectral studies, an octahedral geometry was assigned for all the complexes. Thermal studies of the compounds suggest that the complexes are more stable than the free ligand. This fact was supported by the kinetic parameters calculated using the Horowitz–Metzger (H–M) and Coats–Redfern (C–R) equations. The antibacterial properties of the ligand and its metal complexes were also examined and it was observed that the complexes are more potent bactericides than the free ligand.

Keywords: thiosemicarbazone; Mn(II) and Co(II) complexes; thermal; antibacterial studies.

INTRODUCTION

During the last two decades, thiosemicarbazones have emerged as an important class of sulphur donor ligands for transition metal ions. The interest in the development of the coordination chemistry of thiosemicarbazones is due to their biological and medicinal properties.¹ They present a variety of biological activities ranging from antitumour, antifungal, antibacterial, anticancer anti-inflammatory and antiviral activities.^{2–10} The bacterial and fungicidal activities of transition metal complexes are due to the formation of chelates with the essential metal ions bonding through the nitrogen and the sulphur donor atom of the ligand. The activity of these compounds is also dependent on the nature of the heteroaromatic ring and the position of attachment to the ring, as well as the form of the thiosemicarbazone moiety.^{11,12} Manganese(II) and cobalt(II) complexes of

* Corresponding author. E-mail: schandra_00@yahoo.com; mnk02tyg@yahoo.co.in
doi: 10.2298/JSC0909907C

thiosemicarbazones have been reported as compounds that present biological activity.^{13–15}

In view of the above applications, a spectroscopic, thermal and antimicrobial study of 2-pyridinecarboxaldehyde thiosemicarbazone (L) and its Mn(II), and Co(II) complexes is presented in this paper. The structure of the free ligand is shown in Fig. 1.

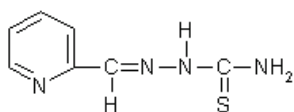


Fig. 1. Structure of the ligand (L).

EXPERIMENTAL

All the employed chemicals were of analytical grade and procured from Sigma-Aldrich and Fluka. The metal salts were purchased from Merck and were used as received.

Synthesis of ligand

A hot ethanolic solution (20 ml) of thiosemicarbazide (4.55 g, 0.0500 mol) and an ethanolic solution (20 ml) of 2-pyridinecarboxaldehyde (4.75 ml, 0.0500 mol) were mixed slowly under constant stirring. This mixture was refluxed at 75–80 °C for 4 h. On cooling, a white coloured compound precipitated out, which was filtered, washed with cold EtOH and dried under vacuum over P₄O₁₀. Yield: 68 %; m.p. 180 °C. Anal. Calcd. for C₇H₈N₄S (FW = 180): C, 46.67; H, 4.45; N, 31.11 %. Found: C, 46.62; H, 4.49; N, 31.20 %.

Synthesis of the complexes

A hot ethanolic (20 ml) solution of the ligand (0.36 g, 0.0020 mol) and an ethanolic (20 ml) solution of the required metal salt (MnCl₂·4H₂O, Mn(NO₃)₂·2H₂O, CoCl₂·6H₂O, Mn(NO₃)₂·2H₂O (0.0010 mol) were mixed together under constant stirring. This reaction mixture was refluxed for 3–4 h at 70–80 °C. The completion of the reaction was confirmed by TLC using ethanol and acetone in a 2:1 ratio as the solvent and silica gel as the adsorbent. The reaction mass was degassed on a rotary-evaporator over a water bath. On cooling, a coloured complex separated out, which was filtered, washed and recrystallized from 50 % ethanol and dried under vacuum over P₄O₁₀.

Physical measurements

C and H were analyzed on a Carlo–Erba EA 1106 elemental analyzer. The nitrogen content of the complexes was determined using the Kjeldahl method.¹⁶ The content of manganese was determined gravimetrically as Mn₂P₂O₇ and cobalt volumetrically using Xylol Orange as the indicator.¹⁷ The molar conductance was measured on an Elico CM82T conductivity bridge. The magnetic susceptibility was measured at room temperature on a Gouy balance using CuSO₄·5H₂O as the calibrant. Correction for diamagnetism was realised using Pascal constants. The electronic impact mass spectrum was recorded on a JEOL, JMS-DX-303 mass spectrometer. The ¹H-NMR spectra of the ligand was recorded at room temperature on a Bruker Advance DPX-300 spectrometer using DMSO-*d*₆ as the solvent. The IR spectra were recorded as KBr pellets on a FTIR BX-II spectrophotometer. The electronic spectra were recorded in DMSO on a Shimadzu UV mini-1240 spectrophotometer. The EPR spectra of the Mn(II) complexes were recorded as polycrystalline sample at room temperature and the Co(II) complexes at liquid nitrogen temperature on an E₄-EPR spectrometer using DPPH as the

g-marker. The thermogravimetric curves were obtained using a Shimadzu TG-50H instrument under a N₂ atmosphere at a heating rate of 15 °C min⁻¹.

RESULTS AND DISCUSSION

Based on elemental analyses, the complexes were found to have the composition shown in Table I. The molar conductance measurements of the complexes in DMSO corresponded to non-electrolytes. Thus, these complexes may be formulated as [M(L)₂X₂] [where M = Mn(II) or Co(II), L = 2-pyridinecarboxaldehyde thiosemicarbazone and X = Cl⁻ or NO₃⁻]. The electron-impact mass spectrum of the ligand is shown in Fig 2. The IR spectra (KBr, cm⁻¹) of the ligand displayed a highest frequency band at 3433 cm⁻¹, which can be assigned to the asymmetric ν(N-H) vibration of the terminal NH₂ group. The other bands at 3261 and 3156 cm⁻¹ may be due to the symmetric ν(N-H) vibrations of the imino and amino groups. The other important IR bands of the ligand and their metal complexes are given in Table II.

TABLE I. Molar conductance and elemental analysis data of the complexes

Complex	Molar conductance S cm ² mol ⁻¹	Colour	M.p. °C	Yield %	Elemental analysis			
					Found (Calcd.), %			
					M	C	H	N
[Mn(L) ₂ Cl ₂]	16	Cream	285	65	11.28	34.50	3.24	23.08
MnC ₁₄ H ₁₆ N ₈ S ₂ Cl ₂					(11.32)	(34.57)	(3.29)	(23.04)
[Mn(L) ₂ (NO ₃) ₂]	12	Cream	289	62	10.16	31.14	2.92	25.92
MnC ₁₄ H ₁₆ N ₁₀ S ₂ O ₆					(10.20)	(31.17)	(2.97)	(25.97)
[Co(L) ₂ Cl ₂]	17	Light pink	298	59	12.06	34.25	3.23	22.82
CoC ₁₄ H ₁₆ N ₈ S ₂ Cl ₂					(12.02)	(34.29)	(3.26)	(22.86)
[Co(L) ₂ (NO ₃) ₂]	20	Shiny pink	295	62	10.82	30.96	2.99	25.72
CoC ₁₄ H ₁₆ N ₁₀ S ₂ O ₆					(10.85)	(30.94)	(2.95)	(25.78)

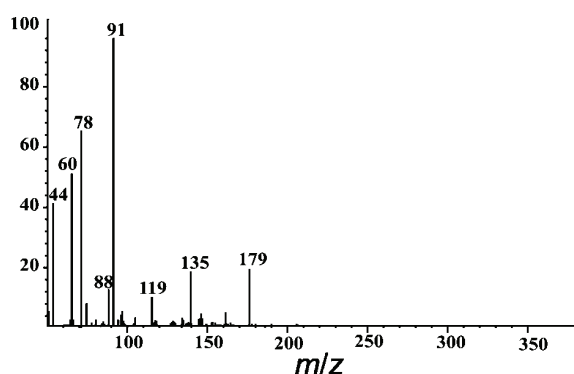


Fig. 2. Electron impact mass spectrum of the ligand (L).

The magnetic moment of the Mn(II) complexes lay in the range 5.92–5.98 μ_B, corresponding to five unpaired electrons. At room temperature, the magnetic moment of the Co(II) complexes lay in the range 4.85–4.90 μ_B, corresponding to

TABLE II. IR Spectral data (cm⁻¹) of ligand and its metal complexes

Compound	$\nu(\text{C}=\text{N})$	$\nu(\text{Py}-\text{N})$	$\nu(\text{C}=\text{S})$	$\nu(\text{M}-\text{N})$
L	1610	559	742	--
[Mn(L) ₂ Cl ₂]	1590	575	742	440
[Mn(L) ₂ (NO ₃) ₂]	1595	572	742	448
[Co(L) ₂ Cl ₂]	1587	580	742	452
[Co(L) ₂ (NO ₃) ₂]	1592	585	742	445

three unpaired electrons (Table III). The electronic spectra of the Mn(II) complexes exhibited four weak intensity absorption bands in the ranges of 533–546, 433–439, 361–364 and 261–274 nm. These bands may be assigned to the transitions: ${}^6\text{A}_{1g} \rightarrow {}^4\text{T}_{1g}$ (${}^4\text{G}$), ${}^6\text{A}_{1g} \rightarrow {}^4\text{E}_g$, ${}^4\text{A}_{1g}$ (${}^4\text{G}$) (10B + 5C), ${}^6\text{A}_{1g} \rightarrow {}^4\text{E}_g$ (${}^4\text{D}$) (17B + 5C) and ${}^6\text{A}_{1g} \rightarrow {}^4\text{T}_{1g}$ (${}^4\text{P}$) (7B + 7C), respectively.^{18,19} The positions of these bands suggest an octahedral geometry around the Mn(II) ion. The electronic spectra of the Co(II) complexes, recorded in DMSO solution, exhibited absorption in the ranges of 962–965, 679–696 and 533–539 nm. These bands may be assigned to the transitions: ${}^4\text{T}_{1g}$ (F) \rightarrow ${}^4\text{T}_{2g}$ (F), ${}^4\text{T}_{1g} \rightarrow {}^4\text{A}_{2g}$ and ${}^4\text{T}_{1g}$ (F) \rightarrow ${}^4\text{T}_{1g}$ (P), respectively.^{20,21} The position of these bands suggests an octahedral environment around the Co(II) ion. The EPR spectra of the Mn(II) and Co(II) complexes were recorded as polycrystalline samples and in DMSO solution at room temperature and liquid nitrogen temperature, respectively. The polycrystalline spectra of the Mn(II) complexes gave an isotropic signal centered at approximately the free electron g -value ($g_0 = 2.0023$). The broadening of the spectra is probably due to spin relaxation. In DMSO solution, the complexes gave six well-resolved lines due to hyperfine interaction between the unpaired electrons with the Mn nucleus ($I = 5/2$). In the spectra of the Co(II) complexes, the g -va-

TABLE III. Magnetic moments and electronic spectral data of the complexes

Complexes	μ_{eff}/μ_B	$\lambda_{\text{max}}/\text{nm}$	$\epsilon/\text{l mol}^{-1}\text{ cm}^{-1}$	Assignments
[Mn(L) ₂ Cl ₂]	5.98	546	30	${}^6\text{A}_{1g} \rightarrow {}^4\text{T}_{1g}$ (${}^4\text{G}$)
		439	41	${}^6\text{A}_{1g} \rightarrow {}^4\text{E}_g, {}^4\text{A}_{1g}$ (${}^4\text{G}$) (10B+5C)
		364	112	${}^6\text{A}_{1g} \rightarrow {}^4\text{E}_g$ (${}^4\text{D}$) (17B+5C)
		261	132	${}^6\text{A}_{1g} \rightarrow {}^4\text{T}_{1g}$ (${}^4\text{P}$) (7B+7C)
[Mn(L) ₂ (NO ₃) ₂]	5.92	533	34	${}^6\text{A}_{1g} \rightarrow {}^4\text{T}_{1g}$ (${}^4\text{G}$)
		433	48	${}^6\text{A}_{1g} \rightarrow {}^4\text{E}_g, {}^4\text{A}_{1g}$ (${}^4\text{G}$) (10B+5C)
		361	119	${}^6\text{A}_{1g} \rightarrow {}^4\text{E}_g$ (${}^4\text{D}$) (17B+5C)
		275	136	${}^6\text{A}_{1g} \rightarrow {}^4\text{T}_{1g}$ (${}^4\text{P}$) (7B+7C)
[Co(L) ₂ Cl ₂]	4.85	965	56	${}^4\text{T}_{1g}$ (F) \rightarrow ${}^4\text{T}_{2g}$ (F)
		696	72	${}^4\text{T}_{1g} \rightarrow {}^4\text{A}_{2g}$
[Co(L) ₂ (NO ₃) ₂]	4.90	533	87	${}^4\text{T}_{1g}$ (F) \rightarrow ${}^4\text{T}_{1g}$ (P)
		962	61	${}^4\text{T}_{1g}$ (F) \rightarrow ${}^4\text{T}_{2g}$ (F)
		679	75	${}^4\text{T}_{1g} \rightarrow {}^4\text{A}_{2g}$
		539	92	${}^4\text{T}_{1g}$ (F) \rightarrow ${}^4\text{T}_{1g}$ (P)

lues were found to be almost the same in both the polycrystalline sample and in solution. This indicates that the complexes had the same geometry in the solid form as in solution (Table IV). Based on of above spectral studies, the structures shown in Fig. 3 may be suggested for the complexes.

TABLE IV. EPR Spectral data of the complexes

Complexes	Temp.	g_{\parallel}	g_{\perp}	g_{iso}	A^0
[Mn(L) ₂ Cl ₂]	RT	–	–	1.9980	109.65
[Mn(L) ₂ (NO ₃) ₂]	RT	–	–	2.0178	112.82
[Co(L) ₂ Cl ₂]	LNT	2.7090	1.8060	2.1070	–
[Co(L) ₂ (NO ₃) ₂]	LNT	2.4951	1.8301	2.0517	–

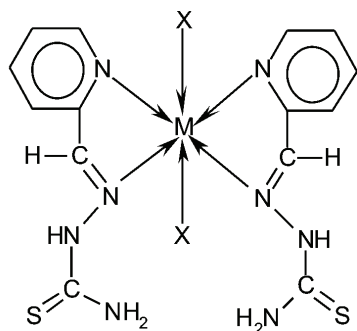


Fig. 3. Suggested structures of the complexes.

Thermogravimetric analysis

The thermal analysis data of the ligand and its metal complexes are given in Table V.

TABLE V. Thermogravimetric results (TG and DTG) for the ligand and its complexes

Compound	Stage	Temperature range, °C	DTG _{max} °C	Residual species	Decomposition species	Total losses, %	
						Found	Calc.
Ligand (L)	1 st	270–800	310	C	C ₂ H ₂ + N ₂ + S	93.30	93.34
	2 nd		600				
	3 rd		725				
[Mn(L) ₂ Cl ₂]	1 st	40–800	216	MnS	7C ₂ H ₂ + Cl ₂ + 4N ₂ + H ₂ S	83.06	82.11
	2 nd		463				
	3 rd		603				
[Mn(L) ₂ (NO ₃) ₂]	1 st	200–800	260	MnO ₂	7C ₂ H ₂ + SO ₂ + 2NO + 4N ₂ + H ₂ S	84.63	83.87
	2 nd		443				
	3 rd		562				
[Co(L) ₂ Cl ₂]	1 st	78–800	145	CoS	7C ₂ H ₂ + Cl ₂ + 4N ₂ + H ₂ S	81.32	81.44
	2 nd		436				
	3 rd		699				
[Co(L) ₂ (NO ₃) ₂]	1 st	59–800	195	CoSO ₄	7C ₂ H ₂ + 2NO + 4N ₂ + H ₂ S	72.19	71.46
	2 nd		480				
	3 rd		628				

Kinetic Parameters. Two methods mentioned in the literature related to decomposition kinetics studies were applied in this study, i.e., the Coats–Redfern²² and Horowitz–Metzger²³ method.

The Coats–Redfern equation (1), which is a typical integral method, can be represented as:

$$\int_0^{\infty} \frac{d\alpha}{(1-\alpha)^n} = \frac{A}{\varphi} \int_{T_1}^{T_2} e^{-\frac{E^*}{RT}} dT \quad (1)$$

For convenience of integration, the lower limit, T_1 , is usually taken as zero. This equation on integration gives:

$$\ln(-\ln(1-\alpha)/T^2) = -E^*/RT + \ln(AR/\Phi e) \quad (2)$$

A plot of the left-hand side (LHS) against $1/T$ was drawn. E^* is the energy of activation in kJ mol^{-1} and is calculated from the slope, and A in s^{-1} from the intercept. The entropy of activation, ΔS^* in $\text{J K}^{-1} \text{mol}^{-1}$, was calculated from the equation:

$$\Delta S^* = R \ln(Ah/kT_s) \quad (3)$$

where k is the Boltzmann constant, h is the Plank constant and T_s is the DTG peak temperature.

The Horowitz–Metzger Equation was written in the form:

$$\log(\log(w_\alpha/w_\gamma)) = E^*\theta/2.303RT_s^2 - \log 2.303 \quad (4)$$

where $\theta = T - T_s$, $w_\gamma = w_\alpha - w$; w_α is the mass loss at the completion of the reaction; w is the mass loss up to time t . From the slope of the linear plot of $\log(\log(w_\alpha/w_\gamma))$ vs. θ , the value of E^* is calculated. The pre-exponential factor, A , is calculated from the equation:

$$E^*\theta/RT_s^2 = A/[\varphi \exp(-E^*/RT_s)] \quad (5)$$

The entropy of activation, ΔS^* , enthalpy of activation, ΔH^* , and Gibbs free energy, ΔG^* , are calculated from:

$$\Delta H^* = E^* - RT \text{ and } \Delta G^* = \Delta H^* - T\Delta S^*$$

The kinetic parameters for the main degradation stages around 700–740 K (decomposition of the ligand) obtained employing the Coats–Redfern and Horowitz–Metzger equations are summarized in Table VI together with the radii of the metal ions. The results show that the values obtained by various methods are comparable. The activation energy of the Mn(II) and Co(II) complexes is expected to increase in relation with the decrease in their radius. The E^* values calculated using the Coats–Redfern method for the definite decomposition stages of the complexes are: $E^*(\text{Mn(II)}) = 1.70 \times 10^5 \text{ kJ mol}^{-1} > E^*(\text{Co(II)}) = 1.24 \times 10^5 \text{ kJ mol}^{-1}$; $r(\text{Mn(II)}) = 46.0 \text{ pm} < r(\text{Co(II)}) = 74.5 \text{ pm}$.

TABLE VI. Thermal behaviour and kinetic parameters determined using the Coats–Redfern (C–R) and Horowitz–Metzger (H–M) method

Compound	Radius pm	T_s K	Method	E^* kJ mol ⁻¹	A s ⁻¹	ΔS^* J K ⁻¹ mol ⁻¹	ΔH^* kJ mol ⁻¹	ΔG^* kJ mol ⁻¹	R
Ligand (L)	–	583	CR	139	25.4	–0.513	134	164	0.9513
			HM	143	86.4	–0.411	138	162	0.9506
[Mn(L) ₂ Cl ₂]	46.0	736	CR	170	1.44×10 ⁶	–1.35	114	213	0.9855
			HM	167	7.98×10 ⁶	–1.20	121	210	0.9814
[Mn(L) ₂ (NO ₃) ₂]		716	CR	178	20.1	–0.550	172	212	0.9906
			HM	188	5.94×10 ¹¹	–0.268	182	202	0.9916
[Co(L) ₂ Cl ₂]	74.5	709	CR	124	7.76×10 ⁹	–0.628	158	203	0.9962
			HM	135	8.15×10 ¹⁰	–0.432	169	199	0.9955
[Co(L) ₂ (NO ₃) ₂]		753	CR	131	6.15×10 ⁶	–1.23	124	217	0.9954
			HM	149	1.74×10 ⁸	–0.994	143	214	0.9920

Antibacterial studies

The antibacterial action of the ligand and its Mn(II) and Co(II) complexes was measured by the disc diffusion method^{24–27} against the bacterial species: *Staphylococcus aureus*, *Pseudomonas striata* and *Escherchia coli*. Sterilized nutrient agar media (NA) (25 ml) was poured into Petri dishes. After solidification, 0.10 ml of test bacteria was spread over the medium using a spreader. Discs of Whatman No. 1 filter paper, diameter 6 mm, were soaked in DMSO solutions in the compounds (1.0 mg cm⁻¹). All the compounds were placed at 4 equidistant places at a distance of 2 cm from the centre of the inoculated Petri dishes. DMSO served as the control and Streptomycin was used as the standard drug. The Petri dishes were kept in a refrigerator for 24 h for pre-diffusion. Finally, the Petri dishes were incubated at 30 °C for 24 h. All determinations were performed in duplicate for each of the compounds. The average of two independent readings for each compound was recorded.

The results of the antibacterial study are given in Fig. 4, from which it can be seen that the bacterial growth inhibitory capacity of the ligand and its complexes followed the order Co(II) > Mn(II) > ligand.

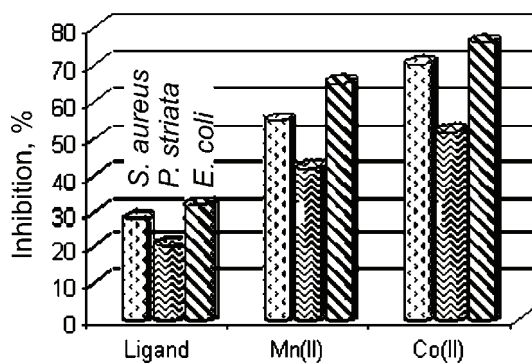


Fig. 4. Antibacterial activity of the compounds.

CONCLUSIONS

The present study confirmed an octahedral geometry around the Mn(II) and Co(II) complexes with the bidentate ligand coordinating through the nitrogen atoms of the of $\nu(\text{Py-N})$ and $\nu(\text{C=N})$ groups. The thermal stability sequence decreased in the following order: Mn(II) > Co(II) > ligand. The activation energy of the Mn(II) and Co(II) complexes, as expected, increased in accordance with their decreasing radius. The activation entropy change in all the complexes had a negative value, meaning that the complexes were more ordered systems than the reactants. The results of antimicrobial activity revealed that all the metal-complexes showed an inhibition capacity slightly higher than the ligand, but much less than the standard drug.

Acknowledgement. The authors are thankful to the DRDO, New Delhi, for financial support.

ИЗВОД

СПЕКТРОСКОПСКА, ТЕРМИЧКА И АНТИБАКТЕРИЈСКА ПРОУЧАВАЊА Mn(II) И Co(II) КОМПЛЕКСА ИЗВЕДЕНИХ ИЗ ТИОСЕМИКАРБАЗОНА

SULEKH CHANDRA¹, MONIKA TYAGI¹ и MOAMEN S. REFAT²¹Department of Chemistry, Zakir Husain College, University of Delhi, JLN-Marg, New Delhi - 110002, India u²Department of Chemistry, Faculty of Science, Port-Said, Suez Canal University, Port-Said, Egypt

Синтетисани су комплекси Mn(II) и Co(II) општег састава $[\text{M}(\text{L})_2\text{X}_2]$ (где је L = 2-пиридинкарбоксилалдехид тиосемикарбазона, M = Mn(II) и Co(II), X = Cl⁻ и NO₃⁻). Сви метални комплекси су окарактерисани елементалном анализом, моларном проводљивошћу, мерењем магнетне суцептибилности, масеним, IR, EPR, електронским спектралним проучавањима и термогравиметријском анализом (TG). На основу спектралних изучавања предложена је октаедарска геометрија за све комплексе. Термичка проучавања једињења сугеришу да су комплекси стабилнији од слободног лиганда. Ово је подржано проучавањем кинетичких параметара применом Horowitz–Metzger (H–M) и Coats–Redfern (C–R) једначина. Антибактеријске особине лиганда и његових металних комплекса су такође изучаване и примећено је да су компелкси моћнији бактерициди него слободни лиганд.

(Примљено 1. децембра 2008, ревидирано 15. априла 2009)

REFERENCES

1. P. Gupta, F. Basuli, S. M. Peng, G. H. Lee, S. Bhattacharya, *Inorg. Chem.* **42** (2003) 2069
2. M. Ruan, Y. Ye, Y. Song, Q. Mauricio, F. Erben, C. O. D. Vedova, *Spectrochim. Acta* **72 A** (2009) 26
3. P. I. Das, M. F. Fernando, R. Pavan, C. Q. F. Leite, F. D. Sousa, A. A. Batista, O. R. Ascimento, J. E. Eduardo, E. Castellano, E. Niquet, V. M. Deflon, *Polyhedron* **28** (2009) 205
4. Z. H. Chohan, *Trans. Met. Chem.* **153** (2009) 153
5. N. K. Singh, A. Srivastava, A. Sodhi, *Trans. Met. Chem.* **25** (2000) 133
6. B. F. Marisa, B. Franco, P. Giorgio, S. Monica, T. Pieralberto, C. Mara, C. Silvia, A. Roberto, P. Silvana, *J. Inorg. Bio. Chem.* **90** (2002) 113
7. N. C. Saha, R. J. Butcher, S. Chaudhuri, N. Saha, *Polyhedron* **22** (2003) 383

8. I. Yilmaz, A. Curkurovali, *Trans. Met. Chem.* **28** (2003) 399
9. M. Akkurt, S. Ozturk, S. Lde, *Anal. Sci.* **16** (2000) 667
10. N. K. Singh, S. B. Singh, A. Srivastav, S. M. Singh, *Proc. Ind. Acad. Sci. (Chem. Sci.)* **113** (2001) 257
11. D. L. Kalyman, J. P. Scovill, J. F. Bartosevich, J. Bruce, *J. Med. Chem.* **26** (1983) 35
12. D. L. Kalyman, J. P. Scovill, J. F. Bartosevich, C. J. Mason, *J. Med. Chem.* **22** (1979) 1367
13. M. Nagar, R. Sharma, S. K. Agarwal, S. Rawat, *Trans. Met. Chem.* **31** (2006) 201
14. Z. H. Abd EI-Wahab, M. M. Mashly, A. A. Salman, B. A. EI-Shertary, A. A. Faheim, *Spectrochim. Acta* **60A** (2004) 2861
15. S. Prasad, R. K. Agarwal, *Trans. Met. Chem.* **32** (2007) 143
16. *Vogel's Text Book Practical Organic Chemistry*, B. S. Furniss, A. J. Hannaford, P. W. G. Smith, A. R. Tatchell, Eds., Longman, London, 1989
17. V. I. Vogel, *Quantitative Inorganic Analysis*, ELBS, 1962, p.p. 536–643
18. A. Castineiras, I. Garcia, Santos, J. M. Varela, *Polyhedron* **28** (2009) 86
19. S. Chandra, M. Tyagi, *J. Ind. Chem. Soc.* **85** (2008) 42
20. S. Chandra, A. Gautam, M. Tyagi, *Trans. Met. Chem.* **32** (2007) 1079
21. S. Chandra, A. Gautam, M. Tyagi, *Russ. J. Coord. Chem.* **35** (2009) 25
22. W. Coats, J. P. Redfern, *Nature* **68** (1964) 201
23. H. H. Horowitz, G. Metzger, *Anal. Chem.* **35** (1963) 1464
24. S. Chandra, S. Raizada, M. Tyagi, A. Gautam, *Bioinorg. Chem. Appl.* **2007** (2007) Article ID 51483
25. S. Chandra, S. Raizada, M. Tyagi and P. K. Sharma, *Spectrochim. Acta* **69A** (2008) 816.
26. G. Puhilbhai, S. Vasudhevan, S. Kutti Rani, G. Rajago, *Spectrochim. Acta* **72A** (2009) 687
27. S. Kumar, P. M. Reddy, Y. P. Ho, V. Ravidda, *J. Ind. Chem. Soc.* **86** (2009) 153.



J. Serb. Chem. Soc. 74 (8–9) 917–926 (2009)
JSCS–3887

Synthesis, characterization, chelation with transition metal ions, and antibacterial and antifungal studies of the 4-[(*E*)-phenyldiazenyl]-2-[(*E*)-(phenylimino)methyl]phenol dye

NURCAN KURTOGLU*

*Kahramanmaraş Sütçü İmam University, Department of Textile Engineering,
Aşar campus, 46050, Kahramanmaraş, Turkey*

(Received 26 November 2008, revised 12 January 2009)

Abstract: New Ni(II), Cu(II) and Co(II) complexes were synthesized with the bidentate azo-azomethine dye, 4-[(*E*)-phenyldiazenyl]-2-[(*E*)-(phenylimino)methyl]phenol (dmpH), which was prepared by the reaction of 2-hydroxy-5-[(*E*)-phenyldiazenyl]benzaldehyde with aniline in EtOH. The syntheses of the metal chelates of the azo-azomethine dye were realized by the precipitation technique. The synthesized metal complexes were characterized by elemental analysis, molar conductance measurements, as well as infrared and UV-Vis spectral data. Based on these characterizations, the metal complexes of the transition metal ions may be formulated as $[M(dmp)Cl(H_2O)]$ where $M = Ni(II), Cu(II)$ and $Co(II)$. The metal complexes were formed by the coordination of N and O atoms of the ligand. The molar conductance values of the Ni(II), Cu(II) and Co(II) complexes of the bidentate ligand indicate their non-ionic character. The free ligand and its metal complexes were tested for their *in vitro* antimicrobial properties against eight bacteria: *Escherichia coli*, *Staphylococcus aureus*, *Klebsiella pneumoniae*, *Mycobacterium smegmatis*, *Pseudomonas aeruginosa*, *Enterococcus cloacae*, *Bacillus megaterium*, and *Micrococcus luteus*, and three fungi, *Kluyveromyces fragilis*, *Rhodotorula rubra* and *Saccharomyces cerevisiae*, in order to assess their antimicrobial potential. The $[Ni(dmp)Cl(H_2O)]$ chelate exhibited high activity against all the bacteria and fungi, except *Rhodotorula rubra*.

Keywords: azo dye; azo-azomethine; transition metals; spectroscopy; antimicrobial activity.

INTRODUCTION

Colorants, which include chromophores of dyes usually consisting of C=C, N=N, C=N, and aromatic and heterocyclic rings, containing oxygen, nitrogen or sulfur, have been widely used as dyes owing to their versatility in various fields

* E-mail: nkurtoglu@ksu.edu.tr

doi: 10.2298/JSC0909917K

and high technologies, including textiles, paper, leather, plastics, biological staining, lasers, liquid crystalline displays, ink-jet printers, and in specialized applications, such as food, drug, cosmetic and photochemical productions.¹⁻⁴ Dyes used before the nineteenth century were either of vegetable (*i.e.*, weld, madder, indigo) or animal origin (*i.e.*, cochineal, shellfish) and belonged to various chemical types, such as flavonoids (yellow), anthraquinones (red) and indigoids (blue and violet).⁵ These chemical types of anthraquinoid dyes provide the most important red dyes and lakes used in artistic paintings. Synthetic dyes are extensively used in industry and a vast amount of the dyes produced enter the environment as waste material.⁶ The main synthetic dye classes include azo, anthraquinone and triarylmethane dyes which constitute more than half of the dyes used in industrial applications. Azo dyes are widely used in the textile industry and are the largest and most versatile group of synthetic organic dyes, with a tremendous number of industrial applications.⁷

Schiff base metal complexes have the ability to reversibly bind oxygen in epoxidation reactions,⁸ biological activity,^{9,10} catalytic activity in hydrogenation of olefins^{11,12} and photochromic properties.¹³ Also, Schiff bases can be used in the degradation of organic compounds¹⁴ and in radiopharmaceuticals.¹⁵

In previous studies, the synthesis and characterization of various bidentate compounds and some of their properties were investigated.¹⁶⁻²⁰ In this article, because of the importance of azo-azomethine compounds and in continuance of present interest in the syntheses of azo and azomethine compounds, the syntheses, complex formation and characterization using different techniques, in particular the elemental analyses, molar conductivity, infrared and electronic spectroscopy, of 4-[(*E*)-phenyldiazenyl]-2-[(*E*)-(phenylimino)methyl]phenol are reported. The ligand was synthesized by the reaction of 2-hydroxy-5-[(*E*)-phenyldiazenyl]benzaldehyde with aniline in EtOH solution at the boiling point. Its complexing ability with Ni(II), Cu(II) and Co(II) salts was examined. The structure of the metal chelates is proposed.

EXPERIMENTAL

Reagents

Aniline and salicylaldehyde were purchased from Aldrich. 2-Hydroxy-5-[(*E*)-phenyldiazenyl]benzaldehyde was prepared as described previously.²¹⁻²³ NiCl₂·6H₂O, CuCl₂·2H₂O and CoCl₂·6H₂O (Merck) were used as purchased with no additional purification. All solvents were of reagent grade and used without further purification.

Physical measurements

The microanalyses for carbon, hydrogen, nitrogen were performed by the TUBITAK Analyses Center. The proton NMR spectrum of the azo ligand was determined in the İnönü University Laboratories, Malatya, Turkey. The infrared spectra (KBr disc) were recorded in the 4000–400 cm⁻¹ range on a Shimadzu 8300 FT-IR spectrometer. The electronic spectra were obtained on a Shimadzu 160A UV spectrometer. The melting points were measured with an Electrothermal LDT 9200 apparatus in open capillaries.

Synthesis of 4-[(E)-phenyldiazenyl]-2-[(E)-(phenylimino)methyl]phenol, dmpH (1)

The azo-azomethine compound was prepared according to a literature method (Fig. 1).¹⁶ Aniline (0.043 g, 0.5 mmol) and 0.104 g (0.460 mmol) 2-hydroxy-5-[(E)-phenyldiazenyl]-benzaldehyde were dissolved in 75 mL absolute EtOH with a few drops of glacial acetic acid as a catalyst. The solution was refluxed for 5 h and then left at room temperature. After cooling, the azo-azomethine dye was obtained as orange microcrystals. The microcrystals were filtered off, washed with 20 mL of cold absolute EtOH and then dried.

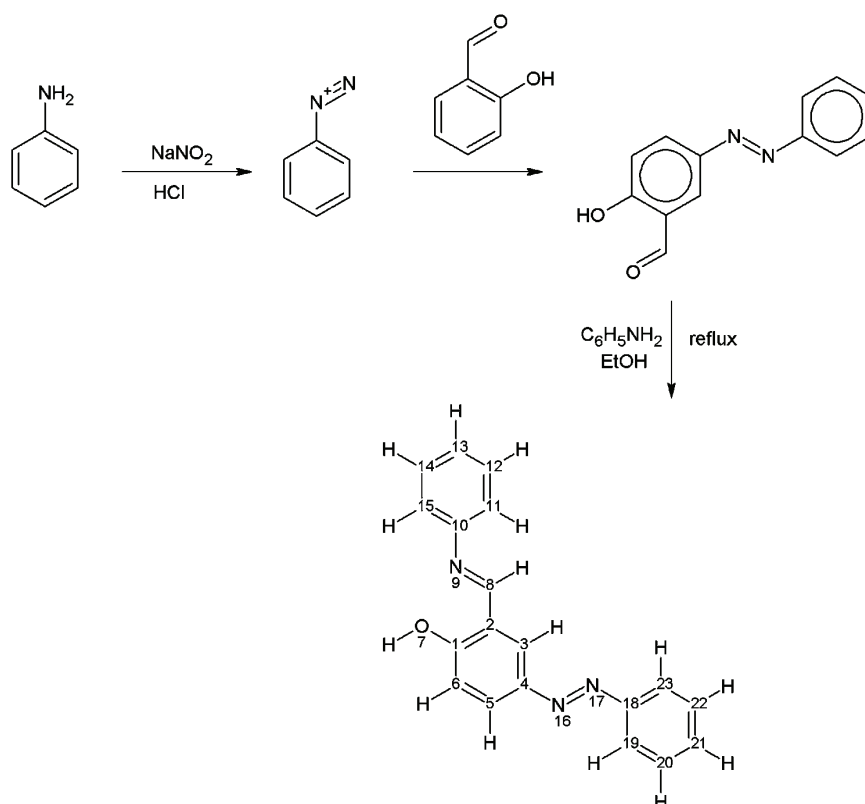


Fig. 1. Preparation of the azo-azomethine dye.

Synthesis of [Ni(dmp)Cl(H₂O)] (2)

A methanolic solution (15 mL) of (0.040 g, 1.66×10^{-4} mol) nickel(II) chloride was added to 15 mL of a clear solution of dmpH (0.050 g, 1.66×10^{-4} mol) in 10 mL MeOH. The resulting mixture was refluxed for 4 h on a water bath. The volume was reduced to half by slow evaporation. After cooling, the red colored complex precipitated out, which was filtered off, washed several times with EtOH and dried *in vacuo*.

Synthesis of [Co(dmp)Cl(H₂O)] (3)

A solution of $\text{CoCl}_2 \cdot 6\text{H}_2\text{O}$ (0.516 g, 0.0200 mmol) in 10 mL of MeOH was added to a magnetically stirred 15 mL MeOH solution containing the ligand (0.653 g, 0.0217 mol) and then refluxed for 2 h. The obtained solution was left at room temperature. The cobalt(II) com-

plex was obtained as a reddish brown precipitate. The product was filtered off, washed with cold EtOH and then dried under vacuum.

Synthesis of [Cu(dmp)Cl(H₂O)] (4)

Copper(II) chloride hexahydrate (0.0524 g, 3.08×10⁻⁴ mol) dissolved in MeOH (10 mL) was added to a hot solution of the azo-azomethine ligand (0.0928 g, 3.08×10⁻⁴ mol) dissolved in MeOH (20 mL). The pH was adjusted to 5–6 using alcoholic sodium hydroxide (0.010 M). The resulting solution was stirred and heated on a hot plate at 70 °C for 30 min. The volume of the obtained solution was reduced to one-half by evaporation. One day later, a greenish brown colored solid of the complex formed, which was filtered, the solid washed with cold EtOH and Et₂O and finally dried under vacuum.

Biological studies

The azo-azomethine dye and its metal complexes were evaluated for both their *in vitro* antibacterial activity against *Escherichia coli*, *Staphylococcus aureus*, *Klebsiella pneumoniae*, *Mycobacterium smegmatis*, *Pseudomonas aeruginosa*, *Enterococcus cloacae*, *Bacillus megaterium* and *Micrococcus luteus*, and their *in vitro* antifungal activity against *Kluyveromyces fragilis*, *Rhodotorula rubra* and *Saccharomyces cerevisiae* by the disc diffusion method.^{24,25}

RESULTS AND DISCUSSION

Synthesis of the coordination compounds

The dye, 4-[(*E*)-phenyldiazenyl]-2-[(*E*)-(phenylimino)methyl]phenol was prepared by reacting aniline with 2-hydroxy-5-[(*E*)-phenyldiazenyl]benzaldehyde, obtained by treating a solution of aniline with salicylaldehyde in EtOH medium with an aqueous solution of NaNO₂ at -5 °C. The structure of the azo-azomethine dye was demonstrated by a combination of analytical, spectroscopic and single crystal X-ray studies. The level of impurity in the product was checked by thin layer chromatography. The single crystal structure of the azo-azomethine ligand has been reported and discussed in a previous paper.¹⁶ In methanolic solution (pH 5–6), the ligand undergoes deprotonation to form 1:1 mononuclear complexes with Ni(II), Co(II) and Cu(II) metal ions:



Characterization and analytic data of the ligand and the complexes

4-[(*E*)-phenyldiazenyl]-2-[(*E*)-(phenylimino)methyl]phenol, *dmpH* (**1**). Yield: 0.12 g (85 %). m.p. 137–138 °C. Anal. Calcd. for C₁₉H₁₅N₃O (301.3 g/mol): C, 75.73; H, 5.02; N, 13.94 %; Found: C, 75.64; H, 5.09; N, 13.86. FTIR (KBr, cm⁻¹): 3420 (Ar-OH), 3049 (Ar-C-H), 1620 (-CH=N-), 1346 (-N=N-). ¹H-NMR (DMSO-*d*₆, δ / ppm): 13.87 (1H, s, -OH), 9.17 (1H, s, -CH=N-), 8.32–8.30 (2H, *d*, *J* = 9.1 Hz, Ar-H), 8.04–7.99 (5H, *dd*, *J* = 8.9 Hz, Ar-H), 7.88–7.85 (1H, *d*, *J* = 8.6 Hz, Ar-H), 7.62–7.57 (5H, *m*, Ar-H). UV-Vis (EtOH, λ_{max} / nm): 272 (π→π*, Ar-C=C), 320 π→π*, -CH=N-), 333 (π→π*, -N=N-), 345 (n→π*, -CH=N-), 452 (n→π*, -N=N-). UV-Vis (DMF, λ_{max} / nm): 277 (π→π*, Ar-

C=C), 326 ($\pi \rightarrow \pi^*$, -CH=N-), 343 ($\pi \rightarrow \pi^*$, -N=N-), 360 ($n \rightarrow \pi^*$, -CH=N-), 460 ($n \rightarrow \pi^*$, -N=N-). $\Lambda_M = 13 \Omega^{-1} \text{ cm}^2 \text{ mol}^{-1}$.

[Ni(dmp)Cl(H₂O)] (2). Yield: 65 %. m.p. 225 °C. Anal. Calcd. for C₁₉H₁₆ClN₃NiO₂ (412.50 g/mol): C, 55.32; H, 3.91; N, 10.19 %; Found: C, 55.07; H, 3.69; Cl, 8.44; N, 10.42 %. FTIR (KBr, cm⁻¹): 3415 ν (OH), 3064 ν (Ar-C-H), 1618 ν (C=N), 1350 ν (-N=N-), 941, 569 ν (Ni-O), 447 ν (Ni-N). UV-Vis (DMF, λ_{max} / nm): 229 ($\pi \rightarrow \pi^*$), 279 ($\pi \rightarrow \pi^*$), 347 ($n \rightarrow \pi^*$), 363 ($n \rightarrow \pi^*$), 443 (d \rightarrow d). $\Lambda_M = 15 \Omega^{-1} \text{ cm}^2 \text{ mol}^{-1}$.

[Co(dmp)Cl(H₂O)] (3). Yield: 69 %. m.p. 258 °C. Anal. Calcd. for C₁₉H₁₆ClCoN₃O₂ (412.74 g/mol): C, 55.29; H, 3.91; Cl, 8.59; N, 10.18; Co, 14.28 %; Found: C, 55.35; H, 3.68; Cl, 8.71; N, 9.96; Co, 14.07 %. FTIR (KBr, cm⁻¹): 3439 ν (OH), 3039 ν (Ar-C-H), 1613 ν (C=N), 1382 ν (-N=N-), 563 ν (Co-O), 447 ν (Co-N). UV-Vis (DMF, λ_{max} / nm): 235 ($\pi \rightarrow \pi^*$), 293 ($\pi \rightarrow \pi^*$), 346 ($n \rightarrow \pi^*$), 428 ($n \rightarrow \pi^*$), 605 (d \rightarrow d), 669 (d \rightarrow d). $\Lambda_M = 25 \Omega^{-1} \text{ cm}^2 \text{ mol}^{-1}$.

[Cu(dmp)Cl(H₂O)] (4). Yield: 71 %. m.p. >250 °C. Anal. Calcd. for C₁₉H₁₆ClCuN₃O₂ (417.35 g/mol): C, 54.68; H, 3.86; Cl, 8.49; N, 10.07; Cu, 15.23 %; Found: C, 54.55; H, 3.74; Cl, 8.27; N, 10.16; Cu, 15.32 %. FTIR (KBr, cm⁻¹): 3458 ν (OH), 3058 ν (Ar-C-H), 1611 ν (C=N), 1379 ν (-N=N-), 530 ν (Cu-O), 455 ν (Cu-N). UV-Vis (DMF, λ_{max} / nm): 234 ($\pi \rightarrow \pi^*$), 274 ($\pi \rightarrow \pi^*$), 352 ($n \rightarrow \pi^*$), 370 ($n \rightarrow \pi^*$), 412 (d \rightarrow d). $\Lambda_M = 21 \Omega^{-1} \text{ cm}^2 \text{ mol}^{-1}$.

The structures of the ligand and corresponding complexes were elucidated based on ¹H-NMR, IR and UV-Vis spectra, elemental analysis and molar conductivity. In the complexes, the chloride ions were found to be coordinated to the metal ions as confirmed by the conductivity measurements.

Solubility and molar conductance

All of the metal chelates, [Ni(dmp)Cl(H₂O)], [Cu(dmp)Cl(H₂O)] and [Co(dmp)Cl(H₂O)] are stable in air and soluble in DMF and insoluble in water and *n*-hexane. Single crystals of the metal chelates could not be isolated from any organic solution, thus no definite structures can be described. However, the analytical, spectroscopic and conductivity data enabled possible structures to be predicted as shown in Fig. 2. The molar conductance values of the complexes 2–4 in DMF were in the range 15–25 $\Omega^{-1} \text{ cm}^2 \text{ mol}^{-1}$, indicating that they are non-electrolytes.

Elemental analyses

The elemental analysis results of the complexes of the ligand 1 are in good agreement with the theoretical calculations. The data show a 1:1 (M:dmpH) ratio of the complexes with formulae [M(dmp)Cl(H₂O)].

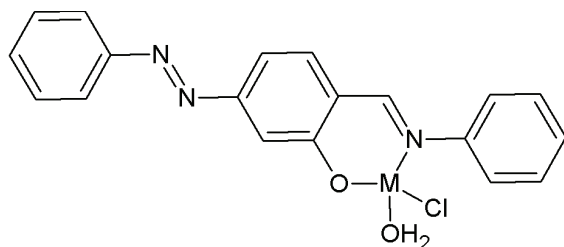


Fig. 2. The proposed general structure of the metal chelates.

¹H-NMR spectrum of the ligand

Proton nuclear magnetic resonance spectral analysis was performed for the synthesized dye which provided further evidence for the structural characteristics of the dye. The ¹H-NMR spectrum of the dye showed a signal at δ 13.87 ppm.²⁶ This chemical shift can be attributed to hydrogen bonded O–H proton. The aldehyde compound containing an azo group exhibited a peak in its ¹H-NMR spectrum at δ 10.32 ppm as a singlet belonging to the proton of the –CHO group. However, the aldehyde peak disappeared in the azo-azomethine dye. The proton of the azomethine group appeared at δ 9.17 ppm as a singlet (Fig. 3). The ¹H-NMR spectrum of the dye showed *d* peaks at δ 8.32–8.30 ppm (H-3), a *dd* at δ 8.04–7.99 ppm (H-5) and a *d* at δ 7.88–7.87 ppm (H-6), which are attributed to phenyl protons, including the –OH group.²² These results show that the azo-azomethine dye shifts to the enol-imine form. The multiple peaks appearing at δ 7.62–7.57 ppm are also attributed to aromatic protons.²

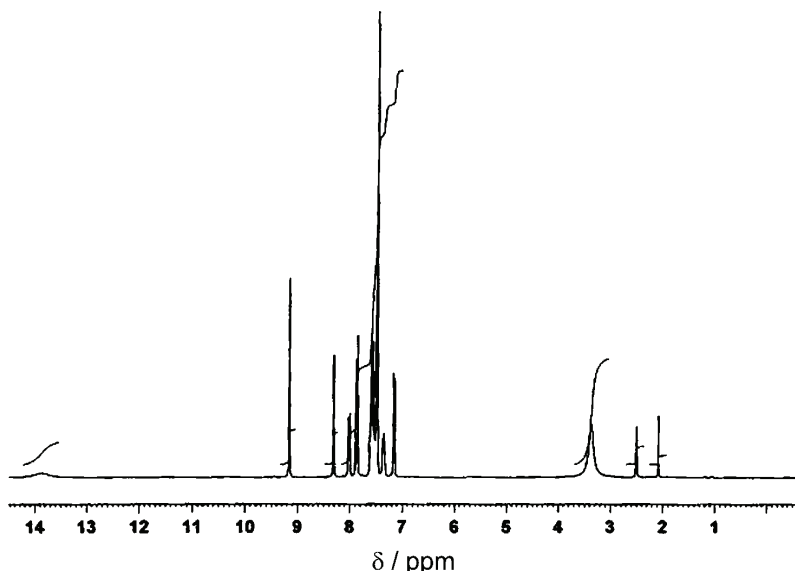


Fig. 3. ¹H-NMR spectrum of the dye.

IR spectra

The IR spectra of the complexes were studied to characterize their structures. The IR spectra of the dmpH ligand **1** and its metal complexes were taken as KBr pellets.

The ligand spectrum revealed a broad band at 3420 cm^{-1} corresponding to the vibration of the O–H group present in the structure.² The band observed at 3049 cm^{-1} is due to the presence of aromatic C–H bonds in the structure. Especially, the band observed at 1620 cm^{-1} indicates the azomethine (–CH=N–) group, which was not present in the starting material but forms in the resulting product as a result of the condensation reaction.²⁷ This band is shifted in the metal chelates toward lower frequencies because of the coordination of the nitrogen to the metal ion. This fact can be explained by the withdrawing of electrons from nitrogen atom to the metal ion on coordination. The band observed at 1346 cm^{-1} is an indication of the –N=N– group. The peak at 3420 cm^{-1} in the spectrum of the ligand corresponding to the OH group was observed at 3415 cm^{-1} in the spectrum of **2**. The peak observed at 3064 cm^{-1} is due to the aromatic C–H group in the complex. The peak at 1618 cm^{-1} is due to C=N. These values are in good accordance with the values cited in the literature. The peak appearing at 3420 cm^{-1} in the IR spectrum of the ligand corresponding to OH group was observed to appear at 3439 cm^{-1} in the IR spectrum of **4**. The peak aromatic C–H group was observed at 3039 cm^{-1} . The peak at 1613 cm^{-1} corresponds to the vibration mode of the C=N group. The peak appearing at 3420 cm^{-1} in the spectrum of the ligand, corresponding to the OH group, was observed at 3458 cm^{-1} in the IR spectrum of **3**. The peak corresponding to the imine group appeared at 1611 cm^{-1} . The peaks appearing at 530 and 455 cm^{-1} were attributed to the Cu–O and Cu–N groups. In the infrared spectra of the complexes, bands assigned to M–O and M–N were identified between 569 – 530 cm^{-1} and 455 – 447 cm^{-1} , respectively.²⁸

Electronic spectra

The electronic spectra of the dye and its metal chelates were recorded in both EtOH and DMF between 200 and 800 nm. The room temperature UV–Vis absorption spectrum of the synthesized dye (dmpH) displayed mainly five bands observed within the range 200–800 nm in EtOH and DMF solution. The first band at 272 nm as a shoulder was assigned to the moderate energy $\pi\rightarrow\pi^*$ transition of the aromatic ring, while the second band at 320 nm is due to the low energy $\pi\rightarrow\pi^*$ transition of the –CH=N– group.

The peaks belonging to the azomethine group in the spectra of **2**, **3** and **4** coordination compounds were observed at 347, 350, 342 nm, respectively. The bands at 333 in EtOH and 343 nm in DMF were assigned to the $\pi\rightarrow\pi^*$ transition of the –N=N– azo group. The other bands in EtOH at 345 and 452 nm were due to $n\rightarrow\pi^*$ transitions of the –CH=N– and –N=N– groups of the dye, respecti-

vely.²⁹ These transitions were observed at 360 and 460 nm in DMF solutions, respectively. The peaks belonging to the –N=N– group in the spectra of the complexes **2**, **3** and **4** appeared at 363, 389 and 370 nm, respectively. The d–d transition bands in the spectra of the azo-azomethine dye complexes were observed at 412–605 nm. The spectroscopic data obtained in this work agreed well with the results of previous studies.

Biological activity

The antibacterial and antifungal activity of the new azo-azomethine chelates were tested by the disc diffusion method. The antibacterial and antifungal activities of the compounds against eight bacteria, namely *E. coli*, *S. aureus*, *K. pneumoniae*, *M. smegmatis*, *P. aeruginosa*, *E. cloacae*, *B. megaterium* and *M. luteus*, and three fungi, namely *K. fragilis*, *R. rubra* and *S. cerevisiae*, are presented in Table I. The results showed that the compound dmpH exhibited high activity against all the tested bacteria and fungi, except for *R. rubra*. The dye, compound **1**, showed the highest effect against *S. aureus* and *K. pneumoniae* among all the tested bacteria and *S. cerevisiae* among all the tested fungi. Compound **2** was quite effective against all the tested bacteria and fungi, with the exception of *R. rubra*, as in the case of compound **1**. However, compound **2** had the highest effect only against one bacterium, namely *S. aureus*, showing an inhibition zone of 22 mm. It is also clear from the data in Table I that compound **3** exhibited high activity against all the tested bacteria and fungi, showing an inhibition zone of 9–15 mm. Compound **4** exhibited moderate activity against all the tested bacteria and fungi, except for *R. rubra*. The copper complex showed the highest effect against *E. coli* and *B. megaterium* among all the tested bacteria and *S. cerevisiae* among all the tested fungi.

TABLE I. Antibacterial and antifungal activities (mm) of the synthesized dye and its complexes

Tested microorganisms	Compound			
	1	2	3	4
<i>E. coli</i>	16	15	13	10
<i>S. aureus</i>	20	22	10	8
<i>K. pneumoniae</i>	20	19	12	8
<i>M. smegmatis</i>	15	15	11	7
<i>P. aeruginosa</i>	15	15	9	7
<i>E. cloacae</i>	15	15	12	7
<i>B. megaterium</i>	16	16	11	10
<i>M. luteus</i>	17	16	12	9
<i>K. fragilis</i>	14	15	15	11
<i>R. rubra</i>	0	0	10	0
<i>S. cerevisiae</i>	17	16	12	16

CONCLUSIONS

In this work, an azo-azomethine dye ligand, 4-[(*E*)-phenyldiazenyl]-2-[(*E*)-(phenylimino)methyl]phenol (dmpH), derived from 2-hydroxy-5-[(*E*)-phenyldiazenyl]benzaldehyde and aniline in EtOH, and some of its transition metal complexes were prepared. The analytical data and spectroscopic studies suggested that the complexes had the general formula of $[M(dmp)Cl(H_2O)]$, where M is nickel(II), cobalt(II) or copper(II). The molar conductance measurements of the complexes showed their non-electrolytic nature. According to UV-Vis and IR data, the phenylazo-linked azo-azomethine dye was coordinated to the metal ion through the azomethine nitrogen and oxygen atom of the hydroxyl group in salicylaldehyde.

Based on the above results, the structure of the investigated coordination compounds can be formulated as in Fig. 2. The studied metal chelates exhibited high activity against *S. cerevisiae*.

ИЗВОД

СИНТЕЗА, КАРАКТЕРИЗАЦИЈА, ХЕЛАЦИЈА ЈОНА ПРЕЛАЗНИХ МЕТАЛА, И АНТИБАКТЕРИЈСКА И АНТИФУНГАЛНА ИСПИТИВАЊА БОЈЕ 4-[(*E*)-ФЕНИЛДИАЗЕНИЛ]-2-[(*E*)-(ФЕНИЛИМИНО)МЕТИЛ]ФЕНОЛА

NURCAN KURTOGLU

*Kahramanmaraş Sütçü İmam University, Department of Textile Engineering,
Avşar campus, 46050, Kahramanmaraş, Turkey*

Синтетисани су нови комплекси Ni(II), Cu(II) и Co(II) са бидентатном азо-азометинском бојом 4-[(*E*)-фенилдиазенил]-2-[(*E*)-(фенилимино)метил]фенолом (dmpH), добијеном у реакцији 5-[(*E*)-фенилдиазенил]-2-хидроксибензалдехида с анилином у EtOH. Синтезе металних хелата азо-азометинске боје изведене су техником таложења. Синтетисани комплекси су окарактерисани елементалном анализом, мерењем моларне проводљивости и на основу инфрацрвених и UV-Vis спектралних података. На основу ове карактеризације формула металних комплекса јона прелазних метала може бити $[M(dmp)Cl(H_2O)]$ где је M = Ni(II), Cu(II) и Co(II). Метални комплекси су формирани координовањем N и O атома лиганда. Вредности моларне проводљивости комплекса Ni(II), Cu(II) и Co(II) бидентатног лиганда указују на њихов нејонски карактер. Испитана су антимикуробна својства *in vitro* слободног лиганда и комплекса на осам бактерија: *Escherichia coli*, *Staphylococcus aureus*, *Klebsiella pneumoniae*, *Mycobacterium smegmatis*, *Pseudomonas aeruginosa*, *Enterococcus cloacae*, *Bacillus megaterium* и *Micrococcus luteus*, и три гљиве: *Kluyveromyces fragilis*, *Rhodotorula rubra* и *Saccharomyces cerevisiae*, како би се проценио њихов антимикуробни потенцијал. Хелат $[Ni(dmp)Cl(H_2O)]$ је показао високу активност на све бактерије и гљиве, сем на гљиву *Rhodotorula rubra*.

(Примљено 26. новембра 2008, ревидирано 12. јануара 2009)

REFERENCES

1. A. T. Peters, H. S. Freeman, *Colour chemistry, the design and synthesis of organic dyes and pigments*, Elsevier App. Sci. Publ., Barking, Essex, UK, 1991, p. 193

2. H. Kocaokutgen, M. Gur, M. S. Soylu, P. Lonnecke, *Dyes Pigm.* **67** (2005) 99
3. P. Gregory, *High-technology applications of organic colorants*, Plenum Press, New York, 1991, p. 1
4. S. C. Catino, R. E. Farris, in: *Concise Encyclopedia of Chemical Technology*, M. Grayson, Ed., John Wiley & Sons, New York, 1985, p. 142
5. W. Nowik, *Encyclopedia of separation sciences*, Academic Press, London, 2000, p. 2602
6. H. Zollinger, *Color Chemistry – Synthesis, Properties and Application of Organic Dyes and Pigments*, VCH Publishers, New York, 1987, p. 1436
7. H. Ollgaard, L. Frost, J. Galster, O. C. Hansen, *Survey of azo-colorants in Denmark: consumption, use, health and environmental aspects*, Ministry of Environment and Energy, Denmark and the Danish Environmental Protection Agency, No. **XX**, 1998, p. 147
8. M. S. El-Medani, O. A. M. Ali, R. M. Ramaden, *J. Mol. Struct.* **738** (2005) 171
9. S. Ren, R. Wang, K. Komastu, P. B. Krause, Y. Zyrianov, C. E. McKenna, C. Csipke, Z. A. Tokes, E. J. Lien, *J. Med. Chem.* **45** (2002) 410
10. M. T. H. Tarafder, M. A. Ali, N. Saravana., W. Y. Weng, S. Kumar, N. U. Tsafe, K. A. Crouse, *Transition Met. Chem.* **25** (2000) 295
11. J. Colman, L. S. Hegedu, *Principles and Applications of Organotransition Metal Chemistry*, University Science Book, Herndon, VA, 1980
12. J. Zhan, B. Zhan, J. Liu, W. J. Xu, Z. Wang, *Spectrochim. Acta A* **57** (2001) 149
13. W. Liu, Y. Zou, Y. Li, Y. G. Yao, Q. J. Meng, *Polyhedron* **23** (2004) 849
14. H. Yoon, T. R. Wagler, K. J. O'Connor, C. J. Burrows, *J. Am. Chem. Soc.* **122** (1990) 4568
15. M. A. Green, H. Luo, P. E. Fanwick, *Inorg. Chem.* **37** (1998) 1127
16. M. Aslantaş, N. Kurtoğlu, E. Şahin, M. Kurtoğlu, *Acta Crystallogr., Section E: Struct. Rep. Online* **E63** (2007) O3637
17. M. Kurtoğlu, N. Birbiçer, U. Kimyonşen, S. Serin, *Dyes Pigments* **41** (1999) 141
18. N. Birbiçer, M. Kurtoğlu, S. Serin, *Synth. React. Inorg. Met. Org. Chem.* **29** (1999) 1353
19. N. Kurtoğlu, M. Kurtoğlu, S. Serin, *Synth. React. Inorg. Met. Org. Chem.* **29** (1999) 1779
20. N. Kurtoğlu, D. Şenol, *Asian J. Chem.* **20** (2008) 1986
21. M. S. Refat, I. M. El-Deen, H. K. Ibrahim, S. El-Ghool, *Spectrochim. Acta.* **65** (2006) 1208
22. M. Odabaşoğlu, Ç. Albayrak, R. Özkanca, F. Z. Akyan, P. Lonnecke, *J. Mol. Struct.* **840** (2006) 71
23. S. Çakır, E. Biçer, M. Odabaşoğlu, Ç. Albayrak, *J. Braz. Chem. Soc.* **16** (2005) 711
24. C. H. Collins, P. M. Lyne, *Microbial Methods*, University Park Press, Baltimore, 1970, p. 422
25. M. Kurtoglu, E. Ispir, N. Kurtoglu, S. Serin, *Dyes Pigments* **77** (2008) 75
26. K. Nejati, I. Z. Rezvani, *New J. Chem.* **27** (2003) 1665
27. V. P. Singh, P. Gupta, *J. Coord. Chem.* **61** (2008) 1532
28. F. Karipcin, E. Kabalcilar, *Acta Chim. Slov.* **54** (2007) 242
29. H. Karaer, I. E. Gümrükçüoğlu, *Turk. J. Chem.* **23** (1999) 67.



J. Serb. Chem. Soc. 74 (8–9) 927–938 (2009)
JSCS–3888

Synthesis, spectral studies and antibacterial activity of Cu(II), Co(II) and Ni(II) complexes of 1-(2-hydroxyphenyl)-3-phenyl-2-propen-1-one, N^2 -[(3,5-dimethyl-1*H*-pyrazol-1-yl)methyl]hydrazone

PAULMONY THARMARAJ^{1*}, DEIVASIGAMANI KODIMUNTHIRI¹, CLARENCE D. SHEELA² and CHAPPANI S. SHANMUGA PRIYA¹

¹Department of Chemistry, Thiagarajar College, Madurai-625009 and ²Department of Chemistry, the American College, Madurai-625002, India

(Received 6 January, revised 16 April 2009)

Abstract: A new series of Cu(II), Co(II) and Ni(II) complexes with the 1-(2-hydroxyphenyl)-3-phenyl-2-propen-1-one, N^2 -[(3,5-dimethyl-1*H*-pyrazol-1-yl)methyl]hydrazone ligand, C₂₁H₂₂N₄O (LH), were synthesized by the reaction of 1-(2-hydroxyphenyl)-3-phenyl-2-propen-1-one, hydrazone with (3,5-dimethyl-1*H*-pyrazol-1-yl)methanol and characterized. The nature of the bonding and geometry of the complexes were deduced from elemental analysis, IR, electronic and ¹H-NMR spectroscopy, and magnetic susceptibility and conductivity measurements. The studies indicated square-planar, tetrahedral and octahedral geometry for the copper(II), cobalt(II) and nickel(II) complexes, respectively. The ESR spectra of the copper(II) complex in acetonitrile at 300 and 77 K were recorded and their salient features are reported. The electrochemical behavior of the copper (II) complex was studied by cyclic voltammetry. The antimicrobial activity of the ligand and its metal complexes were studied against the following strains of microorganism: *Staphylococcus aureus*, *Salmonella enterica typhi*, *Escherichia coli* and *Bacillus subtilis* by the well diffusion method. Metal complexes showed enhanced antimicrobial activity compared with that of the free ligand.

Keywords: 3,5-dimethyl-1-(hydroxymethyl)pyrazole; 2'-hydroxychalcone; metal complexes; pyrazole; Cu(II), Co(II) and Ni(II) complexes; antimicrobial activity.

INTRODUCTION

Pyrazoles belong among the most representative five-membered heterocyclic systems. Despite the fact that the pyrazole ring is rarely a constituent of natural products, numerous synthetic compounds containing the pyrazole moiety have

* Corresponding author. E-mail: ptharma@rediffmail.com

doi: 10.2298/JSC0909927T

been the focus of medicinal chemists for the last 100 years because of their outstanding pharmacological, agrochemical, photographic, catalytic, liquid crystals, antitumor drugs and other applications.^{1–16} Transition-metal complexes containing the pyrazole heterocycle are well studied. The variety of the coordination modes of pyrazole and its derivatives is due to the different chemical natures of the nitrogen atoms in a pyrazole molecule.^{17,18} In the present study, 1-(2-hydroxyphenyl)-3-phenyl-2-propen-1-one, *N*²-[(3,5-dimethyl-1*H*-pyrazol-1-yl)methyl]hydrazone was synthesized *via* the reaction of 1-(2-hydroxyphenyl)-3-phenyl-2-propen-1-one, hydrazone with (3,5-dimethyl-1*H*-pyrazol-1-yl)methanol and characterized by spectral and analytical techniques.

EXPERIMENTAL

The chemicals acetylacetone (A.R.), 2-hydroxyacetophenone (A.R.) and hydrazine hydrate (L.R.) were obtained from E. Merck (India). All the metal salts (L.R.) and solvents (A.R.) were purchased from S. D. Fine Chemicals and used without further purification. The UV–Vis spectra of the ligand and metal complexes were recorded in dichloromethane using a Jasco V-530 spectrophotometer. The IR spectra in KBr discs were recorded on a Shimadzu spectrophotometer Model FTIR-8400S. Cyclic voltammetric measurements were performed using a voltammograph BAS-50 at room temperature in acetonitrile under N₂ using a three electrode cell: a 0.1M Ag/AgCl reference electrode, a Pt wire auxiliary electrode and a glassy carbon working electrode with TBAP as the supporting electrolyte. The ¹H-NMR spectra were recorded in CDCl₃ using a Bruker DRX-300, 300 MHz NMR spectrometer. The ESR spectra were recorded in the solid state at 300 and 77 K using a JEOL TES 100 ESR spectrometer. The magnetic moments of the complexes were measured by a VSM model 7404 at Pondicherry University. The effective magnetic moments were calculated using the formula $\mu_{\text{eff}} = 2.228 (\chi_{\text{M}}T)^{1/2}$, where χ_{M} is the corrected molar susceptibility. The molar conductance of the complexes was measured in methanol at room temperature using a Systronic type conductivity bridge (Oswal).

Synthesis of 1-(2-hydroxyphenyl)-3-phenyl-2-propen-1-one, hydrazone

2'-Hydroxychalcone and 3,5-dimethylpyrazole were synthesized by adopting the literature method.^{19,20} An ethanolic solution of 2'-hydroxychalcone (2.24 g, 10.0 mmol) was added dropwise at room temperature and with stirring over 1 h to hydrazine hydrate (2.5 g, 50 mmol). After completion of the addition, the mixture was stirred for 10 min, and upon cooling in ice, a pale yellow solid appeared, which was collected by filtration, washed with diethyl ether and dried under vacuum.

*Synthesis of 1-(2-hydroxyphenyl)-3-phenyl-2-propen-1-one, N²-[(3,5-dimethyl-1*H*-pyrazol-1-yl)methyl]hydrazone (I) (Fig. 1)*

3,5-Dimethyl-1-(hydroxymethyl)pyrazole (3.15 g, 25.0 mmol) in 25 ml of dichloromethane and 1-(2-hydroxyphenyl)-3-phenyl-2-propen-1-one, hydrazone (5.95 g, 25 mmol) in 15 ml dichloromethane were stirred for 3 h and kept at room temperature for 50 h. The excess water was removed by the addition of anhydrous MgSO₄ and filtrated. The filtrate solution was reduced to one third on a water bath and the thus obtained yellow colored solid was filtered and then dried under vacuum.

Compound I. Yield: 68 % (11.8 g), m.p. 124 °C. Anal. Calcd. for C₂₁H₂₂N₄O: C, 72.83; H, 6.30; N, 16.18 %. Found: C, 72.37; H, 6.28; N, 16.04 %. IR (KBr, cm⁻¹): 1599 (C=N stretching of pyrazole ring), 3342–3360 (O–H stretching of aromatic ring). ¹H-NMR (300

MHz, CDCl_3 , δ / ppm): 7.00–7.43 (9H, *m*, aromatic ring protons), 10.6 (1H, *s*, phenolic O–H), 5.84 (1H, *s*, pyrazole ring proton), 2.8 (6H, *s*, pyrazole ring methyl protons), 5.2 (2H, *s*, N–CH₂–N), 5.6 (1H, *d*, CH=CH), 6.3 (1H, *d*, CH=CH). UV–Vis (CH_3CN , 10^{-3} M) (λ_{max} / nm (cm^{-1}): 318 (31440), 250 (40000), 231 (43290).

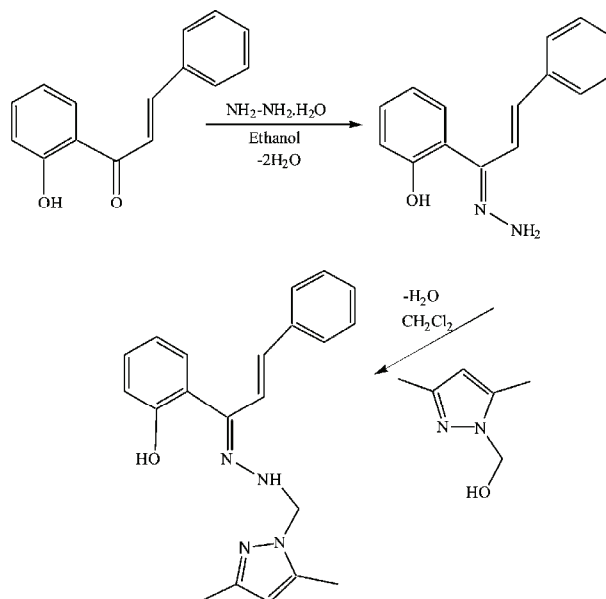


Fig. 1. Synthetic route to the ligand 1-(2-hydroxyphenyl)-3-phenyl-2-propen-1-one, *N*²-[(3,5-dimethyl-1*H*-pyrazol-1-yl)methyl]hydrazone (**1**).

Synthesis of metal complexes

A solution of MCl_2 , $\text{M} = \text{Cu(II)}$, Co(II) or Ni(II) , (10 mmol) in 15 ml of ethanol was mixed with **1** (20 mmol) in 15 ml ethanol. This mixture was refluxed for 3 h and then the solution was reduced to minimum volume. The thus obtained metal complexes (Figs. 2 and 3) were filtered, washed with ether and dried under vacuum.

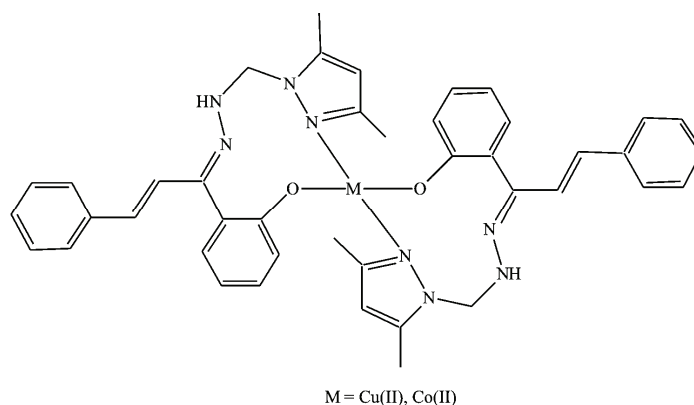


Fig. 2. Suggested structure of the Cu(II) and Co(II) complexes.

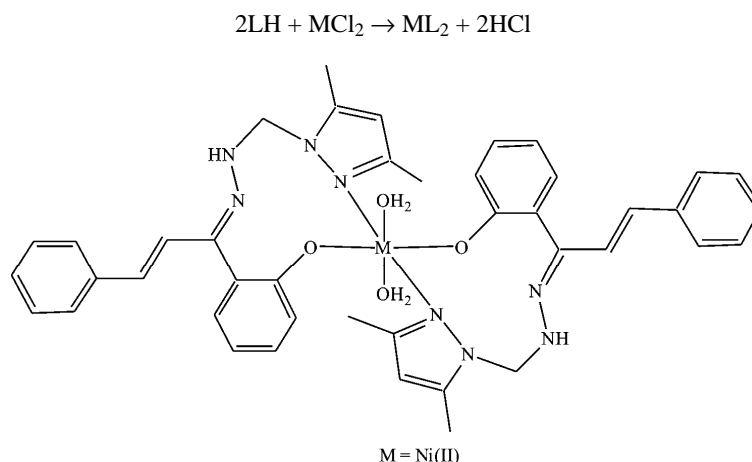


Fig. 3. Suggested structure of the Ni(II) complex.

RESULTS AND DISCUSSION

The analytical data of the ligand and its metal complexes are given in Table I. The found values were in good agreement with the theoretical ones, and correspond well with the general formula $[\text{ML}_2]$, for $\text{M} = \text{Cu(II)}$ and Co(II) , and $[\text{ML}_2(\text{H}_2\text{O})_2]$, for $\text{M} = \text{Ni(II)}$ and $\text{L} = \text{C}_{21}\text{H}_{22}\text{N}_4\text{O}$. The metal complexes were dissolved in acetonitrile and the molar conductivities of their 10^{-3} M solutions were measured at 25 ± 2 °C. The low molar conductivity values of the metal complexes indicate that they are non-electrolytes. The structure of the complexes was predicted based on analytical, spectroscopic and magnetic moment data.

TABLE I. Physical characterization, analytical and molar conductance data of the ligand and its metal complexes

Compound	Found (Calcd.), %						M. p. / °C	$\Lambda_M / \text{S cm}^2 \text{mol}^{-1}$
	Color	M	C	H	N			
Ligand (LH)	Yellow	–	72.37 (72.83)	6.28 (6.36)	16.04 (16.18)		124	–
$[\text{CuL}_2]$	Pale Green	8.10 (8.42)	66.12 (66.87)	5.13 (5.61)	14.58 (14.85)		293	13.31
$[\text{CoL}_2]$	Green	7.53 (7.86)	67.17 (67.28)	5.65 (5.36)	14.95 (14.65)		245	14.08
$[\text{NiL}_2(\text{H}_2\text{O})_2]$	Blue	7.02 (7.47)	64.04 (64.22)	5.54 (5.90)	14.10 (14.26)		278	11.20

IR Spectra

The IR spectral data of the ligand and its complexes are given in Table II. In order to study the binding mode of the ligand in the metal complexes, the IR spectrum of the free ligand was compared with those of the corresponding metal

complex. The free ligand exhibited a strong band at 3342 cm^{-1} assignable to the $\nu(\text{N-H})$ stretching vibration. The hydrogen bonded $\nu(\text{O-H})$ shows a broad band in the region $3320\text{--}2990\text{ cm}^{-1}$, which is obviously absent in the spectra of the complexes, indicating the deprotonation and the involvement of the phenol O in the chelation. The absorption bands around 1304 , 1599 and 976 cm^{-1} may be assigned to $\nu(\text{C-O})$, $\nu(\text{C=N})$ and $\nu(\text{N-N})$, respectively. The $\nu(\text{C-O})$ band has a positive shift of $20\text{--}40\text{ cm}^{-1}$ in the complexes due to chelation of the phenolic oxygen atom to the metal ion. On coordination, the negative shift in $\nu(\text{C=N})$ and positive shift in $\nu(\text{N-N})$ ($15\text{--}55\text{ cm}^{-1}$) are indicative of the coordination of the tertiary nitrogen of pyrazoline to the metal. The increased $\nu(\text{N-N})$ stretching frequency in the complexes may be attributed to the loss of the repulsive forces of the lone pair on the nitrogen atom. The $\nu(\text{NH})$ stretching frequency shows irregular variation in the complexes, which ruled out the possibility of its coordination. The oxygen and nitrogen coordination to the metal ion is proved by the bands that appeared in the range $590\text{--}550\text{ cm}^{-1}$ and $450\text{--}400\text{ cm}^{-1}$, assigned to M-O and M-N modes,²¹⁻²³ respectively. In the Ni(II) complex, IR bands of coordinated water appeared at 832 and 1469 cm^{-1} , indicating the binding of water molecules to the metal ion.²⁴

TABLE II. IR Spectral data of the ligand and its metal complexes

Compound	Frequency, cm^{-1}						
	$\nu(\text{O-H})$	$\nu(\text{C-O})$	$\nu(\text{C=C})$	$\nu(\text{C=N})$	$\nu(\text{N-N})$	$\nu(\text{M-O})$	$\nu(\text{M-N})$
Ligand (LH)	3342–3360	1304	1627	1599	976	–	–
[CuL ₂]	–	1328	1643	1573	980	435	574
[CoL ₂]	–	1331	1634	1582	985	465	537
[NiL ₂ (H ₂ O) ₂]	3450	1338	1642	1569	976	443	549
	(Coordinated water)						

Magnetic properties and electronic absorption spectra

The magnetic moments and electronic spectral data of the ligand and its complexes are summarized in Table III. The spectrum of the ligand in acetonitrile showed three prominent bands at 31440 , 40000 and 43290 cm^{-1} , which were assigned as intra-ligand charge transfer (INCT) bands. The spectrum of the copper(II) complex showed a broad band at 16120 cm^{-1} , which was assigned as a (${}^2\text{B}_{1g} \rightarrow {}^2\text{A}_{1g}$) d-d transition and is interpreted in terms of square-planar geometry. The absence of any bands below 10000 cm^{-1} eliminates the possibility of a tetrahedral or pseudo tetrahedral environment in this complex. The magnetic moment of Cu(II) complex is $1.78\ \mu_{\text{B}}$, indicating square-planar geometry.^{25,26} The Co(II) complex exhibited three bands, *viz.* 14410 , 15010 and 15870 cm^{-1} , which were assigned as ${}^4\text{A}_{2g} \rightarrow {}^4\text{T}_{2g}(\text{F})$, ${}^4\text{A}_{2g}(\text{F}) \rightarrow {}^4\text{T}_{1g}(\text{F})$ and ${}^4\text{A}_{2g}(\text{F}) \rightarrow {}^4\text{T}_{1g}(\text{P})$ transitions, respectively. The intensity and band width strongly suggested tetrahedral geometry. The magnetic moment of the Co(II) complex was $3.59\ \mu_{\text{B}}$,

which is characteristic for a tetrahedral environment. The electronic spectrum of the Ni(II) complex showed three prominent bands at 10449, 15878 and 19920 cm^{-1} , which may be tentatively assigned to ${}^3A_{2g} \rightarrow {}^3T_{2g}(\text{F})$, ${}^3A_{2g}(\text{F}) \rightarrow {}^3T_{1g}(\text{F})$ and ${}^3A_{2g}(\text{F}) \rightarrow {}^3T_{1g}(\text{P})$ transitions, arising from octahedral geometry.²⁷ The Ni(II) complex possessed a magnetic moment value of $2.84 \mu_{\text{B}}$ found for a regular octahedral arrangement.

TABLE III. Electronic spectral data and magnetic moments of the prepared compounds

Compounds	Frequency, cm^{-1}	Transition	Geometry	$\mu_{\text{eff}} / \mu_{\text{B}}$
Ligand (LH)	31440	INCT	–	–
	40000	INCT		
	43290	INCT		
[CuL ₂]	16120	${}^2B_{1g} \rightarrow {}^2A_{1g}$	Distorted octahedral	1.71
[CoL ₂]	14410	${}^4A_{2g}(\text{F}) \rightarrow {}^4T_{2g}(\text{F})$	Octahedral	3.59
	15010	${}^4A_{2g}(\text{F}) \rightarrow {}^4T_{1g}(\text{F})$		
	15872	${}^4A_{2g}(\text{F}) \rightarrow {}^4T_{1g}(\text{P})$		
[NiL ₂ (H ₂ O) ₂]	10449	${}^3A_{2g}(\text{F}) \rightarrow {}^3T_{2g}(\text{F})$	Octahedral	2.84
	15878	${}^3A_{2g}(\text{F}) \rightarrow {}^3T_{1g}(\text{F})$		
	19920	${}^3A_{2g}(\text{F}) \rightarrow {}^3T_{1g}(\text{P})$		

Adduct formation

The tendency of the Co(II) complex to form additional compounds with coordinating bases, such as pyrazole and imidazole, was studied in solution. The variations of the peak pattern in the electronic spectra upon addition of heterocyclic bases, indicating geometrical changes in the Co(II) complex due to adduct formation, are shown in Figs. 4 and 5. The addition of pyrazole and imidazole to the chelate complex revealed the weak nature of the ligand field, which was susceptible for further coordination to give six-coordinated complexes.

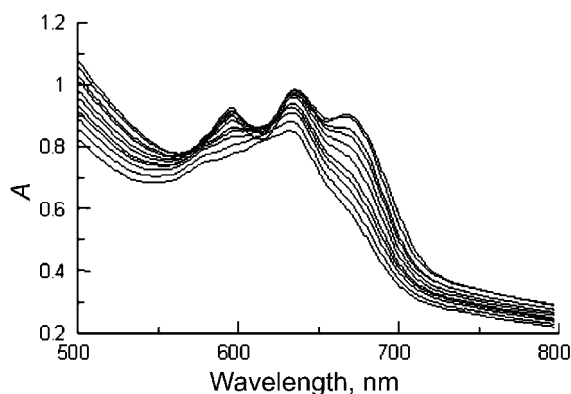


Fig. 4. Electronic spectra of the Co(II) complex in acetonitrile after addition of pyrazole.

In order to study the effect of coordination bases on the geometry of the [CoL₂] complex, a comparison of electronic spectra of the [CoL₂Y₂]⁻ (Y = 3,5-

-dimethylpyrazole) complex (formed by the addition of 3,5-dimethylpyrazole) with that of $[\text{CoL}_2]$ showed that the band at around 15010 cm^{-1} decreased in intensity due to adduct formation. The bands at 14410 and 15870 cm^{-1} of the Co(II) complex vanished completely in pyrazole solution. Thus the Co(II) complex in pyrazole solution showed adduct formation with a possible change in geometry from tetrahedral to octahedral.²⁸

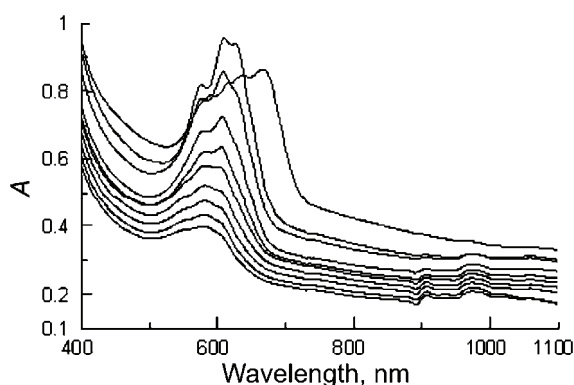


Fig. 5. Electronic spectra of the Co(II) complex in acetonitrile after addition of imidazole.

The electronic spectra of the Co(II) complex in imidazole solution gave rise to a new band at 10362 cm^{-1} and the bands at 15010 and 15870 cm^{-1} were shifted to 16393 and 16863 cm^{-1} , respectively, with a decrease in intensity due to interaction of the base with the metal ion. This led to a change in geometry to octahedral. The ligand exchange behavior on the chelated complex was also studied with acetylacetonone. Addition of a small amount of acetylacetonone shifted the broad band in the spectrum of the Co(II) complex to 16025 cm^{-1} (Fig. 6).

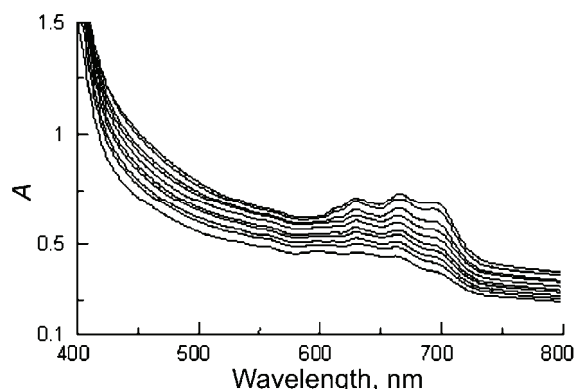


Fig. 6. Electronic spectra of the Co(II) complex in acetonitrile after addition of acetylacetonone.

ESR Spectra

ESR spectra of the Cu(II) complex were recorded at room temperature and liquid nitrogen temperature (Fig. 7). There are four well resolved peaks in the low field region corresponding to g_{\parallel} (2.264) and g_{\perp} (2.0419). The trend g_{\parallel} (2.264) $>$ g (2.0419) $>$ g_e (2.0023) observed for the copper complex suggests that the unpaired electron is localized in the $d_{x^2-y^2}$ orbital of the copper ion.^{29,30} The fact that the unpaired electron lies predominately in the $d_{x^2-y^2}$ orbital is also supported by the value of the exchange interaction term G estimated from expression:

$$G = (g_{\parallel} - 2.0023) / (g_{\perp} - 2.0023)$$

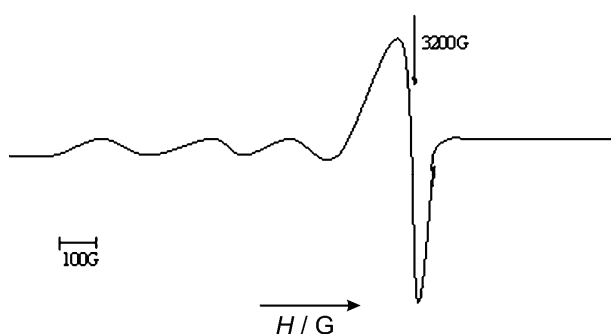


Fig. 7. ESR spectrum of the Cu(II) complex in acetonitrile at 77 K.

If $G > 4.0$, the local axes are aligned parallel or only slightly misaligned. If $G < 4.0$, significant exchange coupling is present and the misalignment is appreciable. The observed value for the exchange interaction parameter for the Cu(II) complex ($G = 6.60$) suggests that the local tetragonal axes are aligned parallel or slightly misaligned and that the unpaired electron is present in the $d_{x^2-y^2}$ orbital. The spin orbit coupling constant, λ (value: -15938 cm^{-1}), calculated using the relation, $g_{\text{av}} = 1/3(g_{\parallel} + 2g_{\perp})$ and $g_{\text{av}} = 2(1 - 2\lambda/10Dq)$, is less than that for the free Cu(II) ion, -12019 cm^{-1} , which also supports the covalent character of M-L band in the complex. The covalency parameter, α^2 , was calculated using the following equation:

$$\alpha^2(\text{Cu}) = A_{\parallel}/p + (g_{\parallel} - 2.0023) + 3/7(g_{\perp} - 2.0023) + 0.004$$

The observed value of α^2 of the complex is less than unity and slightly higher than 0.5, which indicates that the complex had some covalent character in the ligand environment.³¹ The observed g_{\parallel} value for the copper complex was less than 2.3, suggesting a covalent character of the M-L bond, which is in agreement with the observation of Kivelson and Neiman.

Redox behavior

The redox behavior of the Cu(II) complex was investigated in acetonitrile by cyclic voltammetric studies using a glassy carbon working electrode. The cathodic current function values were found to be independent of the scan rate. The repeated scans as well as the different scan rates showed that dissociation of this complex did not occur. The reduction peak of the Cu(II)/Cu(I) couple for the copper complex (Fig. 8) was observed in the potential range from $E_{pa} = 0.450$ V vs. Ag/AgCl to $E_{pc} = 0.575$ V vs. Ag/AgCl, which is similar to the value reported earlier. The ratio of the anodic and cathodic peak currents ($I_{pc}/I_{pa} \approx 1$) corresponds to a one electron process. Copper complex had a large separation between the cathodic and anodic peak of 125 mV, indicating a quasi-reversible character.^{32,33}

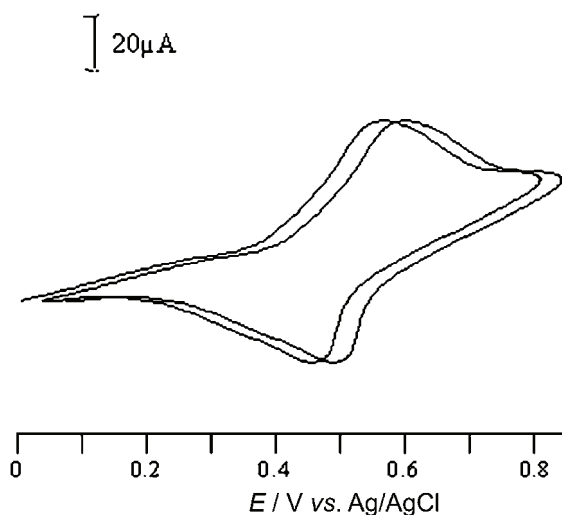


Fig. 8. Cyclic voltammograms of the Cu(II) complex in acetonitrile solution at various scan rates, viz. 50 and 150 mV s^{-1} .

Antibacterial activity

The antimicrobial activity of the ligand and its metal complexes were tested against the following stains of bacteria: *Staphylococcus aureus*, *Escherichia coli*, *Salmonella enterica typhi* and *Bacillus subtilis* by the well diffusion method.³⁴ The test solutions were prepared in acetonitrile, nutrient agar was used as the culture medium. The zone of inhibition was measured in mm and the values of the investigated compounds are summarized in Table IV.

The values indicate that the metal complexes had a higher antibacterial activity than the free ligand. Such increased activity of the metal complexes can be explained on the basis of the overtone concept³⁵ and chelation theory.³⁶ According to the overtone concept of cell permeability, the lipid membrane that surrounds the cell favors the passage of only lipid soluble materials, due to which liposolu-

bility is an important factor controlling the antimicrobial activity. On chelation, the polarity of the metal ion is reduced to a great extent due to the overlap of the ligand orbital and the partial sharing of the positive charge of the metal ion with donor groups. Furthermore, it increases the delocalization of electrons over the whole chelate ring and enhances the lipophilicity of the complex. This increased lipophilicity enhances the penetration of the complex into the lipid membrane and blocks the metal binding sites on the enzymes of the microorganism. However, the antibacterial activities of the ligand and its metal complexes were lower than those found for the standard antibacterial drug ciprofloxacin.

TABLE IV. Antibacterial activity data of the ligand and its metal complexes; concentration of the test solutions: 10^{-3} M; diameter of the well: 7 mm

Compound	Zone of inhibition, mm			
	Gram (+)		Gram (-)	
	<i>Bacillus subtilis</i>	<i>Staphylococcus aureus</i>	<i>Escherichia coli</i>	<i>Salmonella enterica typhi</i>
Ligand (LH)	10	11	14	13
[CuL ₂]	16	17	18	18
[CoL ₂]	19	14	16	16
[NiL ₂ (H ₂ O) ₂]	17	17	19	15
Ciprofloxacin	23	24	22	23

CONCLUSIONS

The available experimental data suggest that the prepared 1-(2-hydroxyphenyl)-3-phenyl-2-propen-1-one, *N*²-[(3,5-dimethyl-1*H*-pyrazol-1-yl)methyl]hydrazine possesses four coordinating sites. Physical and spectroscopic characterization of the complexes revealed that the OH group of the chalcone and the azomethine nitrogen of pyrazole were involved in the coordination and that the Cu(II) complex had square-planar geometry, whereas the Ni(II) and Co(II) complexes had octahedral and tetrahedral geometry, respectively. On addition of bases to the Co(II) complex, a change in geometry occurred due to adduct formation. Generally, antimicrobial activity is due to the hetero atom of multiple bonds or a cyclic ring system. The metal complexes had more pronounced antibacterial activities than the free ligand, probably due to a reduction of the polarity of the metal ion.

Acknowledgments. The authors are grateful to the management, principal and Department of Chemistry, Thiagarajar College, Madurai, Tamil Nadu, India, for their support.

ИЗВОД

СИНТЕЗА, СПЕКТРАЛНО ПРОУЧАВАЊЕ И АНТИБАКТЕРИЈСКА АКТИВНОСТ Cu(II), Co(II) И Ni(II) КОМПЛЕКСА СА N^2 -[(3,5-ДИМЕТИЛ-1H-ПИРАЗОЛ-1-ИЛ)МЕТИЛ]ХИДРАЗОНОМ 1-(2-ХИДРОКСИФЕНИЛ)-3-ФЕНИЛ-2-ПРОПЕН-1-ОНА

PAULMONY THARMARAJ¹, DEIVASIGAMANI KODIMUNTHIRI¹,
CLARENCE D. SHEELA² И CHAPPANI S. SHANMUGA PRIYA¹

¹Department of Chemistry, Thiagarajar College, Madurai-625009 и ²Department of Chemistry, The American College, Madurai-625002, India

Нова серија комплекса Cu(II), Co(II) и Ni(II) са N^2 -[(3,5-диметил-1H-пиразол-1-ил)метил]хидразоном 1-(2-хидроксифенил)-3-фенил-2-пропен-1-она као лигандом, C₂₁H₂₂N₄O (LH), добијена је реакцијом хидразона 1-(2-хидроксифенил)-3-фенил-2-пропен-1-она са (3,5-диметил-1H-пиразол-1-ил)метанолом и окарактерисана. Природа везе и геометрија комплекса су изведени на основу елементалне анализе, IR, електронских и ¹H-NMR спектра, магнетне суспектибилности и мерења проводљивости. Проучавање је показало квадратну, тетраедарску и октаедарску геометрију за бакар(II), кобалт(II), односно никал(II) комплексе. ESR спектри бакар(II) комплекса у ацетонитрилу на 300 и 77 K су снимљени и дате су њихове истакнуте карактеристике. Електрохемијско понашање бакар(II) комплекса изучавано је циклчном волтаметријом. Антимикробна активност лиганда и његових металних комплекса тестирана је на следећим сојевима микроорганизама: *Staphylococcus aureus*, *Salmonella enterica typhi*, *Escherchia coli* и *Bacillus subtilis* дифузионом методом. Метални комплекси показали су повећану антимикробну активност у односу на слободни лиганд.

(Примљено 6. јануара, ревидирано 16. априла 2009)

REFERENCES

1. W. Klaui, D. Schramm, G. Schramm, *Inorg. Chim. Acta* **357** (2004) 1642
2. M. C. Torralba, M. Cano, J. A. Campo, J. V. Heras, E. Pinilla, M. R. Torres, *Inorg. Chem. Commun.* **5** (2002) 887
3. A. A. Bekhit, T. Abdel-Aziem, *Bioorg. Med. Chem.* **12** (2004) 1935
4. P. M. Takahashi, A. V. G. Netto, A. E. Mauro, R. C. G. Frem, *J. Therm. Anal. Calorim.* **79** (2005) 335
5. S. G. Kucukguzel, S. Rollas, H. Erdeniz, M. Kiraz, A. C. Ekinici, A. Vidin, *Eur. J. Med. Chem.* **35** (2000) 761
6. I. Schepetkin, A. Potapov, A. Khlebnikov, E. Korotkova, A. Lukina, G. Malovichko, L. Kirpotina, M. T. Quinn, *J. Biol. Inorg. Chem.* **11** (2006) 499
7. J. J. Baldwin, P. K. Lumma, F. C. Novello, G. S. Ponticello, J. M. Sprague, D. E. Duggan, *J. Med. Chem.* **20** (1977) 1189
8. J. R. Beck, M. P. Lynch [C.A. 103/1985 141938]
9. I. Okada, S. Okui, Y. Takahashi, T. Fukuchi [C.A. 110/1989 96234]
10. H. Ishikawa, T. Morita, T. Oono, T. Nakamura, M. Taniguchi, H. Yoshizawa, M. Yochihara [C.A. 120/1994 99438]
11. A. Gursoy, S. Demirayak, G. Capan, K. Erol, *Eur. J. Med. Chem.* **35** (2000) 359
12. B. S. Hammes, C. J. Carrano, *Chem. Commun.* (2000) 1635
13. T. C. Higgs, R. S. Czernuscewicz, G. J. Carrano, *Inorg. Chim. Acta*, **273** (1998) 14
14. T. N. Sorrell, *Tetrahedron* **45** (1989) 3
15. E. Bouwmann, W. L. Driessen, J. Reedijk, *Coord. Chem. Rev.* **104** (1990) 143

16. F. Mani, *Coord. Chem. Rev.* **120** (1992) 325
17. T. O. Denisova, E. V. A. Chenkova, I. S. Kislina, N. B. Librovich, S. E. Nefedov, *Russ. J. Inorg. Chem.* **51** (2006) 1755
18. R. C. Elderfield, *Heterocyclic compounds*, John Wiley, New York, 1959, p. 565
19. C. H. Lin, C. T. Lin, C. L. Yeh, *J. Chin. Chem. Soc. (Taipei)* **9** (1967) 14
20. B. S. Furnis, A. J. Hannaford, P. W. G. Smith, A. R. Tatchen, *Vogel's Textbook of Practical Organic Chemistry*, Longman, London, 1989, p. 1149
21. K. Nakamoto, *Spectroscopy and Structure of Metal Chelate Compounds*, John Wiley, New York, 1988, p. 214
22. K. Gudasi, M. Patil, R. Vadavi, R. Shenoy, S. Patil, *J. Serb. Chem. Soc.* **72** (2007) 357
23. C. Natarajan, P. Tharmaraj, *Indian J. Chem. Sec A.* **29A** (1990) 666
24. C. M. Sharaby, *Spectrochim. Acta A* **66** (2007) 1271
25. A. B. P. Lever, *Inorganic Electronic Spectroscopy*, 2nd ed., New York, 1968, p. 317
26. R. L. Dutta, A. Syamal, *Elements of Magnetochemistry*, 2nd ed., New Delhi, 1992, p. 206
27. K. Gudasi, S. A. Patil, R. Vadavi, V. Rashmi, R. Shenoy, M. S. Patil, *J. Serb. Chem. Soc.* **71** (2006) 357
28. E. K. Barefield, D. H. Busch, S. M. Nelson, *Quart. Rev.* **22** (1986) 457
29. B. J. Hathaway, A. A. G. Tomlinson, *Coord. Chem. Rev.* **5** (1970) 1
30. I. M. Procter, B. J. Hathaway, D. E. Billing, P. Nicholls, *J. Chem. Soc. A* (1968) 1678
31. A. G. Tomlinson, B. J. Hathaway, P. Nicholls, *J. Chem. Soc. A* (1969) 65
32. K. G. Dutton, G. D. Fallon, K. S. Murray, *Inorg. Chem.* **27** (1998) 34
33. P. Knopp, K. Weighardt, B. Nuber, J. Weiss, W. S. Scheldrick, *Inorg. Chem.* **29** (1990) 363
34. C. Perez, M. Pauli, P. Bazevque, *Acta Biol. Med. Exp.* **15** (1990) 113
35. Y. Anjaneyulu, R. P. Rao, *Synth. React. Inorg. Met. Org. Chem.* **16** (1986) 257
36. L. Mishra, V. K. Singh, *Indian J. Chem.* **32A** (1993) 446.



J. Serb. Chem. Soc. 74 (8–9) 939–951 (2009)
JSCS–3889

Journal of
the Serbian
Chemical Society

JSCS@tmf.bg.ac.rs • www.shd.org.rs/JSCS

UDC 546.732:742:562:472:547.217.2+
547.556.3:541.123.2

Original scientific paper

Metal ion controlled synthesis of 16- and 18-membered binuclear octaazamacrocyclic complexes with Co(II), Ni(II), Cu(II) and Zn(II): a comparative spectroscopic approach to DNA binding to Cu(II) complexes

FARHA FIRDAUS^{1*}, KANEEZ FATMA¹, ASAD U. KHAN²
and MOHAMMAD SHAKIR^{1‡}

¹Division of Inorganic Chemistry, Department of Chemistry, Aligarh Muslim University, Aligarh-202002, and ²Interdisciplinary Biotechnology Unit, Aligarh Muslim University, Aligarh-202002, India

(Received 12 January, revised 7 May 2009)

Abstract: A series of 16- and 18-membered binuclear octaazamacrocyclic complexes, $[M_2L_1(NO_3)_4]$ and $[M_2L_2(NO_3)_4]$ ($M = Co(II), Ni(II), Cu(II), Zn(II)$, $L_1 = 3,8,11,16$ -tetramethyl-1,2,4,7,9,10,12,15-octaaza-3,7,11,15-cyclohexadecatetraene and $L_2 = 3,9,12,18$ -tetramethyl-1,2,4,8,10,11,13,17-octaaza-3,8,12,17-cyclooctadecatetraene) were synthesized by metal template condensation of *N,N'*-diacetylhydrazine with 1,2-diaminoethane and 1,3-diaminopropane in methanol. The formation of macrocyclic ligand frameworks, the bonding of the macrocyclic moieties in the complexes and the overall geometry of the complexes were deduced based on the results obtained from elemental analyses as well as molar conductivity, FTIR, ¹H-, ¹³C-NMR, EPR, ESI-mass, UV–Vis spectral studies and magnetic measurements. An octahedral geometry is proposed for all the complexes, while a distortion in the octahedral geometry was registered for the Cu(II) complexes. Comparative fluorescence and UV–Vis studies on the Cu(II) complexes proved a significant binding to calf thymus DNA.

Keywords: octaazamacrocycles; Cu(II), Co(II), Ni(II) and Zn(II) binuclear complexes; template condensation; DNA binding studies.

INTRODUCTION

In the last few years, a great deal of research has been aimed at designing macrocyclic compounds and studying their physico–chemical properties.^{1,2} These investigations emphasized the great relevance of these systems in basic and applied chemistry. Several synthetic strategies are nowadays available for the

* Corresponding author. E-mail: farha_firdaus@yahoo.co.in

‡ Present address: Chemistry Department, College of Science King Khaled University, Abha, Saudi-Arabia.

doi: 10.2298/JSC0909939F



preparation of well-organized molecular systems or molecular devices, which exhibit peculiar physico-chemical properties or have well defined properties.¹⁻⁴ Among the various synthetic strategies proposed, template condensation is one of the most highlighted. Metal template condensation provides selective routes towards products that are not obtainable in the absence of the metal ion.⁵ The high thermodynamic stability and extreme kinetic inertness of many transition metal complexes with polyazamacrocyclic ligands are significant, as they enhance important industrial applications.⁵⁻⁷ In particular, the chemistry of tetraazamacrocycles has received special attention due to their applications in a variety of catalysis, biochemical and industrial processes.⁸ Hexa- and octa-azamacrocycles are known to give several mononuclear complexes, in spite of the large size of the cavity formed by the macrocyclic backbones, as well as to stabilize various anions in their protonated forms.⁹⁻¹¹ The synthesis of binuclear complexes has become a point of increasing interest due to their mimicry in terms of physical and chemical properties with the binuclear metal centers in enzymes.¹² A number of binuclear complexes were reported earlier due to their potential relevance in bioinorganic,¹³ magneto,¹⁴ redox¹⁵ and coordination chemistry,^{16,17} as well as in homogeneous catalysis.¹⁸ In these systems, there is often an additional internal or external bridging group which completes the structure of the binuclear species and has the advantage of being relatively rigid, thus giving structurally well defined moieties.¹⁹ Binuclear copper-containing proteins play an important role in biology, including dioxygen transport or activation, electron transfer, reduction of nitrogen oxides and hydrolytic consequences.²⁰ Hence, the design and synthesis of model compounds that mimic the physical and chemical properties of the active sites present in metalloenzymes are essential and the study of such compounds is becoming increasingly important in understanding the biological functions of bimetallic cores of enzymes.²¹ In order to extend this work, herein, the synthesis and characterization is reported of novel binuclear octaazamacrocyclic complexes resulting from the template condensation of *N,N'*-diacetylhydrazine with 1,2-diaminoethane and 1,3-diaminopropane, $[M_2L_1(NO_3)_4]$ and $[M_2L_2(NO_3)_4]$, where $M = Co(II), Ni(II), Cu(II), Zn(II)$, $L_1 = 3,8,11,16$ -tetramethyl-1,2,4,7,9,10,12,15-octaaza-3,7,11,15-cyclohexadecatetraene and $L_2 = 3,9,12,18$ -tetramethyl-1,2,4,8,10,11,13,17-octaaza-3,8,12,17-cyclooctadecatetraene. Finally, the binding of the $Cu(II)$ complexes with DNA were screened.

EXPERIMENTAL

Materials and methods

The metal salts, $Co(NO_3)_2 \cdot 6H_2O$, $Ni(NO_3)_2 \cdot 6H_2O$, $Cu(NO_3)_2 \cdot 3H_2O$, and $Zn(NO_3)_2 \cdot 6H_2O$, 1,2-diaminoethane, 1,3-diaminopropane (all E. Merck) and *N,N'*-diacetylhydrazine (Acros) were commercially available as pure chemicals. Methanol used as the solvent was of A.R. grade (E. Merck). Highly polymerized calf thymus DNA sodium salt (containing 7 % of Na) was purchased from Sigma. Other chemicals were of reagent grade and used without further

purification. The calf thymus DNA was dissolved to 0.50 % w/w (12.5 mM DNA/phosphate) in 0.10 M sodium phosphate buffer (pH 7.40) at 310 K for 24 h with occasional stirring to ensure the formation of a homogeneous solution. The purity of the DNA solution was checked from the absorbance ratio A_{260}/A_{280} . Since the absorption ratio lay in the range $1.8 < A_{260}/A_{280} < 1.9$, no further deproteinization of the DNA was required. Stock solutions of the complexes $[\text{Cu}_2\text{L}_1(\text{NO}_3)_4]$ and $[\text{Cu}_2\text{L}_2(\text{NO}_3)_4]$, synthesized as described below (abbreviated with **1c** and **2c**) ($c = 5 \text{ mg/ml}$) were also prepared.

Synthesis of tetranitrato(3,8,11,16-tetramethyl-1,2,4,7,9,10,12,15-octaza-3,7,11,15-cyclohexadecatetraene)bimetal(II) type of complexes

A methanolic solution ($\approx 25 \text{ ml}$) of 1,2-diaminoethane (0.54 ml, 8.0 mmol) and N,N' -diacetylhydrazine (0.93 g, 8.0 mmol) in methanol ($\approx 25 \text{ ml}$) were simultaneously added dropwise to stirred methanolic solution ($\approx 25 \text{ ml}$) of metal salt (8.0 mmol). The resultant mixture was stirred for several hours leading to isolation of the solid product, which was then filtered off, washed several times with methanol and dried under vacuum to give the complex $[\text{M}_2\text{L}_1(\text{NO}_3)_4]$ ($\text{M} = \text{Co(II)}$ (**1a**), Ni(II) (**1b**), Cu(II) (**1c**) and Zn(II) (**1d**)).

Synthesis of tetranitrato(3,9,12,18-tetramethyl-1,2,4,8,10,11,13,17-octaza-3,8,12,17-cyclooctadecatetraene)bimetal(II) type of complexes

The procedure was similar to the one mentioned above, except 1,3-diaminopropane (0.67 ml, 8.0 mmol) was used instead of 1,2-diaminoethane, whereby the complexes $[\text{M}_2\text{L}_2(\text{NO}_3)_4]$ ($\text{M} = \text{Co(II)}$ (**2a**), Ni(II) (**2b**), Cu(II) (**2c**) and Zn(II) (**2d**)) were obtained.

Binding analysis of complexes 1c and 2c

To elaborate the fluorescence quenching mechanism, the Stern-Volmer equation was used for data analysis:²²

$$F_0/F = 1 + K_{SV}[Q] \quad (1)$$

where F_0 and F are the steady-state fluorescence intensities in the absence and presence of quencher, respectively. K_{SV} is the Stern–Volmer quenching constant and $[Q]$ is the concentration of quencher (DNA). The values of K_{SV} for complexes **1c** and **2c** were found to be of the order of 10^4 . The linearity of the F_0/F vs. $[Q]$ (Stern–Volmer) plots for the DNA–**1c** and DNA–**2c** complexes (Fig. 1) indicates that the quenching may be static or dynamic, since the

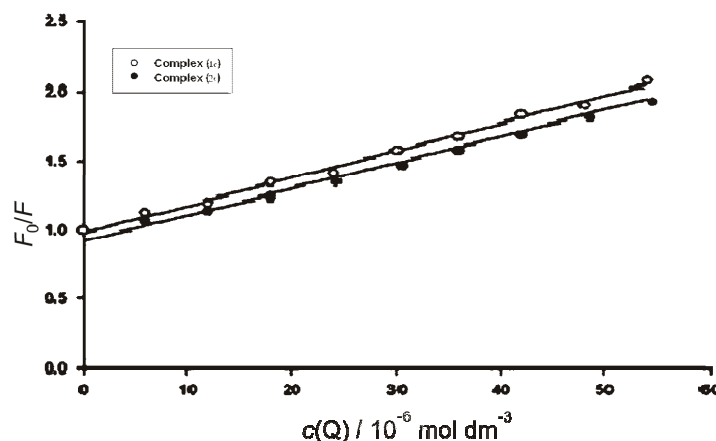


Fig. 1. Stern–Volmer plot for the binding of complex **1c** and **2c** with DNA at 298 K, pH 7.4.

characteristic Stern–Volmer plot of combined quenching (both static and dynamic) has an upward curvature. When ligand molecules bind independently to a set of equivalent sites on a macromolecule, the equilibrium between free and bound molecules is given by the equation:²³

$$\log [(F_0 - F)/F] = \log K + n \log [Q] \quad (2)$$

where K and n are the binding constant and the number of binding sites, respectively. Thus, a plot of $\log (F_0 - F)/F$ vs. $\log [Q]$ can be used to determine K as well as n .

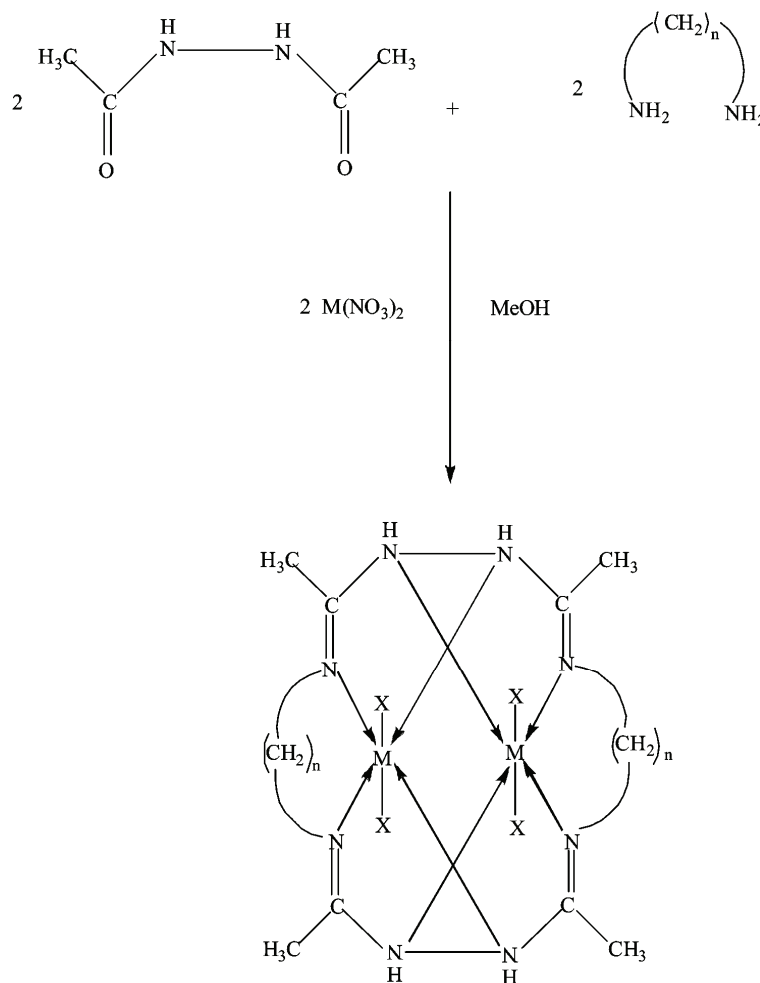
Physical measurements

Elemental analyses were obtained from C. D. R. I. Lucknow, India. The IR spectra (4000–200 cm^{-1}) of the complexes were recorded as CsI/KBr discs on a Perkin-Elmer-621 spectrophotometer. The ESI-mass spectra were obtained by electrospray ionization on a Micromass Quattro II triple quadrupole mass spectrometer from C.D.R.I. Lucknow. The ^1H - and ^{13}C -NMR spectra were recorded in DMSO- d_6 using a Jeol FT NMR AL-300 MHz spectrometer with Me_4Si from G. N. D. U. Amritsar India as the internal standard. The electronic spectra of the complexes in DMSO were recorded on Pye-Unicam 8800 spectrophotometer. The magnetic susceptibility measurements were performed using a Faraday balance at 25 °C. The data were corrected for diamagnetic susceptibilities using Pascal's constants. The EPR spectra of the Cu(II) complexes were recorded as powder samples at room temperature on an E-4 spectrometer using DPPH as the g -marker. The molar conductivity data for 10^{-3} M solution in DMSO were recorded on a Systronic type 302 conductivity bridge thermostated at 25.00 ± 0.05 °C. The contents of metals were determined volumetrically.²⁴ Fluorescence measurements were performed on a spectrofluorimeter Model RF-5301PC (Shimadzu, Japan) equipped with a 150W Xenon lamp using a slit width of 5 nm. A 1.00 cm quartz cell was used for the measurements. For the determination of binding parameters, 30 μM of complex solution was taken in a quartz cell and increasing amounts of CT DNA solution were titrated. Fluorescence spectra were recorded at 310 K in the range of 740–880 nm with excitation at 280 (λ_{em} was 770 nm). The UV measurements of calf thymus DNA were recorded on a Shimadzu double beam spectrophotometer model UV 1700 using a 1 cm path length cuvette. Absorbance values of DNA in the absence and presence of complex were measured in the range of 220–300 nm. DNA concentration was fixed at 0.10 mM, while the compound was added in increasing concentrations.

RESULTS AND DISCUSSION

The metal ion controlled reaction of the 1,2-diaminoethane and 1,3-diaminopropane with N,N' -diacetylhydrazine in 1:1:1 molar ratio resulted in the formation of new series of 16- and 18-membered binuclear Schiff-base macrocyclic complexes of the types $[\text{M}_2\text{L}_1(\text{NO}_3)_4]$ and $[\text{M}_2\text{L}_2(\text{NO}_3)_4]$, where $\text{M} = \text{Co(II)}$, Ni(II) , Cu(II) and Zn(II) (Scheme 1). The resulting complexes were obtained as colored solids in moderate yields (54–65 %). All the complexes were soluble in polar solvents and were stable at room temperature. The purity of the complexes was checked by TLC on a silica gel coated plate using EtOAc–MeOH (6:4 v/v) as the eluent. The elemental analyses (Table I) agree well with the proposed stoichiometry of the binuclear octaazamacrocyclic complexes. The positions of the molecular ion peaks in the mass spectra were consistent with the empirical mole-

cular formulae (Table I). The molar conductivities (Table I) of all the complexes in DMSO corresponded to a non-electrolytic²⁵ nature of these complexes.



Scheme 1. M = Co(II), Ni(II), Cu(II) and Zn(II), X = NO₃⁻, n = 2 for the complex [M₂L₁(NO₃)₄] and n = 3 for the complex [M₂L₂(NO₃)₄].

Elemental analyses

Anal. Calcd. for [Co₂L₁(NO₃)₄] (C₁₂H₂₄Co₂N₁₂O₁₂): C, 22.22; H, 3.58; N, 25.82; Co, 18.00. Found: C, 22.30; H, 3.74; N, 26.00; Co, 18.23. Anal. Calcd. for [Co₂L₂(NO₃)₄] (C₁₄H₂₈Co₂N₁₂O₁₂): C, 24.66; H, 4.09; N, 24.77; Co, 17.38. Found: C, 24.93; H, 4.18; N, 24.92; Co, 17.47. Anal. Calcd. for [Ni₂L₁(NO₃)₄] (C₁₂H₂₄Ni₂O₁₂): C, 22.0; H, 3.62; N, 26.00; Ni, 18.14. Found: C, 22.31; H, 3.74; N, 26.02; Ni, 18.17. Anal. Calcd. for [Ni₂L₂(NO₃)₄] (C₁₄H₂₈Ni₂O₁₂):

C, 24.73; H, 4.15; N, 24.52; Ni, 17.22. Found: C, 24.95; H, 4.18; N, 24.94; Ni, 17.42. Anal. Calcd. for $[\text{Cu}_2\text{L}_1(\text{NO}_3)_4]$ ($\text{C}_{12}\text{H}_{24}\text{Cu}_2\text{N}_{12}\text{O}_{12}$): C, 21.82; H, 3.37; N, 25.32; Cu, 19.00. Found: C, 21.98; H, 3.69; N, 25.64; Cu, 19.38. Anal. Calcd. for $[\text{Cu}_2\text{L}_2(\text{NO}_3)_4]$ ($\text{C}_{14}\text{H}_{28}\text{Cu}_2\text{N}_{12}\text{O}_{12}$): C, 24.52; H, 4.10; N, 24.32; Cu, 18.28. Found: C, 24.60; H, 4.12; N, 24.58; Cu, 18.59. Anal. Calcd. for $[\text{Zn}_2\text{L}_1(\text{NO}_3)_4]$ ($\text{C}_{12}\text{H}_{24}\text{N}_{12}\text{O}_{12}\text{Zn}_2$): C, 21.73; H, 3.54; N, 25.21; Zn, 19.62. Found: C, 21.86; H, 3.66; N, 25.49; Zn, 19.83. Anal. Calcd. for $[\text{Zn}_2\text{L}_2(\text{NO}_3)_4]$ ($\text{C}_{14}\text{H}_{28}\text{N}_{12}\text{O}_{12}\text{Zn}_2$): C, 24.30; H, 4.01; N, 24.39; Zn, 19.00. Found: C, 24.46; H, 4.10; N, 24.45; Zn, 19.02.

TABLE I. Elemental analyses, m/z values, color, yield, molar conductance and melting point values of the prepared complexes

Compound	m/z Found (Calcd.)	Color	Yield, %	Molar conductance $\text{S mol}^{-1} \text{cm}^2$	M.p. $^\circ\text{C}$
$[\text{Co}_2\text{L}_1(\text{NO}_3)_4]$ (1a) $\text{C}_{12}\text{H}_{24}\text{N}_{12}\text{Co}_2\text{O}_{12}$	646.20 (646.25)	Brown	58	13	>300 $^\circ\text{C}$
$[\text{Co}_2\text{L}_2(\text{NO}_3)_4]$ (2a) $\text{C}_{14}\text{H}_{28}\text{N}_{12}\text{Co}_2\text{O}_{12}$	674.00 (674.31)	Dark brown	65	17	>300 $^\circ\text{C}$
$[\text{Ni}_3\text{L}_1(\text{NO}_3)_4]$ (1b) $\text{C}_{12}\text{H}_{24}\text{N}_{12}\text{Ni}_2\text{O}_{12}$	645.52 (645.77)	Violet	55	19	>300 $^\circ\text{C}$
$[\text{Ni}_3\text{L}_2(\text{NO}_3)_4]$ (2b) $\text{C}_{14}\text{H}_{28}\text{N}_{12}\text{Ni}_2\text{O}_{12}$	673.80 (673.82)	Purple	63	21	>300 $^\circ\text{C}$
$[\text{Cu}_2\text{L}_1(\text{NO}_3)_4]$ (1c) $\text{C}_{12}\text{H}_{24}\text{N}_{12}\text{Cu}_2\text{O}_{12}$	655.25 (655.48)	Blue	62	23	>300 $^\circ\text{C}$
$[\text{Cu}_2\text{L}_2(\text{NO}_3)_4]$ (2c) $\text{C}_{14}\text{H}_{28}\text{N}_{12}\text{Cu}_2\text{O}_{12}$	683.50 (683.54)	Dark blue	65	18	>300 $^\circ\text{C}$
$[\text{Zn}_2\text{L}_1(\text{NO}_3)_4]$ (1d) $\text{C}_{12}\text{H}_{24}\text{N}_{12}\text{Zn}_2\text{O}_{12}$	659.10 (659.15)	Colorless	60	24	>300 $^\circ\text{C}$
$[\text{Zn}_2\text{L}_2(\text{NO}_3)_4]$ (2d) $\text{C}_{14}\text{H}_{28}\text{N}_{12}\text{Zn}_2\text{O}_{12}$	687.09 (687.20)	Colorless	54	20	>300 $^\circ\text{C}$

FTIR spectra

The IR spectra of the binuclear complexes of the type $[\text{M}_2\text{L}_1(\text{NO}_3)_4]$ and $[\text{M}_2\text{L}_2(\text{NO}_3)_4]$ exhibited characteristic bands of the expected functional groups and relevant data are given in Table II. The formation of the macrocyclic complexes was confirmed by the appearance of a $\nu(\text{C}=\text{N})$ band²⁶ in the region 1600–1620 cm^{-1} and the absence of the $\nu(\text{NH}_2)$ bands at $\approx 3400 \text{ cm}^{-1}$, indicating that a Schiff base condensation between the carbonyl group of diacetylhydrazine and the amino group of the alkylamine had occurred. This fact is further supported by the presence of a medium intensity $\nu(\text{M}-\text{N})$ band, observed in the 382–400 cm^{-1} region.²⁶ In addition to the above, a medium intensity band appeared in the region 3230–3250 cm^{-1} , which may be assigned to the $\nu(\text{N}-\text{H})$ stretching vibration of the secondary amine of the condensed diacetylhydrazine moiety.²⁷ The absorption band appearing in the region 2870–2920 cm^{-1} may be due to the $\nu(\text{C}-\text{H})$

stretching vibration. Moreover, the strong band at around 950–973 cm^{-1} may be ascribed to the $\nu(\text{N-N})$ stretching mode of the condensed diacetylhydrazine moiety.²⁸ The coordination of the nitrate group with the metal was ascertained by the bands in the 230–245 cm^{-1} region, which may reasonably be assigned to the $\nu(\text{M-O})$ of the (O-NO_2) group. The spectra of the metal complexes gave additional bands at around 1235–1260, 1028–1060 and 855–870 cm^{-1} , which are consistent with the monodentate coordination of nitrate anions.²⁹

TABLE II. IR spectral data (cm^{-1}) of the complexes

Compound	$\nu(\text{C=N})$	$\nu(\text{N-N})$	$\nu(\text{N-H})$	$\nu(\text{M-N})$	$\nu(\text{M-O})$
$[\text{Co}_2\text{L}_1(\text{NO}_3)_4]$	1608(<i>s</i>)	952(<i>s</i>)	3236(<i>m</i>)	382(<i>m</i>)	242(<i>m</i>)
$[\text{Co}_2\text{L}_2(\text{NO}_3)_4]$	1600(<i>s</i>)	970(<i>s</i>)	3248(<i>m</i>)	394(<i>m</i>)	230(<i>m</i>)
$[\text{Ni}_2\text{L}_1(\text{NO}_3)_4]$	1617(<i>s</i>)	962(<i>s</i>)	3233(<i>m</i>)	395(<i>m</i>)	245(<i>m</i>)
$[\text{Ni}_2\text{L}_2(\text{NO}_3)_4]$	1603(<i>s</i>)	955(<i>s</i>)	3245(<i>m</i>)	390(<i>m</i>)	233(<i>m</i>)
$[\text{Cu}_2\text{L}_1(\text{NO}_3)_4]$	1619(<i>s</i>)	966(<i>s</i>)	3230(<i>m</i>)	386(<i>m</i>)	238(<i>m</i>)
$[\text{Cu}_2\text{L}_2(\text{NO}_3)_4]$	1610(<i>s</i>)	950(<i>s</i>)	3250(<i>m</i>)	388(<i>m</i>)	240(<i>m</i>)
$[\text{Zn}_2\text{L}_1(\text{NO}_3)_4]$	1615(<i>s</i>)	958(<i>s</i>)	3240(<i>m</i>)	398(<i>m</i>)	235(<i>m</i>)
$[\text{Zn}_2\text{L}_2(\text{NO}_3)_4]$	1620(<i>s</i>)	973(<i>s</i>)	3242(<i>m</i>)	400(<i>m</i>)	244(<i>m</i>)

¹H-NMR spectra

The ¹H-NMR spectra of the **1d** and **2d** complexes exhibited resonance peaks at δ 6.20 and 6.23 ppm for secondary amino protons (4H, $-\text{C-NH-N-}$) and δ 2.09 and 2.15 ppm for imine methyl³⁰ protons (12H, $\text{CH}_3\text{C=N-}$) of the condensed diacetylhydrazine moiety. A singlet at δ 3.16 and 3.25 ppm for **1d** and **2d**, respectively, may reasonably be assigned to methylene protons (8H, $-\text{N-CH}_2-\text{C-}$) of the condensed amino moiety. While another singlet observed at δ 1.98 ppm may reasonably be assigned to the middle methylene protons (4H, $-\text{C-CH}_2-\text{C-}$) of the propane moiety in **2d**.³¹

¹³C-NMR spectra

The ¹³C-NMR spectra for Zn(II) complexes revealed the presence of the imine moiety ($>\text{C=N-}$) at 158 and 160 ppm in both complexes.³² The chemical shifts of the ($>\text{N-CH}_2-$) carbons appear at 45 and 43 ppm for 1,2-diaminoethane and 1,3-diaminopropane, respectively.³⁰ Moreover, the resonance peaks observed at 22 and 23 ppm correspond to the four methyl carbon adjacent to imine group.³⁰ Another signal observed at 33 ppm was assigned to the middle carbon atom ($-\text{CH}_2-$) of the 1,3-diaminopropane moiety.³²

EPR spectra

The EPR spectra of the complexes **1c** and **2c** were recorded at room temperature and their g_{\parallel} and g_{\perp} values were calculated (Table III). Both the complexes exhibited a similar single absorption band (Figs. 2 and 3). The absence of hyperfine lines in the spectra of these complexes may be due to the strong dipolar and ex-

change interactions between the Cu(II) ions in the unit cell. The calculated g_{\parallel} values of 2.112 and 2.147 and the g_{\perp} values of 2.071 and 2.047 for **1c** and **2c**, respectively, support the fact that ${}^2B_{1g}$ is the ground state, having an unpaired electron in the $d_{x^2-y^2}$ orbital of the Cu(II) ion. Both the complexes show $g_{\parallel} < 2.3$, indicating that the present complexes exhibit appreciable covalent nature.³³ The observed $g_{\parallel} < 2.0023$ for the complexes show that the unpaired electron is localized in the $d_{x^2-y^2}$ orbital of the Cu(II) ion, which is characteristic of the axial symmetry. Tetragonally elongated geometry³⁴ is thus confirmed for the aforesaid complexes.

Table III. Magnetic moment values, electronic spectral data with their assignments and EPR spectral parameters of the complexes

Compound	μ_{eff} / μ_B	Band position cm^{-1}	Assignments	EPR parameters		
				g_{\parallel}	g_{\perp}	G
[Co ₂ L ₁ (NO ₃) ₄]	4.60	9000	${}^4T_{1g}(\text{F}) \rightarrow {}^4T_{2g}(\text{F})$	2.112	2.071	1.577
		17000	${}^4T_{1g}(\text{F}) \rightarrow {}^4A_{2g}(\text{F})$			
		21850	${}^4T_{1g}(\text{F}) \rightarrow {}^4T_{1g}(\text{P})$			
[Co ₂ L ₂ (NO ₃) ₄]	4.57	9090	${}^4T_{1g}(\text{F}) \rightarrow {}^4T_{2g}(\text{F})$	2.147	2.047	3.127
		16750	${}^4T_{1g}(\text{F}) \rightarrow {}^4A_{2g}(\text{F})$			
		21600	${}^4T_{1g}(\text{F}) \rightarrow {}^4T_{1g}(\text{P})$			
[Ni ₂ L ₁ (NO ₃) ₄]	3.34	11400	${}^3A_{2g}(\text{F}) \rightarrow {}^3T_{2g}(\text{F})$	2.112	2.071	1.577
		17500	${}^3A_{2g}(\text{F}) \rightarrow {}^3T_{1g}(\text{P})$			
[Ni ₂ L ₁ (NO ₃) ₄]	3.40	11200	${}^3A_{2g}(\text{F}) \rightarrow {}^3T_{2g}(\text{F})$	2.147	2.047	3.127
		17600	${}^3A_{2g}(\text{F}) \rightarrow {}^3T_{1g}(\text{P})$			
[Cu ₂ L ₁ (NO ₃) ₄]	1.90	13000	${}^2B_{1g} \rightarrow {}^2A_{1g}$	2.112	2.071	1.577
		17000	${}^2B_{1g} \rightarrow {}^2E_g$			
[Cu ₂ L ₂ (NO ₃) ₄]	1.87	13750	${}^2B_{1g} \rightarrow {}^2A_{1g}$	2.147	2.047	3.127
		16650	${}^2B_{1g} \rightarrow {}^2E_g$			



Fig. 2. X-band EPR spectrum of the **1c** complex at room temperature.

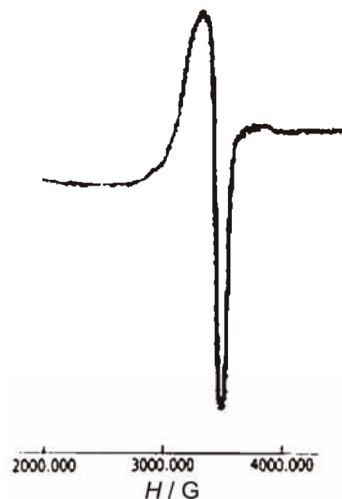


Fig. 3. X-band EPR spectrum of the **2c** complex at room temperature.

The G values are related by the expression $G = (g_{\parallel} - 2) / (g_{\perp} - 2)$, and lie in the range 1.577 and 3.127 for the complexes **1c** and **2c**, indicating a significant exchange interaction³⁵ among the Cu(II) ions in these complexes, as the G values were less than 4.

Electronic spectra and magnetic susceptibility data

The electronic spectra of the binuclear Co(II) complexes (Table III) showed three bands in the range 9,000, 17,000 and 21,850 cm^{-1} for **1a** and 9,090, 16,750 and 21,600 cm^{-1} for **2a** complexes, attributed to ${}^4\text{T}_{1g}(\text{F}) \rightarrow {}^4\text{T}_{2g}(\text{F})$, ${}^4\text{T}_{1g}(\text{F}) \rightarrow {}^4\text{A}_{2g}(\text{F})$ and ${}^4\text{T}_{1g}(\text{F}) \rightarrow {}^4\text{T}_{1g}(\text{P})$ transitions, respectively, consistent with an octahedral geometry³⁶ around the Co(II) ion. The magnetic moment values of 4.60 μ_{B} for the **1a** and 4.57 μ_{B} for the **2a** complex (Table III) correspond to high spin Co(II) in an octahedral environment. The relatively higher values of the observed magnetic moments than that of the spin only moment (3.89 μ_{B}) may be attributed in terms of the orbital contribution³⁶ generally observed for Co(II) compounds.

The Ni(II) ion complexes exhibit two absorption bands in the region 11,400 and 17,500 cm^{-1} for the **1b**, and 11,200 and 17,600 cm^{-1} for the **2b** complex, corresponding to ${}^3\text{A}_{2g}(\text{F}) \rightarrow {}^3\text{T}_{2g}(\text{F})$ and ${}^3\text{A}_{2g}(\text{F}) \rightarrow {}^3\text{T}_{1g}(\text{P})$ transitions, respectively, suggesting an octahedral geometry.³⁷ Further confirmation regarding the octahedral environment around the Ni(II) ion was deduced from the magnetic moment values of 3.34 μ_{B} and 3.40 μ_{B} for the **1b** and **2b** complexes, respectively (Table III).

The electronic spectra of the hexacoordinated Cu(II) complexes showed three spin allowed transitions in the visible and near IR regions. These bands were assigned as ${}^2\text{B}_{1g} \rightarrow {}^2\text{A}_{1g}$ ($d_{x^2-y^2} - d_{z^2}$), ${}^2\text{B}_{1g} \rightarrow {}^2\text{B}_{2g}$ ($d_{x^2-y^2} - d_{xy}$) and ${}^2\text{B}_{1g} \rightarrow {}^2\text{E}_g$ ($d_{x^2-y^2} - d_{xz}$, d_{yz}) transitions in the increasing order of their energies. The energy level sequence will depend on the amount of tetragonal distortion due to the ligand field and the Jahn–Teller effect.^{38,39} The electronic spectra of the complexes reported here show two characteristic bands in the range 13000 and 17000 cm^{-1} for the **1c** and 13750 and 16650 cm^{-1} for the **2c** complex. These may reasonably be assigned to ${}^2\text{B}_{1g} \rightarrow {}^2\text{A}_{1g}$ and ${}^2\text{B}_{1g} \rightarrow {}^2\text{E}_g$ transitions, respectively. A band corresponding to the ${}^2\text{B}_{1g} \rightarrow {}^2\text{B}_{2g}$ transition was not observed as a separate band, which may be due to tetragonal distortion.³⁹ The observed magnetic moments of 1.90 μ_{B} for the **1c** and 1.87 μ_{B} for the **2c** complex further supplement the electronic spectral findings (Table III).

Fluorescence measurements

Interactions of DNA with complexes 1c and 2c. Fluorescence spectroscopy provides insight into changes occurring in the DNA microenvironment on addition of the complexes. The interaction of the compounds with calf thymus DNA was studied by monitoring the changes in the intrinsic fluorescence of these com-

pounds at varying DNA concentrations. Representative fluorescence emission spectra of the compounds upon excitation at 290 nm are shown in Figs. 4A and 4B. The addition of DNA caused a gradual decrease in the fluorescence emission intensity of both compounds, with a conspicuous change in the emission spectra. The spectra illustrate that higher excesses of DNA led to more effective quenching of the fluorescence of the fluorophore molecule. The quenching of fluorescence clearly indicates that the binding of the DNA to complexes **1c** and **2c** changed the microenvironment of the fluorophore residue. The shift in emission peak of the synthesized molecules further depicts an effective interaction at higher DNA concentration, which was more prominent in the case of **1c**. The reduction in the intrinsic fluorescence upon interaction with DNA could be due to masking or burial of the fluorophore between the stacked bases within the helix and/or surface binding at the reactive nucleophilic sites on the heterocyclic nitrogenous bases of DNA.

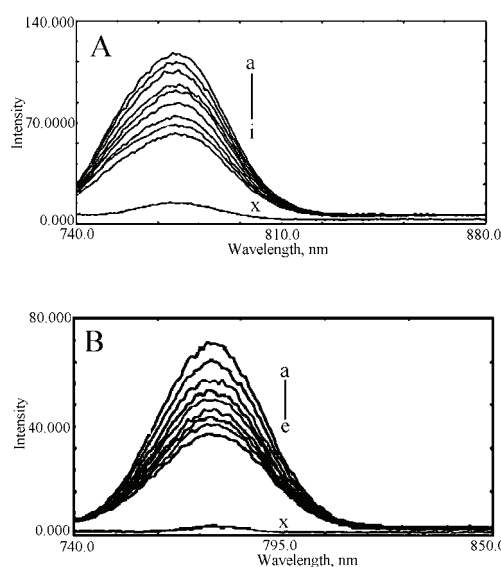


Fig. 4. Fluorescence emission spectra of the complexes in the absence and presence of increasing amounts of DNA. Excitation 290 nm. Fixed concentration of complex (*i.e.*, 4 μM) was titrated in each titration. A concentration of 4 μM DNA (x) was used for DNA alone. Spectra (A) and (B) represent complex **1c** and **2c**, respectively.

The binding parameters for complex **1c** and **2c** were found to be $K = (8.21 \pm 0.21) \times 10^4 \text{ mol}^{-1} \text{ dm}^3$, $n = 1.1$ and $K = (0.74 \pm 0.11) \times 10^4 \text{ mol}^{-1} \text{ dm}^3$, $n = 0.92$, respectively. Pronounced bathochromism was observed with complex **1c**, which was negligible with complex **2c**. The results suggest that the compounds have varying degrees of affinity toward the DNA molecule. This differential binding of **1c** and **2c** is attributed in terms of different molecular structures around the Cu(II) ion.

Absorption spectroscopy. UV–Vis absorption studies were performed to further ascertain the DNA–complex **1c** and **2c** interaction. The UV absorbance show-

ed an increase with increasing complex **1c/2c** concentrations (Fig. 5A). Since complexes **1c** and **2c** do not show any peak in this region (Fig. 5B), the increase in the DNA absorbance is indicative of interaction between DNA and the complexes. Both complexes (**1c** and **2c**) exhibited hyperchromism but of varying degrees. Hyperchromism means the breakage of the secondary structure of DNA. Hence, it is primarily speculated that the complexes interact with the secondary structure of calf thymus DNA, resulting in its breakage and perturbation. After interaction with the base pairs of DNA, the $\pi \rightarrow \pi^*$ orbital of the bound ligand can couple with the π orbital of the base pairs, due to the decrease in $\pi \rightarrow \pi^*$ transition energy, which results in a bathochromic shift.⁴⁰ The prominent shift in the spectra of **1c** suggests more interference of the orbital by the complex **1c** molecule. The above changes are indicative of conformational alteration of DNA but of varied extent.

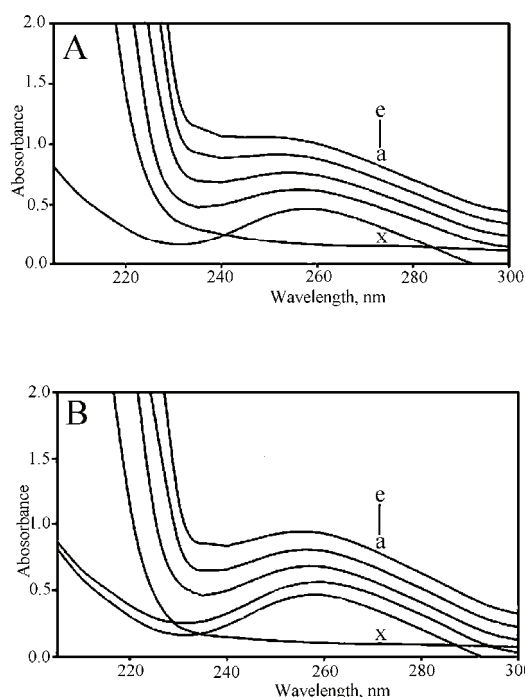


Fig. 5. Absorbance spectra of DNA and DNA-**1c** (A)/**2c** (B) system. The DNA concentration was 0.10 mM (a); complex concentration for DNA-**1c** and **2c** complex systems was a) 10, b) 20, c) 30 and d) 40 μ M.

CONCLUSIONS

A novel series of 16- and 18-membered Schiff-base binuclear N_8 -macrocyclic complexes were synthesized and characterized by spectral and elemental analyses. The IR spectra of the complexes showed the absence of bands corresponding to the $\nu(\text{C}=\text{O})$ and $\nu(\text{NH}_2)$ group of diacetylhydrazine and alkylamine moieties, respectively, and the appearance of a new well-defined band corresponding

to the $\nu(\text{C}=\text{N})$ stretching vibration. This suggests the formation of the macrocyclic framework, which was further substantiated by the ^1H - and ^{13}C -NMR spectra. Confirmation regarding the stoichiometry, nature and overall geometry around the metal ion was further deduced from the electronic, ESI-mass, EPR spectra, magnetic moment values and conductivity measurements. Fluorescence and absorption measurements demonstrated a considerable interaction between the Cu(II) complexes **1c** and **2c** and CT DNA.

Acknowledgements. The Chairman, Department of Chemistry, Aligarh Muslim University, Aligarh, India, is acknowledged for providing the necessary research facilities. The authors are thankful to Prof. R. J. Singh, Department of Physics, AMU, Aligarh, for the discussion of the EPR spectra.

ИЗВОД

СИНТЕЗА 16- И 18-ОЧЛАНИХ БИНУКЛЕАРНИХ ОКТААЗАМАКРОЦИКЛИЧНИХ КОМПЛЕКСА Co(II), Ni(II), Cu(II) И Zn(II) КОНТРОЛИСАНА МЕТАЛНИМ ЈОНИМА: УПОРЕДНИ СПЕКТРОСКОПСКИ ПРИКАЗ ВЕЗИВАЊА DNA ЗА Cu(II) КОМПЛЕКСЕ

FARHA FIRDAUS¹, KANEER FATMA¹, ASAD U. KHAN² и MOHAMMAD SHAKIR¹

¹*Division of Inorganic Chemistry, Department of Chemistry, Aligarh Muslim University, Aligarh-202002 u*

²*Interdisciplinary Biotechnology Unit, Aligarh Muslim University, Aligarh -202002, India*

Добијена је серија 16- и 18-очланих бинуклеарних октаазамакроцикличних комплекса, $[\text{M}_2\text{L}_1(\text{NO}_3)_4]$ и $[\text{M}_2\text{L}_2(\text{NO}_3)_4]$ ($\text{M} = \text{Co}(\text{II}), \text{Ni}(\text{II}), \text{Cu}(\text{II}), \text{Zn}(\text{II}), \text{L}_1 = 3,8,11,16$ -тетраметил-1,2,4,7,9,10,12,15-октааза-3,7,11,15-циклохексадекатетрен и $\text{L}_2 = 3,9,12,18$ -тетраметил-1,2,4,8,10,11,13,17-октааза-3,8,12,17-циклооктадекатетраен) металном темплатном кондензацијом N,N' -диацетилхидразина са 1,2-диаминоетаном и 1,3-диаминопропаном у метанолу. Грађење макроцикличне лигандне структуре, везивање макроцикличне средине комплекса у општу геометрију изведено је на основу резултата елементарне анализе, моларне проводљивости, FT-IR, ^1H , ^{13}C -NMR, EPR, ESI-масеног, UV-Vis спектралног проучавања и магнетних мерења. Октаедарска геометрија је предложена за све комплексе, док је дисторгована октаедарска геометрија примећена код Cu(II) комплекса. Упоредна флуоресцентна и UV-Vis проучавања Cu(II) комплекса доказала су значајно везивање за DNA телећег тимуса.

(Примљено 12. јануара, ревидирано 7. маја 2009)

REFERENCES

1. S. Anbu, M. Kandaswamy, P. S. Moorthy, M. Balasubramanian, M. N. Ponnuswamy, *Polyhedron* **28** (2009) 49
2. H. Zhou, Z. H. Peng, Z. Q. Pana, Y. Song, Q. M. Huang, X. L. Hu, *Polyhedron* **26** (2007) 3233
3. P. Zanello, S. Tamburini, P. A. Vigato, G. A. Mazzocchin, *Coord. Chem. Rev.* **77** (1987) 165
4. J. M. Lehn, *Pure. Appl. Chem.* **50** (1978) 871
5. F. Firdaus, K. Fatma, M. Azam, S. N. Khan, A. U. Khan, M. Shakir, *Transition Met. Chem.* **33** (2008) 467
6. L. Mishra, K. Bindu, S. Bhattacharya, *Spectrochim. Acta A* **61** (2005) 807
7. J. M. M. Sanchez, R. B. D. L. Calle, A. Macias, P. P. Lourido, L. V. Matarranz, *Polyhedron* **25** (2006) 3495

8. A. K. Mohamed, K. S. Islam, S. S. Hasan, M. Shakir, *Transition Met. Chem.* **24** (1999) 198
9. L. Branco, J. Costa, R. Delgado, M. G. B. Drew, V. Felix, B. J. Goodfellow, *J. Chem. Soc. Dalton Trans.* (2002) 3539
10. J. L. Karn, D. H. Busch, *Inorg. Chem.* **8** (1969) 1149
11. C. Cruz, S. Carvalho, R. Delgado, M. G. B. Drew, V. Felix, B. J. Goodfellow, *J. Chem. Soc. Dalton Trans.* (2003) 3172
12. H. Adams, D. E. Fenton, S. R. Haque, S. L. Heath, M. Ohba, H. Okawa, S. E. Spey, *J. Chem. Soc. Dalton Trans.* (2000) 1849
13. S. L. Jain, P. Bhattacharyya, H. L. Milton, A. M. Z. Salwin, J. A. Crayston, J. D. Woollins, *J. Chem. Soc. Dalton Trans.* (2004) 862
14. M. H. Klingele, B. Moubaraki, J. D. Cashion, K. S. Murray, S. Brooker, *Chem. Commun.* (2005) 987
15. S. Brooker, *Coord. Chem. Rev.* **222** (2001) 33
16. E. Jabri, M. B. Carr, R. P. Hausinger, P. A. Karplus, *Science* **268** (1995) 998
17. B. Linton, A. D. Hamilton, *Chem. Rev.* **97** (1997) 1669
18. S. O. Kang, M. Kim, *J. Am. Chem. Soc.* **125** (2003) 4684
19. C. Lodeiro, R. Bastida, E. Bertola, A. Macias, A. Rodriguez, *Polyhedron* **22** (2003) 1701
20. M.A. De Rosch, W. C. Trogler, *Inorg. Chem.* **29** (1990) 2409
21. D. E. Fenton, H. Okawa, *Perspectives in Bioinorganic Chemistry*, JAI Press, London, 1993, p. 8
22. A. M. Pyle, J. P. Rehmann, R. Meshoyrer, C. V. Kumar, N. J. Turro, J. K. Barton, *J. Am. Chem. Soc.* **111** (1989) 3051
23. X. Z. Feng, Z. Lin, L. J. Yang, C. L. Bai, *Talanta* **47** (1998) 1223
24. C. N. Reilly, R. W. Schmid, F. A. Sadak, *J. Chem. Educ.* **36** (1959) 619
25. W. J. Geary, *Coord. Chem. Rev.* **7** (1971) 81
26. D. P. Singh, R. Kumar, V. Malik, P. Tyagi, *J. Enzyme Inhib. Med. Chem.* **22** (2007) 177
27. S. I. Mostafa, T. H. Rakha, M. M. El-Agez, *Indian J. Chem.* **39A** (2000) 1301
28. X. Wang, X. Han, W. Lu, X. Liu, D. Sun, *Synth. React. Inorg. Met.-Org. Chem.* **22** (1992) 1169
29. K. Fujisawa, T. Kobayashi, K. Fujita, N. Kitajima, Y. Moro-oka, Y. Miyashita, Y. Yamada, K. Okamoto, *Bull. Chem. Soc. Jpn.* **73** (2000) 1797
30. M. Shakir, N. Begum, S. Parveen, P. Chingsubam, S. Tabassum, *Synth. React. Inorg. Met.-Org. Chem.* **34** (2004) 1135
31. M. Shakir, Y. Azim, H. T. N. Chishti, N. Begum, P. Chingsubam, M. Y. Siddiqi, *J. Braz. Chem. Soc.* **17** (2006) 272
32. A. Bansal, S. Kumar, R. V. Singh, *Synth. React. Inorg. Met.-Org. Chem.* **31** (2001) 1085
33. B. Jezowska, J. Lisowski, A. Vogt, P. Chemielewski, *Polyhedron* **7** (1988) 337
34. S. Chandra, L. K. Gupta, *Spectrochim. Acta, Part A* **60** (2004) 2767
35. I. M. Procter, B. N. Hathaway, P. Nicholls, *J. Chem. Soc. A* (1968) 1678
36. A. B. P. Lever, *Inorganic Electronic Spectroscopy*, 2nd ed., Elsevier, Amsterdam, 1984
37. F. A. Cotton, G. Wilkinson, *Advanced Inorganic Chemistry*, 5th Ed., Wiley, New York, 1988
38. K. G. Kocwin, W. Wojciechowski, *Transition Met. Chem.* **21** (1996) 312
39. S. N. Choi, E. R. Menzel, J. R. Wasson, *J. Inorg. Nucl. Chem.* **39** (1977) 477
40. X. F. He, H. Chen, L. Xu, L. N. Ji, *Polyhedron* **17** (1998) 3161.



J. Serb. Chem. Soc. 74 (8–9) 953–964 (2009)
JSCS–3890

Journal of
the Serbian
Chemical Society

JSCS@tmf.bg.ac.rs • www.shd.org.rs/JSCS

UDC 546.763+66.081+54–145.2:624.131.27

Original scientific paper

Studies on chromium(III) removal from aqueous solutions by sorption on *Sphagnum* moss peat

CATALIN BALAN, DOINA BILBA* and MATEI MACOVEANU

Department of Environmental Engineering and Management, Faculty of Chemical Engineering and Environmental Protection, Technical University of Iasi, D. Mangeron Blvd. 71A, 700050, Iasi, Romania

(Received 16 November, revised 13 April 2009)

Abstract: Batch sorption experiments were performed for the removal of chromium(III) ions from aqueous solutions using Romanian *Sphagnum* moss peat (untreated and treated with NaCl solution) as sorbent. In order to establish the best conditions for the sorption of chromium(III), the influence of initial pH, contact time, peat dose and metal ion concentration was investigated. The Freundlich, Langmuir and Dubinin–Radushkevich models were applied to describe the sorption isotherms and to calculate its constants. The experimental data fitted well to the Langmuir model with a maximum sorption capacity of 18.6 mg Cr(III)/g of peat. The mean free energy of sorption suggests that the binding of Cr(III) on peat occurred through an ion exchange mechanism. The kinetic data evaluated by pseudo-first order and pseudo-second order kinetic models showed that the sorption of chromium onto the peat followed a pseudo-second order rate equation. The chromium(III) could be easily eluted from the loaded peat using 0.10 M HCl and the peat may be reused in several sorption/desorption cycles. The experimental results indicated the potential of *Sphagnum* moss peat for removal of Cr(III) from wastewaters.

Keywords: *Sphagnum* moss peat; Cr(III), sorption; equilibrium studies; kinetics.

INTRODUCTION

Chromium is an important metal used in many industrial activities, including electroplating, leather tanning, electric-power production, pulp production, paint and pigment manufacture and ore and petroleum refining. These activities produce significant quantities of chromium wastes, which can generate a considerable pollution of water and soil.

The stable oxidation states of chromium in the environments are Cr(III) and Cr(VI), which are found in several different forms according to pH.¹ The toxicity of soluble chromium species and their mobility in aquatic and terrestrial envi-

* Corresponding author. E-mail: dbilba@ch.tuiasi.ro
doi: 10.2298/JSC0909953B

ronments depends on their oxidation state. Cr(III) is considered less toxic than Cr(VI) and even essential to human health in trace concentrations. However, at increasing concentrations, Cr(III) can cause adverse effects because of its high capability to coordinate various organic compounds, resulting in inhibition of some metallic-enzyme systems.^{1,2} Meanwhile, Cr(VI) is a confirmed human carcinogen and epithelial irritant.^{2,3} The tolerance limit for aqueous effluents discharge into inland waters is 1.0 mg/L for total chromium (Cr(III) and Cr(VI)) and 0.10 mg L⁻¹ for Cr(VI).⁴

Several technologies have been developed to remove heavy metals, particularly chromium, from industrial wastewater; these include chemical precipitation, coagulation/flocculation processes, membrane filtration, oxidation processes, activated carbon adsorption, reverse osmosis, ion exchange and solvent extraction.⁵ Many of these processes are often complicated and time consuming, generate slugs or other toxic wastes and may be ineffective or expensive. Adsorption is one of the important methods for the removal of heavy metals at medium and low concentrations (1–100 mg/L) from wastewaters. The high cost of commercial activated carbons has stimulated the search for cheaper alternatives and, recently, non-conventional and low cost agricultural by-products have been employed as adsorbents in the removal of heavy metals.^{6–9} Various materials of this type have been investigated for the removal of chromium species; these include agricultural or industrial wastes processed into activated carbons,^{10–13} peat,^{14,15} sawdust,¹⁶ and several biomasses.^{17–20}

Peat is an inexpensive and widely available natural material, consisting of organic matter at various stages of decomposition; the main components are lignin, cellulose, and humic and fulvic acids. These components contain various polar functional groups, especially weakly acidic groups such as carboxyl and phenolic hydroxide that can be involved in chemical bonding of transition metals and polar organics.²¹ The ability of peat to remove heavy metals, such as copper, cadmium, lead, nickel and chromium, has been reported by many authors.^{21–30}

In this study, the sorption capacity of Romanian *Sphagnum* moss peat for chromium(III) ions was investigated under batch conditions, whereby various process parameters, such as initial pH, adsorbent dose, chromium concentration and contact time, were considered. The sorption data were tested fitted to a number of isotherm and kinetic models, with the view of understanding the mechanism of Cr(III) sorption using moss peat as the adsorbent.

EXPERIMENTAL

Materials

In this study, a commercially available *Sphagnum* moss peat (Poiana Stampei, Romania) was used. The material was air-dried, ground and sieved to particles size 1–2 mm. Some of the main characteristics of the peat were determined according to standard methods; the

results (Table I) suggest a peat with a low degree of decomposition. This was designated P-H (peat in hydrogen form).

TABLE I. Characteristics of the *Sphagnum* moss peat

Property	Value
pH (1:50, w/v deionised water)	4.05±0.05
Ash content, mass % w/w	4.85
Organic mater, mass %	84–85
Moisture content, mass %	10.5–11
Cation exchange capacity, meq g ⁻¹ of peat ^a	0.575

^aDetermined by pH-metric titration in 0.1 M NaCl solution

In order to improve the dissociation of the weak carboxylic groups from the peat, an amount of sorbent was treated for 24 h with 1.0 M NaCl solution, washed with distilled water and dried. This sorbent was designated P-Na (peat in sodium form).

A stock solution of Cr(III) (520 mg/L) was prepared by dissolving analytical reagent grade chromium nitrate (Cr(NO₃)₃·9H₂O) (Sigma) in distilled water. All working solutions were prepared by adequate dilution of the stock solution with distilled water.

Sorption experiments

Batch sorption experiments were performed in 250 mL conical flasks by shaking the required amount of peat (P-H or P-Na) with 50 mL of aqueous solutions of Cr(III) of known concentration, at a constant temperature (20±1 °C). The pH of the solutions was adjusted to a constant value by the addition of dilute solutions of H₂SO₄ and NaOH or acetate buffer solution and measured with a pH-meter, Radelkis OP-271 pH/Ion analyzer. After a specified contact time, the peat was separated by filtration and the residual concentration of Cr(III) in the solution (previously oxidized with KMnO₄) was analyzed by a spectrophotometric method with diphenylcarbazide using a UV–Vis digital spectrophotometer, model S 104D/WPA.

The amount of Cr(III) adsorbed on the peat at equilibrium, q (mg g⁻¹), and the percentage of Cr(III) removed, R (%), were calculated using the following equations:

$$q = (c_0 - c)V / m \quad (1)$$

$$R = (c_0 - c)100 / c_0 \quad (2)$$

where c_0 and c are the Cr(III) concentrations (mg L⁻¹) in initial solution and after equilibrium, respectively, V is the volume of the solution (L) and m is the mass of *Sphagnum* moss peat (g).

The effect of operating process parameters on the removal of chromium(III) by peat was investigated according to Table II.

TABLE II. Experimental conditions used for the sorption of Cr(III) onto *Sphagnum* moss peat

Operating variable	Initial pH	Amount of peat g L ⁻¹	Cr(III) Concentration mg L ⁻¹	Contact time h
pH	1.0–5.5	4	26 and 52	24
Peat dose	4	2.0–12	83.2	24
Cr(III) concentration	4 and 5	4	10.4–104	24
Contact time	4	4	41.6 and 83.2	15 min–4 h

Adsorption isotherm models

The equilibrium data for Cr(III) removal using peat as the sorbent were analysed using different isotherm models available in the literature.^{24,31-33}

The Freundlich isotherm, which assumes a heterogeneous adsorption surface, was tested using the following linear equation:

$$\log q = \log K_F + 1/n \log c \quad (3)$$

where K_F and $1/n$ are constants related to the adsorption capacity and adsorption intensity (efficiency), respectively.

The Langmuir isotherm adsorption model is based on the assumption that maximum adsorption corresponds to a monolayer of solute species on the sorbent surface, containing a finite number of energetically equivalent sites. The Langmuir equation can be used in following linearized form:

$$1/q = (1/q_0 K_L c) + 1/q_0 \quad (4)$$

where q_0 is the maximum amount of solute adsorbed (mg g^{-1}) and K_L is a constant related to the binding energy of the solute (L mg^{-1}).

In order to appreciate the nature – physical or chemical – of the sorption process, the isotherms data were analyzed by the Dubinin–Radushkevich (D–R) model, expressed by the following equation:

$$\ln q = \ln q_{\max} - \beta \varepsilon^2 \quad (5)$$

where q_{\max} is the maximum amount of solute adsorbed under optimized experimental conditions (mg g^{-1}), β is a constant related to the sorption energy ($\text{mol}^2 \text{kJ}^{-2}$) and ε (the Polanyi potential) is defined by the mathematical relation:

$$\varepsilon = RT \ln(1 + 1/c) \quad (6)$$

where R is the gas constant ($\text{kJ mol}^{-1} \text{K}^{-1}$), T is the absolute temperature and c is the equilibrium concentration in solution (mol L^{-1}).

The mean free energy of sorption, E (kJ mol^{-1}), can be calculated using the following equation:

$$E = 1/\sqrt{2\beta} \quad (7)$$

Values of the mean free energy less than 8 kJ mol^{-1} are characteristic of a physical sorption mechanism and values between 8 and 16 kJ mol^{-1} indicate an ion exchange mechanism.

Kinetic models

The kinetic adsorption data were evaluated using pseudo-first order and pseudo-second order kinetic models.^{32,34}

The pseudo first-order Lagergren model is usually expressed as:

$$\log(q_e - q) = \log q_e - \frac{k_1}{2.303} t \quad (8)$$

where q_e and q are the amounts of sorbed Cr(III) (mg g^{-1}) at equilibrium (24 h) and at any time t (min), respectively, and k_1 is the Lagergren rate constant of the first-order sorption (min^{-1}).

The pseudo-second order model (Ho model) assumes that the sorption follows a second order mechanism and that the rate limiting step may be chemical sorption involving valence

forces or covalent forces between the sorbent and the adsorbate. The rate of pseudo-second order reaction is expressed by the equation:

$$\frac{t}{q} = \frac{1}{q_e^2 k_2} + \frac{1}{q_e} t \quad (9)$$

where k_2 is the rate constant of second order sorption ($\text{g mg}^{-1} \text{min}^{-1}$) and $q_e^2 k_2 = h$ can be regarded as the initial sorption rate ($\text{mg g}^{-1} \text{min}^{-1}$) as t approaches zero.

RESULTS AND DISCUSSION

Effect of solution pH value

The solution pH value is one of the most important controlling parameters in the sorptive removal of heavy metals, influencing not only the dissociation of functional groups and surface charge of the sorbent, but also the solution chemistry of the heavy metals.^{7,35} According to the speciation diagram for Cr(III) complexes,^{36,37} in aqueous solutions at medium and low concentrations (below 10 mmol L^{-1}), about 98 % of the total amount of chromium is present as Cr^{3+} at pH 2, while this value decreases to 40 and the rest 60 % of chromium is in the hydroxylated CrOH^{2+} form at pH 4. The effect of the initial pH value (adjusted with sulphuric acid or sodium hydroxide) on the removal of Cr(III) ions on P-H and P-Na *Sphagnum* moss peat from two solutions of different initial concentration is shown in Fig. 1.

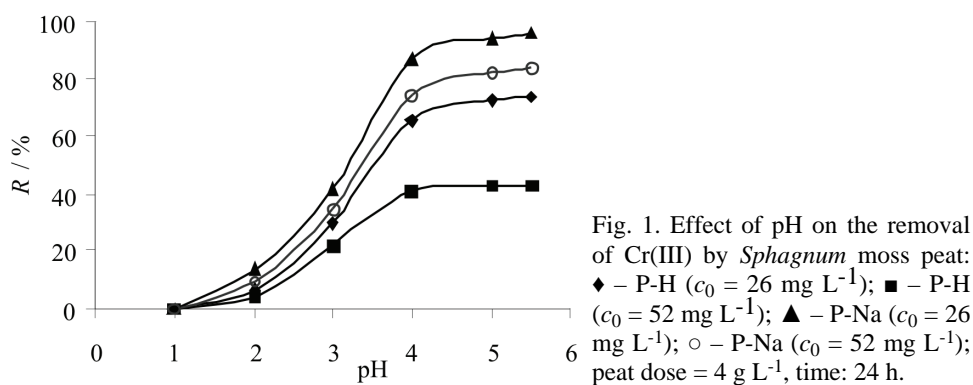


Fig. 1. Effect of pH on the removal of Cr(III) by *Sphagnum* moss peat: \blacklozenge – P-H ($c_0 = 26 \text{ mg L}^{-1}$); \blacksquare – P-H ($c_0 = 52 \text{ mg L}^{-1}$); \blacktriangle – P-Na ($c_0 = 26 \text{ mg L}^{-1}$); \circ – P-Na ($c_0 = 52 \text{ mg L}^{-1}$); peat dose = 4 g L^{-1} , time = 24 h.

It is evident that at a pH lower than 2.0, the adsorption of Cr(III) was negligible but increased rapidly with increasing pH value, with a maximum in the pH range 4.0–5.5. This increase in the percent removal of chromium (from 6.8 to 74 % from solutions of 26 mg Cr L^{-1}) with increasing pH (from 2.0 to 5.5) is due to lower competition of protons for the binding sites and also to the increase in the concentration of CrOH^{2+} species, which exchange with H^+ from the carboxyl groups more readily than Cr^{3+} . For the sodium form of the peat (P-Na), the increase in the dissociation of the carboxyl groups generates a more negatively charged surface and electrostatic interactions with cationic species of Cr(III) is

increased, thus enhancing the sorption. The percentage of chromium removed is smaller when a higher initial concentration was used.

Effect of adsorbent dose

The effect of the concentration of *Sphagnum* moss peat (P-H and P-Na) on the sorption of chromium(III) from solutions of initial concentration 83.2 mg L^{-1} and pH 4.0 is shown in Fig. 2.

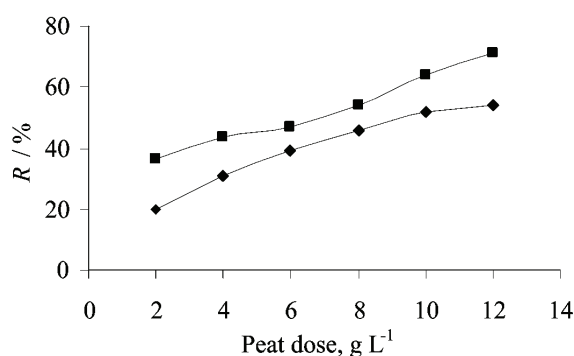


Fig. 2. Effect of *Sphagnum* moss peat dose on the sorption of Cr(III): \blacklozenge – P-H; \blacksquare – P-Na; pH 4, $c_0 = 83.2 \text{ mg L}^{-1}$, time: 24 h.

The sorption of chromium(III) increased with increasing peat dose from 2.0 to 12 g L^{-1} for both P-H and P-Na, probably due to the greater surface area and to more sorption sites on the sorbent. The chromium removal percent was higher for the sodium form of the peat.

Effect of chromium(III) concentration

The effect of the initial Cr(III) concentration on the sorption of chromium (III) onto *Sphagnum* moss peat untreated and treated with NaCl from solutions of various initial pH values is presented in Fig. 3.

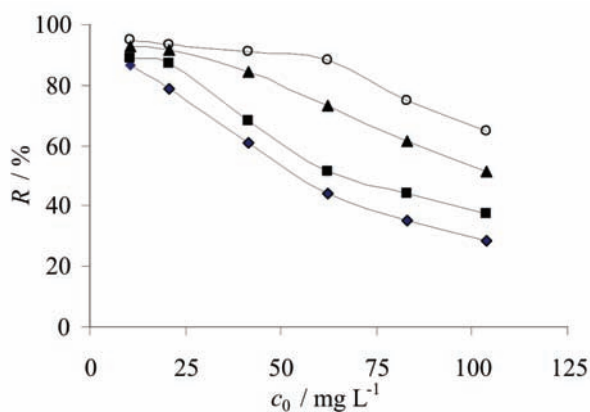


Fig. 3. Influence of initial Cr(III) concentration on the removal of chromium by *Sphagnum* moss peat: \blacklozenge – P-H (pH 4.0); \blacksquare – P-Na (pH 4.0); \blacktriangle – P-Na (pH 5.0, NaOH); \circ – P-Na (pH 5.0, acetate); peat dose: 4 g L^{-1} , time: 24 h.

Increasing the initial Cr(III) concentration from 10.4 mg L^{-1} to 104 mg L^{-1} in solutions with an initial pH 4 decreased the percent removal of Cr(III) by P-H samples from about 86.5 to 28.5 %. This is explained by increasing ratios between the initial number of moles of Cr(III) and the limited number of available sorption sites on the peat. Chromium sorption onto P-Na samples slightly increased, showing that the replacement of protons with Na^+ enhanced the accessibility of the sorption sites as well as the swelling of the peat.³⁸ Also, increasing the initial pH of the solution had a favourable effect on chromium(III) removal; the best results were obtained from solutions of pH 5 adjusted with $\text{CH}_3\text{COOH}-\text{CH}_3\text{COONa}$ buffer.

Equilibrium modelling

Sorption isotherms describe the distribution of adsorbate species between the liquid phase and the solid phase when the sorption process reaches its equilibrium state. An analysis of equilibrium data by fitting them to different isotherm models is important for an estimation of the practical sorption capacity and optimization of the design of sorption systems.

The sorption isotherms of chromium(III) on *Sphagnum* moss peat (in the H- and Na-form) from solutions of various initial pH values are shown in Fig. 4.

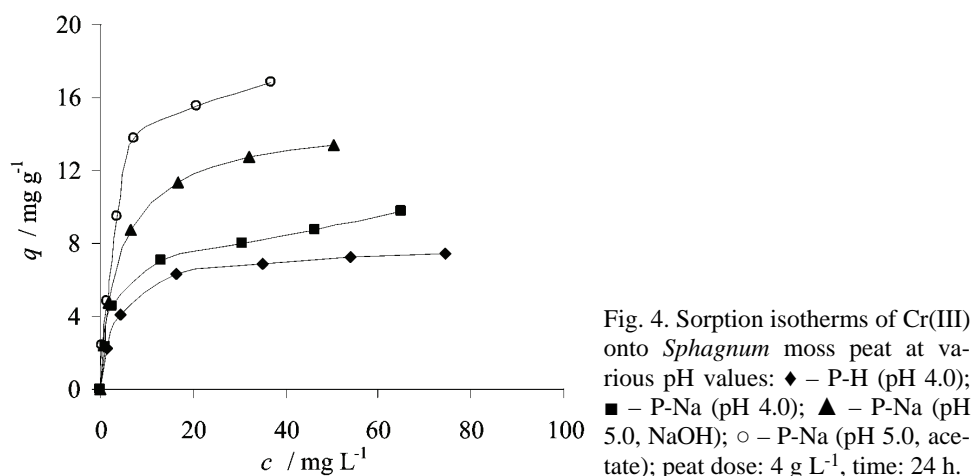


Fig. 4. Sorption isotherms of Cr(III) onto *Sphagnum* moss peat at various pH values: \blacklozenge – P-H (pH 4.0); \blacksquare – P-Na (pH 4.0); \blacktriangle – P-Na (pH 5.0, NaOH); \circ – P-Na (pH 5.0, acetate); peat dose: 4 g L^{-1} , time: 24 h.

The experimental equilibrium sorption data were compared with three adsorption isotherm models: the Freundlich, Langmuir and Dubinin–Radushkevich models, and the best-fit equilibrium model was established based on the linear regression correlation coefficients, R^2 .

The numerical values of the Freundlich, Langmuir and D–R isotherm parameters, evaluated from the slope and the intercept of the corresponding plots ($\log q$ vs. $\log c$; $1/q$ vs. $1/c$ and $\log q$ vs. ε^2 , respectively) are summarized in Table III.

TABLE III. Parameters for the sorption of Cr(III) on *Sphagnum* moss peat

Isotherm parameter		P-H (pH 4.0)	P-Na (pH 4.0)	P-Na (pH 5.0, NaOH)	P-Na (pH 5.0, acetate buffer)
Freundlich	$1/n$	0.299	0.315	0.396	0.454
	$K_F / (\text{mg g}^{-1})(\text{L mg}^{-1})^{1/n}$	2.367	2.762	3.372	4.158
	R^2	0.927	0.911	0.938	0.909
Langmuir	$q_0 / \text{mg g}^{-1}$	7.547	9.609	13.89	18.62
	$K_L / \text{L mg}^{-1}$	0.300	0.279	0.286	0.278
	R^2	0.998	0.991	0.999	0.998
Dubinin–Radushkevich	$q_{max} / \text{mg g}^{-1}$	13.67	17.80	34.74	56.60
	$\beta / \text{mol}^2 \text{kJ}^{-2}$	0.0030	0.0032	0.0038	0.0042
	$E / \text{kJ mol}^{-1}$	12.91	12.50	11.47	10.91
	R^2	0.955	0.949	0.964	0.943

The correlation coefficients higher than 0.9 show that the sorption of Cr(III) ions followed the Freundlich isotherm; the fractional values of $1/n$ ($0 < 1/n < 1$) suggest heterogeneity of the sorbent surface (the closer the $1/n$ value is to zero, the more heterogeneous is the surface³¹) and, simultaneously, indicates a beneficial adsorption of Cr(III) on the peat.

However, the R^2 values from Table III show that the isotherms data of chromium(III) ions sorption can be better described by the Langmuir model, indicating the formation of a monolayer coverage of the adsorbate at the outer surface of the peat. The obtained maximum sorption capacity was slightly higher on the Na-form of the peat than that on the untreated peat and increased with increasing solution pH. The highest capacity was obtained in acetate buffer solutions of pH 5.0. The high sorption equilibrium constant K_L suggests a strong interaction between chromium(III) cations and the binding sites of the peat.

The D–R isotherm parameter q_{max} (mg g^{-1}) indicates the porous structure of the peat sorbent (the maximum amounts of Cr(III) ions that could be sorbed under optimized conditions were much higher than the experimental values). The values of the mean free sorption energy were between 10.9 and 12.9 kJ mol^{-1} , which correspond to an ion exchange mechanism for the sorption of chromium(III) ions on the peat. A slight decrease of the energy sorption values with increasing pH was observed, probably due to an increase of the physical sorption of neutral chromium species.

Kinetic studies

Information on the sorption rate is required for the selection of the optimum conditions for operation in a full-scale batch process.

The results of Cr(III) sorption at pH 4.0 on the *Sphagnum* moss peat in the Na form as a function of contact time between the sorbent and aqueous solutions of adsorbate are presented in Fig. 5.

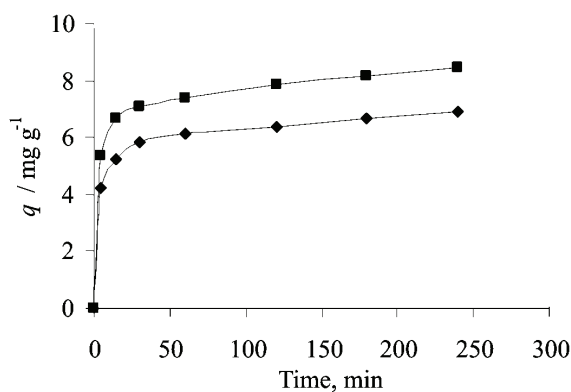


Fig. 5. Effect of contact time on the sorption of Cr(III) onto *Sphagnum* moss peat: \blacklozenge – $c_0 = 41.6 \text{ mg L}^{-1}$; \blacksquare – $c_0 = 83.2 \text{ mg L}^{-1}$; pH 4.0, peat dose (P-Na): 4 g L^{-1} .

As can be seen in Fig. 5, the sorption of Cr(III) ions was extremely rapid during the first 20 min and, thereafter, it decreased significantly near the equilibrium, which can be considered to have been obtained after 4 h (the values of the amount sorbed after 24 h were found to be 2.8 and 3.28 % higher, respectively, than those after 4 h contact). The fast sorption kinetics is typical for sorption of metal due to purely physico-chemical interactions between adsorbent and adsorbate.

The experimental data were interpreted by means of pseudo-first and pseudo-second order kinetic models. The constants of these kinetic models calculated from the linear plots ($\log(q_e - q)$ vs. t and t/q vs. t) and the corresponding correlation coefficients are presented in Table IV.

TABLE IV. Kinetic constants for Cr(III) sorption onto *Sphagnum* moss peat

Kinetic parameter		$c_0 = 41.6 \text{ mg Cr L}^{-1}$	$c_0 = 83.2 \text{ mg Cr L}^{-1}$
Pseudo-first order model	$q_0 / \text{mg g}^{-1}$	9.343	9.813
	k_1 / min^{-1}	1.396	1.282
	R^2	0.8868	0.8947
Pseudo-second order model	$q_0 / \text{mg g}^{-1}$	6.887	8.525
	$h / \text{mg g}^{-1} \text{ min}^{-1}$	1.148	1.404
	$k_2 / \text{g mg}^{-1} \text{ min}^{-1}$	0.0242	0.0193
	R^2	0.9976	0.9988

The R^2 values below 0.90 suggest that the Lagergren model is not a good model for the kinetic data; in addition, the estimated values of q_e do not agree very well with the experimental values.

The experimental data complied very well with the pseudo-second order kinetic model, with correlation coefficients higher than 0.99. It was observed that the initial metal ion concentration influenced the kinetic parameters. The values of the initial sorption rate, h , increased with increasing initial Cr(III) concentration, probably due to the greater concentration gradient between the sorbent and

solution. However, the values of rate constant, k_2 , decreased with increasing initial concentration. In addition, the good correspondence between the calculated and experimental values of the sorption capacity showed that the kinetic data are in agreement with the pseudo-second order rate equation.

Desorption studies

In order to check the reusability of the both the peat and Cr(III), several loading and elution experiments were performed. The desorption of Cr(III) ions from loaded peat was tested under batch conditions using different concentrations of aqueous solutions of mineral acids (as proton exchanging agents). The results indicate that the chromium(III) ions can be readily eluted with 0.10 M solutions of HCl or H₂SO₄ (about 96 % chromium recovery for a mass peat: acid volume ratio of 1:10). This fact is in agreement with the pH dependence of the chromium removal onto the peat and confirms the prevalence of the ion exchange mechanism of the sorption. The peat (rinsed with distilled water before reloading) was reused in fives sorption/desorption cycles without a significant loss in sorption capacity.

CONCLUSIONS

The removal of chromium(III) ions from aqueous solutions by sorption onto Romanian *Sphagnum* moss peat was studied as a function of solution pH value, metal ion concentration, peat dose and contact time. The results showed that the highest percentages of Cr(III) removal were attained using peat in the sodium form (4 g L⁻¹) from solutions of pH 5.0 (acetate buffer) with Cr(III) concentrations below 50 mg L⁻¹. The equilibrium data were analyzed against the Freundlich, Langmuir and Dubinin–Radushkevich models. The experimental data were best correlated by the Langmuir isotherm; under optimized conditions, the monolayer adsorption capacity was of 18.6 mg Cr(III) g⁻¹ of peat. Ion exchange was the major mechanism for the adsorption of Cr(III) on the peat particles with the sorption kinetics following a pseudo-second order rate equation. The Cr (III)-loaded peat could be regenerated by treatment with 0.10 M HCl and the sorbent may be reused in several sorption–desorption cycles. The results of this study showed that Romanian *Sphagnum* moss peat, a natural, cheap and available material, could be employed as a sorbent for the removal of chromium(III) from aqueous waste solutions.

ИЗВОД

ИСПИТИВАЊЕ УКЛАЊАЊА ХРОМА(III) ИЗ ВОДЕНИХ РАСТВОРА
СОРПЦИЈОМ НА ТРЕСЕТНОЈ МАХОВИНИ *Sphagnum*

CATALIN BALAN, DOINA BILBA и MATEI MACOVEANU

Department of Environmental Engineering and Management, Faculty of Chemical Engineering and Environmental Protection, Technical University of Iasi, D. Mangeron Blvd. 71A, 700050, Iasi, Romania

Изведена је група сорпционих експеримената за уклањање јона хрома (III) из водених раствора помоћу тресетне маховине *Sphagnum* са подручја Румуније (нетретирани и третирано раствором NaCl) као сорбентом. У циљу успостављања најпогоднијих услова за сорпцију хрома(III), испитивани су утицаји рН, времена контакта, количине маховине и концентрације јона. Примењени су модели Фројндлиха (Freundlich), Ленгмира (Langmuir) и Дубинин–Радушевича (Dubinin–Radushkevich) за опис сорпционих изотерми и за израчунавање одговарајућих константи. Експериментални резултати одговарају Ленгмировом моделу са максималним сорпционим капацитетом од 18,6 mg Cr(III) по граму маховине. Вредност средње енергије сорпције указује на то да се Cr(III) везује за маховину по механизму измене јона. Кинетички подаци, добијени на основу псеудо-првог и псеудо-другог кинетичког модела, показују да процес сорпције хрома на маховини следи закон брзине псеудо-другог реда. Сорбовани хром(III) лако може бити одвојен од маховине испирањем раствором 0,10 М HCl, док се иста маховина може користити у неколико циклуса сорпција/десорпције. Експериментални резултати указују на то да тресетна маховина *Sphagnum* има потенцијал за примену уклањања Cr(III) из отпадних вода.

(Примљено 16. новембра, ревидирано 13. априла 2009)

REFERENCES

1. J. Kotas, Z. Stasicka, *Environ. Pollut.* **107** (2000) 263
2. S. Goswami, U. C. Ghosh, *Water SA* **31** (2005) 597
3. E. Oguz, *Colloids Surfaces A* **252** (2005) 121
4. NTPA 001/2002 – Romanian Norm setting the pollutant concentrations in waste waters at release into natural receptors
5. J. W. Patterson, *Industrial wastewater treatment technology*, 2nd ed., Butterworth – Heinemann, London, 1985
6. S. E. Bailey, T. J. Olin, R. M. Bricka, D. D. Adrian, *Water Res.* **33** (1999) 2469
7. J. L. Gardea-Torresdey, G de la Rosa, J. R. Peralta-Videa, *Pure Appl. Chem.* **76** (2004) 801
8. U. Kumar, *Sci. Res. Essay* **1** (2006) 33
9. J. C. Igwe, A. A. Abia, *Afr. J. Biotech.* **5** (2006) 1167
10. E. Demirbas, M. Kobya, E. Senturk, T. Ozkan, *Water SA* **30** (2004) 533
11. N. F. Fahim, B. N. Barsoum, A. E. Eid, M. S. Khalil, *J. Hazard. Mater.* **136** (2006) 303
12. D. Mohan, K. P. Singh, V. K. Singh, *J. Hazard. Mater.* **135** (2006) 280
13. E. I. El-Shafey, *Water Air Soil Pollut.* **163** (2005) 81
14. S. A. Dean, J. M. Tobin, *Resource. Conservation Recycling* **27** (1999) 151
15. J. Kyziol, *Polish J. Environ. Studies* **11** (2002) 713
16. S. S. Baral, S. N. Das, P. Rath, *Biochem. Eng. J.* **13** (2006) 216
17. M. X. Loukidou, A. I. Zouboulis, T. D. Karapantsios, K. A. Matis, *Colloids Surfaces A* **242** (2004) 93

18. J. Romero-Gonzalez, J. L. Gardea-Torresdey, J. R. Peralta-Videa, E. Rodríguez, *Bioinorg. Chem. Appl.* **3** (2005) 55
19. N. T. Abdel-Ghani, R. M. El-Nashar, G. A. El-Chaghaby, *EJEAFChe* **7** (2008) 3126
20. J. R. Memon, S. Q. Memon, M. I. Bhanger, M. Y. Khuhawar, *Pak. J. Anal. Environ. Chem.* **9** (2008) 20
21. P. A. Brown, S. A. Gill, S. J. Allen, *Water Res.* **34** (2000) 3907
22. Y. S. Ho, G. McKay, D. A. J. Wase, C. F. Forster, *Trans. I. Chem. E.* **81B** (2000) 639
23. Y. S. Ho, G. McKay, *Water Res.* **34** (2000) 735
24. Y. S. Ho, J. F. Porter, G. McKay, *Water Air Soil Pollut.* **141** (2002) 1
25. D. C. K. Ko, J. F. Porter, G. McKay, *Trans. I. Chem. E.* **81B** (2003) 73
26. W. Ma, J. M. Tobin, *Biochem. Eng. J.* **18** (2004) 33
27. A. Kicsi, D. Bilba, M. Macoveanu, *Env. Eng. Manag. J.* **5** (2006) 19
28. A. Kicsi, D. Bilba, M. Macoveanu, *Env. Eng. Manag. J.* **6** (2007) 205
29. L. Bulgariu, C. Cojocaru, B. Robu, M. Macoveanu, *Env. Eng. Manag. J.* **6** (2007) 425
30. C. Balan, D. Bilba, M. Macoveanu, *Env. Eng. Manag. J.* **7** (2008) 17
31. N. Khalid, S. Ali, A. Iqbal, S. Pervez, *Sep. Sci. Technol.* **42** (2007) 203
32. V. C. Srivastava, M. M. Swamy, I. D. Mall, B. Prasad, I. M. Mishra, *Colloids Surfaces A* **272** (2006) 89
33. B. Noroozi, G. A. Sorial, H. Bahrami, M. Arami, *J. Hazard. Mater.* **139** (2007) 167
34. Y. S. Ho, *J. Hazard. Mater.* **136** (2006) 681
35. A. Esposito, F. Pagnelli, F. Veglio, *Chem. Eng. Sci.* **57** (2002) 307
36. R. L. Ramos, L. F. Rubio, R. M. G. Coronado, J. M. Barron, *J. Chem. Technol. Biotechnol.* **62** (1995) 64
37. M. M. Araujo, J. A. Teixeira, *Int. Biodeter. Biodegrad.* **40** (1997) 63
38. P. Fine, A. Scagnossi, Y. Chen, U. Mingelgrin, *Environ. Pollut.* **138** (2005) 358.



J. Serb. Chem. Soc. 74 (8–9) 965–975 (2009)
JSCS–3891

Activity of carbon supported Pt₃Ru₂ nanocatalyst in CO oxidation

KSENIJA DJ. POPOVIĆ^{1*#}, JELENA D. LOVIĆ^{1#}, AMALIJA V. TRIPKOVIĆ^{1#}
and PIOTR K. OLSZEWSKI²

¹ICTM – Institute of Electrochemistry, University of Belgrade, Njegoševa 12, P.O. Box 473,
11000 Belgrade, Serbia and ²Institute of Catalysis and Surface Chemistry,
Polish Academy of Sciences, Krakow, Niezapominajek 8, 30-239, Poland

(Received 23 February, revised 24 April 2009)

Abstract: The electrocatalytic activity of Pt₃Ru₂/C nanocatalyst toward the electro-oxidation of bulk CO was examined in acid and alkaline solution at ambient temperature using the thin-film, rotating disk electrode (RDE) method. The catalyst was characterized by XRD analysis. The XRD pattern revealed that the Pt₃Ru₂/C catalyst consisted of two structures, *i.e.*, Pt–Ru-fcc and Ru-hcp (a solid solution of Ru in Pt and a small amount of Ru or a solid solution of Pt in Ru). Electrocatalytic activities were measured by applying potentiodynamic and steady state techniques. The oxidation of CO on the Pt₃Ru₂/C catalyst was influenced by pH and anions from the supporting electrolytes. The Pt₃Ru₂/C was more active in alkaline than in acid solution, as well as in perchloric than in sulfuric acid. Comparison of CO oxidation on Pt₃Ru₂/C and Pt/C revealed that the Pt₃Ru₂/C was more active than Pt/C in acid solution, while both catalysts had a similar activity in alkaline solution.

Keywords: CO oxidation; Pt₃Ru₂/C nanocatalyst; XRD; pH effect; anion effect.

INTRODUCTION

The major interest for the electro-oxidation of CO on a Pt₃Ru₂/C catalyst originated from previous studies of the electrocatalytic activity on PtRu-supported nanocatalysts in the electro-oxidation of methanol and formic acid.^{1–6} The electro-oxidations of methanol and formic acid, anodic reactions in fuel cells, belong to typical auto-inhibiting reactions producing strongly bound intermediates (predominantly CO-type species), well known as catalytic poisons.⁷ The oxidative removal of adsorbed CO by adsorbed oxygen containing species plays a dominant role in determining the catalyst activity in these reactions.

* Corresponding author. E-mail: ksenija@tmf.bg.ac.rs

Serbian Chemical Society member.

doi: 10.2298/JSC0909965P

It is believed that the electro-oxidation of CO_{ad} on an electrode surface in an electrolyte occurs analogously to the oxidative removal of CO on a Pt surface in the gas phase, which proceeds *via* the Langmuir–Hinshelwood mechanism, *i.e.*, by reaction of chemisorbed CO with chemisorbed oxygen.^{8,9}

The superior activity of PtRu among other catalytic materials has been explained by a bifunctional mechanism in which the oxidation of adsorbed CO is facilitated by the presence of OH_{ad} species formed by the electrochemical dissociation of water on oxophilic surface atoms, such as Ru, at lower anodic overpotentials compared with pure Pt.^{10,11} Consequently, the Ru sites act as collectors for OH_{ad} species, which then catalyze the oxidation of CO molecules preferentially bonded to neighboring Pt atoms. Additionally, the so-called ligand or electronic effect, in which the Ru alters the electronic properties of the Pt, might also be considered.^{8,12}

In this study, the electrocatalytic activity of a $\text{Pt}_3\text{Ru}_2/\text{C}$ catalyst in the electro-oxidation of bulk CO was examined in acid and alkaline solution at ambient temperature in order to study the effects of pH and anions of the electrolytes. Activity of the $\text{Pt}_3\text{Ru}_2/\text{C}$ was compared with activity of a Pt/C catalyst. A quasi-bifunctional mechanism for CO bulk oxidation on both catalysts in acid and alkaline solution is proposed.

EXPERIMENTAL

Electrode preparation

High area carbon supported platinum–ruthenium ($\text{Pt}_3\text{Ru}_2/\text{C}$) and platinum (Pt/C) nanocatalysts with 33.5 wt % alloy and 47.5 wt % Pt (Tanaka Precious Metal Group, Tokyo, Japan) were applied to a glassy carbon substrate in the form of a thin-film.¹³ A suspension of $\text{Pt}_3\text{Ru}_2/\text{C}$ or Pt/C in water was prepared in an ultrasonic bath and a drop of the suspension was placed onto the substrate, resulting in the constant loading of $15 \mu\text{g}_{\text{Alloy}} \text{cm}^{-2}$ or $20 \mu\text{g}_{\text{Pt}} \text{cm}^{-2}$, respectively. After drying in a stream of high-purity nitrogen at room temperature, the deposited catalyst layer was covered with 20 μl of a diluted aqueous Nafion[®] solution (thickness *ca.* 0.1 μm) and left to dry completely.

Mass transfer resistance through the Nafion[®] film covering the $\text{Pt}_3\text{Ru}_2/\text{C}$ layer was determined by recording the diffusion limiting currents of hydrogen oxidation on the rotating disk electrode. Since a Levich–Koutecky plot with an intercept close to zero was obtained, it was concluded that the mass transfer resistance through the Nafion[®] film was negligible.¹

Electrode characterization

The carbon supported Pt and Pt_3Ru_2 catalysts were characterized by X-ray powder diffraction analysis using a Siemens D5005 (Bruker-AXS, Germany) diffractometer system, equipped with a $\text{CuK}\alpha$ source operating at 40 mA and 40 kV and graphite monochromator. The XRD patterns were obtained in the 2θ range 10–100°, with 0.01°/s steps. The quantitative analysis of the phase content and crystallite size calculations were performed by multiphase Rietveld refinement using Topas software and the Fundamental Parameters approach for the modeling of the peak shape.

Electrochemical measurements

All electrochemical measurements were conducted in a thermostated three-compartment electrochemical cell at ambient temperature. The reference electrode was a standard calomel electrode (SCE) separated from the working electrode compartment to avoid chloride contamination. The potentials in this study were referred to the reversible hydrogen electrode (RHE).

The thin film rotating disk method was used for the determination of the catalytic activity. The rotation rate was 2000 rpm. All solutions were prepared with high purity water ("Millipore", 18 MΩ cm resistivity) and p.a. (H₂SO₄ and NaOH) or ultra high purity (HClO₄) grade chemicals (Merck). The HClO₄ was without any trace of Cl ions. The prepared electrodes were immersed in nitrogen purged perchloric or sulfuric acid or sodium hydroxide solution to record the basic voltammograms.

Carbon monoxide adsorption was performed in CO saturated solution holding the electrodes at 0.05 V for 3 min. The supporting electrolytes were saturated with CO by bubbling high purity CO through the solution for 30 min. The cyclic voltammograms were recorded using a sweep rate of 50 or 1 mV s⁻¹.

RESULTS AND DISCUSSION

Characterization of the catalysts

The XRD patterns of the carbon-supported Pt and Pt₃Ru₂ catalysts are shown in Fig. 1. The four characteristic peaks of the face-centered cubic (fcc) crystalline structure of Pt/C are seen: (111), (200), (220) and (311).

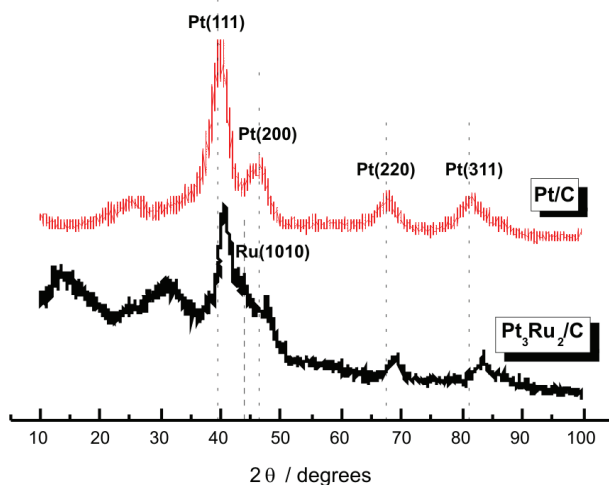


Fig. 1. XRD Patterns of Pt₃Ru₂/C and Pt/C catalysts. The vertical lines represent the positions of the peaks of pure Pt and pure Ru.

Two phases were identified in the diffraction pattern of the Pt₃Ru₂/C catalyst: a solid solution of ruthenium in platinum (fcc) and a phase associated with a weak peak at 43.8° assigned to the strongest Ru(1010) peak in the hexagonal phase of ruthenium (hcp). The first two broad peaks at 14.0 and 30.9° were assigned to the carbon support material. The Pt–Ru–fcc reflections in the Pt₃Ru₂/C

pattern were systematically shifted towards higher angles in relation to the pure platinum peaks in the pattern of the Pt/C catalyst, due to the incorporation of smaller ruthenium atoms into platinum crystal lattice.¹⁴ The lattice parameter for the Pt₃Ru₂/C catalyst (3.859(8) Å) was smaller than that of Pt/C (3.916(6) Å), due to a lattice contraction caused by the incorporation of Ru into the *fcc* structure of platinum after alloying. On the other hand, the presence of the 43.8° peak, attributed to the Ru-hcp phase, indicates that this incorporation was only partial. It was assumed in the calculations that the second phase is Ru-hcp.

The two structures, *i.e.*, Pt–Ru-*fcc* and Ru-hcp, were refined using the Rietveld method. The presence of the carbon support was not taken into account. The crystallite size determined using the Scherrer method, based on the broadening of the (220) peak, was 3.1 nm for the Pt and 4.5 nm for Pt–Ru-*fcc* phase, respectively. Similar crystallite sizes for both catalysts were calculated from the charge under the CO stripping peaks.

The carbon supported Pt₃Ru₂ nanocatalyst was examined in acid and alkaline solution at ambient temperature. The obtained voltammetric profiles (Fig. 2) can be divided into two regions: hydrogen desorption/adsorption between 0.05 V and 0.30 V and adsorption/desorption of reversible and irreversible oxygen-containing species, such as RuOH, Ru₂O, RuO_xH₂O, *etc.*,^{15,16} at more positive potentials. The continuous and fast transition from the reversible to irreversible state of the oxides resulted in a broad capacitive feature in the profile of the PtRu alloy. The anodic limit was set to 0.80 V to prevent any Ru dissolution.¹⁷

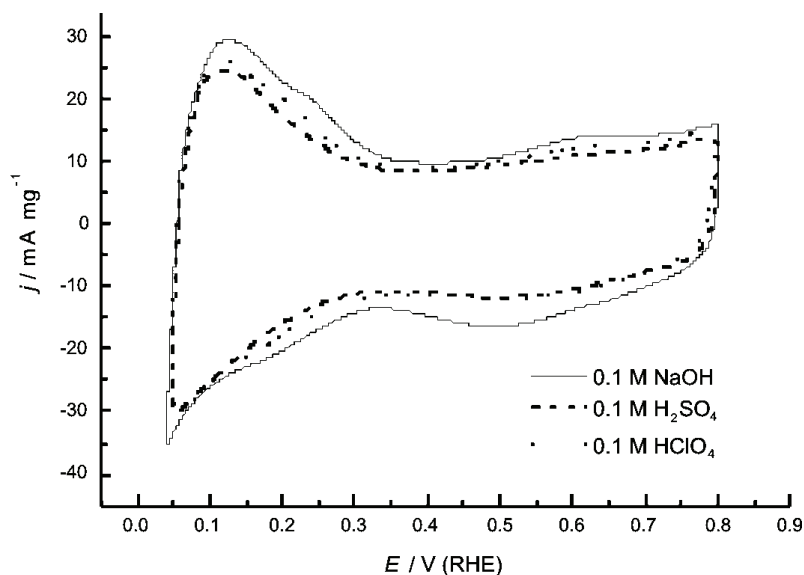


Fig. 2. Cyclic voltammograms of a high surface area Pt₃Ru₂ catalyst in alkaline and two different acid solutions. $\omega = 2000$ rpm; $\nu = 50$ mV s⁻¹; $T = 295$ K.

Potentiodynamic measurements

The electrocatalytic activities of Pt₃Ru₂/C catalyst in the bulk oxidation of CO were examined in acid and alkaline electrolytes in order to establish the effects of anions and the pH of the solution.

Effect of anions. The role of anions in the supporting electrolyte (HClO₄ and H₂SO₄) on the kinetics of CO oxidation can be seen from the corresponding voltammograms given in Fig. 3. To avoid any influence of chlorides present in *p.a.* perchloric acid, ultra high pure HClO₄ (without any traces of Cl⁻) was employed. Evidently, bisulfates influence the beginning of the reaction, slightly shifting the onset potential towards higher values relative to HClO₄. This phenomenon was also observed in methanol oxidation.^{5,18} Bisulfates decrease the activity of Pt₃Ru₂/C in the oxidation of CO due to their competition with OH and CO for adsorption on Pt sites freed from CO_{ad}.

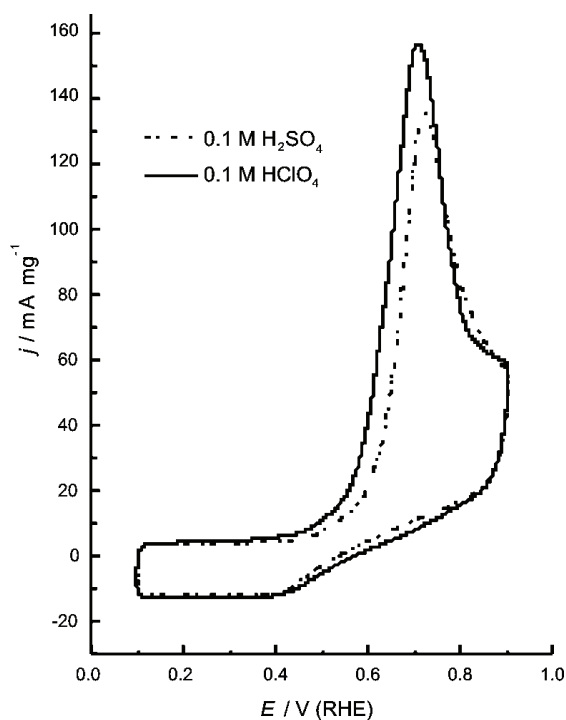


Fig. 3. Cyclic voltammograms for the oxidation of bulk CO on a Pt₃Ru₂/C electrode in 0.10 M H₂SO₄ and 0.10 M HClO₄ solutions. $\omega = 2000$ rpm; $\nu = 50$ mV s⁻¹; $T = 295$ K.

Effect of pH. The cyclic voltammograms for CO oxidation in acid (HClO₄) and alkaline (NaOH) solutions are shown in Fig. 4. The reaction commences at a ≈ 0.1 V more negative potential in NaOH than in HClO₄ media, suggesting clearly that the alkaline solution promotes CO oxidation. This is evidence that Pt can adsorb OH species in alkaline solution at significantly lower potentials than in acid solutions.

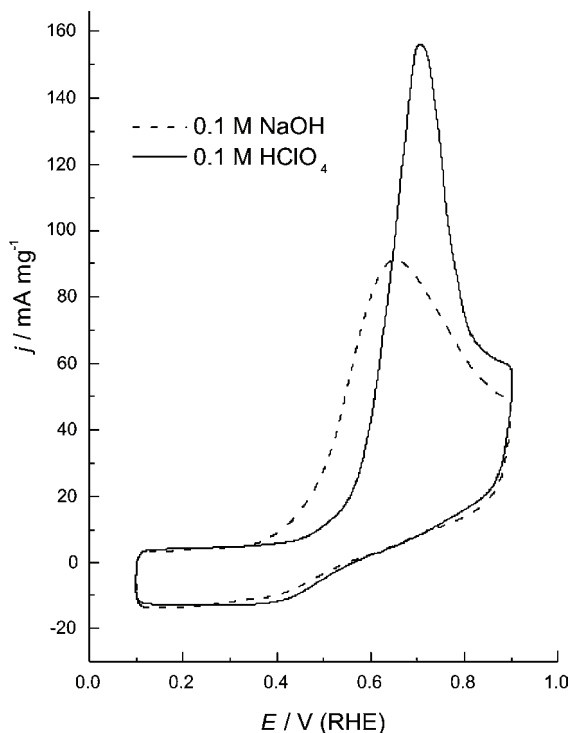


Fig. 4. Cyclic voltammograms for CO bulk oxidation on a $\text{Pt}_3\text{Ru}_2/\text{C}$ electrode in 0.10 M NaOH and 0.10 M HClO_4 solutions. $\omega = 2000$ rpm; $\nu = 50$ mV s^{-1} ; $T = 295$ K.

Quasi-steady state measurements

The quasi-steady state curves for CO oxidation recorded at a slow sweep of 1 mV s^{-1} in acid and alkaline solutions are presented in Fig. 5. The general trends observed in the potentiodynamic experiments were also observed in the quasi-steady state measurements. The oxidation of CO was significantly enhanced in alkaline relative to acid media. The onset of the reaction was shifted by ≈ 0.10 V towards less positive potentials and the current densities were higher by more than one order of magnitude. The faster kinetics achieved in perchloric acid than in sulfuric acid by a factor of ≈ 2 indicates inhibition of CO oxidation caused by bisulfate adsorption.

The slopes of the Tafel lines for CO bulk oxidation on the $\text{Pt}_3\text{Ru}_2/\text{C}$ catalyst were ≈ 120 mV dec^{-1} . This fact implies the same limiting step in CO oxidation according to a Langmuir–Hinshelwood type reaction⁸ in all the studied media.

Comparison of CO oxidation on $\text{Pt}_3\text{Ru}_2/\text{C}$ and on Pt/C catalysts

The oxidation of CO on $\text{Pt}_3\text{Ru}_2/\text{C}$ and Pt/C catalysts in acid and alkaline solutions are shown in Fig. 6a and 6b, respectively.

CO oxidation on a Pt/C catalyst in H_2SO_4 solution is represented by a sharp, symmetric peak centered at approximately 0.90 V and by a so-called pre-wave, in

the potential region $0.40 \text{ V} < E < 0.80 \text{ V}$. The pre-wave, appearing in the pre-ignition region of CO oxidation, is related to the oxidation of CO on defect sites on the facets.¹⁹ It is also a characteristic of CO oxidation on low-index Pt single crystal surfaces, where it was correlated with the presence of nano-islands on the terraces.²⁰

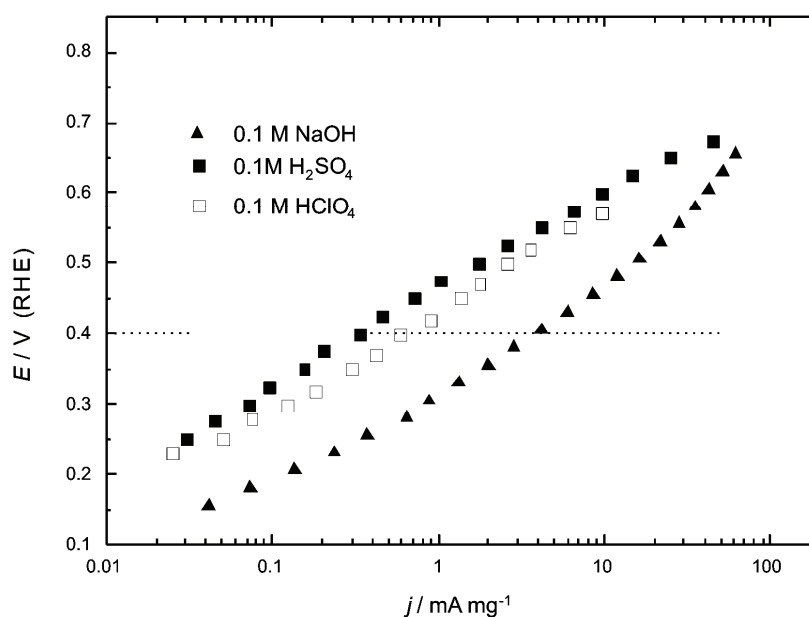


Fig. 5. Mass-specific quasi-steady state current densities for CO oxidation on a Pt₃Ru₂/C nanocatalyst in three different solutions. $\omega = 2000 \text{ rpm}$; $\nu = 1 \text{ mV s}^{-1}$; $T = 295 \text{ K}$.

Interestingly, CO oxidation on Pt₃Ru₂/C occurs in the potential region assigned as the preignition region on Pt/C, but the reaction rate is significantly enhanced compared to Pt/C. This is important datum suggesting that both metals, Ru and Pt, are able to adsorb OH species at $\approx 0.40 \text{ V}$. However, the reaction rate on Pt₃Ru₂/C is significantly increased, implying that the coverage by OH_{ad} species is larger on Ru than on Pt sites. It should be noted that under these experimental conditions, a high and constant coverage by CO_{ad} was achieved on both electrodes at the onset potential.^{21,22} Anions (bisulfates) did not affect CO adsorption at 0.05 V , which is in accordance with the results reported in the literature.²³

In alkaline solution, CO oxidation commenced at $\approx 0.3 \text{ V}$ on both catalysts. Additionally, both catalysts exhibit similar activity at potentials of technical interest ($E < 0.6 \text{ V}$). This is clear evidence that in alkaline solution not only Ru but also Pt becomes able to form OH_{ad} species at low potentials.

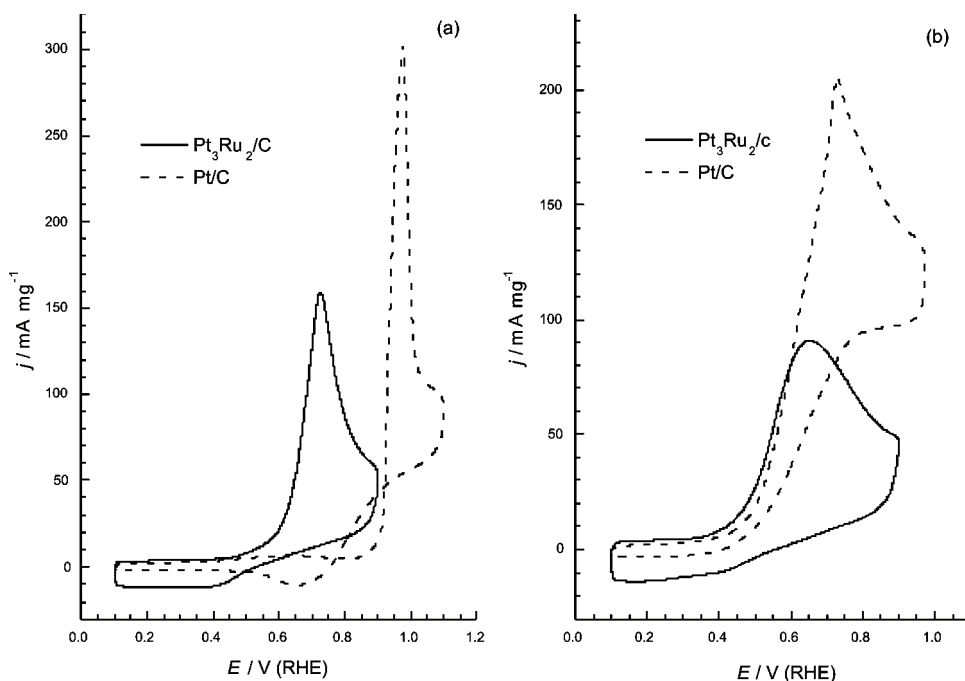
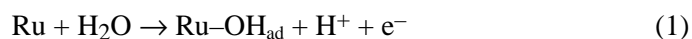


Fig. 6. Cyclic voltammograms for the oxidation of bulk CO on Pt₃Ru₂/C and Pt/C catalysts in (a) 0.10 M H₂SO₄ and (b) in 0.10 M NaOH solutions. $\omega = 2000$ rpm; $\nu = 50$ mV s⁻¹; $T = 295$ K.

CO electro-oxidation mechanism

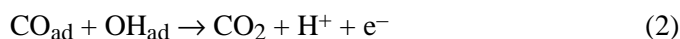
The oxidation of CO on Pt and PtRu alloy surfaces is consistent with a Langmuir–Hinshelwood reaction mechanism between adsorbed CO and oxygen-containing species, OH_{ad}. The formation of CO_{ad} occurs with equal facility on Ru and Pt sites, while the nucleation of OH_{ad} at low electrode potentials is specific to Ru surface atoms in acid solution.

According to the bifunctional mechanism,¹⁰ the electro-oxidation of CO molecules on a Pt₃Ru₂/C surface could be presented in two major steps. The first step is nucleation and growth of oxygen-containing species on the Ru sites at significantly more negative potentials compared to Pt sites:



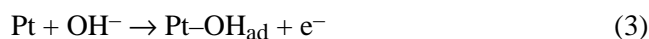
which can then initiate further electro-oxidation of CO molecules adsorbed on either Pt or Ru neighboring sites. This step occurs at surface sites referred to as “active sites”. On bulk Pt electrodes, the splitting of water probably occurs on particular sites, such as crystalline defects.²⁴ On carbon-supported Pt nanoparticles, it was proposed that these sites are defects of cubo-octahedral structure.²⁵

The second step is the reaction between the adsorbed oxygenated species and CO_{ad}, yielding CO₂ as the final product:



In this study, the onset potential for the oxidation of CO_{ad} at a Pt₃Ru₂/C catalyst was shifted towards negative potentials in acid solution compared to Pt, which is characteristic of a bimetal Pt/Ru structure. As the coverage with CO_{ad} was high, the reaction was limited by water splitting (Eq. (1)), which may explain the higher activity of Pt₃Ru₂/C than Pt/C in acid solution.

In alkaline solution, the adsorption of oxygen-containing species also occurred on the Pt sites (Eq. (3)), *i.e.*, Pt was able to adsorb OH species at almost as low potentials as Ru, causing reaction also on Pt. Ru in alkaline media is not the only donor of OH_{ad} species, as is the case in acid solution:



In fact, the oxidation of CO proceeds through a quasi-bifunctional mechanism on a Pt₃Ru₂/C catalyst in acid and in alkaline solution because Pt and Ru sites adsorb CO in acid media and both metals adsorb OH species in alkaline media.

CONCLUSIONS

The presented results can be summarized as follows:

- At a Pt₃Ru₂/C catalyst, anions (bisulfates) slightly shift the onset of the reaction towards higher potentials, thereby decreasing the reaction rate.
- A Pt₃Ru₂/C catalyst is more active in alkaline than in acid solution, since as well as Ru, Pt becomes able to adsorb OH at low potentials, thus enhancing the reaction rate compared to acid solution.
- In acid solution, the oxidation of CO proceeds on Pt₃Ru₂/C significantly faster than on Pt/C at low potentials because Ru provides more OH_{ad} species than pure Pt.
- In alkaline solution, the oxidation of CO commences at approximately the same potential at Pt/C and at Pt₃Ru₂/C and both catalyst show similar activity at potentials up to 0.6 V.
- The oxidation of CO proceeds through a quasi-bifunctional mechanism on a Pt₃Ru₂/C catalyst in acid and in alkaline solution.

Acknowledgements. This work was financially supported by the Ministry of Science and Technological Development of the Republic of Serbia, Contract No. H-142056.

ИЗВОД

АКТИВНОСТ Pt₃Ru₂/C НАНОКАТАЛИЗАТОРА У ОКСИДАЦИЈИ СОКСЕНИЈА Ђ. ПОПОВИЋ¹, ЈЕЛЕНА Д. ЛОВИЋ¹, АМАЛИЈА В. ТРИПКОВИЋ¹ и PIOTR K. OLSZEWSKI²¹ИХТМ - Центар за електрохемију, Универзитет у Београду, Њеџишева 12, б. бр. 473, 11000 Београд и²Institute of Catalysis and Surface Chemistry, Polish Academy of Sciences, Krakow, Niezapominajek 8, 30-239, Poland

Електрохемијска оксидација СО испитивана је на нанокатализатору Pt₃Ru₂ диспергованом на активном угљу као носачу у киселој и алкалној средини на собној температури коришћењем методе ротирајуће диск електроде (РДЕ). Катализатор је окарактерисан дифракцијом X-зрака (XRD) и добијени резултати су показали да се легура Pt₃Ru₂ састоји од две фазе: чврстог раствора Ru и Pt и од малих количина чистог Ru или чврстог раствора Pt у Ru. Електрокаталитичка активност овог катализатора за оксидацију СО је испитивана цикличном волтаметријом и показан је ефекат рН и ефекат анјона из носећег електролита. Pt₃Ru₂/C катализатор је активнији у алкалној него у киселој средини, указујући на чињеницу да у алкалији Pt може да адсорбује ОН честице на исто тако ниским потенцијалима као и Ru и на тај начин убрзава реакцију оксидације СО у поређењу са киселином. Показано је да адсорпција бисулфатних анјона из носећег електролита помера почетни потенцијал реакције ка позитивнијим вредностима и смањује брзину оксидације СО. Поређењем активности Pt/C и Pt₃Ru₂/C катализатора у оксидацији СО у киселој и алкалној средини показано је да је та разлика знатно мања у алкалној него у киселој средини.

(Примљено 23. фебруара, ревидирано 24. априла 2009)

REFERENCES

1. A. V. Tripković, K. Dj. Popović, B. N. Grgur, B. Blizanac, P. N. Ross, N. M. Marković, *Electrochim. Acta* **47** (2002) 3707
2. A. V. Tripković, S. Štrbac, K. Dj. Popović, *Electrochem. Commun.* **5** (2003) 484
3. J. D. Lović, A. V. Tripković, S. Lj. Gojković, K. Dj. Popović, D. V. Tripković, P. Olszewski, A. Kowal, *J. Electroanal. Chem.* **581** (2005) 294
4. A. V. Tripković, S. Lj. Gojković, K. Dj. Popović, J. D. Lović, A. Kowal, *Electrochim. Acta* **53** (2007) 887
5. A. V. Tripković, S. Lj. Gojković, K. Dj. Popović, J. D. Lović, *J. Serb. Chem. Soc.* **71** (2006) 1333
6. A. V. Tripković, K. Dj. Popović, J. D. Lović, *J. Serb. Chem. Soc.* **72** (2007) 1094
7. R. Parsons, T. van der Noot, *J. Electroanal. Chem.* **257** (1988) 9
8. H. A. Gasteiger, N. Marković, P. N. Ross Jr., E. J. Cairns, *J. Phys. Chem.* **98** (1994) 617
9. H. A. Gasteiger, N. Marković, P. N. Ross Jr., *J. Phys. Chem.* **99** (1995) 8290
10. M. Watanabe, S. Motoo, *J. Electroanal. Chem.* **60** (1975) 267
11. M. Watanabe, S. Motoo, *J. Electroanal. Chem.* **60** (1975) 275
12. A. Kabbibi, R. Faure, R. Durand, B. Beden, F. Hahn, J. M. Leger, C. Lamy, *J. Electroanal. Chem.* **444** (1998) 41
13. T. J. Schmidt, H. A. Gasteiger, R. J. Behm, *Electrochem. Commun.* **1** (1999) 1
14. A. Kowal, P. Olszewski, D. Tripković, R. Stevanović, *Mat. Sci. Forum* **518** (2006) 271
15. A. H. C. Sirk, J. M. Hill, S. K. Y. Kung, V. I. Birss, *J. Phys. Chem. B* **108** (2004) 689
16. G. Wu, L. Li, B.-Q. Xu, *Electrochim. Acta* **50** (2004) 1

17. S. Hadži-Jordanov, H. Angerstein-Kozłowska, M. Vuković, B. Conway, *J. Electrochem. Soc.* **125** (1978) 1471
18. T. Iwasita, *Electrochim. Acta* **47** (2002) 3663
19. K. J. J. Mayrhofer, B. B. Blizanac, M. Arenz, V. R. Stamenković, P. N. Ross, N. M. Marković, *J. Phys. Chem. B* **109** (2005) 14433
20. M. Arenz, K. J. J. Mayrhofer, V. R. Stamenković, B. B. Blizanac, T. Tomoyuki, P. N. Ross, N. M. Marković, *J. Am. Chem. Soc.* **127** (2005) 6819
21. E. A. Batista, T. Iwasita, W. Vielstich, *J. Phys. Chem. B* **108** (2004) 14216
22. Z. Jusys, J. Kaiser, R. J. Behm, *Electrochim. Acta* **47** (2002) 3693
23. D. V. Tripković, D. Strmcnik, D. van der Vilet, V. Stamenković, N. M. Marković, *Faraday Discuss.* **140** (2009) 25
24. N. P. Lebedeva, M. T. M. Koper, J. M. Feliu, R. A. van Santen, *J. Phys. Chem. B* **106** (2002) 12938
25. K. J. J. Mayrhofer, M. Arenz, B. B. Blizanac, V. R. Stamenković, P. N. Ross, N. M. Marković, *Electrochim. Acta* **50** (2005) 5144.



J. Serb. Chem. Soc. 74 (8–9) 977–984 (2009)
JSCS–3892

Journal of
the Serbian
Chemical Society

JSCS@tmf.bg.ac.rs • www.shd.org.rs/JSCS

UDC 546.873+543.23+543.4/.5+542.97

Short communication

SHORT COMMUNICATION

Kinetic spectrophotometric determination of Bi(III) based on its catalytic effect on the oxidation of phenylfluorone by hydrogen peroxide

SOFIJA M. RANČIĆ^{1*} and SNEŽANA D. NIKOLIĆ-MANDIĆ²

¹Faculty of Science, Department of Chemistry, University of Niš, Višegradska 33, 18000 Niš and ²Faculty of Chemistry, University of Belgrade, Studentski trg 16–22, 11000 Belgrade, Serbia

(Received 1 December 2008, revised 15 April 2009)

Abstract: A new reaction was suggested and a new kinetic method was elaborated for determination of Bi(III) in solution, based on its catalytic effect on the oxidation of phenyl-fluorone (PF) by hydrogen peroxide in ammonia buffer. By application of spectrophotometric technique, a limit of quantification (LQ) of 128 ng cm⁻³ was reached, and the limit of detection (LD) of 37 ng cm⁻³ was obtained, where LQ was defined as the ratio signal:noise = 10:1 and LD was defined as signal 3:1 against the blank. The *RSD* value was found to be in the range 2.8–4.8 % for the investigated concentration range of Bi(III). The influence of some ions upon the reaction rate was tested. The method was confirmed by determining Bi(III) in a stomach ulcer drug (“Bicit HP”, Hemofarm A.D.). The obtained results were compared to those obtained by AAS and good agreement of results was obtained.

Keywords: kinetic method; catalytic reaction; Bi(III) determination.

INTRODUCTION

The most important methods of bismuth determination are kinetic, spectrophotometric and atomic absorption spectroscopy (AAS) methods.^{1–21} An interesting electrothermal atomic absorption spectroscopy (ET AAS) method was published for the determination of bismuth traces in sea water.²² Some photometric, chromatographic (HPLC) and flow-injection analysis (FIA) methods are also reported.^{23–25} There are relatively small number of kinetic methods for Bi(III) determination, compared to a great number of spectrophotometric ones based on its ability to form complexes, mainly colored, with organic and inorganic compounds.

* Corresponding author. E-mail: sofija_rancic@yahoo.com
doi: 10.2298/JSC0909977R



An interesting kinetic method, described by Murty, points out the catalytic effect of Bi(III) in the molybdenum phosphorous acid reduction by ascorbic acid,¹ although a new method, employing the same reaction system, but with better sensitivity, was also reported.² The method was used to determine the traces of Bi(III) in alloys. A method based on the catalytic effect of Bi(III) ions is employed in the oxidation of hematoxylin (HT) by H₂O₂ in a strong acid solution.³ Kinetic catalytic method for bismuth determination in strong acid medium with KIO₄ as the oxidant and dibrom-nitro-arsenazo (DBN-arsenazo) as the reductant was used for bismuth determination in drinking water.⁴ Another kinetic method employed for the determination of Bi(III) in alloys and drinking water⁵ is based on the catalytic effect of bismuth on the oxidation of carboxyazo I by KIO₄. The inhibitory effect of Bi(III) on the fading reaction of crystal violet oxidized by H₂O₂ in the acetate buffer solution was followed by kinetic spectrophotometric method.⁶ Of all reported kinetic methods, only the method reported by Sanz et al. was used to determine bismuth in drugs.⁷

The aim of this communication is to present the results obtained in a new kinetic spectrophotometric determination of Bi(III) using its catalytic effect in the oxidation of phenylfluorone (PF) by hydrogen peroxide in ammonia buffer. The method is employed for the determination of Bi(III) in a stomach ulcer drug.

EXPERIMENTAL

Apparatus

The spectrophotometric measurements were performed on a Perkin-Elmer UV-Vis Lambda 15 spectrophotometer. The cylindrical cells were thermostated at 20±0.1 °C using a thermocirculating bath. The pH measurements were performed using a Radiometer PHM 29 b pH-meter with a combined glass-calomel electrode GK 2311 C.

Reagents

All solutions were prepared by dissolving p.a. quality "Merck" reagents in deionized water (0.4–0.8 μS cm⁻¹) and ammonia buffer. Adequate polyethylene vessels were used for storage of the solutions. Ammonia buffers were prepared by mixing NH₃(aq) and NH₄Cl solutions (0.2 mol dm⁻³)²⁶ and their pH values were checked using pH-meter. A stock Bi(III) solution (1.0×10⁻³ g cm⁻³) was prepared by dissolving 1.00 g of metallic bismuth (99.999 %) in a minimal volume of HNO₃ (1:1) and diluting it to 1 dm³ with 2 % HNO₃ solution. The concentration of the stock solution was checked by EDTA titration.²⁷ The concentrations of H₂O₂ solutions were verified by KMnO₄ titration. The phenylfluorone solution was prepared by dissolving the exactly measured amount of dry substance in ammonia buffer (pH 10.4).

Procedure

Selected volumes of reactants and deionized water were poured separately into four-legged Budarin vessel up to a predetermined total volume of 10 cm³. The solution of Bi(III) was measured into one leg of Budarin vessel for catalytic reaction and the same volume of deionized water was measured for the non-catalytic reaction. After thermostating for 10 min the reagents were mixed and absorbance was measured in 15 s intervals 45 s after beginning of the reaction. Absorbance measurements were performed at 20±0.1 °C.

RESULTS AND DISCUSSION

While the reaction proceeds, the initial red color of solution fades and a colorless reaction product is formed. Neither the exact mechanism of reaction nor the chemical nature of the products was of major interest in this investigation. The spectrophotometric measurements were performed at the wavelength of the absorption maximum of phenyl fluorone in ammonia buffer (493.6 nm, Fig. 1). The logarithm of absorbance-time curves are linear during the first 5–10 min of reaction for different Bi(III) concentrations. The rate of the reaction was obtained using the slope of the kinetic curves of the absorbance–time plot.²⁸

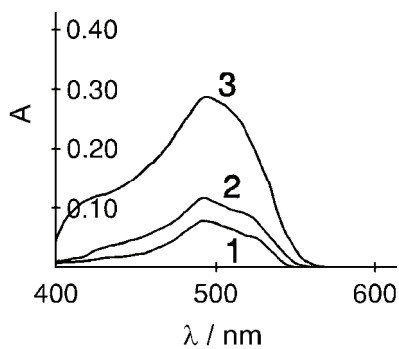


Fig. 1. Absorption spectra of PF in ammonia buffer. Initial conditions: $1.5 \times 10^{-5} \text{ mol dm}^{-3}$ PF; $20 \pm 0.1 \text{ }^\circ\text{C}$; pH: 1) 10.2, 2) 10.6; 3) 11.9.

According to the previous results,²⁹ borate and phosphate buffers are inadequate for this reaction. Hence, the influence of the pH value of selected ammonia buffers on the rate of both the catalytic and non-catalytic reaction was examined in pH interval of about 9 to about 11. Within this range, the non-catalytic reaction showed zero order dependence on the pH value of the ammonia buffer, while the catalytic reaction exhibited a complex dependence (Fig. 2). The value of 10.4 was selected as the most appropriate one, because it provides the largest difference of the reaction rates of the catalytic and non-catalytic reaction.

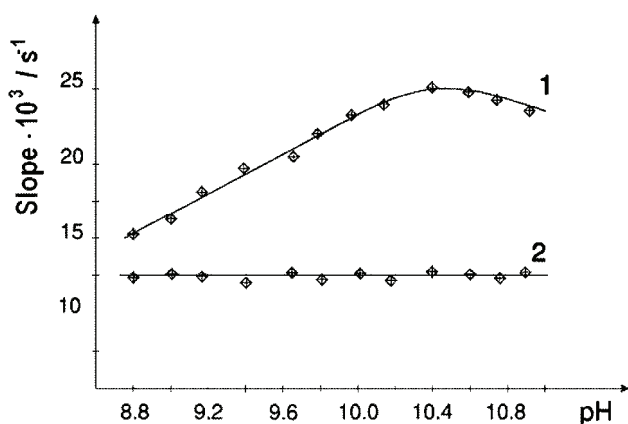


Fig. 2. Dependence of the reaction rate on pH. Initial conditions: $4 \times 10^{-5} \text{ mol dm}^{-3}$ PF; $3.9 \text{ mol dm}^{-3} \text{ H}_2\text{O}_2$; $2.5 \text{ } \mu\text{g cm}^{-3}$ Bi(III); $20 \pm 0.1 \text{ }^\circ\text{C}$; 1 – catalytic reaction, 2 – non-catalytic reaction.

Hence, the ammonia buffer pH 10.4 was used in all subsequent investigations.

The rates of both reactions are of the first order dependence on the reductant concentration (Fig. 3) within the range of 1.0×10^{-5} to 4.0×10^{-5} mol dm⁻³. Consequently, a concentration of 3.0×10^{-5} mol dm⁻³ was selected as optimal for the subsequent measurements.

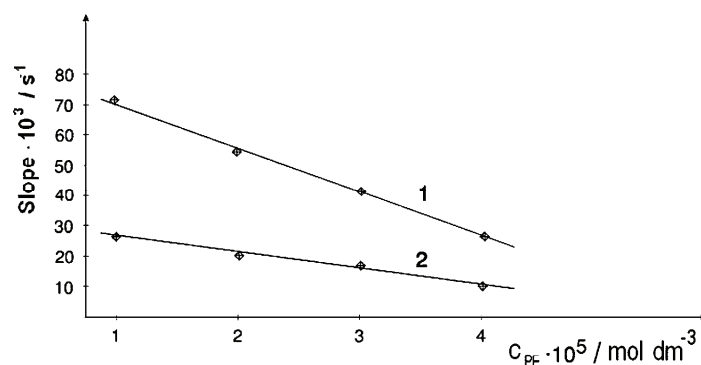


Fig. 3. Dependence of the reaction rate on the PF concentration. Initial conditions: $3.9 \text{ mol dm}^{-3} \text{ H}_2\text{O}_2$; $2.5 \mu\text{g cm}^{-3} \text{ Bi(III)}$; $20 \pm 0.1 \text{ }^\circ\text{C}$; 1 – catalytic reaction, 2 – non-catalytic reaction.

Based on the previous investigations,²⁹ the dependence of rate of the catalytic and non-catalytic reaction on the oxidant concentration was monitored within the concentration range of about 2.0 to about $4.0 \text{ mol dm}^{-3} \text{ H}_2\text{O}_2$. Within this interval, the catalytic reaction rate increases with oxidant concentration, whereas the non-catalytic one does not depend on oxidant concentration (Fig. 4). As optimal, a concentration of $3.9 \text{ mol dm}^{-3} \text{ H}_2\text{O}_2$ was selected, because at this concentration (in the investigated range) the difference between the reaction rates of catalytic and non-catalytic reaction was the greatest.

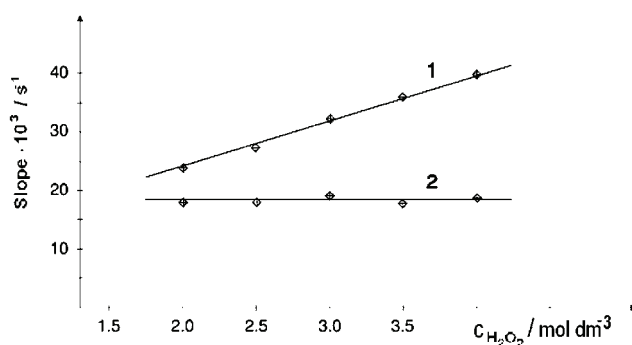


Fig. 4. Dependence of the reaction rate on the H_2O_2 concentration. Initial conditions: $3 \times 10^{-5} \text{ mol dm}^{-3} \text{ PF}$; $2.5 \mu\text{g cm}^{-3} \text{ Bi(III)}$; $20 \pm 0.1 \text{ }^\circ\text{C}$; 1 – catalytic reaction, 2 – non-catalytic reaction.

Hence, the optimal conditions for performing the reaction were found to be: pH 10.4, $c_{PF} = 3.0 \times 10^{-5} \text{ mol dm}^{-3}$, $c_{H_2O_2} = 3.9 \text{ mol dm}^{-3}$.

Under the selected conditions, the dependence of catalytic reaction rate on the Bi(III) concentration was observed at three temperatures: 20 ± 0.1 , 23 ± 0.1 and 25 ± 0.1 °C. The linear dependence of calibration curves falls within the range of 6.0×10^{-7} to $3.0 \times 10^{-6} \text{ g cm}^{-3}$ Bi (III) (Fig. 5).

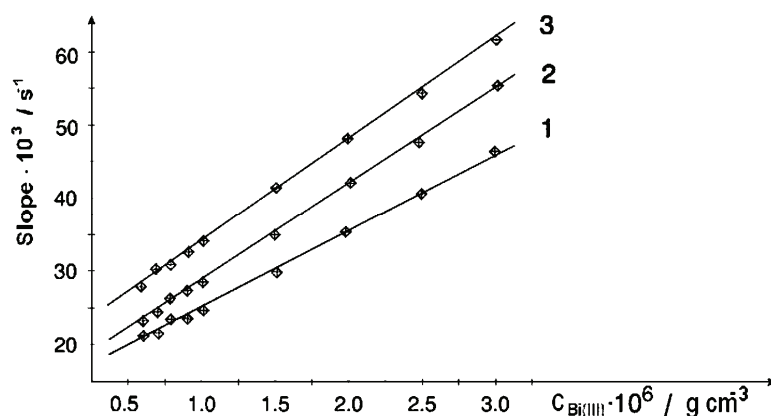


Fig. 5. Calibration curve at different temperatures: 1 – 20 ± 0.1 , 2 – 23 ± 0.1 and 3 – 25 ± 0.1 °C.

The adequate equations of calibration curves for 20 ± 0.1 , 23 ± 0.1 and 25 ± 0.1 °C, were calculated as follows:

$$\text{Slope} = (0.01027 \pm 0.00001)c + (0.01495 \pm 0.00017) \quad (1)$$

$$\text{Slope} = (0.01234 \pm 0.00003)c + (0.01811 \pm 0.00015) \quad (2)$$

$$\text{Slope} = (0.01325 \pm 0.00002)c + (0.02246 \pm 0.00011) \quad (3)$$

where c is the Bi(III) concentration in $\mu\text{g cm}^{-3}$.

The accuracy and precision of the method were checked for three different Bi(III) concentrations within the range of calibration curve. Five repeated measurements were performed for each concentration. Satisfactory results were obtained since the Bi(III) concentrations of 1.0, 2.0 and $3.0 \mu\text{g cm}^{-3}$ gave the RSD values of 4.8, 3.6 and 2.8 %, respectively.

The accuracy and precision of the method were checked for three different Bi(III) concentrations within the range of calibration curve. Five repeated measurements were performed for each concentration. Satisfactory results were obtained since the Bi(III) concentrations of 1.0, 2.0 and $3.0 \mu\text{g cm}^{-3}$ gave the RSD values of 4.8, 3.6 and 2.8 %, respectively.

The selectivity of reaction was established by separately adding the selected ions to the reaction mixture. Each ion was added in six known concentration ratios (0.001:1, 0.01:1, 1:1, 10:1, 100:1 and 1000:1) to the constant Bi(III) concentration ($2.0 \mu\text{g cm}^{-3}$). The measurements were performed at 20 ± 0.1 °C,

and 30 most frequently used cations and anions were tested (Na^+ , K^+ , Ag^+ , Ca^{2+} , Sr^{2+} , Ba^{2+} , Mg^{2+} , Zn^{2+} , Cu^{2+} , Pb^{2+} , Ni^{2+} , Co^{2+} , Hg^{2+} , Sn^{2+} , Fe^{3+} , Al^{3+} , As^{3+} , Sb^{3+} , acetate, tartarate, oxalate, molybdate, wolframate, bromide, iodide, chloride, nitrate, sulphate, carbonate, phosphate). The method was found to have extremely good selectivity. Only the presence of As(III), Sb(III), Hg(II), molybdate and wolframate, in the ratio 1:1, interferes the determination of bismuth; Sn(II) in the ratio 1:1 inhibits the determination, and Co(II) in the ratio 0.01:1 catalyzes the determination of Bi(III) by this method.

The method was successfully applied to the determination of Bi(III) in stomach ulcer drug "Bicit HP" (Hemofarm A.D.). This drug contains bismuth in the form of subcitrate. Solutions containing a known quantity of bismuth were prepared by dissolving the drug in deionized water. The solutions were analyzed by application of both the presented kinetic method and the AAS method. The results are given in Table I, from which the good agreement between the results of both methods can be seen.

TABLE I. Bi(III) determination in a drug

Measured $\mu\text{g cm}^{-3}$	Kinetic determination ^a $\mu\text{g cm}^{-3}$	RSD %	Determined by AAS ^a $\mu\text{g cm}^{-3}$	RSD %
1.0	1.16±0.18	4.6	1.05±0.02	1.0
2.0	2.08±0.13	3.7	2.01±0.02	0.9
3.0	2.93±0.10	2.6	3.00±0.02	0.6

^aThe mean value of five measurements $\pm 2SD$

CONCLUSIONS

A new method for the determination of Bi(III) was developed, providing rapid and easy performance at room temperature, giving precise, reproducible results and exhibiting exceptional selectivity. On the grounds of the obtained results, the method is highly recommendable for the determination of Bi(III) in drug solutions. It could also be a good basis for further investigation in the area of kinetic methods for the determination of bismuth.

ИЗВОД

КИНЕТИЧКО СПЕКТРОФОТОМЕТРИЈСКО ОДРЕЂИВАЊЕ Bi(III) НА ОСНОВУ ЊЕГОВОГ КАТАЛИТИЧКОГ ДЕЈСТВА НА ОКСИДАЦИЈУ ФЕНИЛФЛУОРОНА ВОДОНИК-ПЕРОКСИДОМ

СОФИЈА М.РАНЧИЋ¹ И СНЕЖАНА Д. НИКОЛИЋ-МАНДИЋ²

¹Природно-математички факултет, Одсек за хемију, Универзитет у Нишу, Вишеградска 33, 18000 Ниш и

²Хемијски факултет, Универзитет у Београду, Студенски тирз 16–22, 11000 Београд

Предложена је нова реакција и развијена нова кинетичка метода за одређивање Bi(III) у раствору, на основу његовог каталитичког дејства на оксидацију фенилфлуорона (PF) водоник-пероксидом у амонијачном пуферу. Применом спектрофотометријске методе, под

оптimalним условима, постигнута је граница одређивања (LQ) од 128 ng cm⁻³ и остварена граница детекције(LD) од 37 ng cm⁻³. LQ је дефинисана као однос сигнал:шум = 10:1, а LD као сигнал 3:1 према слепој проби. RSD се креће од 2,8 до 4,8 % у испитиваном интервалу концентрација Bi(III). Испитан је и утицај присуства других јона у реакционој смеши на брзину основне реакције. Метода је примењена за одређивање бизмута у леку за чир на желуцу, ("Bicit HP", Хемофарм А.Д.). Добијени резултати показују добро слагање с резултатима добијеним ААС методом која је коришћена као референтна метода.

(Примљено 1. децембра, ревидирано 15. априла 2009)

REFERENCES

1. J. A. Murty, *Chem. Anal. (Warsaw)* **5** (1992) 37 (in Polish)
2. J. Li, J. Zhu, *J. Guilin Univer. Technol.* **16** (1996) 174 (in Chinese)
3. T. G. Pecev, R. P. Igov, V. P. Stankov-Jovanović, V. D. Mitić, *J. Serb. Chem. Soc.* **55** (1995) 64
4. J. Yu, Y. Lei, *Phys. Testing Chem. Anal. B* **37** (2001) 349 (in Chinese)
5. S. Ge, J. Yu, K. Cui, *Sichuan Univer. J., Natur. Sci.* **18** (2004) 299 (in Chinese)
6. L. Zhang, Y. Yang, J. Xu, C. Xu, Z. Ye, *Chin. J. Anal. Labor.* **26** (2007) 52 (in Chinese)
7. J. Sanz, S. de Marcos, J. Galban, F. Gallarta, *Analisis* **21** (1993) 27
8. L. Zhang, S. B. Mulrooney, A. F. K. Leung, Y. Zeng, B. B. C. Ko, R. P. Hausinger, H. un, *Biometals* **19** (2006) 503
9. L. Jin, K. Y. Szeto, L. Zhang, W. Du, H. Sun, *J. Inorg. Biochem.* **98** (2004) 1331
10. L. Chen, Y. Shu, *Acta Sci. Circumstant.* **12** (1990) 63 (in Chinese)
11. H. Liu, *Chin. J. Anal. Chem. Jiliang Univer.* **15** (2006) 55 (in Chinese)
12. W. Wang, T. Jiang, W. Hu, J. Shao, X. Mu, Z. Zhang, X. Zhang, Q. Zhai, *Metall. Anal.* **25** (2005) 80 (in Chinese)
13. R. P. Mihajlović, V. M. Kaljević, M. P. Vukasinović, Lj. V. Mihajlović, I. D. Pantić, *Water SA* **33** (2007) 513
14. X. Zheng, *Metall. Anal.* **28** (2008) 77 (in Chinese)
15. G. Zhao, Y. Yan, J. Xie, *Metall. Anal.* **26** (2006) 53 (in Chinese)
16. Y. Dong, A. Wang, *Uran. Min. Metall.* **24** (2005) 163 (in Chinese)
17. L. Gao, H. Song, C. Wang, J. Yao, *Chin. J. Anal. Chem. Jiliang Univer.* **14** (2005) 57 (in Chinese)
18. X. Ge, T. Hang, N. Liu, *Chin. J. Pharm. Anal.* **25** (2005) 670 (in Chinese)
19. W. Chen, W. Ma, X. Xu, S. Li, *Chin. J. Anal. Labor.* **24** (2005) 10 (in Chinese)
20. G. Gemus, H. Filik, B. Demirata, *Anal. Chim. Acta* **547** (2005) 138
21. Y. Li, W. Chen, J. Sun, Q. Zhang, B. Lu, *Chin. J. Anal. Labor.* **24** (2005) 33 (in Chinese)
22. Y. Shiyo, M. Mitsuhashi, T. Shimizu, S. Sakurai, *Analyst* **117** (1992) 1929
23. K. Shibata, M. Nakahara, *J. Res.* **7** (2007) 20 (in Japanese)
24. T. Muramoto, Y. Yukishita, T. Shimizu, N. Uehara, *J. Iron Steel Inst. Japan* **2** (2007) 94 (in Japanese)
25. K. Agrawal, G. L. Mundhara, K. S. Patel, P. Hoffman, *Anal. Lett.* **10** (2004) 37
26. Y. Y. Luruye, *Spravochnik po analiticheskoi khimiyi*, Khimiya, Moskva, 1989, p. 76 (in Russian)
27. M. J. Bulatov, J. P. Kalinkin, *Prakticheskoe rukovodstvo po fotometricheskim metodam analiza*, Khimiya, Leningrad, 1986, p. 93 (in Russian)

28. D. Perez-Bendito, M.Silva, *Kinetic methods in analytical chemistry*, John Wiley and Sons, Chichester, 1988, p. 22
29. S. Rančić, *Ph.D. Thesis*, Faculty of Chemistry, University of Belgrade, Belgrade, 2005.



SHORT COMMUNICATION

Spectrophotometric determination of nitrite based on its catalytic effect on the reaction of nuclear fast red and potassium bromate

HASSAN ZAVVAR MOUSAVI^{1*} and HAMID SHIRKHANDLOO²

¹*Chemistry Department, College of Sciences, Semnan University, Semnan and* ²*Research Institute of Petroleum Industry, Medical Industrial Laboratory, Tehran, Iran*

(Received 16 January, revised 24 April 2009)

Abstract: A highly selective and sensitive catalytic spectrophotometric method was developed for the determination of nitrite in water samples. The method is based on its catalytic effect on the nuclear fast red–potassium bromate redox reaction in acidic medium. The reaction was followed spectrophotometrically by measuring the change in the absorbance at 518 nm of nuclear fast red 5 min after initiation of the reaction. In this study, the experimental parameters were optimized and the effects of other cations and anions on the determination of nitrite were examined. The calibration graph was linear in the range 2.0–45 $\mu\text{g mL}^{-1}$ of nitrite. The relative standard deviations for the determination of 15 and 30 $\mu\text{g mL}^{-1}$ of nitrite were 3.1 and 1.75 %, respectively ($n = 8$). The detection limit calculated from three times the standard deviation of the blank $3S_b$ was 0.7 $\mu\text{g mL}^{-1}$. The method was successfully applied to the determination of nitrite in spiked tap, natural and wastewater samples.

Keywords: nitrite; catalytic reaction; spectrophotometric; nuclear fast red.

INTRODUCTION

The determination of nitrite is of increasing interest in a variety of fields, such as food, water and environmental samples. Nitrite and nitrate ions participate in several important environmental transformations involving nitrogen. The toxicity of nitrite is primarily due to the fact that it can react with secondary or tertiary amines present in the human body to form nitrosamines, which are known to be carcinogens and mutagenic.^{1–3} It is well known that the nitrite ion is an important intermediate in the biological nitrogen cycle and is present in soils and surface water.⁴ Nitrite salts are versatile chemical agents that have found numerous applications, such as in dye manufacture, the food industry and corrosion inhibition of industrial process water.⁵

* Corresponding author. E-mail: hzmousavi@semnan.ac.ir
doi: 10.2298/JSC0909985M

As nitrite shows potential toxicity by forming carcinogenic nitrosamines, the determination of nitrite is important in environmental protection and public health. Therefore, many methods for nitrite determination have been developed in recent years, such as kinetic methods,^{6,7} chromatography,^{8,9} potentiometry,^{10,11} amperometry,¹² polarography,¹³ capillary electrophoresis,¹⁴ spectrophotometry¹⁵ and flow injection analysis (FIA) systems.¹⁶ However, these methods have the disadvantage of the employment of large volumes of toxic reagents, low sample frequency, application of complicated flow injection systems, poor reproducibility, expensive and time-consuming separation procedures and, for certain methods, the requirement of high temperatures.^{17,18}

Kinetic methods^{19,20} can be implemented on very simple, inexpensive equipment and provide for low level determinations comparable to those typically offered by much more expensive techniques, such as inductively coupled plasma, atomic emission spectrometry (ICP-AES) or electro thermal atomic absorption spectrometry (ETAAS). In this paper, a simple, sensitive, and highly selective catalytic method for the determination of nitrite based on its catalytic effect on the redox reaction of nuclear fast red–potassium bromate is described.

EXPERIMENTAL

Reagents and solutions

All employed reagents were of analytical-reagent grade and double distilled water (DDW) was used throughout. Nuclear fast red (Aldrich), potassium bromate and sulfuric acid (Merck) were used without further purification. A nitrite stock solution 100 mg L^{-1} was freshly prepared before each measurement by dissolving 0.1500 g sodium nitrite (Merck) in 1000 mL water. This solution was transferred into a brown bottle and stored under diffused sunlight. A bromate solution (0.25 mol L^{-1}) was prepared by dissolving 4.1752 g of KBrO_3 in water in a 100 mL volumetric flask. A nuclear fast red solution ($5 \times 10^{-4} \text{ mol L}^{-1}$) was prepared by dissolving 0.0178 g of nuclear fast red in water and diluting with water in a 100 mL volumetric flask. A sulfuric acid solution (2 mol L^{-1}) was prepared by diluting an appropriate volume of concentrated acid. Stock solutions interfering ions, $1000 \text{ } \mu\text{g mL}^{-1}$, were prepared by dissolving appropriate amounts of their suitable salts in water.

Apparatus

A UV-visible spectrophotometer (Shimadzu) was used for recording and measuring the absorbance at 518 nm . A Colora C-1668 thermostat, in which the temperature could be fixed to within $\pm 0.10 \text{ }^\circ\text{C}$, was used for maintaining the temperature.

Procedure

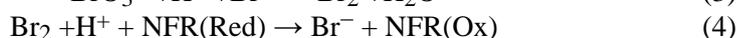
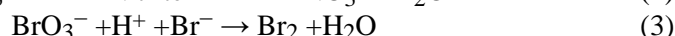
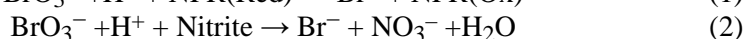
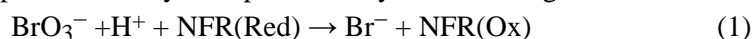
To a series of 10 mL volumetric flasks, 2.0 mL of $5.0 \times 10^{-4} \text{ mol L}^{-1}$ nuclear fast red solution, 1 mL of 2.0 mol L^{-1} sulfuric acid and 1.0 mL of different concentrations of nitrite were added in sequence. Then 2.0 mL of 0.2 mol L^{-1} bromate solution was added and the solution was diluted to the mark with DDW and the solution was mixed well. The zero time was taken as the moment at which the last drop of bromate solution was added. After 5 min , a portion of the solution was transferred into a 1.0 cm quartz cell and the absorbance was measured against DDW at 518 nm (A_S). The blank reaction was performed according to the same procedure without addition of nitrite and the change in absorbance was labeled as A_0 . A

standard curve showing the difference in absorbance between A_s and A_0 (ΔA) vs. the nitrite concentration was obtained. For each sample and blank, five replicate determinations were made and the mean signals were used. The catalytic and non-catalytic reactions (blank reaction) were simultaneously measured.

RESULTS AND DISCUSSION

Absorption spectra

Nuclear fast red, NFR, is a dye with an absorption spectrum in acidic medium that shows an absorbance maximum at 518 nm. In acidic medium, nuclear fast red is oxidized by bromate to produce a colorless compound. However, in the absence of nitrite, the reaction between nuclear fast red and bromate is slow and in the presence of trace amounts of nitrite, the rate of reaction is increased. This oxidation process was observed by the decrease in absorbance of the characteristic band for nuclear fast red. The catalytic effect of nitrite on the reaction was monitored spectrophotometrically by measuring the change in absorbance of nuclear fast red at 518 nm with time. The possible mechanism of the nuclear fast red reaction in its simplest form may be represented by the following reactions:



where Red is the reduced form and Ox is the oxidized form of nuclear fast red. Reaction (1) is slow in the absence of nitrite, BrO_3^- oxidizes nuclear fast red to produce a small reduction in the absorbance of dye. When nitrite is added to this system, reactions (2) and (3) are very fast and the Br_2 generated *in situ* in this system is a nascent oxidant.²¹ To determine the optimum experimental conditions, several parameters having the biggest influence on the rate of reaction, *i.e.*, time of reaction, temperature, sulfuric acid concentration, bromate concentration and concentration of nuclear fast red, were studied.

Effect of reaction time

As shown in Fig. 1, when the reaction time was between 0 and 5 min, ΔA ($A_s - A_0$) was a linear function of the reaction time. After 5 min, ΔA changed very slowly with elapsed time; ΔA was first stable and then showed a decreasing tendency. The change in absorbance, ΔA , reached its maximum in 5 min. Therefore, a fixed time of 5 min was applied for all the experiments because the highest ΔA was obtained after this time (see Fig. 1).

Effect of reaction variables

In order to find the optimal conditions for the catalytic determination of nitrite, the effects of acids and acidity, the concentration of the reagents, interfering ions and temperature were examined, in both the catalyzed and uncatalyzed reactions.

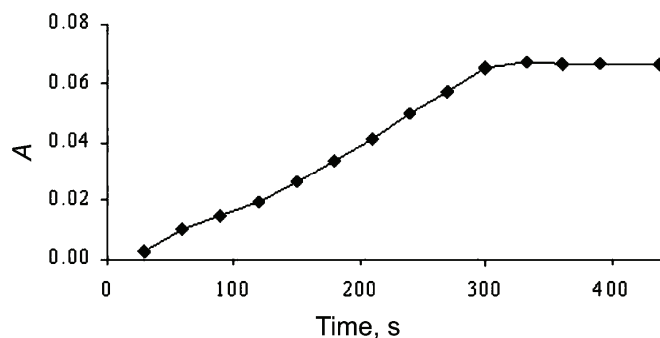


Fig. 1. Effect of time on ΔA .

Effect of acidity. Since the reaction proceeds in acidic media, the effect of the type and concentration of acid on the reaction rate was studied. The effects of various types of acids, *i.e.*, sulfuric, hydrochloric, phosphoric and nitric acid, of similar concentration were studied and sulfuric acid was selected. The effect of acidity was studied by varying the volume of the employed 2.0 mol L^{-1} sulfuric acid solution between 1.0–5.0 mL. The results showed that with increasing acidity, the sensitivity of the determination of nitrite decreased. Therefore, 1.0 mL of sulfuric acid was chosen for further studies.

Optimization of the concentrations of the reagents. The effect of the nuclear fast red concentration on the reaction rate is shown in Fig. 2. When the nuclear fast red concentration was increased in the range 5.0×10^{-6} to $2.0 \times 10^{-4} \text{ mol L}^{-1}$, the difference in the absorbance (ΔA) increased. A concentration of $1.0 \times 10^{-4} \text{ mol L}^{-1}$ of nuclear fast red in the final solution was selected. At higher concentrations of nuclear fast red, the absorbance of the solution became too high (see Fig. 2).

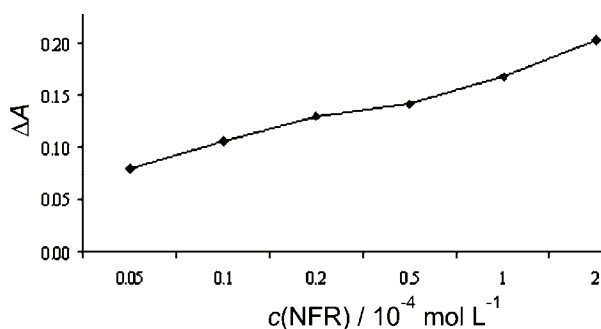


Fig. 2. Effect of the nuclear fast red concentration on ΔA . Conditions: $10 \mu\text{g mL}^{-1}$ nitrite; 0.20 mol L^{-1} sulfuric acid; 0.020 mol L^{-1} potassium bromate; temperature: $25 \text{ }^\circ\text{C}$; reaction time: 5 min.

The influence of bromate concentration on the reaction rate was also studied by adding different concentration of the potassium bromate and applying the re-

commended procedure. A concentration of 0.040 mol L^{-1} of potassium bromate in final solution gave the highest ΔA and was selected for further work (see Fig. 3).

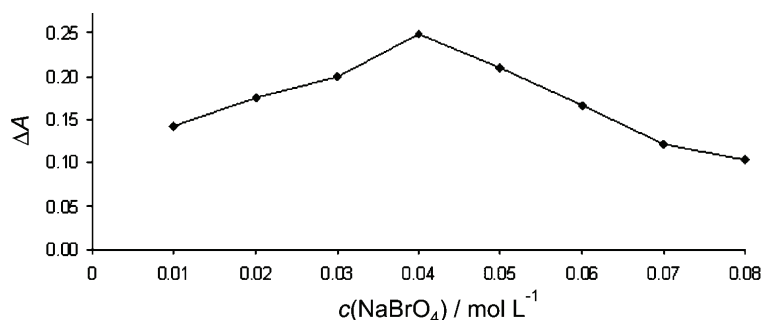


Fig. 3. Effect of the potassium bromate concentration on ΔA . Conditions: $10 \mu\text{g mL}^{-1}$ nitrite; 0.20 mol L^{-1} sulfuric acid; $1.0 \times 10^{-4} \text{ mol L}^{-1}$ nuclear fast red, temperature: $25 \text{ }^\circ\text{C}$; reaction time: 5 min

Effect of temperature. The effect of temperature on the sensitivity was examined in the range of $20\text{--}50 \text{ }^\circ\text{C}$. At high temperatures, the absorbance difference (ΔA) decreased. At temperatures from 20 to $25 \text{ }^\circ\text{C}$, the highest absorbance difference (ΔA) was obtained. In this study, the laboratory temperature ($25 \pm 0.1 \text{ }^\circ\text{C}$) was used for further experiments.

Effect of interfering ions. To study the selectivity of the proposed method, the interference of several ions that could occur in real water samples besides nitrite was studied by adding various concentrations of the different ions to a solution containing $20 \mu\text{g mL}^{-1}$ of nitrite. The results are summarized in Table I. The tolerance limit was defined as the concentration of added ion causing a relative error less than 3 %. The results indicate that most of common anions and cations did not interfere in the determination of nitrite by the proposed method.

TABLE I. Interference of various ions in the determination of $20 \mu\text{g mL}^{-1}$ of nitrite

Ions	Tolerance ratio
K^+ , Ca^{2+} , Na^+ , Cl^- , Cd^{2+} , Mg^{2+} , NH_4^+ , IO_3^- , NO_3^- , PO_4^{3-} , Cr^{3+} , Mn^{2+}	1000
Cu^{2+} , Ni^{2+} , Zn^{2+} , Co^{2+} , Li^+ , Sn^{2+} , CH_3COO^- , Pb^{2+} , F^-	500

Calibration graph and precision

A calibration graph was obtained by plotting ΔA vs. the nitrite concentration using the developed method under the optimal conditions. From the results of the experiments, 5 min was chosen as the optimal time because it provided the best correlation coefficient and sensitivity. The calibration graph was linear in the range of $2.0\text{--}45 \mu\text{g mL}^{-1}$ of nitrite ions. The equation of the line was $y = 0.0046 + 0.014c$, where y is ΔA , and c is the concentration of nitrite in $\mu\text{g mL}^{-1}$, with a correlation coefficient $r = 0.997$. The correlation coefficient indicates a good

linear correlation between ΔA and the concentration of nitrite. Each point in the calibration graph was the average of five replicates. The experimental limit of detection ($3S_b/m$, three times the blank standard deviation divided by the slope of the equation) was $0.70 \mu\text{g mL}^{-1}$ and LOQ of the proposed method was $2.5 \mu\text{g mL}^{-1}$. The relative standard deviation for 5 replicate determinations of 15 and $35 \mu\text{g mL}^{-1}$ of nitrite were 3.1 and 1.75 %, respectively.

Analytical applications

The proposed method was applied for the determination of nitrites in some natural waters. The samples were collected from the city of Semnan, Iran, and its surroundings. The river water sample was sampled at the Heshmat River (North of Iran) and the tap water sample was obtained from local pipes. All samples were filtered through a $0.45 \mu\text{m}$ filter (glass fiber) to remove the suspended solids and then stored in clean polyethylene bottles. When water samples spiked with nitrite standards of different concentrations were treated by the proposed method, the recoveries were all in the range of 97–99 %, with a RSD of 1.0–4.0 %. The characteristics of the tap water samples are given in Table II. The determination results and recoveries are listed in Table III. They show good accuracy in comparison to the standard method.²²

TABLE II. Some parameters of the tap water sample

pH	7.6
Turbidity (NTU)	0.3
Conductivity, S cm^{-1}	670
Total dissolved solid, mg/L	374
Alkalinity, mg/L	140

TABLE III. Determination of nitrite in various samples

Sample	Nitrite added $\mu\text{g mL}^{-1}$	Proposed method ^a $\mu\text{g mL}^{-1}$	Standard method ²⁴ $\mu\text{g mL}^{-1}$	Recovery %
Tap water	–	Trace (< 2)	Trace (< 2)	–
	12.0	11.8	11.9	98.3
Waste water ^b	–	2.54	2.63	–
	10.0	12.31	12.46	97.5
	20.0	22.43	22.50	99.5
River water	–	Trace (< 2)	Trace (< 2)	–
	10.0	9.86	9.90	98.6
	20.0	19.8	19.9	99.0

^aMean of four determinations; ^bSemnan University wastewater

CONCLUSIONS

Nitrite, formed during the biodegradation of nitrate and ammoniacal nitrogen or nitrogenous organic matter, is an important indicator of fecal pollution of natural water. The determination of nitrite is of general importance because of its

harmful impact on human health. In comparison with the high cost techniques for nitrite determination, the present paper describes a low-cost, very simple, selective and highly sensitive method for the determination up to 2.0–45 $\mu\text{g mL}^{-1}$ of nitrite with a detection limit of 0.70 $\mu\text{g mL}^{-1}$. In addition, the new proposed method involves neither solvent extraction²³ nor requires any separation or pre-concentration steps, nor critical control of pH²⁴ or temperature²⁵ nor employs sophisticated instruments²⁶ and can be directly applied for the determination of nitrite in tap, natural and industrial waste water samples. In practice, the system showed high tolerance to interference from matrix elements. The results presented in this paper clearly demonstrate that the proposed method is sensitive, simple and selective and that it can also be conveniently applied for the analysis of different water samples.

Acknowledgements. The authors are thankful to the Semnan University Research Council for the support of this work.

ИЗВОД

СПЕКТРОФОТОМЕТРИЈСКО ОДРЕЂИВАЊЕ НИТРИТА ЗАСНОВАНО НА ЊЕГОВОМ КАТАЛИТИЧКОМ ЕФЕКТУ НА РЕАКЦИЈУ ИЗМЕЂУ НУКЛЕАРНО БРЗО ЦРВЕНОГ И НАТРИЈУМ-БРОМАТА

HASSAN ZAVVAR MOUSAVI¹ и HAMID SHIRKHANLOO²¹Chemistry Department, College of Sciences, Semnan University, Semnan и ²Research Institute of Petroleum Industry, Medical Industrial Laboratory, Tehran, Iran

Развијена је високоселективна и осетљива каталитичка спектрофотометријска метода за одређивање нитрита у узорцима воде. Метода је заснована на каталитичком ефекту нитрита на нуклеарно брзо црвено–натријум-бромат редокс реакцији у киселој средини. Реакција је праћена спектрофотометријски, мерењем промене апсорбанције нуклеарно брзо црвеног на 418 nm, 5 min након почетка реакције. Испитивањем су оптимизовани експериментални параметри и утврђен ефекат других катјона и анјона на одређивање нитрита. Калибрациони график је линеаран у области концентрације нитрита 2,0–45 $\mu\text{g mL}^{-1}$. Релативно стандардно одступање за одређивање 15 и 30 $\mu\text{g mL}^{-1}$ нитрата износило је 3,1 и 1,75 %, редом ($n = 8$). Граница детекције израчуната из троструког стандардног одступања слепе пробе, $3S_b$, износила је 0,70 $\mu\text{g mL}^{-1}$. Метода је успешно примењена за одређивање нитрита у узорцима бунарске, природне и отпадне воде.

(Примљено 16. јануара, ревидирано 24. априла 2009)

REFERENCES

1. M. Masuda, H. F. Mower, B. Pignatelli, I. Celan, M. D. Friesen, H. Nishino, H. Ohshima, *Chem. Res. Toxicol.* **13** (2000) 301
2. J. G. Henery, G. W. Heinke, *Environmental Science and Engineering*, 2nd ed., Prentice Hall, New Jersey, 1996
3. R. D. Cox, C. W. Frank, *J. Anal. Toxicol.* **6** (1982) 148
4. J. Davis, K. J. McKeegan, M. F. Cardosi, D. H. Vaughan, *Talanta* **50** (1999) 103
5. J. L. Manzoori, M. H. Sorouraddin, A. M. Haji-Shabani, *Talanta* **46** (1988) 1379

6. M. A. Koupparis, K. M. Walczak, H. V. Malmstadt, *Analyst* **107** (1982) 1309
7. B. Liang, M. Iwatsuki, T. Fukasawa, *Analyst* **119** (1994) 2113
8. S. B. Butt, M. Riaz, M. Z. Iqbal, *Talanta* **55** (2001) 789
9. D. C. Siu, A. Henshall, *J. Chromatogr. A* **604** (1998) 157
10. J. Z. Li, X. C. Wu, R. Yuan, H. G. Lin, R. Q. Yu, *Analyst* **119** (1994) 1363
11. U. Schaller, E. Bakker, U. E. Spichiger, E. Pretsch, *Talanta* **41** (1994) 1001
12. M. Bertotti, D. Pletcher, *Anal. Chim. Acta* **337** (1997) 49
13. M. I. N. Ximenes, S. Rath, F. G. R. Reyes, *Talanta* **51** (2000) 49
14. N. O. Ztekin, M. S. Nutku, F. B. Erim, *Food Chem.* **76** (2002) 103
15. T. Kawakami, S. Igrashi, *Anal. Chim. Acta* **333** (1996) 175
16. R. Andradea, C. O. Viana, S. G. Guadagnin, F. G. R. Reyesb, S. Ratha, *Food Chem.* **80** (2003) 597
17. M. Mir, W. Frenzel, V. Cerda, J. M. Estela, *Anal. Chim. Acta* **437** (2001) 55
18. S. Motomizu, S. C. Rui, M. Oshima, K. Toei, *Analyst* **112** (1987) 1261
19. H. A. Mottola, D. Perez-Bendito, *Anal. Chem.* **68** (1996) 257
20. M. Shamsipur, M. F. Mousavi, *Iranian J. Chem. Chem. Eng.* **14** (1995) 1
21. X. Zheng, M. Yang, Z. Zhang, *Acta Chim. Sin.* **59** (2001) 945
22. *Official Method of Analysis of the Association of Official Analytical Chemists*, 15th ed., K. Helrich, Ed., Association of Official Analytical Chemists, Arlington, VA, 1990
23. A. Afkhami, T. Madrakian, A. Maleki, *Anal Biochem.* **347** (2005) 162
24. A. Chaube, A. K. Baveja, V. K. Gupta, A. K. Baveja, V. K. Gupta, *Talanta* **31** (1984) 391
25. Q.-F. Wu, P.-F. Liu, *Talanta* **30** (1983) 374
26. A. Kazem Zadeh, A. A. Ensafi, *Microchem. J.* **69** (2001) 159.



J. Serb. Chem. Soc. 74 (8–9) 993–1007 (2009)
JSCS–3894

Alkali-catalyzed production of biodiesel from waste frying oils

ZLATICA J. PREDOJEVIĆ* and BILJANA D. ŠKRBIĆ

Faculty of Technology, University of Novi Sad, Bulevar cara Lazara 1, 21000 Novi Sad, Serbia

(Received 18 February, revised 8 April 2009)

Abstract: The effects of the transesterification parameters on the yield and quality of the methyl esters (MEs) produced from waste frying oil (WFO) were investigated. A two-step alkali transesterification reaction followed by silica gel purification step was applied. The investigated reaction parameters were the methanol/oil molar ratio (6:1 and 9:1), the catalyst/oil weight ratio (1.0 and 1.5 mass %) and the type of catalyst (NaOH and KOH). The physical and chemical properties of the employed feedstock and the obtained biodiesel were determined in order to investigate the effects of both the properties of the WFO and the reaction parameters on the characteristics and yields of the product. It was found that the properties of the feedstock had a determinant effect on the physical and chemical properties of the MEs, as the majority of them did not differ significantly under the studied reaction parameters. However, the reaction parameters influenced the yields of the product. Higher yields were obtained with a 1.0 than with a 1.5 mass % catalyst to oil ratio. The increasing yield with decreasing catalyst/oil ratio was more pronounced with NaOH (9.15–14.35 %) than with KOH (2.84–6.45 %). When KOH was used as the catalyst, the yields were always higher (the mean yield was 94.86 %) in comparison to those obtained with NaOH (the mean was 84.28 %). Furthermore, the efficiency of KOH in conversion of WFO to purified MEs in comparison to NaOH was even more pronounced in the case of the higher methanol/oil ratio, *i.e.*, for the 9:1 methanol/oil ratio, the yield increase with KOH was about 2 times higher than the yield with NaOH, regardless of the applied catalyst/oil ratio.

Keywords: biodiesel; waste frying oil; alkaline two-step transesterification.

INTRODUCTION

Biodiesel is a non-petroleum-based fuel used in diesel engines and heating systems; hence, this fuel could be regarded as a mineral diesel substitute with the advantage of reducing greenhouse emissions because it is a renewable resource.¹ Sharmer *et al.*² estimated that CO₂ production could be reduced by 3.2 kg by using 1 kg of pure biodiesel instead of the same amount of fossil fuel. Although

* Corresponding author. E-mail: pzlatica@uns.ns.ac.yu
doi: 10.2298/JSC0909993P

the amount of biofuels produced in the EU is growing, the quantities remain small compared to the total volume of mineral-based transport fuels. There are few obstacles that have hindered the wider use of biodiesel. The most important of which is that the selling price of biofuels is higher than that of mineral oil fuels. The biodiesel produced from vegetable oil or animal fat is usually more expensive than petroleum-based diesel fuel by 10 to 50 %.³ Compared to neat vegetable oils, waste frying oils (WFOs) are lower cost feedstocks, making biodiesel production more competitive to that of petroleum-based diesel fuel. In addition, as WFOs are regularly poured down the drain, resulting in problems for wastewater treatment plants and energy loss, or integrated into the food chain as animal fodder, causing human health problems, the use of waste frying oils in biodiesel production offers a solution to the growing global problem of increased oil waste from households and industrial sources.

Biodiesel is a product of transesterification of triglycerides (the main constituents of vegetable oils or animal fats) with a short chain alcohol (primarily, methanol) in the presence of a suitable catalyst; chemically, it represents a mixture of fatty acid alkyl (primarily methyl) esters. Alkali catalysts, such as sodium or potassium hydroxide, and sodium or potassium methoxide, are most commonly employed in the transesterification. These catalysts are also preferred due to the resulting high yields. The methylate salts are more reactive than the corresponding hydroxides, but are expensive, cause the formation of various by-products and require high quality oils and water-free methanol.¹ Contrary to the numerous references concerning base catalyzed one step transesterification reactions, only a limited number were found for two-step base catalyzed transesterification reactions: two studies were based on experiments with refined oils,^{4,5} while waste cooking oil was used in another two.^{6,7} In a two-stage alkali transesterification process, the majority of mono-, di-, and triglycerides are removed in the first stage and those remaining in the second stage, resulting in a more purified product. Cayh and Kusefoglul⁶ concluded that two-step transesterification of used cooking oil had superiority over a one step method, especially in terms of the high yields obtained. They suggested that the removal of glycerol at the end of the first step may be one of the main reasons why the equilibrium is shifted to the products.

The purpose of this study was to characterize biodiesels (methyl esters) produced from WFO by two-step alkali transesterification with varying parameters in order to examine the influence of the feedstock properties and the reaction conditions on the yield and properties of the obtained product. The varied reaction parameters were the ratio of methanol to oil, the type of catalyst and its amount relative to the amount of feedstock.

EXPERIMENTAL

Materials and methods

Waste frying sunflower oils were collected from local restaurants and were used as feedstocks. Prior to transesterification, the WFO samples were dried over calcium chloride (CaCl_2) and filtered through a cellulose filter to remove any suspended matter and CaCl_2 crystals. Chromatographic grade methanol (99.5 %), phosphoric acid, potassium hydroxide, sodium hydroxide, anhydrous sodium sulfate and calcium chloride were supplied by Lachema (Neratovice, Czech Republic), silica gel from Fluka (Buchs, Switzerland), while the reference standard for the gas chromatographic determination of fatty acid methyl esters was obtained from Supelco (Bellefonte, USA).

Transesterification procedure

Methyl esters (biodiesel) were synthesized in a batch type reactor using alkali catalysts. The ester preparation involved a two-step transesterification followed by purification and drying. The amount of WFO used in the reaction was 200 g, which was placed in a dry two-necked flask equipped with a thermometer and a reflux condenser. Dryness was absolutely necessary as water in the reactor would consume some of the catalyst, thereby slowing the reaction. The methanol and catalyst were added into the flask in the quantities to obtain the desired ratios relative to the oil. Namely, the study was realized using a mole ratio of methanol to WFO of 6:1 and of 9:1, whereas the catalyst (either NaOH or KOH) was added in quantities equivalent to 1 and 1.5 mass % of WFO. In the first step, the mixture was stirred for 30 min at 30 °C and 400 rpm, and then it was poured into a separation funnel. After one hour separation, glycerol was removed from the bottom of the flask, while the top esters layer was transferred into second two-necked flask, heated to 60 °C and mixed with a second methanol/catalyst solution. After stirring the mixture for 30 min at 400 rpm, it was poured into a separation funnel and allowed to separate for 12 h. The glycerol was removed by gravity settling and the methanol was removed from the thus-obtained crude esters layer by rotary evaporation at 65 °C and 20 kPa. The obtained crude methyl esters were weighed and further purified by passing them through a bed of silica gel with a top layer of anhydrous sodium sulfate in order to remove the remaining salts and glycerol, as it was shown previously that high yields could be obtained in this manner from acidic feedstocks, such as WFOs.⁷ The obtained dried methyl esters were then bottled and kept for characterization studies.

Characterization of feedstocks and methyl esters

The feedstock WFO was characterized after drying and filtering (*i.e.*, prior to transesterification) in a series of tests. Furthermore, the physical and chemical properties of the methyl esters (ME) obtained by two-step alkali transesterification after purification on silica gel were determined by the methods listed in the JUS EN 14214:2004 standard.⁸ This standard is equivalent to EN 14214: 2004 and defines the requirements and test methods for fatty acid methyl esters (FAME) to be used in diesel engines. The procedures employed for characterization are summarized in Table I. Even though it is not required by JUS EN 14214:2004, the saponification value (S_v) was also determined using the titration method described in ISO 3657:2002. The iodine value (I_v) and S_v were also calculated based on the fatty acid (methyl ester) composition determined by gas chromatography and using the equations (given in Table I) proposed by Kalayasiri *et al.*⁹ In this way, an attempt was made to see if the calculated values could predict satisfactorily these two properties and be alternatively employed instead of the corresponding experimental procedures for their determination. A method for an estimation of the cetane index (CI) based on S_v and I_v was previously described,¹⁰ as a simpler

and more convenient method than the experimental procedure, for the determination of the cetane number utilizing a cetane engine (EN ISO 5165:1998). In this work, the experimentally obtained values of S_v and I_v were used for calculating CI . However, the proposed equation for CI is not recommended for feedstock characterization as it has been previously documented that the cetane indexes of oils are generally much lower than those of methyl ester derivatives, despite the fact that they have similar S_v and I_v values.¹⁰ Thus, the CI of the WFO will not be discussed.

TABLE I. Methods used to characterize the feedstocks and the methyl esters

Property	Method
Density at 15 °C ^a , $\rho / \text{kg m}^{-3}$	JUS EN ISO 3675:2005 Crude petroleum and liquid petroleum products – laboratory determination of density – hydrometer method
Kinematic viscosity at 40 °C ^a , $\nu / \text{mm}^2 \text{ s}^{-1}$	JUS ISO 3104:2003 Petroleum products – transparent and opaque liquids – determination of kinematic viscosity and calculation of dynamic viscosity
Acid value (A_v) ^a , mg KOH/g oil	EN 14104:2003 Fatty and oil derivatives – fatty acid methyl esters – determination of the acid value
Iodine value (I_v) ^a , g J ₂ /100 g (experimental)	EN 14111: 2003 Fatty and oil derivatives – fatty acid methyl esters – determination of the iodine value
Iodine value (I_v), g J ₂ /100 g (calculated)	Azam <i>et al.</i> : ⁹ $I_v = \Sigma(254DA_i)/MW_i^b$
Cold filter plugging point (CFPP) ^a	EN 116: 1981 Determination of the cold filter plugging point of diesel and domestic heating fuels
Saponification value (S_v), mg KOH/g oil (experimental)	ISO 3657: 2002 Animal and vegetable fats and oils – determination of the saponification value
Saponification value (S_v), mg KOH/g oil (calculated)	Azam <i>et al.</i> : ⁹ $S_v = \Sigma(560A_i)/MW_i^b$
Cetane index (CI)	Krisnangkura Equation: ¹⁰ $CI = 46.3 + 5458/S_v - 0.225I_v$
Fatty acid methyl ester composition, mass %	Capillary gas chromatography (GC) with flame ionization detection
Mean molecular mass of WFOs, kg mol^{-1}	Calculated according to the fatty acid profile obtained by GC

^aProperties and respective test methods required for characterization of methyl esters to be used as fuel in diesel engine by SRPS EN 14214 standard; ^b A_i is in %, D is the number of double bonds and MW_i is the molecular mass of each component

The methyl ester composition was obtained using a gas chromatograph equipped with a DB-WAX 52 column (Supelco) and a flame ionization detector.

All the properties were determined in two replicates and the final results are given as average values.

RESULTS AND DISCUSSION

Feedstock properties

The physical and chemical properties of the waste frying oil, WFO, used as the feedstock for the two-step alkali transesterification are given in Table II. The WFO had an acid value higher than 2.0 mg KOH/g (Table II), which has often been recommended as the limit acid value for an efficient transesterification.¹¹ Namely, the base catalyzed reaction was reported to be very sensitive to the content of free fatty acids, which should not exceed the recommended limit to avoid deactivation of the catalyst, and the formation of soaps and emulsion.^{11,12–14} An elevated content of free fatty acids, expressed as the acid value, is not surprising for waste frying oils, as it is known that during the frying process under high temperatures in the presence of air and moisture, a variety of degradation reactions can occur, leading eventually to changes in the properties of the oil, including an increase in the viscosity and in the content of free fatty acids.¹⁵

TABLE II. The characteristics of waste frying oil used as the feedstock

Characterization test	Waste frying oil from restaurant (WFOR)	
Density, ρ , at 15 °C, g/cm ³	0.933	
Kinematic viscosity, ν , at 40 °C, mm ² /s	44.85	
Acid value, mg KOH/g oil	2.58	
Saponification value, S_v , mg KOH/g oil	Experimental	Calculated
	197	198
Iodine value, g J ₂ /100 g oil	Experimental	Calculated
	119	124
Fatty acid composition, mass %		
C12:0	–	
C14:0	0.25	
C16:0	9.44	
C16:1	1.02	
C18:0	5.71	
C18:1	28.19	
C18:2	53.50	
C18:3	0.34	
C20:0	0.44	
Total unsaturated	83.05	
Total saturated	15.84	

Considering the fatty acid composition of the WFO used in this study, it consisted mainly of methyl esters of linoleic (C18:2) > oleic (C18:1) > palmitic (C16:0) > stearic (C18:0) acids. The contents of the other evidenced acids were about 1 mass % or less. Such a composition reflects the sunflower origin of the WFO. The iodine value of the feedstock, which is a measure of the degree of unsaturation, was approximately 120 mg I₂/100 g. The calculated iodine values were about 4 % higher than the experimentally determined ones. The iodine value of

the WFO was lower than the values (120 and 140 mg I₂/100 g) reported for frying sunflower oils used in Portugal.¹ However, the used oils have a variety of qualities as a consequence of the different frying conditions and the periods of use. Comparing sunflower oils with other vegetable oils, it is well known that, typically, the former have higher iodine values because of their higher levels of unsaturated fatty acids, primarily linoleic acid (two double bonds), than other vegetable oils.⁵ Considering the saponification value, good agreement between the experimental and calculated values was obtained.

Influence of the transesterification parameters on methyl ester yields

The product yield considering either crude or purified esters is defined as the mass percentage of the final product relative to the initial mass of WFO introduced into the transesterification. The yields of methyl esters (MEs) obtained by two-step alkali transesterification of the WFO under varying reaction conditions are given in Table III. The obtained yields coincide with the previous findings of Predojević⁷ that a two-step alkali transesterification with a silica gel purification treatment could be recommended for obtaining high biodiesel yields from waste frying oils, despite the elevated acid values. Namely, it is known that the more acidic the feedstock is, the lower yield that could be obtained by base transesterification because of the more pronounced deactivation of the catalyst and soap formation by the free fatty acids in the feedstock.¹ It was previously reported⁷ that a two-step transesterification procedure, also applied in this study, could be satisfactorily employed for biodiesel production from waste frying oils with acid values up to ≈ 2.5 mg KOH/g, without a significant decrease in the MEs yields.

TABLE III. Comparison of methyl esters (MEs) yields (%) obtained with varying reaction parameters during the employed two-step alkali transesterification

Catalyst	Catalyst amount mass %	Methanol/oil mole ration			
		6:1		9:1	
		Crude MEs	Purified MEs	Crude MEs	Purified MEs
NaOH	1.0	92.95	86.81	96.04	79.53
	1.5	82.85	79.53	86.98	69.55
KOH	1.0	97.33	96.17	98.15	95.84
	1.5	92.94	90.34	95.44	92.66

In order to compare the yields obtained under different reaction conditions, the relative yields are shown in Figs. 1 and 2. It can be seen that the yields were always higher with the lower quantity of catalyst, *i.e.*, higher yields were obtained with 1.0 mass % than with 1.5 mass % catalyst to oil (Table III; Fig. 1). The yield increase with decreasing catalyst/oil ration was more pronounced for NaOH (9.15–14.35 %) than for KOH (2.84–6.45 %, Fig. 1). In other words, the mass ratios of KOH studied here had a similar influence on the methyl ester conversion, whereas the higher ratio of NaOH (*i.e.*, 1.5 mass % of oil) suppressed

the conversion in comparison to the lower ratio (*i.e.*, 1.0 mass %). Furthermore, the bar diagram shown in Fig. 2 shows that yields were always higher when KOH was used as the catalyst (the mean yield was 94.86 %) in comparison to the yields obtained with NaOH (the mean yield was 84.28 %), which coincides with the findings of other authors.^{1,16,17} Sharma *et al.*¹¹ reported a better yield with NaOH as the catalyst than with KOH when a magnetic stirrer was used, while when a mechanical stirrer was employed, the yield was same with an equal amount of NaOH and KOH (0.50 mass %). These authors also observed that during the separation of the final products from glycerol, KOH was more convenient. Potassium soaps, being softer than sodium soaps, did not block the bottom of separation funnel, unlike the later, and were easily removed. Hence, KOH as the catalyst is preferred over NaOH on the industrial level of application.¹¹

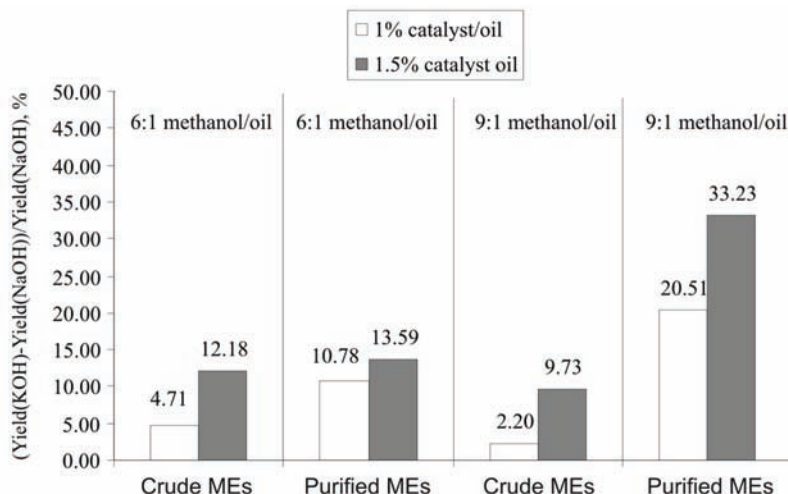


Fig. 1. Comparison of methyl esters yields obtained with different transesterification parameters: the percentage increase of the yield with 1.0 mass % of catalyst to oil relative to the yield with 1.5 mass %.

It can be also seen that the efficiency of KOH the in conversion of the WFO to purified MEs in comparison to NaOH was even more pronounced in the case of the higher methanol/oil ratio, *i.e.*, for the 9:1 methanol/oil ratio, the yield increase with KOH was about 2 times higher than the yield with NaOH, regardless of the catalyst/oil ratio applied (Fig. 2). The methanol/WFO ratio is one of the most important variables because of its influence on the separation of the methyl esters from the glycerol layer and, consequently, on the yield of biodiesel. Stoichiometrically, three moles of alcohol are required for each mole of triglyceride but, in general, a higher molar ratio is often employed for maximum ester production, depending on the type of feedstock, amount of catalyst, temperature,

*etc.*¹¹ The presence of a sufficient amount of methanol during the transesterification reaction is essential to break the glycerin-fatty acid linkages.¹¹ However, a large excess of alcohol should be avoided as it aggravates the separation of glycerol by increasing its solubility in alcohol, causing the reaction equilibrium to be shifted in the direction that favors the product decomposition reaction, with a consequential decrease in the yield of methyl esters. Leung and Guo¹⁸ suggested that the hydroxyl group of methanol can act as an emulsifier and cause emulsification, making the separation of the ester layer from the aqueous layer difficult. Hence, it could be concluded that the KOH-catalyzed two-step transesterification was less sensitive to the excess of alcohol than the reaction with NaOH, further indication that KOH is more appropriate for practical employment.

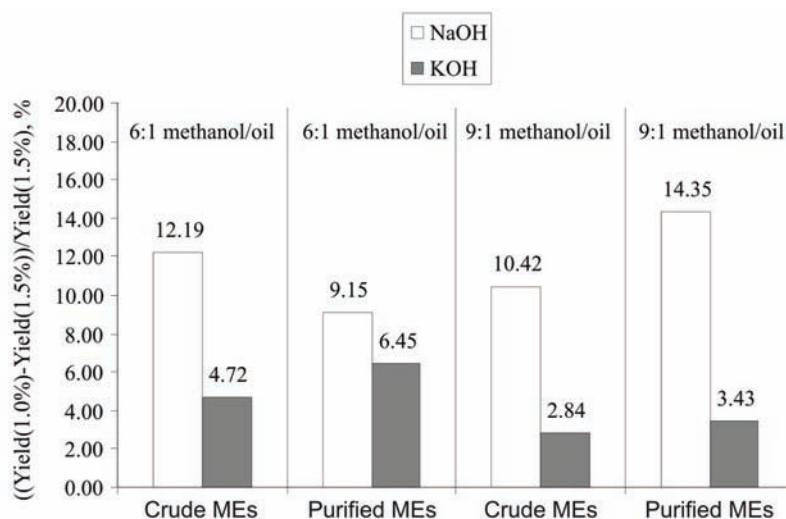


Fig. 2. Comparison of methyl esters yields obtained with different transesterification parameters: the percentage increase of the yield with KOH relative to the yield with NaOH.

Properties of the methyl ester

The physical and chemical properties of the methyl esters obtained by two-step alkali transesterification of the WFO after applying different experimental conditions are shown in Table IV. The properties are compared with the quality of biodiesel required for use in diesel engine in accordance to the JUS EN 14214 standard.⁸ In general, very little differences could be observed in the properties of the methyl esters obtained by application of different reaction parameters.

The overall relative standard deviation (RSD_{overall}) as a measure of the dispersion of the results was used to detect if there were major differences in the studied properties. RSD_{overall} was calculated by dividing the standard deviation of all values obtained for a particular property, regardless of the reaction con-

ditions applied, with their mean value and then multiplied with 100 to obtain percentage. Considering that the RSD_{overall} for density, saponification value (experimental), iodine value (experimental), cetane index and the content of total unsaturated acids were estimated to be 0.37, 0.66, 0.67, 0.82 and 0.68 %, respectively, it could be concluded that the reaction parameters examined in this study did not significantly influence these properties of the produced methyl esters. The RSD_{overall} for the kinematic viscosities and the total saturated fatty acid content were slightly elevated (2.18 and 3.09 %, respectively), while it was significantly higher (14.67 %) for the acid value, suggesting that the later was influenced by the reaction parameters investigated here.

TABLE IV. The characteristics of the methyl esters obtained with different reaction parameters during the employed two-step alkali transesterification of waste frying oils

Property	MeOH/oil mole ratio							
	6:1		9:1		6:1		9:1	
	Catalyst amount, mass %							
	NaOH				KOH			
	1	1.5	1	1.5	1	1.5	1	1.5
ρ , 15 °C, g/cm ³	0.891	0.889	0.890	0.889	0.893	0.891	0.892	0.898
ν , 40 °C, mm ² /s	4.75	4.56	4.63	4.59	4.77	4.70	4.81	4.75
Av , mg KOH/g	0.38	0.39	0.39	0.27	0.39	0.36	0.43	0.41
Iv , gJ ₂ /100g (Experimental)	119	119	118	118	119	120	119	118
Iv , gJ ₂ /100g (Calculated)	119	118	117	117	119	119	119	118
PP , °C	±0	±0	±0	±0	+1	±0	±0	+1
$CFPP$, °C	-1	±0	-3	-4	-2	-2	-4	-5
Sv , mg KOH/g (Experimental)	193	193	193	191	191	192	192	190
Sv , mg KOH/g (Calculated)	192	192	192	191	192	191	191	190
CI	47.7	47.9	48.1	48.4	48.1	47.8	47.9	48.8
	Fatty acid composition, mass %							
C12:0	0.10	0.05	-	-	0.29	-	-	-
C14:0	0.33	0.29	0.37	0.62	0.35	0.29	0.29	0.66
C16:0	9.61	9.95	10.60	10.17	9.61	9.59	9.55	9.53
C16:1	1.16	1.09	1.14	1.05	1.10	1.17	1.16	1.03
C18:0	6.29	6.30	6.23	6.44	5.87	5.77	5.87	5.79
C18:1	28.26	28.74	28.44	28.34	28.32	28.33	28.22	28.32
C18:2	53.94	53.13	53.22	52.86	53.66	54.23	54.18	53.75
C18:3	0.19	0.31	-	0.41	0.29	0.20	0.32	0.37
C20:0	0.12	0.14	-	0.11	0.50	0.42	0.42	0.55
Total unsaturated	83.55	83.27	82.8	82.66	83.37	83.93	83.87	83.47
Total saturated	16.45	16.73	17.2	17.34	16.63	16.07	16.13	16.53

Density at 15 °C. This property is important mainly in airless combustion systems because it influences the efficiency of atomization of the fuel.¹ The results obtained (Table IV) showed that all the methyl ester produced in this study had a density in the range 0.86–0.90 g/cm³, specified according to the standard JUS EN 14214.⁸ The mean value (\pm standard deviation) of the densities calculated for the MEs obtained with NaOH was 0.890 \pm 0.001 g/cm³, while the MEs produced with KOH had slightly higher densities with a mean value 0.893 \pm 0.003 g/cm³.

Kinematic viscosity at 40 °C. Even more than the density, the kinematic viscosity at 40 °C is an important property regarding fuel atomization and distribution. The higher is the viscosity, the greater is the tendency of the fuel to form engine deposits. The viscosities of the MEs (Table IV) were much lower than that of the feedstock oil (about 10 times) and they met the required values that must be between 3.5–5.0 mm²/s.⁸ As in the case of the densities, the values of kinematic viscosities were slightly higher for the MEs obtained with KOH (4.76 \pm 0.05 mm²/s) than those obtained with NaOH (4.63 \pm 0.08 mm²/s). It is known that viscosity increases with chain length and with increasing degree of saturation (*i.e.*, with decreasing degree of unsaturation).¹⁹ However, this could not be observed in this study, as the differences in the iodine value, as a measure of the unsaturation, were negligible (the RSD_{overall} was 0.67 %). Additionally, it was observed that when the methanol/WFO or the catalyst/WFO ratios were increased, the viscosity of the methyl esters decreased (see Table IV).

Acid value. The acid value is defined as the milligrams of potassium hydroxide required to neutralize the free acids in 1 g of sample. The acid values of the MEs varied from low 0.266 to 0.429 mg KOH/g and they were less than the 0.5 mg KOH/g specified as the maximum value according to JUS EN 14214.⁸ As was previously mentioned, the greatest dispersion of the results was obtained for this property of the MEs produced under varying conditions (the RSD_{overall} was 14.67 %). Again, the mean acid value of the MEs obtained with NaOH (0.354 \pm 0.060 mg KOH/g) was lower than the mean of that obtained by transesterification with KOH (0.400 \pm 0.029 mg KOH/g). However, the greatest differences in the acid values were only observed for the higher methanol/oil ratio (9:1), whereas in the case of the lower ratio (6:1), acid values were almost the same regardless of the catalyst type or the catalyst/oil ratio.

Iodine value. The iodine value is an important measure for the determination of the unsaturation in fatty acids, which is only dependent on the vegetable oil. This property greatly influences fuel oxidation and the deposits formed in the injector of diesel engines.¹ With increasing iodine value of unsaturated fatty acids, the effect of polymerization is stronger. According to JUS EN 14214,⁸ MEs used as diesel fuel must have an iodine value of less than 120 g I₂ per 100 g of sample. The MEs obtained in this study had an iodine value in the very narrow range of 118–120 g I₂/100 g. The mean iodine value of the MEs produced using NaOH

was 118 ± 1 g I₂/100 g and of those using KOH was 119 ± 1 g I₂/100 g. The calculated iodine values were in a very good agreement with those experimentally obtained.

Saponification value. The saponification value represents the milligrams of potassium hydroxide required to saponify one gram of fat or oil. The saponification value is not a property of biodiesel restricted according to EU or Serbian standards, which is the reason why it was not regularly determined in the relevant literature studies.

The difference in the saponification values of the MEs produced in this study was negligible, with a mean value for the MEs obtained using NaOH of 192 ± 1 mg NaOH/g, and for those using KOH of 191 ± 1 mg KOH/g. There was no significant difference in the calculated and experimental saponification values. The values were only slightly lower than that of the WFO (197 mg KOH/g). It is generally expected that an oil and the corresponding MEs have the same saponification value, as it is known that a triglyceride has 3 associated fatty acid chains and that each triglyceride will give three methyl esters; hence, stoichiometrically, it is to be expected that the same amount of fatty acid carbon chain in the neat feedstock oil and the biodiesel will react with the same amount of KOH giving soaps. However, is this assumption applicable to waste frying oils knowing that their properties differ significantly from the neat oils as a consequence of polymerization and degradation of the triglycerides that occur during frying.¹⁵

Cold flow properties. Compared with fossil diesel fuel, one of the major problems with the employment of biodiesel is its poor low temperature properties, such as cloud point (*CP*), pour point (*PP*) and cold filter plugging point (*CFPP*). The *CP* is the temperature at which a liquid is cloudy due to formation of crystals of size up to 1 mm, which make the suspension cloudy or hazy.²⁰ The *PP* is the lowest temperature at which a material will still flow due to crystal agglomeration. The *PP* is useful for characterizing the suitability of a fuel for large storage and pipeline distribution.^{20,21} The *CFPP* is defined as the lowest temperature at which 20 ml of oil safely passes through a filter within 60 s. The cold flow properties of methyl esters such as the *PP* and *CFPP* depend on the structure of the fatty acids. In general, biodiesel made from feedstocks containing higher concentration of high melting point saturated long-chain fatty acids have relatively poor cold flow properties.^{19,22} It was previously found that the difference between the *CP* and *PP* of methyl esters is relatively small²⁰ so that the filterability test, *i.e.*, *CFPP*, could better a better indication of engine performance during low temperature operation.

The experimentally determined values of the *CFPP* and *PP* for the methyl esters samples were in the range from -5 – 0 °C and around 0 °C, respectively (Table IV), implying that the obtained biodiesels could be suitable for use in summer time. The low temperature properties of a biodiesel depend on the quality and

composition of the raw material, but they can be improved by blending with diesel fuel D2 or with polymer additives.¹⁹

Cetane index. This property could be regarded as an indicator of the cetane number, which is a property that reflects the ignition quality of biodiesel. The cetane number is related to the time that passes between injection of the fuel into the cylinder and the onset of ignition. It is known that the exhaust emission of nitrogen oxides (NO_x) is lower with increasing time. The reduction of NO_x exhaust emissions is an important problem facing biodiesel as it is known that it is slightly increased when using biodiesel in comparison to fossil diesel.²³ The structure of fatty esters can also influence emissions, with the NO_x emissions being lower with increasing saturation. Saturated compounds have higher cetane numbers (*i.e.*, cetane index) than unsaturated compounds. For instance, Freedman and Bagby²⁴ reported cetane numbers for methyl palmitate (C16:0) and methyl stearate (C18:0) as 74.3 and 75.6, while Klopfenstein²⁵ reported 74.5 and 86.9, respectively. Unsaturated methyl oleate (C18:1) and methyl linoleate (C18:2) have much lower cetane numbers, *i.e.*, 47.2 and 28.5, respectively.²⁶ Contrary to the determination of the cetane number that requires tedious experimental procedure, the cetane index can be obtained by simple calculation.

The mean cetane index, *CI*, obtained for the MEs produced with NaOH was 48.03 ± 0.29 and 48.15 ± 0.44 for the MEs obtained using KOH. Šiler-Marinković and Tomasević¹⁶ also used the Krisnangkura equation to calculate the *CI* for the characterization of MEs produced from crude sunflower oils and the estimated values were very similar to the values obtained in this study, ranging from 49.7 to 50.9.

Fatty acid composition. As can be observed from Table IV, the fatty acid methyl ester profiles of the produced biodiesels reflected the fatty acid composition of feedstock. A typical gas chromatogram of the obtained methyl esters is shown in Fig. 3. The biodiesels consisted mainly of methyl esters of palmitic (C16:0), stearic (C18:0), oleic (C18:1), and linoleic (C18:2) acids, which also occurred in large amounts in the feedstock. Mittelbach²⁷ proposed to limit the content of unsaturated fatty acids in biodiesel, especially unsaturated fatty acids such as linolenic acid (C18:3). The maximum content of linolenic acid in the MEs obtained in this study was less than 0.4 mass %.

CONCLUSIONS

The production of biodiesel by alkali two-step transesterification of waste frying oil (WFO) with an acid value higher than 2 mg KOH/g is feasible without any previous treatment under the conditions applied in this study. On varying the type of the catalyst (NaOH or KOH), the methanol/oil mole ratio (6:1 or 9:1) and the catalyst/oil mass ratio (1 mass % and 1.5 mass %) it was found that the investigated characteristics of the methyl esters (MEs) were not influenced significantly by the transesterification parameters. The exception was the acid va-

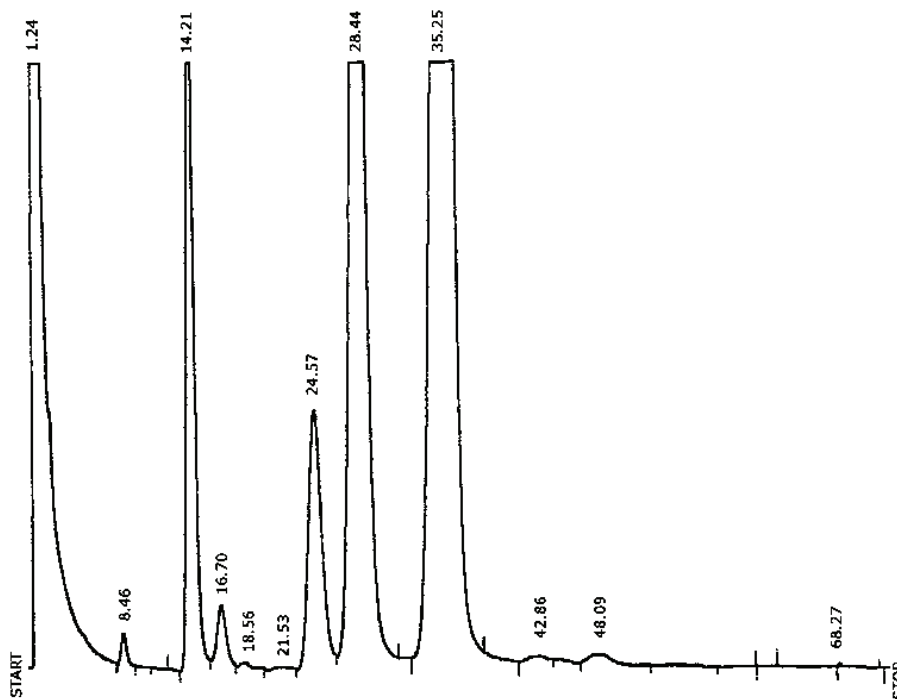


Fig. 3. Typical gas chromatogram of the investigated methyl esters obtained by transesterification of waste frying oil.

lues obtained with the higher methanol/oil ratio, but further investigations are required in order to elucidate the found deviations. Good agreement was observed between the experimental and calculated iodine and saponification values of MEs, suggesting that the results of gas chromatographic analysis of the composition of the fatty acid methyl esters could be satisfactory used for the prediction of these properties as an alternative to the experimental procedures. The reaction conditions influenced the yields of the produced biodiesel in a following way: KOH induced a more efficient conversion of WFO to MEs than NaOH; higher yields were obtained with the lower catalyst/oil ratio (1.0 mass%) than with the higher (1.5 mass %). In the case of KOH, the methanol/oil mole ratio had no marked influence on the yield of MEs.

Acknowledgement. This work was supported by the Ministry of Science and Technological Development of the Republic of Serbia project 142024.

ИЗВОД

ДОБИЈАЊЕ БИОДИЗЕЛА ИЗ ОТПАДНОГ УЉА БАЗНО-КАТАЛИЗОВАНОМ
ТРАНСЕСТЕРИФИКАЦИЈОМ

ЗЛАТИЦА Ј. ПРЕДОЈЕВИЋ И БИЉАНА Д. ШКРБИЋ

Технолошки факултет, Универзитет у Новом Саду, Булевар Цара Лазара 1, Нови Сад

Испитиван је утицај параметара трансестерификације на принос и квалитет метил естра, МЕ, добијеног из коришћеног, отпадног уља. Алкална трансестерификација је вођена у два степена, а за пречишћавање сировог метил естра коришћен је силика гел. Варијациони параметри: однос алкохол/уље (6:1 и 9:1), масени однос катализатор/уље (1 и 1,5 mass %) и тип катализатора (NaOH и KOH). Одређене су физичко-хемијске карактеристике коришћене сировине и добијеног биодизела, да би се испитао утицај и сировине и параметара реакције на карактеристике и принос продукта. Уочено је да карактеристике сировине имају одлучујући утицај на физичко-хемијске карактеристике метил естера. Већина од одређених карактеристика се значајно не разликују за испитиване параметре реакције. Међутим, реакциони параметри имају утицај на принос производа. Већи принос се добија при односу катализатор/уље 1,0 у односу на 1,5 mass %. Принос се повећава смањењем односа катализатор/уље и то изразитије за NaOH (9,15–14,35 %) у односу на KOH (2,84–6,45 %). Принос је увек већи при коришћењу KOH катализатора (средња вредност приноса је 94,86 %) у поређењу са приносом добијеним са NaOH (средња вредност приноса је 84,28 %). Штавише, ефикасност KOH у степену конверзије сировине у пречишћен МЕ је изразитија при већем односу метанол/уље, односно при односу метанол/уље 9:1, остварен принос са KOH је већи у односу на принос са NaOH, без обзира на однос катализатор/уље. Релативно повећање приноса са KOH је два пута веће у односу на NaOH.

(Примљено 18. фебруара, ревидирано 8. априла 2009)

REFERENCES

1. P. Felizardo, M. Joana Neiva Correia, L. Rapaso, J. F. Mendes, R. Berkemeier, J. M. Bordado, *Waste Management* **26** (2006) 487
2. K. Sharmar, *Umweltaspekte bei Herstellung und Verwendung von RME*, in *RME Hearing*, Ministry for Agriculture, Vienna, 1993
3. D. Y. C. Leung, Y. Guo, *Fuel Proc. Technol.* **87** (2006) 883
4. S. L. Dmytryshyn, A. K. Dalai, S. T. Chaudhari, H. K. Mishra, M. J. Reaney, *Biores. Technol.* **92** (2004) 55
5. X. Lang, A. K. Dalai, N. N. Bakhshi, J. Reahey, P. B. Hertz, *Biores. Technol.* **80** (2001) 53
6. G. Cayh, S. Kusefoglul, *Fuel Proc. Technol.* **89** (2008) 118
7. Z. Predojević, *Fuel* **87** (2008) 3522
8. JUS EN 14214:2004, *Automotive fuels. Fatty acid methyl esters (FAME) for diesel engines – requirements and test methods*, Standardization Institute, Belgrade, Serbia
9. M. M. Azam, A. Waris, N. M. Naihar, *Biomass Bioenergy* **29** (2005) 293
10. K. Krisnangkura, *J. Am. Oil Chem. Soc.* **63** (1986) 552
11. Y. C. Sharma, B. Singh, S. N. Upadhyay, *Fuel* **87** (2008) 2355
12. B. Freedman, E. H. Pryde, T. L. Mounts, *J. Am. Oil Chem. Soc.* **61** (1984) 1638
13. L. C. Meher, D. Vidya Sagar, S. N. Naik, *Renew. Sust. Energy Rev.* **10** (2004) 248
14. J. Van Gerpen, *Fuel Proc. Technol.* **86** (2005) 1097

15. J. McNeill, Y. Kakuda, B. Kamel, *J. Am. Oil Chem. Soc.* **63** (1986) 1564
16. S. S. Šiler-Marinković, V. A. Tomašević, V. Lj. Mojović, D. S. Petrović, *Hem. Ind.* **50** (1996) 303 (in Serbian)
17. G. Viecente, M. Martinez, J. Araci, *Biores. Technol.* **92** (2004) 297
18. D. Y. C. Leung, Y. Guo, *Fuel Proc. Technol.* **87** (2006) 883
19. G. Knothe, *Fuel Proc. Technol.* **86** (2005) 1059
20. R. O. Dunn, M. O. Bagby, *J. Am. Oil Chem. Soc.* **72** (1995) 895
21. Ch-W. Chiu, L. G. Schumacher, G. J. Suppes, *Biomass Bioenergy* **27** (2004) 485
22. T. A. Foglia, L. A. Nelson, R. O. Dunn, W. N. Marmer, *J. Am. Oil Chem. Soc.* **74** (1997) 951
23. N. Ladommatos, M. Parsi, A. Knowles, *Fuel* **75** (1996) 8
24. B. Freedman, M. O. Bagby, *J. Am. Oil Chem. Soc.* **67** (1990) 565
25. W. E. Klopfenstein, *J. Am. Oil Chem. Soc.* **62** (1985) 1029
26. University of New Hampshire, Biodiesel Group, www.unh.edu/p2/biodiesel (December 2008)
27. M. Mittelbach, *Bioresour. Technol* **56** (1996) 7.



J. Serb. Chem. Soc. 74 (8–9) 1009–1017 (2009)
JSCS–3895

The effects of some agrotechnical measures on the uptake of nickel by maize plants

BRANKA M. ŽARKOVIĆ and SRDJAN D. BLAGOJEVIĆ*#

Faculty of Agriculture, University of Belgrade, Nemanjina 6, 11081, Belgrade, Serbia

(Received 21 January, revised 11 March 2009)

Abstract: Nickel is a non-essential element in the nutrition of the majority of plant species and can be toxic to plants when its concentration in soils is high. Several soil properties have an effect on the uptake of this heavy metal by plants. The purpose of this investigation was to determine the effect of fertilization, soil acidification and liming on the uptake of Ni by maize plants grown on some alluvial soils. A pot experiment with maize plants grown on soils having various properties and elevated content of Ni was set up. The experiment lasted six weeks. The roots and shoots were analyzed for the concentration of Ni. From the results of the experiment, it can be concluded that the roots had higher concentrations of Ni than the shoots. The addition of mineral fertilizers (without application of other measures) mainly decreased the concentration and uptake of Ni by the roots and the transport of Ni to the shoots. Soil acidification (to pH 4.5) caused an increase in the Ni concentration in the plants and in its removal from the soil. Liming of acid soils had a positive effect on the uptake of Ni by young maize plants. The obtained results are important from the standpoint of reducing the pollution of plants by potentially toxic heavy metals.

Keywords: agrotechnical measures; Ni; uptake; concentration; maize.

INTRODUCTION

Nickel is a heavy metal that is not essential for the growth and development of the majority of plant species. Under normal conditions, plants take up small quantities of Ni from soils. However, Ni can be toxic to plants when its concentration in the soil is high. This is the case with severely polluted soils. It is well known that the main sources of Ni and other heavy metals in a soil are the substrate from which the soil was originally formed and anthropogenic pollution. Significant amounts of Ni can be introduced into soils through application of high doses of sewage sludge and certain mineral and organic fertilizers.

* Corresponding author. E-mail: sblagoje@eunet.rs

Serbian Chemical Society member.

doi: 10.2298/JSC0909009Z

The most common symptom of Ni phytotoxicity is chlorosis, which seems to be Fe-induced. In plants under Ni stress, the absorption of nutrients, root development and metabolism are strongly retarded. Before acute Ni toxicity symptoms are evident, elevated concentrations of this metal in plant tissues are known to inhibit photosynthesis and transpiration.¹ Both plant and pedological factors affect Ni uptake by plants, but the soil pH has the most pronounced influence. As Berrow and Burrige² found, increasing the soil pH from 4.5 to 6.5 decreased the Ni content in oat grain by a factor of about 8. Apart from the soil pH, soil organic matter and clay minerals have significant influence on the uptake of Ni by plants.

Agrotechnical measures can change some of the soil properties and, in this way, affect the uptake of Ni and other heavy metals by plants. Liming and addition of organic matter result in a decrease of both the available Ni and the amount taken up by plants.³ In Serbia, there have not been many studies in which this problem was addressed. Zarković and Blagojević⁴ studied the effect of some agrotechnical measures on the uptake of lead (Pb) by maize plants. They found that the application of mineral fertilizers decreased the uptake of Pb by the roots and its transport to the shoots.

The purpose of the present investigation was to determine the effect of fertilization, soil acidification and liming on the uptake of Ni by maize plants grown on some alluvial soils.

EXPERIMENTAL

A pot experiment was set up with maize (hybrid ZP 704) that was grown on alluvial soils collected from the following locations in Serbia: Salinac, Velika Plana, Lipe, Osipaonica, Mala Krsna and Kragujevac. Before the experiment was set up, the soil samples were analyzed for the following chemical properties:

- the soil pH in water and 1.0 M KCl (potentiometrically with a glass electrode);
- the humus content (the Tiurin method modified by Simakov);
- the total N content (the Kjeldahl method modified by Bremner);
- the available phosphorus and potassium (the AL-method according to Egner–Riehm);
- total Ni content (atomic absorption spectrophotometry after digestion of the samples with a mixture of nitric, perchloric and hydrofluoric acid).

All the aforementioned methods are described in detail in the *Laboratory Manual in Agrochemistry*.⁵

After determination of the pH, it was decided that the pot experiment would be performed with 4 neutral to weakly alkaline soils (pH in H₂O from 7.16 to 7.58) and 2 acid soils (pH in H₂O 5.76 and 6.36).

The following treatments were applied on the neutral and weakly alkaline soils:

1. control (without fertilizers);
2. NPKI (50 mg N/kg, 50 mg P₂O₅/kg and 50 mg K₂O/kg);
3. NPKII (100 mg N/kg, 100 mg P₂O₅/kg and 100 mg K₂O/kg);
4. NPKI (soil acidified to pH 5.5 in 1M KCl);
5. NPKI (soil acidified to pH 4.5 in 1M KCl).

The following treatments were applied on the two acid soils:

1. control (without fertilizers);
2. NPKI (50 mg N/kg, 50 mg P₂O₅/kg and 50 mg K₂O/kg);
3. NPKII (100 mg N/kg, 100 mg P₂O₅/kg and 100 mg K₂O/kg);
4. NPKI + 1/2 of the amount of CaCO₃ required for soil neutralization;
5. NPKI + the amount of CaCO₃ required for soil neutralization.

Nitrogen was added as NH₄NO₃, phosphorus as Na₂HPO₄·12H₂O and potassium in the form of KCl. All three nutrients were added as solutions of the aforementioned salts. Soil acidification (to pH 5.5 and 4.5 in 1.0 M KCl) was performed with 5.0 M H₂SO₄. Partial and full neutralization of the two acid soils was realized by means of calcium carbonate, the amount of which was calculated on the basis of the value for hydrolytic acidity.

Each experimental treatment was repeated three times. The soil moisture was maintained at 60 % of the water holding capacity during the experiment. The experiment lasted for 6 weeks. At the end of the experiment, the yield of young maize plants was measured. The roots and the aerial part of the maize plants were analyzed for the concentration of Ni by atomic absorption spectrophotometry, which was performed after digestion of the samples with nitric and perchloric acid.⁶

The obtained analytical data were subjected to statistical analysis (analysis of variance and correlation analysis). It is important to mention that the LSD test was performed only in cases where statistical significance of the corresponding *F* values was found.

RESULTS AND DISCUSSION

The results of the determination of some chemical properties of the alluvial soils are presented in Table I.

TABLE I. Some important chemical properties of alluvial soils

Soil-location	pH		Humus %	Total N %	Available		Total Ni mg/kg
	H ₂ O	nKCl			P (mg P ₂ O ₅ /100 g)	K (mg K ₂ O/100 g)	
1-Salinac	7.42	6.76	2.09	0.134	8.1	21.7	116
2-Velika Plana	7.58	6.70	2.70	0.200	5.2	36.0	148
3-Lipe	7.16	6.27	3.55	0.228	35.0	40.0	115
4-Osipaonica	7.22	6.18	3.25	0.275	17.5	21.6	144,5
5-Mala Krsna	6.36	5.28	3.37	0.216	1.4	22.5	122,5
6-Kragujevac	5.76	4.66	2.49	0.171	4.1	14.9	45

According to the pH values in water, four soils (Lipe, Osipaonica, Salinac and Velika Plana) are neutral to weakly alkaline, while the soils from Mala Krsna and Kragujevac are acid. The content of organic matter in the soils is medium. The obtained values indicate that soils 1, 2, 5 and 6 have low content of available phosphorus, while it is high in soil from Lipe. All soils are well supplied with available potassium. It can be seen from the Table I that the total Ni concentration is in the interval from 45 to 148 mg/kg. The highest value was found in the soil sample from Velika Plana. Maximum allowed Ni concentration in agricultural soils is 50 mg/kg.⁷

The concentration of Ni found in the roots is shown in Tables II and III. Statistical analysis of data (analysis of variance) indicates that the treatment as an

experimental factor had a significant influence on the concentration of Ni in the roots of young maize plants that were grown on neutral and weakly alkaline soils. Namely, the corresponding *F*-values were significant at the 0.01 probability level. The average Ni concentration in the roots ranged from 52.1 to 78.1 µg/g, while corresponding removal of Ni from the soil ranged from 37.1 to 64.1 µg/pot. The highest average value for Ni concentration in plant tissues and its removal from the soil was found with the treatment NPKI (pH 4.5), while the lowest was found with the treatment NPKII. From the results presented in Table II, it can be seen that the higher dose of mineral fertilizers (treatment NPKII) caused a significant decrease in the Ni concentration in the plant roots and its removal from the soil by the roots. It can be assumed that part of the available Ni was transformed into less soluble compounds under the influence of the applied phosphate ions. Soil acidification (to pH 5.5 and 4.5) increased the root Ni concentration and its removal from the soil. This effect was especially pronounced with treatment NPKI (pH 4.5), which can be explained by the considerably higher mobility of Ni at this pH value. It is well known from the literature⁸ that the mobility and availability of Ni is higher in acid in relation to neutral and weakly alkaline soils. Ni phytotoxicity occurs when highly contaminated soils are strongly acidic.⁹ Soil as an experimental factor also exerted a statistically significant influence on the uptake of Ni by maize roots. Comparison of the average values for the uptake of Ni from the investigated soils indicates that the highest average removal of Ni from the soil was found for soil 3 (70.2 µg/pot), while it was the lowest for soil 1 (42.3 µg/pot). There was no significant difference between soils 3 and 4 with respect to Ni removal from the soil.

TABLE II. Concentration of Ni in the roots and its removal from treated neutral and weakly alkaline soils; results of the LSD test for Ni concentration: treatment – LSD (0.05) = 13.8 and LSD (0.01) = 18.4; results of the LSD test for Ni uptake: treatment – LSD (0.05) = 16.7 and LSD (0.01) = 22.3, soil – LSD (0.05) = 13.6 and LSD (0.01) = 18.2

Treatment	Soil 1		Soil 2		Soil 3		Soil 4		Average value	
	µg/g	µg/pot	µg/g	µg/pot	µg/g	µg/pot	µg/g	µg/pot	µg/g	µg/pot
Control	47.5	31.1	50.5	27.3	75.5	85.2	78	67.4	62.9	52.8
NPKI	73.5	48.1	76.5	62.9	64	66	78	66.9	73.0	61.0
NPKII	46	30.1	48	25.6	45	41.9	69.5	50.9	52.1	37.1
NPKI (pH 5.5)	60	50	54.5	37.8	79	91.5	76	65.2	67.4	61.1
NPKI (pH 4.5)	68.5	52.2	84	62.5	74.5	66.6	85.5	74.9	78.1	64.1
Average	59.1	42.3	62.7	43.2	67.6	70.2	77.4	65.1	66.7	55.2

Only soil as an experimental factor had a statistically significant influence on the concentration of Ni in maize roots and Ni removal by roots from acid soils (Table III). This was determined by statistical analysis. The average values for the Ni concentration in plant roots and Ni removal from the soil were higher for the treatments of soil 5 than of soil 6. This was connected with the fact that soil 5

had a higher concentration of total Ni than soil 6. From the Table III, it can be seen that with treatments NPKI and NPKII, root Ni concentration and Ni removal from the soil were lower than in the control. Full neutralization of the acid soils increased Ni removal from the soil by the roots in relation to all other experimental treatments. However, it must be bear in mind that the registered changes in the root Ni concentration and Ni removal from the soil were not significant at the 0.05 probability level.

TABLE III. Concentration of Ni in the roots and its removal from the treated acid soils; results of the LSD test for Ni concentration: soil – LSD (0.05) = 16.8 and LSD (0.01) = 22.8; results of the LSD test for Ni uptake: soil – LSD (0.05) = 23.2 and LSD (0.01) = 31.5

Treatment	Soil 5		Soil 6		Average value	
	µg/g	µg/pot	µg/g	µg/pot	µg/g	µg/pot
Control	105.0	78.8	53.5	26.0	79.3	52.4
NPKI	74.5	76.9	45.5	19.9	60.0	48.4
NPKII	57.5	55.9	46.0	17.9	51.8	36.9
NPKI +1/2 CaCO ₃	66.0	57.4	55.5	21.0	60.8	39.2
NPKI + CaCO ₃	102.0	132.8	57.0	32.5	79.5	82.7
Average	81.0	80.4	51.5	23.5	66.3	51.9

The found values for the Ni concentration in the shoots and for the uptake of Ni from treated neutral and weakly alkaline soils are given in Table IV. The average values (according to treatments for all 4 soils) for the Ni concentration in the shoots ranged from 6.8 to 12.0 µg/g, while the corresponding values for Ni removal ranged from 8.8 to 16.7 µg/pot. Analysis of the variance showed that none of the experimental factors had a statistically significant influence on the shoot Ni concentration and its removal from the soil. In other words, the differences in the Ni concentration and its removal (in shoots and by shoots, respectively), which existed between the treatments and the soils were not significant at the 0.05 probability level.

TABLE IV. Concentration of Ni in the shoots and its removal from the treated neutral and weakly alkaline soils

Treatment	Soil 1		Soil 2		Soil 3		Soil 4		Average value	
	µg/g	µg/pot	µg/g	µg/pot	µg/g	µg/pot	µg/g	µg/pot	µg/g	µg/pot
Control	14.0	15.3	11.5	10.4	8.0	15.0	8.5	12.2	10.5	13.2
NPKI	6.0	6.5	6.5	8.9	7.5	12.9	7.0	10.0	6.8	9.6
NPKII	7.0	7.6	7.0	6.2	7.5	11.6	8.0	9.8	7.4	8.8
NPKI (pH 5.5)	6.5	9.0	7.5	8.7	7.0	13.5	6.0	8.6	6.8	10.0
NPKI (pH 4.5)	6.0	7.6	10.0	12.4	8.0	11.9	24.0	35.0	12.0	16.7
Average	7.9	9.2	8.5	9.3	7.6	13.0	10.7	15.1	8.7	11.7

Comparison of the treatments with fertilizers and the control showed that the Ni concentration in the shoots and its removal were lower for soils to which only

mineral fertilizers were applied. Soil acidification to pH 4.5 increased the shoot Ni concentration and Ni removal from the soil in relation to the control and other treatments on neutral and weakly alkaline soils. However, as mentioned earlier, the registered changes were not significant at the 0.05 probability level.

Differences between soils with respect to the total Ni concentration did not have a significant effect on the concentration and transfer of Ni into the maize shoots. The highest average values for the Ni concentration and uptake were found for the treatments of soil 4.

The results presented in Table V indicate that treatment, as an experimental factor, did not have a significant influence on the concentration of Ni in the plants (aerial part) and its transfer to the shoots in the experiment with the acid soils. On the other hand, soil, as an experimental factor, did exert a significant influence on the uptake of this metal. The average value of Ni removal from soil 5 was 13.5 $\mu\text{g}/\text{pot}$, while the corresponding value for soil 6 was 6.4 $\mu\text{g}/\text{pot}$. The reason for this lies in the fact that average maize yield on soil 5 was two times higher than that on soil 6.¹⁰ The highest average value for Ni removal from the soil by maize was found for the treatment NPKI + CaCO_3 . However, this increase, with respect to the other treatments, was not significant at the 0.05 probability level.

TABLE V. Concentration of Ni in the maize shoots and its removal from the treated acid soils; results of the LSD test for Ni uptake: soil – LSD (0.05) = 5.0 and LSD (0.01) = 6.7

Treatment	Soil 5		Soil 6		Average value	
	$\mu\text{g}/\text{g}$	$\mu\text{g}/\text{pot}$	$\mu\text{g}/\text{g}$	$\mu\text{g}/\text{pot}$	$\mu\text{g}/\text{g}$	$\mu\text{g}/\text{pot}$
Control	7.0	8.8	9.0	7.3	8.0	8.1
NPKI	7.5	12.9	9.0	6.6	8.3	9.8
NPKII	6.5	10.5	9.5	6.2	8.0	8.4
NPKI + 1/2 CaCO_3	10.0	14.5	8.5	5.4	9.3	10.0
NPKI + CaCO_3	9.5	20.6	7.0	6.7	8.3	13.7
Average	8.1	13.5	8.6	6.4	8.4	10.0

The results that are presented in Tables II–V indicate that the concentration of Ni was higher in the roots than in the shoots of maize plants. Thus, for example, the average Ni concentration in the roots of maize plants on neutral and weakly alkaline soils was 66.7 $\mu\text{g}/\text{g}$, while the corresponding value for the shoots was 8.7 $\mu\text{g}/\text{g}$. The results obtained by Radulović¹¹ also indicated that the concentration of Ni was higher in the roots than in the shoots. These investigations refer to oat plants that were grown under controlled conditions on the brown and alluvial soils of the Zeta Plain in Montenegro. This author found that the ratio between Ni concentration in roots and shoots of oat grown on brown soils was 1:0.12, while the corresponding value on the alluvial soils was 1:0.15. Investigations carried out by Sauerbeck and Hein¹² showed that the concentration of Ni

was the highest in the roots. Namely, they investigated the uptake of Ni by 13 plant species grown on two types of soil containing Ni in different concentrations and forms.

Correlation analysis was employed to investigate the relationship between the Ni concentration (in roots and shoots of maize) and the chemical properties of the investigated soils. For the calculation of correlation coefficients, results referring to all three replications of unfertilized treatment (controls) were used. The results of the correlation analysis are presented in Table VI.

TABLE VI. Correlation coefficients between the Ni concentration in maize and some important chemical properties of soil

Soil property	Correlation coefficient	
	Roots	Shoots
pH (H ₂ O)	ns ^a	0.530 ^b
pH (1M KCl)	ns	0.624 ^c
Humus	0.821 ^c	-0.860 ^c
Total N	0.619 ^c	-0.708 ^c
Available phosphorus	ns	ns
Available potassium	ns	ns
Total Ni	ns	ns

^aNot significant; ^bstatistically significant at the 0.05 probability level; ^cstatistically significant at the 0.01 probability level

The results presented in Table VI indicate that only the content of humus and total nitrogen had a significant influence on the concentration of Ni in the roots of young maize plants. Therefore, it can be supposed that the Ni present in the roots originated partly from its organic forms in the soil. In other words, the fraction of Ni bound to the organic matter of the soil contributed to the supply of plants with this element.

Concerning the concentration of Ni in the shoots, medium and statistically significant correlations were obtained with pH (in H₂O and 1 M KCl), the humus content and the total soil nitrogen. It can be seen that an increase in the humus and nitrogen content bring about a decrease in the Ni concentration in maize shoots. A good explanation for the positive effect of soil pH and the negative effect of humus content on the Ni concentration in maize shoots cannot be given at present.

There is a negative and statistically very significant correlation between concentrations of Ni in the roots and shoots ($r = -0.811$).

Multiple linear regression was employed to determine the simultaneous impact of several soil properties on the Ni concentration in maize roots and shoots. The investigated chemical properties were assumed as independent variables for the equation constructed by progressive stepwise regression. The following soil

characteristics were considered in the equation describing the Ni concentration in the roots and the aerial parts of the tested plants:

$$\begin{aligned} \text{Ni}_{\text{roots}} &= -24.712 + 40.477\text{humus} - 120.956\text{N} \\ \text{Ni}_{\text{shoot}} &= 11.226 - 0.660\text{pH}_{\text{H}_2\text{O}} + 2.207\text{pH}_{\text{KCl}} - 3.161\text{humus} - 4.836\text{N} \end{aligned}$$

where humus is the humus content in % and N is the total nitrogen content in %.

CONCLUSIONS

Based on the results obtained in this investigation, the following conclusions can be drawn:

- The addition of mineral fertilizers (without application of other measures) mainly decreased the Ni concentration in maize and Ni removal from the soil by the plants.
- Soil acidification (to pH 4.5) caused an increase in the Ni concentration in the plants and its removal from the soil.
- Liming of acid soils had a positive effect on the removal of Ni from the soil by young maize plants.
- The concentration of Ni in the roots was on average 8 times higher than in the shoots. The obtained results are important from the standpoint of reducing the pollution of plants with potentially toxic heavy metals.
- Correlation analysis indicated that some of the chemical properties of the investigated soils had a statistically significant influence on the concentration of Ni in the roots and shoots of young maize plants. The strongest effect was expressed by the humus content.

ИЗВОД

УТИЦАЈ НЕКИХ АГРОТЕХНИЧКИХ МЕРА НА УСВАЈАЊЕ НИКЛА БИЉКАМА КУКУРУЗА

БРАНКА ЖАРКОВИЋ И СРЂАН БЛАГОЈЕВИЋ

Пољопривредни факултет, Немањина 6, 11080 Београд

Никл није неопходан елемент за исхрану већине биљних врста и он може бити токсичан за биљке када је његова концентрација у земљишту висока. Неколико особина земљишта има утицаја на усвајање овог метала биљкама. Циљ овог истраживања је био да се утврди утицај ђубрења, закисељавања земљишта и калцизације на усвајање Ni биљкама кукуруза гајеним на неким алувијалним земљиштима. Постављен је оглед у судовима са биљкама кукуруза које су гајене на поменутом земљиштима. Оглед је трајао 6 недеља. Коренови и надземни делови су анализирани на садржај Ni. Може се закључити из резултата огледа да коренови имају веће концентрације Ni у односу на надземне делове. Додавање минералних ђубрива (без примене других мера) углавном је смањило концентрацију и усвајање Ni кореновима као и његов транспорт до надземних делова. Закисељавање земљишта (до pH 4,5) повећало је усвајање Ni кореновима и његов транспорт до надземних делова биљака. Калцизација киселих земљишта је имала позитиван утицај на усвајање Ni младим биљкама кукуруза. Добијени резултати су значајни за смањење загађивања биљака потенцијално токсичним тешким металима.

(Примљено 21. јануара, ревидирано 11. марта 2009)

REFERENCES

1. A. Kabata-Pendias, *Trace elements in soils and plants*, CRC Press, Boca Raton, FL, 2001
2. M. L. Berrow, J. C. Burridge, *Sources and distribution of trace elements in soils and related crops*, CEP Consultants Ltd., Edinburgh, 1979
3. R. L. Halstead, B. J. Finn, A. J. MacLean, *Can. J. Soil Sci.* **49** (1969) 335
4. B. Žarković, S. Blagojević, *J. Environ. Prot. Ecol.* **8** (2007) 535
5. D. Stevanović, R. Džamić, M. Jakovljević, *Practicum in Agrochemistry*, Faculty of Agriculture, Belgrade, 1996
6. J. B. Jones, V. W. Case, in *Soil Testing and Plant Analysis*, R. L. Westerman, Ed., Soil Science Society of America, Madison, WI, 1990, p. 404
7. *Regulatives of allowed concentrations of heavy metals and organic matter in soil*, Official Gazette, Official Informatory of the Republic of Serbia, 1990, p. 11
8. W. H. Fuller, in *Movement of selected metals, asbestos and cyanide in soil: application to waste disposal problem*, US-EPA, Cincinnati, OH, 1977, p. 243.
9. G. Siebielec, L. R. Chaney, U. Kukier, *Plant and Soil* **299** (2007) 117
10. B. Žarković, *Ph.D. Thesis*, Faculty of Agriculture, Belgrade, 2005
11. M. Radulović, *Ph.D. Thesis*, Faculty of Agriculture, Belgrade, 2001
12. D. R. Sauerbeck, A. Hein, *Water Air Soil Pollut.* **57–58** (1991) 861.



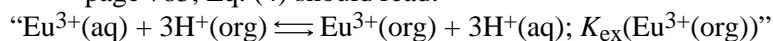
J. Serb. Chem. Soc. 74 (8–9) 1019 (2009)

Errata (printed version)

Issue No. 7 (2009), Vol. 74:

– page 781, lines 5 and 6 from the top should read: “EMANUEL MARKLÍK^{1*}, PETR VAŇURA², PAVEL SELUCKÝ³, VASILYI A. BABAIN⁴ and IGOR V. SMIRNOV^{4*}”.

– page 783, Eq. (4) should read:



– page 783, line 15 from the bottom should read: “...to which the equilibrium constants: K_{D} , $\beta(\text{HL}^+(\text{org}))$, $\beta(\text{HL}_2^+(\text{org}))$, $K_{\text{ex}}(\text{Eu}^{3+}(\text{org}))$...”

– page 784, line 11 from the top should read: “... $\log(K_{\text{ex}}(\text{Eu}^{3+}(\text{aq}))) = 1.3^{26}$ were used for the respective calculations. The results...”

– page 784, line 12 from the bottom should read: “...rithmic scale using the approximate expression $\log K \pm \{\log(K + 1.5\sigma(K)) - \log(K - 1.5\sigma(K))\}$. For $\sigma(K) > 0.2$...”

– page 784, line 9 from the bottom should read: “Knowing the value $\log K_{\text{ex}}(\text{Eu}^{3+}(\text{org})) = 1.30$,²⁶ as well as the extraction...”